# AFCEE Source Zone Initiative

# Final Report

Colorado State University

Environmental Science and Engineering
SCHOOL OF MINES
1874
COLORADO
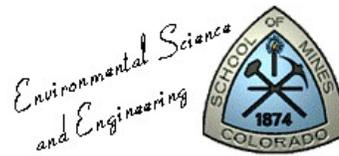
Submitted to

Air Force Center for Environmental Excellence

May 2007

# Executive Summary

### Introduction

A fundamental question associated with managing historical releases of chlorinated solvents is how source depletion, and/or source zone containment, will affect downgradient water quality over time (Figure 1). The focus of this project was to build a set of tools that will assist stakeholders in addressing this issue. These include a comprehensive description of governing processes, illustrative laboratory experiments, predictive models, and supporting field data. The key theme that arises from this work is that contaminants in low permeability layers can act as long-term sources of contaminants in source zones and downgradient plumes.
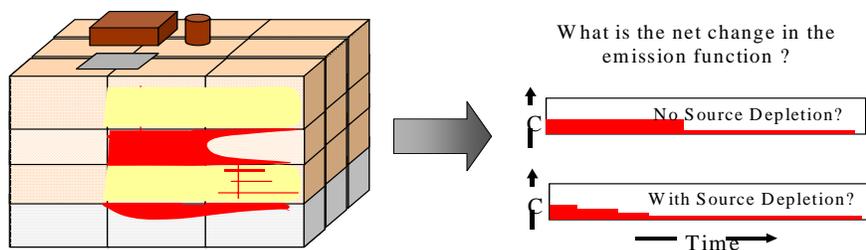


Figure 1 - Chlorinated solvent source zone (after Poulson and Kueper, 1992, Kueper et al., 1993) and conceptual source emission functions.

### Project Basis

Interactions between staff at the Air Force Center for Environmental Excellence (AFCEE) and faculty at Colorado State University (CSU) and Colorado School of Mines (CSM) led to a vision of developing a set of tools that would assist stakeholders in resolving how best to manage chlorinated solvents released at

Department of Defense (DoD) facilities.  The motivation for this is recognition that historical efforts to remediate contaminated sites have sometimes fallen short of expectations and that there are potential opportunities to "do things better."

**Governing Processes**

As a first step, governing processes were reviewed.  This provided a theoretical basis for laboratory experiments, mathematical models, and interpretations of field data.   Key concepts are noted in the following text.

Dense nonaqueous phase liquids (DNAPLs) are thought to occur in sparse horizontal subzones (referred to as pools) that are interconnected by sparse vertical fingers and zones of residual saturation (Figure 2). The occurrence of horizontal DNAPL subzones is related to the presence of fine-grained layers that have sufficiently large displacement pressures to preclude downward migration of DNAPL. This results in the condition of DNAPL perched on low permeability layers.
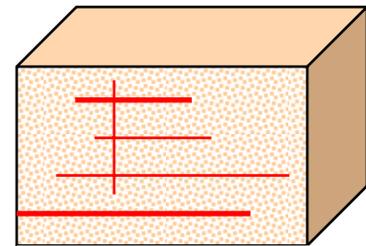


Figure 2 - DNAPL pools and fingers

With dissolution, DNAPL constituents are transferred to aqueous and sorbed phases in transmissive and low permeability zones.  Figure 3 presents the simple case of a DNAPL subzone in a transmissive layer (sand) resting on a low permeability layer (silt) that behaves as a capillary barrier.  Primary processes that govern release of contaminants to groundwater are:  (1) transverse diffusion-dispersion from the DNAPL to the transmissive zone, (2) transverse diffusion into the silt layer through the pool, (3) longitudinal advection, and  (4) transverse diffusion into the silt from the plume.  Inspection of the graph in Figure 3 (based on assumed conditions and simple analytical solutions) reveals that the majority of the dissolved contaminant mass released from the DNAPL zone ends up in the silt after 1000 days.
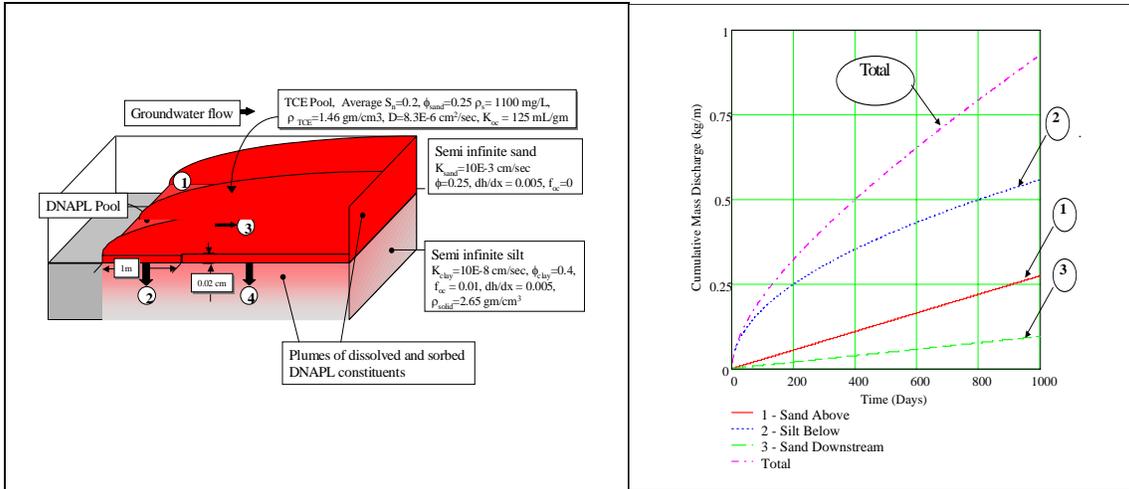
Figure 3 -DNAPL perched on a capillary barrier and cumulative mass discharges to transmissive and stagnant zones

Two additional processes (2` and 4`) are identified in Figure 4.  Processes 2` and 4` are the reversal of processes 2 and 4, respectively.  They reflect back diffusion of contaminants into the transmissive zone after the DNAPL is exhausted.   Back diffusion is a primary topic of this study.  This focus reflects the fact that back diffusion has the potential to sustain plumes (after source depletion) and to govern time to cleanup.
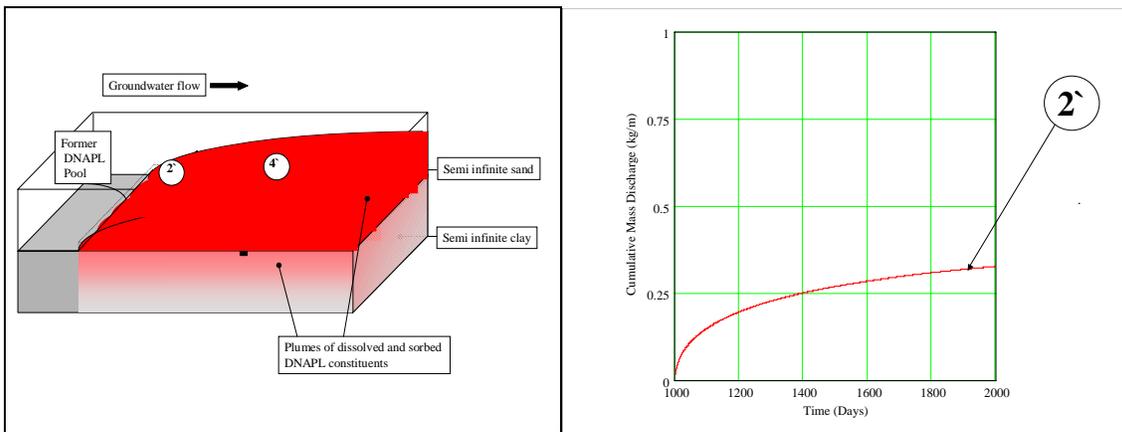


Figure 4 - Back diffusion from low permeability zones 2` and 4` and estimated cumulative discharge due to 2` after removal of a DNAPL pool.

## Laboratory Studies

A primary cornerstone of this project is laboratory studies conducted in sand tanks at a variety of scales.  The main objectives of the tank studies are to resolve fundamental processes and to generate data to test predictive models.

CSU conducted small-scale tank studies using soils from F.E. Warren Air Force Base (FEW), Cheyenne, Wyoming.  Highly idealized two-layer and multiple-layer configurations were investigated.  The primary goal was to resolve the effect of low permeability layers on the discharge of dissolved contaminants from the tanks.  Inclusive to this is resolving how adsorption and degradation of contaminants in low permeability layers controls contaminant storage and release.  This was accomplished by using contaminants with different tendencies to adsorb (different $K_{oc}$ values) and silt layers amended with organic carbon and reactive media.  Results show that low permeability layers play dramatic roles in (1) attenuating plumes while sources are active and (2) sustaining plumes after sources are removed.  In addition, results indicate that (1) elevated adsorption in low permeability layers greatly increases contaminant storage and (2) that even modest degradation rates can dramatically reduce contaminant release from low permeability layers.

Experiments conducted at CSM include small, intermediate, and large-scale tank studies conducted in conjunction with X-ray analysis to monitor DNAPL depletion.  X-ray analysis provides a means of resolving when DNAPL is and is not present and knowing when the source of aqueous phase contaminants is DNAPL or back diffusion.  Soils used in the CSM studies are a combination of laboratory sand and soil obtained from Naval Air Station Fort Worth (NASFtW) and former Carswell AFB, Texas.

Preliminary experiments conducted in the small-scale tanks at CSM allowed development of experimental methods and conceptual models. These formed the basis for subsequent intermediate and large-scale tank experiments.

Results from the intermediate-scale tanks suggest, that at the scale of observation (centimeters), dissolution of common DNAPL contaminants proceeded in a relatively quick and steady fashion. The results (which are for only one highly uniform sand) suggest that DNAPL blobs or pools are not particularly long-lived. Despite the relatively rapid depletion of DNAPL pools and residuals (<10 days), downstream concentrations remained well above U.S. Environmental Protection Agency (USEPA) maximum contaminant levels (MCLs) for weeks to months. The contradiction between relatively quick DNAPL dissolution and long-term effluent concentration tails is best explained by matrix storage and subsequent back diffusion.

Large-scale tanks were employed to study governing processes at larger scales over longer periods. The greater length of the tanks (~ 5 m) allowed for the creation of both the source zone (where DNAPL is entrapped) and downgradient plume with reasonable spatial dimensions. Through this experimental process the four primary contaminant fluxes (Figure 3) were addressed in one experiment. Three separate tanks were packed with different configurations of the field soil collected from NASFtW and various laboratory sands. The large tank studies show that matrix diffusion and subsequent back diffusion play a primary role in defining the longevity of dissolved phase contaminants in plumes. Furthermore, results from the large tank model provide a basis for testing numerical models.

**Modeling**

Two modeling efforts were undertaken. The first involved the development of analytical solutions. Analytical solutions provide insight to governing basic

6

processes and a basis for testing numerical models. The second modeling effort involved numerical models. Numerical models offer the opportunity to consider more realistic physical settings.

As indicated by the estimated contaminant fluxes in Figure 3, a primary process governing DNAPL dissolution in the two-layer case is transverse diffusion into the low permeability layer. Once the DNAPL has fully dissolved, back diffusion from the low permeability zones (also a transverse diffusion process) sustains contaminant concentrations in the transmissive layer. Figure 4 identifies back diffusion processes 2` and 4`. It also presents an estimate of cumulative contaminant discharge from the stagnant zone beneath a fully dissolved DNAPL pool as a function of time. Clearly, for the conditions considered, complete removal of DNAPL should not be equated to complete removal of the source.

Building on Sudicky et al. (1985), analytical solutions for processes 4 and 4` were developed. A sample problem is presented in Figure 5. The general condition is a DNAPL-like source at the sand-silt contact. The source is active for 1000 days and then removed. Normalized concentrations in the sand and silt are presented in Figure 6 at various times while the source is active and off. The contour plots illustrate the effects of sub-processes 4 and 4` on water quality in the transmissive sand and low permeability silt layers.
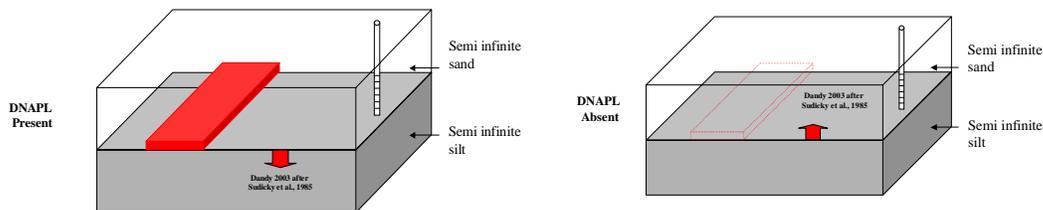


Figure 5 - Plume attenuation with DNAPL present (left) and back diffusion after DNAPL depletion (right).
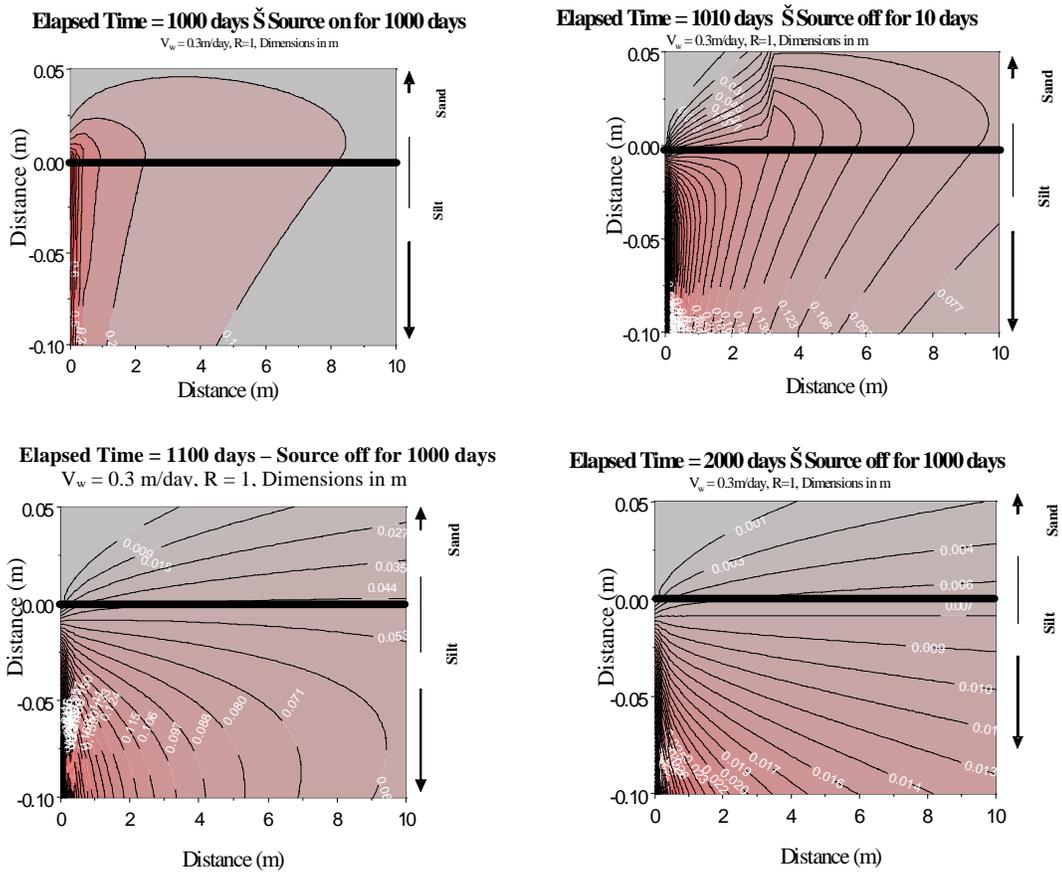
Figure 6 - Normalized concentration in sand and silt layers downgradient of a DNAPL source that persists for 1000 days – axis dimensions in meters.

Using the analytical solution for sub-processes 4 and 4`, Figure 7 presents estimates of concentration in monitoring wells located 1, 10, and 100 m, downgradient a DNAPL –like source.  The source is active for the first five years of the twenty-year period considered.  Concentrations in wells are obtained by averaging modeled concentrations over a 3 m interval immediately above the sand layer.  Initially, transverse diffusion into the silt attenuates plume concentrations.  After the source is removed, back diffusion sustains plume concentrations.  For the conditions considered, complete source removal provides approximate one to two orders of magnitude improvements in wells

8

located 10 and 100 m downgradient water quality 15 years after complete source removal. Regrettably, this result indicates that contaminants stored in low permeability layers can sustain plumes for extended periods after complete source removal. More favorable results are observed for conditions with lower adsorption and higher degradation rates in the low permeability layer.
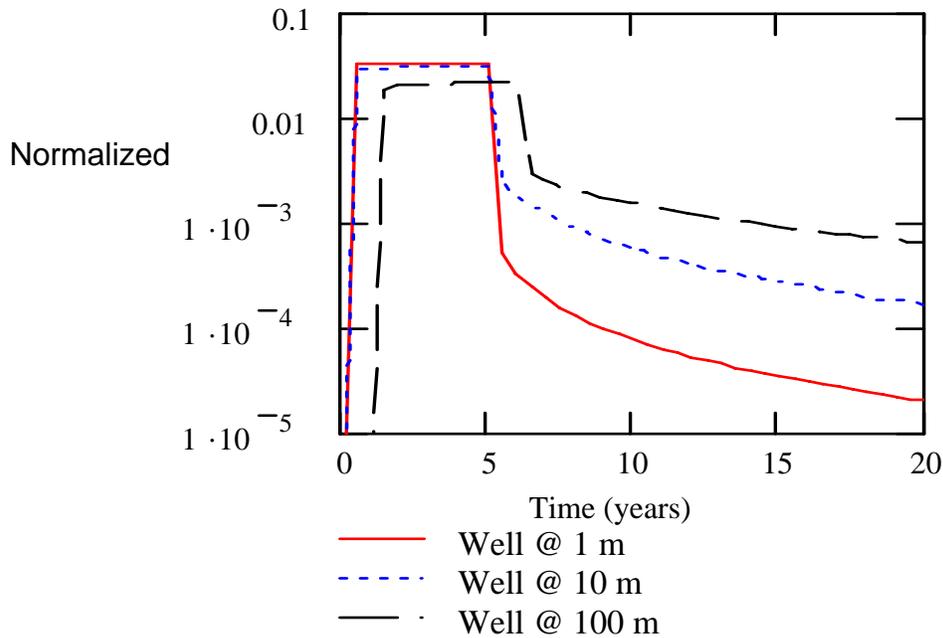
Figure 7 - Concentrations of TCE in downgradient wells as a function of time.

More realistic physical settings were considered using numerical models. As a starting point, conventional numerical transport models are challenged to capture transverse transport process due to the issue with domain discretization. In addition, the nature of the paths traveled by a contaminant in an aquifer is strongly influenced by the heterogeneity of the subsurface, which determines the underlying flow field. Considering the limitations of the conventional advection-dispersion models, a dual-porosity model is utilized. Specifically, the dual-porosity module of Finite Element Heat and Mass (FEHM) transfer is used in conjunction with the flow and transport modules to simulate the physical conditions in the tanks.

9

For each experimental domain, the transient source function that was calculated from the measured pure phase mass depletion curve. This was used as the source term in the model. The results of the numerical simulations show that FEHM is able to predict the observed diffusion into and out of the lower permeability layer in the experimental domain. For each simulation, sensitivity analyses were performed to determine which parameter(s) had the greatest effect on the effluent breakthrough curve. Results indicate that the amount of pure phase DNAPL initially injected, flow rate through the system, and the heterogeneity of the system are the key parameters defining downgradient water quality. Through the numerical modeling effort a predictive tool is demonstrated that can simultaneously address sources and contaminant storage-release from low permeability zones.

**Field Studies**

Similar issues with contaminant storage and release from low permeability layers are seen in field data. For example, an iron permeable reactive barrier (PRB) was installed at Spill Site 7, F.E. Warren AFB, Wyoming in 2000. This action reduced TCE concentrations at the barrier by multiple orders of magnitude to values less than 5 *u*g/L, the USEPA MCL. After five years, TCE concentrations forty and sixty feet downgradient of the barrier dropped by only one order of magnitude (Figure 8). Sustained concentrations of TCE downgradient of the barrier are attributed to desorption and back diffusion from low flow zones. A key observation from the field data is that contaminant storage and release from low permeability zones (as observed in laboratory and modeling studies) also occurs at field sites.
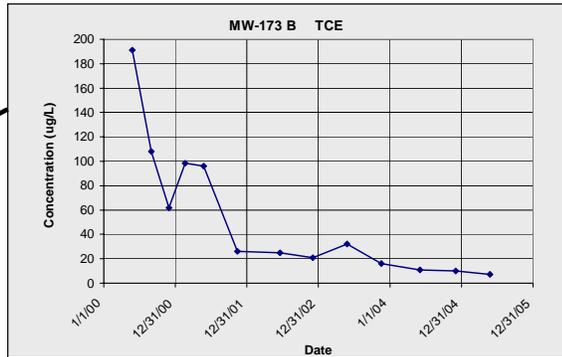
Figure 8 - Concentrations of TCE in wells 40 and 60 feet downgradient of an iron PRB

## Summary

Through this project, a set of tools were developed to assist stakeholders in resolving the benefits of source management measures. Key elements include a description of governing processes, illustrative laboratory studies, predictive models, and demonstrative field data. Results from this work indicate that transverse diffusion can drive contaminants into low permeability zones. Initially, this has the effect of attenuating contaminants in transmissive layers. After the DNAPL has been depleted, back diffusion from low permeability zones sustains contaminant concentrations in transmissive layers in source zones and plumes. Primary implications of contaminant storage and release in low permeability zones include:

- Release of stored contaminants can sustain contaminant discharge from source zones. This can explain persistent releases of contaminant from plume heads where little, if any, DNAPL can be found.

- Source zone treatments that solely address transmissive zones may miss substantial contaminant mass in low permeability zones and be subject to post treatment contaminant rebound.

- Given near perfect depletion and/or containment of sources, back diffusion can sustain downgradient plumes for extended periods. As such, removal and/or containment of sources may not provide substantial near-term improvement in groundwater quality.

Per the original objective for this project, the project team hopes that the information presented herein provides an improved basis for selection remedies for releases of chlorinated solvents and other persistent contaminants at DoD facilities.

**Acknowledgements**

# Table of Contents

# Appendices

# Table of Figures

# List of Tables

# 1.0   Introduction

Beginning in 2000, interactions between staff at the Air Force Center for Environmental Excellence (AFCEE) and faculty at Colorado State University (CSU) and Colorado School of Mines (CSM) led to a vision of developing a protocol that addresses the management of historical releases of chlorinated solvents at Department of Defense (DoD) facilities. The motivation for this was recognition that historical efforts to remediate contaminated sites have sometimes fallen short of expectations and there is an opportunity to "do things better". Originally, this project was envisioned as developing both supporting science and a protocol. Due to a reduction in project funding, the objectives for this work were constrained to developing supporting science and tools for a source zone protocol. However, the DoD Environmental Security Technology and Certification Program (ESTCP) will provide support for the originally envisioned protocol for source zones. Information compiled herein provides a scientific foundation for the ESTCP source zone protocol.

## 1.1   Scope

As finally defined, the primary elements of the project are:

1) Laboratory studies conducted at different test scales designed to investigate the governing processes of contaminant release and transport under idealized conditions. These experiments will help in obtaining a qualitative and quantitative understanding of the fundamental processes with the goal to build a technical foundation for subsequent work and an effective means of illustrating critical processes to decision makers.

2) Evaluation of governing processes at a field-scale based on data from projects at F.E. Warren Air Force Base (FEW), Naval Air Station Fort Worth (NASFtW), and Air Force Plant 4 (AFP4) located adjacent to NASFtW. For the first year this included technical support to the operators of these facilities.

3) Development of models that provide *a priori* estimates of the effect of source control measures on groundwater quality. These models are tested using results from the laboratory studies.

4) Development of a set of tools, including responses to frequently asked questions, to assist Air Force staff and contractors in formulating optimal strategies for managing issues related to chlorinated solvent releases at DoD facilities.

## *1.2   Report Content*

The report is organized as follows:

**Section 2 - Process Conceptualization** – This section describes our conceptual understanding of processes governing the effectiveness of source control measures. This description departs from conventional thinking in that it emphasizes the importance of contaminant mass stored in low permeability groundwater zones. This is a topic that is often given little attention in granular porous media. It is our hypothesis that this storage mechanism is responsible, in part, for the limited effectiveness of many technologies used to improve water quality at sites impacted with chlorinated solvents.

**Section 3 - Laboratory Studies** – Governing processes can be systematically investigated through laboratory studies involving idealized conditions. Once the processes are understood at various test scales, tools can be developed to generalize these results to field-scale problems. Large- and small-scale tank studies have been conducted. Inclusive to this has been the collection and use of field soils from FEW and NASFtW. The laboratory results provide a dramatic demonstration of the importance of hydraulically stagnant zones and a basis for validating analytical and numerical models developed in later parts of the report.

**Section 4 – Models** – The goal of modeling is to quantitatively advance our understanding of governing processes and apply our knowledge of the processes to field conditions, the primary scale of interest. Final solutions will serve as a foundation for *a priori* analyses of the water quality improvements associated with source control measures.

**Section 5 - Field Studies** – Evaluation of source control measures at field sites provides a critical opportunity for understanding how laboratory-scale processes come into play at the field-scale. Twenty-one source control projects at FEW, NAS, and AFP4 were reviewed. This evaluation provides important insights into the factors affecting the success of source control measures, including those classified as innovative technologies. Regrettably funds to complete this initiative were not available.

**Section 6 - Future Work** – Through our compilation of this document, we have developed a list of issues that deserve further consideration. This is provided for those who might follow on with the initiatives of this project.

**Appendices** – Numerous appendices are included in this document. These appendices provide rigorous backup for the content presented in the main text of the report. Our goal in organizing this document is to avoid burdening the reader with too much technical detail in the main text. Ultimately, we hope to present much of this material in peer reviewed publications and/or theses.

# 2.0 Process Conceptualization

## 2.1 Introduction

The following provides an overview of processes governing the impacts of DNAPL releases on groundwater quality. The primary objective is to build a conceptual foundation for DNAPL releases that can be used to make sound decisions regarding management of impacts from the releases. In addition, this section provides the theoretical basis for subsequent laboratory experiments, mathematical developments, and interpretations of field data.

## 2.2 Dense Nonaqueous Phase Liquids

DNAPL is a convenient label for nonaqueous phase chlorinated solvents in soils and groundwater. The acronym stands for Dense Nonaqueous Phase Liquid. Dense highlights the fact that chlorinated solvents have mass per unit volume (density) that is greater than water. As such, they have a tendency to sink within aquifers. "Nonaqueous" emphasizes the fact that DNAPL and water do not mix; that is, they are immiscible. A primary consequence of not mixing with water (being immiscible) is that water and DNAPL occupy different portions of the pore space when present in granular or fractured media. This "sharing of pore space" complicates the flow of DNAPL and water, and the mechanics of the DNAPL dissolution into water. Other DNAPLs, such as coal tar and creosote, are not a primary concern of the DoD, and their behavior can be substantially different from that of chlorinated solvents. Therefore, "other DNAPLs" are not considered herein.

## 2.3 Relevant Processes

### 2.3.1 DNAPL Releases

Standard industrial practices of past decades have resulted in inadvertent releases of chlorinated solvents to the environment. Commonly this has been

associated with storage and/or disposal practices at industrial facilities. Fortunately, recognition of the resultant problems has led to dramatically improved storage/use/disposal practices and greatly reduced the frequencies of releases. A primary outcome of improved practices is that most DNAPL releases are old (10, 20 or even 50 years). Subsequent discussions show that the age of a release can have a strong bearing on distribution of contaminants in a source zone and efficacy of source control technologies.

### 2.3.2  DNAPL Migration

Subsurface sediments consist of solids (e.g., soil grains) and void space (soil pores). The void space of subsurface porous media always contains water, whether it is above and below the water table. In the unsaturated zone (that is, above the capillary fringe), air coexists with water in the pore space. Compared to air, water is preferentially attracted to the solids and forms a continuous **wetting phase** that "coats" the soil grains and tends to fill the smaller pore spaces. In larger pores, water tends to occupy margins, leaving the remaining central portions filled with air, a **non-wetting phase** that is immiscible to water.

In porous media, DNAPL is non-wetting when it exists in the presence of water. Figure 9 is a photograph of porous media that contains both wetting and non-wetting phases. In this case, the wetting phase is water and the non-wetting phase could be either air or DNAPL.
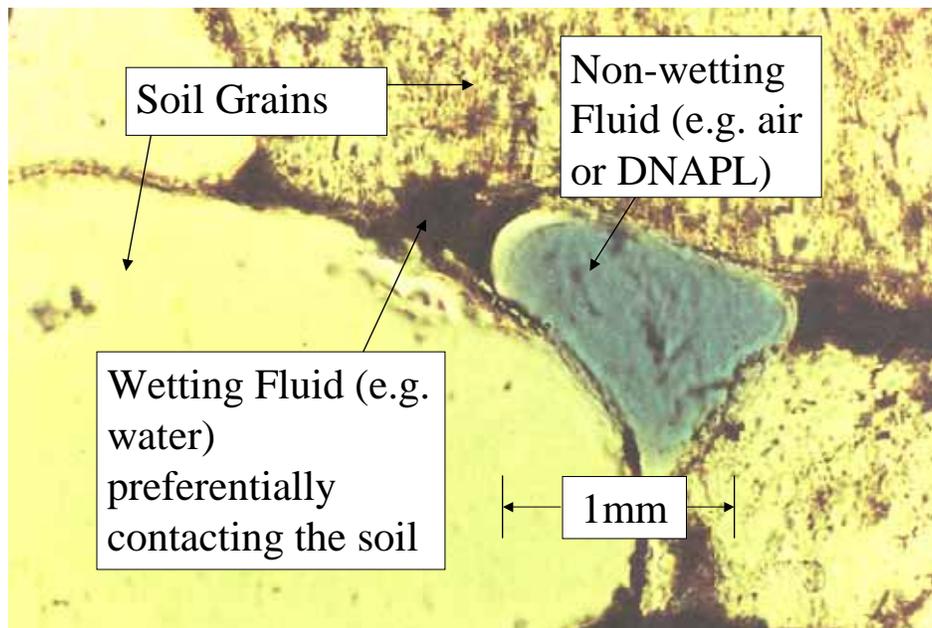
Figure 9 - Immiscible fluids in the pore space of a granular porous media (From Wilson et al., 1990)

Released DNAPL migrates downward through the subsurface under the influence of gravity and capillary forces. Above the capillary fringe, DNAPL displaces air and occurs as an intermediate wetting phase between the water and air. Volatile DNAPL components partition into soil gas and vapor plumes forming local releases. Given a large enough release, DNAPL will migrate downward to the groundwater zone. In the groundwater zone DNAPL displaces water and occurs (typically) as a non-wetting phase within the porous or fractured medium.

The non-wetting and immiscible nature of DNAPL influences its movement and distribution in the subsurface. For DNAPL to invade water-saturated media, it must displace the water, which requires that the DNAPL pressure be higher than the water pressure. Note that the pressures of DNAPL and water are different at the *same location*, due to the surface tension that develops at the interface

between the two fluids. The DNAPL pressure (that is, pressure greater than water) needed to displace water from a pore and allow DNAPL to invade is referred to as **displacement pressure**. For a given DNAPL, the displacement pressure is related to the size of the pore. For larger pores, the displacement pressure for DNAPL invasion is smaller. As a consequence, DNAPL tends to migrate preferentially into the largest pores first. Rigorous development of these concepts is presented in Kueper et al (1989; 1991).

Selective movement along paths of least resistance, along with the results from experimental releases at Canadian Forces Base, Borden, Ontario (Poulson and Kueper, 1992; Kueper et al., 1993), have led to the conceptualization of DNAPL occurring in sparse horizontal subzones (referred to as pools) that are interconnected by sparse vertical fingers as shown in Figure 10. The occurrence of the horizontal DNAPL subzones is related to the presences of fine-grained layers that have sufficiently large displacement pressures that they preclude downward migration (invasion) of DNAPL into their pore space This leads to the important observations that: (1) DNAPL pools are often perched above fine-grained layers and (2) the architecture of DNAPL occurrence is highly dependent on the geologic heterogeneity of the source zone (Illangasekare et al., 1995). Figure 10 presents none of the geologic detail that governs the distribution of the DNAPL. As such, it is a gross simplification. In addition, the conceptualization in Figure 10 does not convey the importance of dissolved DNAPL that has migrated by diffusion into hydraulically low permeability groundwater zones. As discussed below, this can be the most important component of a source zone.
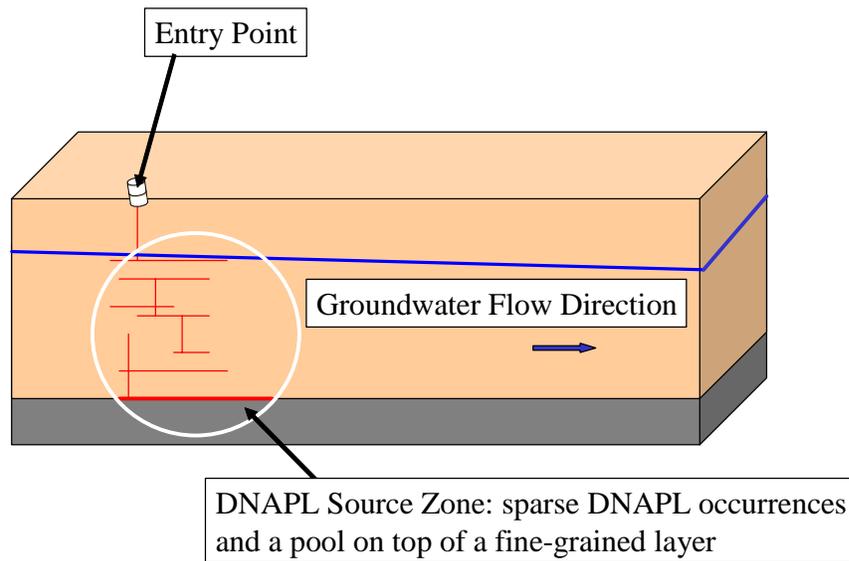
Figure 10 - Simple conceptualization of DNAPL occurring in horizontal pools and vertical fingers (e.g. Kueper et al., 1993)

### 2.3.3  DNAPL Dissolution

Where DNAPL is in contact with gas or water, chemical potentials drive DNAPL constituents into the surrounding fluid(s).  Saturation of the aqueous or gas phase occurs when the chemical potential of the respective phases are equal. Dissolution of DNAPL constituents into the gas and/or water phases depletes the remaining DNAPL.  Transport processes, such as advection, dispersion, and diffusion, carry dissolved constituents away from the source and drive further DNAPL dissolution.  In addition, dissolved DNAPL constituents in water can adsorb onto the solids that make up the porous media.  Sorption acts as a sink that accelerates rates of DNAPL dissolution.  The total chemical mass in a source zone is thus comprised of the DNAPL, dissolved DNAPL constituents in the aqueous phase, vaporized DNAPL constituents in the gas phase, and DNAPL constituents sorbed to matrix solids (Cohen and Mercer, 1993).

During, or immediately after a release, DNAPL will be the largest component of contaminant mass in the source zone. With time, mass transfer to the aqueous, gas, and solid phases depletes the amount of DNAPL. As this occurs, the mass stored in the aqueous phase and sorbed to solids can become the dominant fraction of the source mass. This mass is subsequently referred to as Non-DNAPL Source Mass. This is a topic that has seen limited attention (Sudicky et al., 1985; Parker et al., 1993; Parker et al., 1997). Its introduction and study is one of the primary contributions of this report.

Figure 11 illustrates dissolved chemical concentrations about a set of DNAPL pools in a uniform porous media based on Sale and McWhorter (2001). Most of the mass transfer from the DNAPL occurs at the leading edge of the pools where the gradients in concentration (the driving force for dissolution) are the largest. Thus, most of the contaminant loading comes from the leading edges of the pools. An interesting consequence of this is that contaminant loading from the pool to groundwater water flowing past the pool is relatively insensitive to the pool length. Following Sale and McWhorter (2001), it can be argued that the narrow vertical DNAPL fingers identified in many DNAPL source zones will tend to be short lived, and horizontal DNAPL pools will last longer. With this, pools are envisioned as the primary DNAPL form associated older historical releases.
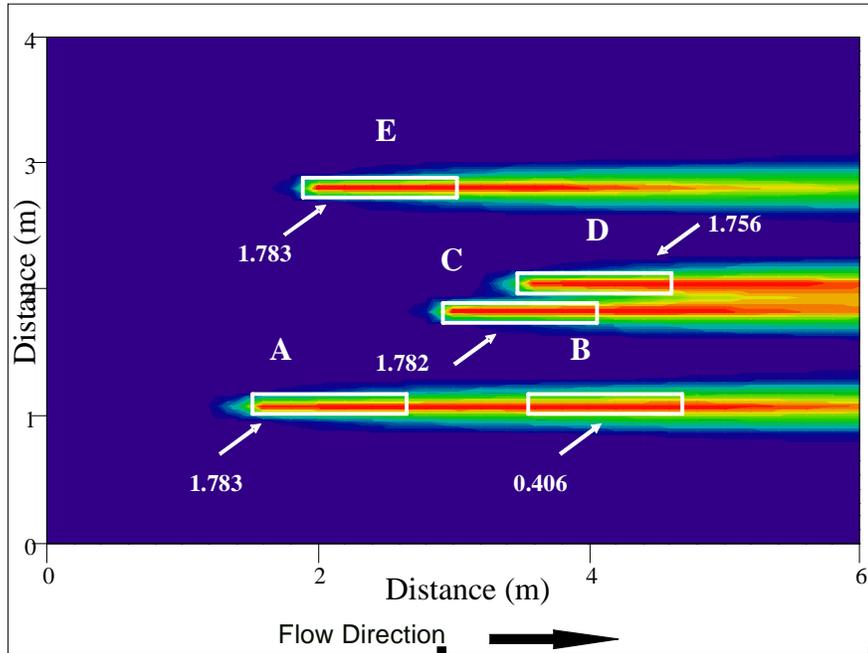
Figure 11 - DNAPL pools and associated aqueous phase plumes in uniform porous media. (Numerical values reflect mass transfer rates.  From Sale and McWhorter, 2001)

## 2.4    Significance of Heterogeneity

The conceptualization of mass transfer presented in Figure 11 is limited by the assumption of a uniform porous media.   In actuality, porous media, even materials that visually appear to be uniform, are typically very heterogeneous (e.g. Sudicky 1986).   Groundwater flow velocities can easily vary by orders of magnitude within different layers of natural sediments (e.g., sand and silt).   Also, the capacity of different sediments to store sorbed contaminant mass can vary by orders of magnitude.   All of this has great relevance to the mechanisms by which contaminants are stored and released from source zone to downgradient plumes.

In this study, our inspection of the significance of heterogeneity begins with a two-layer system referred to as "the simple case".  The value of the simple case

is that we can rigorously analyze governing processes via laboratory experiments and analytical models developed from first principles.  In subsequent phases of this project the simple case principles were extended to more complex settings using numerical models (e.g., multiple layer and nonuniform geometries) in an effort to understand field-scale processes.

Figure 12 introduces the "Simple Case."  A horizontal semi-infinite sand layer is conceptualized as overlying a semi-infinite silt layer.  The contrast in permeability between the two layers is large enough that the sand layer is viewed as hydraulically transmissive and the silt is viewed as hydraulically low permeability.  This presents an important conceptualization of porous media as being comprised of low permeability and high-permeability groundwater units.
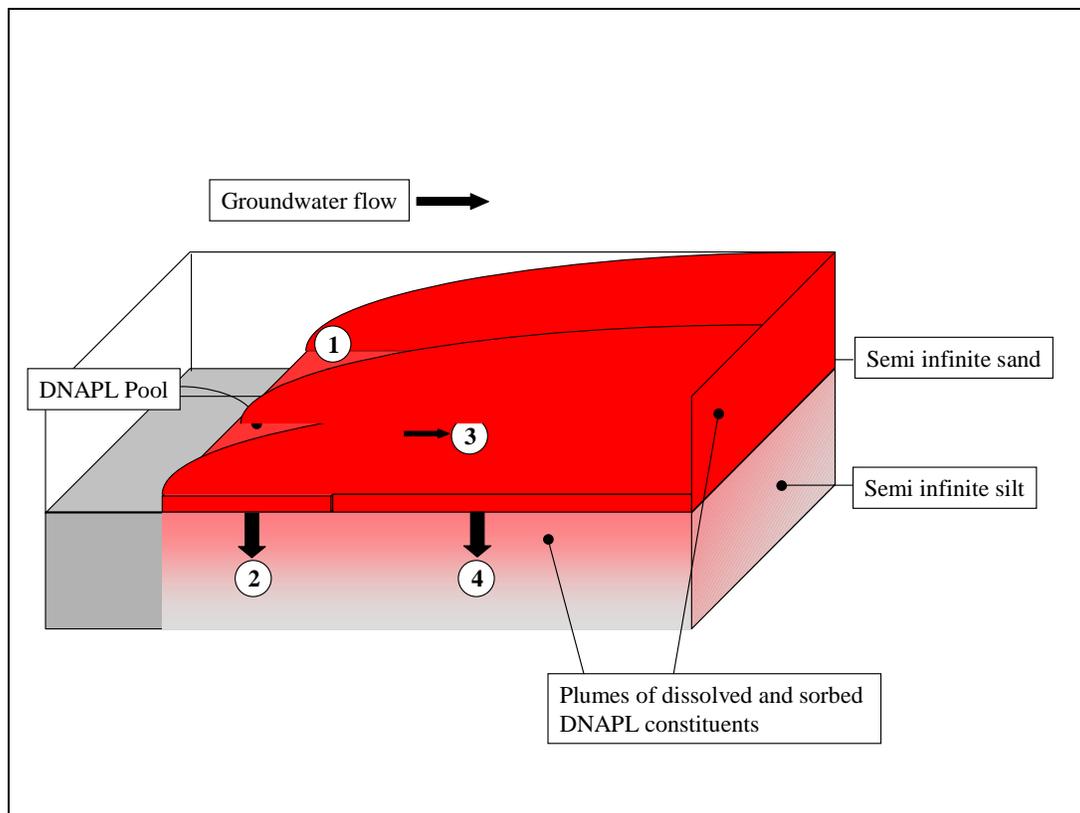
Figure 12  -The "Simple Case" (Numbers identify different flux mechanisms that transport dissolved chemicals away from the pool)

Continuing with Figure 12, a finite pool of DNAPL is present above the silt layer. The occurrence of the pool at the sand/silt contact reflects small pore sizes in the silt and correspondingly large displacement pressure that prevents DNAPL invasion into the silt (a capillary barrier). The chemical gradient near the DNAPL, that is, the gradient driving DNAPL dissolution, is sustained via transport of dissolved DNAPL constituents away from the DNAPL zone. This occurs through:

1) Transverse diffusion into the groundwater above the pool and subsequent horizontal advection along the top of the pool,
2) Diffusion into the silt below the pool, and
3) Advective transport through the pool.

These are identified as fluxes 1 through 3 in Figure 12. Given a pool with small height relative to its length, flux 3 will be a small component of the chemical transport compared to fluxes 1 and 2 (Sale and McWhorter, 2001). Flux three is also minimized by the presence of the DNAPL, which reduces the flow of water through the pore space.

An additional contaminant flux (4) is identified downgradient of the DNAPL. This reflects transport of dissolved aqueous phase constituents from the sand (active groundwater flow) into the silt (low groundwater flow). This is driven by depletion of aqueous phase constituents from the transmissive sand into the low permeability silt via transverse diffusion. An interesting aspect of flux 4 is its potential to operate over an area that is much large than the footprint of the DNAPL.

Note fluxes 1, 2, and 4 are all driven by transverse diffusion. This presents a challenge. The diffusion processes of concern occur over relatively small dimensions (e.g. centimeters). In this project our ultimate interests are at field-scale (e.g. tens to hundreds of meters). Needing to address a small-scale process, to resolve field-scale trends in water quality, is a major impediment to

developing practical modeling approaches for heterogeneous systems. This issue is addressed further in subsequent sections addressing modeling.

Given sufficient time, the DNAPL will be completely depleted as depicted in Figure 13. This reduces the contaminant concentration at the sand-silt boundary and drives reverse or "back" diffusion from the low permeability zone (silt) into the transmissive zone (sand). In Figure 13, fluxes 2 and 4 are primed to indicate back diffusion. The primary factors controlling mass stored in the silt are:

1) The duration of DNAPL presence at the sand-silt interface
2) The solubility of the DNAPL constituents
3) The amount of adsorption to solids
4) Rates of biotic or abiotic degradation of contaminants in the low permeability zones

For the simple case, the silt layer has two important effects:

1) Initially, it attenuates contaminants in the transmissive zone due to diffusion into the low permeability zone. This reduces contaminant concentration in the transmissive zones in the source while the DNAPL is present.
2) After the DNAPL is depleted, the silt layer acts as a "non-DNAPL source". Following Sudicky et al., 1985; Parker et al., 1993; Wilson 1997; Parker et al., 1997; and Liu and Ball 2002, back diffusion from the low permeability zones can sustain contaminant release from a source zone. In general, the older a release the more likely it is that back diffusion is driver for contaminant concentrations at the heads of persistent plumes.

A similar attenuation and release mechanism is conceptualized in a plume downstream of a source in Figure 14.
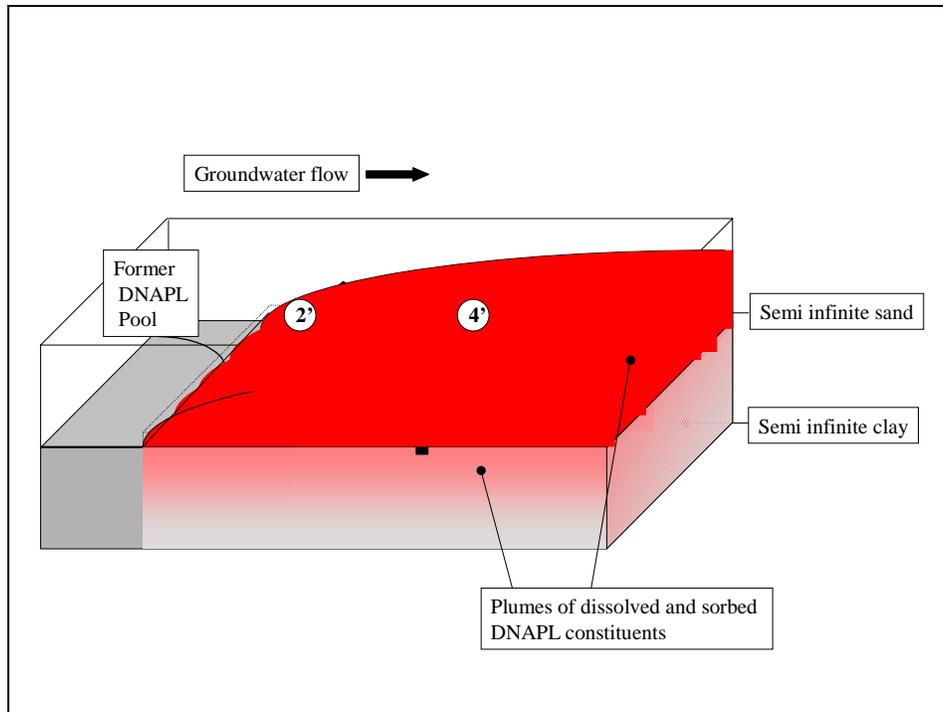
Figure 13 - Diffusion of contaminants out of low permeability zones after DNAPL depletion (building on Parker et al., 1997)
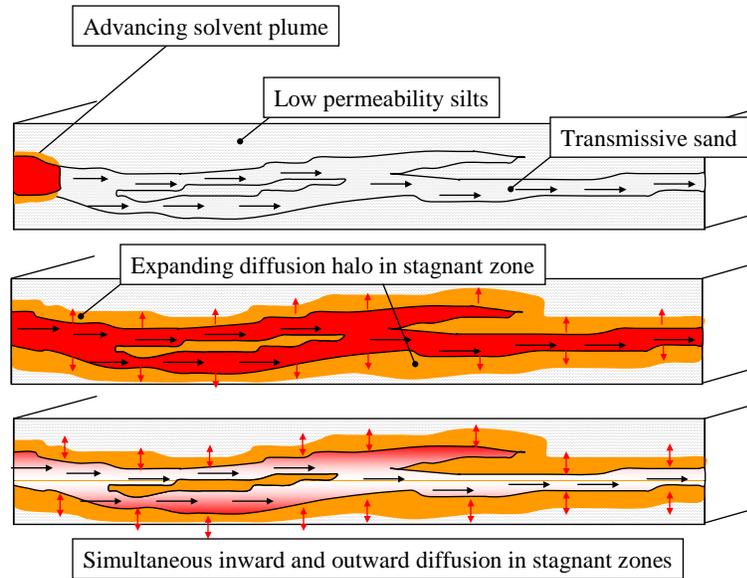
Figure 14 - Diffusive mechanism leading to plume attenuation and plume persistence

The implications of non-DNAPL source mass are potentially large. They include:

1) DNAPL may not be present at all plume heads that are sustaining dissolved chlorinated solvent plumes in groundwater. This explains why at many sites it is difficult to find DNAPL at the heads of persistent chlorinated solvent plumes. In this case, the DNAPL may be depleted and the plume is sustained by back diffusion.

2) Source treatment technologies that completely remove DNAPL (few if any) may have small effect on water quality if significant Non-DNAPL source mass is left in place within low permeability zones (Saenton et al, 2000). This supports the observation that, worldwide, USEPA MCLs have not been achieved in any significant DNAPL source zone after remediation.

3) Chronic low-level concentrations of chlorinated solvents produced by pump and treat systems may have more to do with the presence of widely dispersed non-DNAPL source mass than discrete DNAPL zones. In this

case, reverse diffusion provides a long-term source for low concentrations of aqueous phase DNAPL constituents.

Two other idealized systems considered in this report are parallel layers of transmissive and low permeability zones (uniform layers) and systems where the orientation of low permeability and transmissive layers hydraulically drive contaminants into low permeability zones (non-uniform layers).  These are conceptualized in Figure 15.  The uniform layered scenario is reviewed in detail in Sudicky et al., (1985).  It provides a plausible variant of the simple case that may be a more appropriate model for select settings.   Interestingly, it is directly analogous to a heat exchanger.

The non-uniform layer scenario is of interest in that it introduces the concept that aqueous-phase contaminants can be driven into and out of low permeability zones via advection.   Since aquifers are rarely composed of parallel beds, and/or gradients can be across bedding, advective storage and release of contaminants from low permeability zones is a potentially important process.

Uniform Layers



Non-uniform Layers
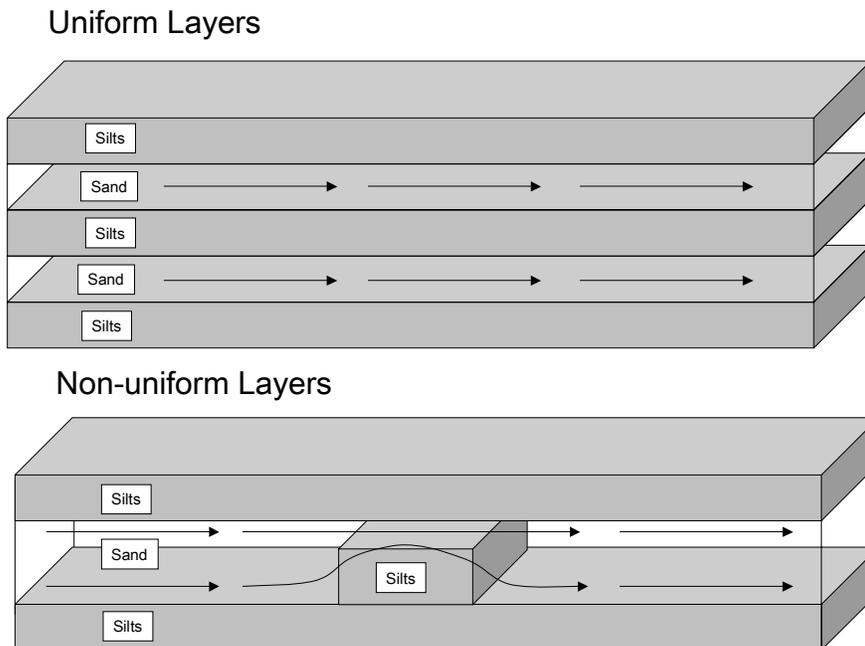


Figure 15– Other idealized architectures

38

## 2.5 Geo-Contaminant Type Settings

Given our emphasis on heterogeneity, it is important to reflect on the general types of heterogeneity that are commonly encountered. Figure 16 presents five general "Geology-Contaminant Type Settings". These setting were initially introduced in the Year One Progress Report for this project (Sale et al., 2003). Subsequently, the US Army funded National Research Council Committee studying source zone (Fountain et al., 2005) adopted and updated the described geologic type settings. The following builds on related developments in Fountain et al., (2005). Sections that are direct quotes are presented in italics.

In the interest of simplicity, we have used the fewest number of settings we feel can be developed. We recognize that real field setting can be much more complicated that those depicted in Figure 16. Relative to our interests, the distinguishing characteristic between each of the five type settings is how they store and release contaminants.
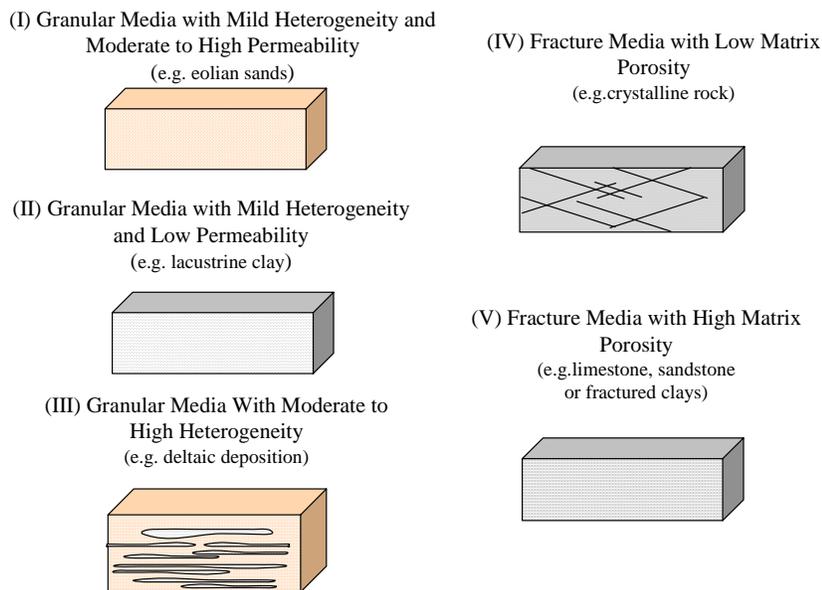


Figure 16– Geology -Contaminant Type Settings

## Type I – Granular Media with Mild Heterogeneity and Moderate to High Permeability

*Type I media include systems with porosities that are consistent with typical granular media (e.g., 5 percent to 40 percent), with permeabilities that are consistent with sand or gravel deposits ($>10^{-14}$ $m^2$ or hydraulic conductivity $>10^{-7}$ m/s), and mild heterogeneity (less than three orders of magnitude). As conceptualized here, this material is about as uniform as it can be in nature and thus is relatively uncommon. Deposits of this nature are encountered in association with windblown sands and beach deposits. Examples include beach sands at the Canadian Forces Base Borden, Canada, and dune deposits at Great Sand Dunes National Park, Colorado (Figure 17).*

Due to mild heterogeneity and moderate to high permeability, low permeability zones are not dominant in Type I settings. As such, there is little low permeability zone mass storage (sorbed or dissolved). The dominant storage/release mechanism will be associated with DNAPL dissolution and solid-phase sorption. In general, contaminated Type I settings are rare.



Figure 17 - Example of Type I media (Great Sand Dunes National Monument. SOURCE: http://www.nps.gov/grsa)

## Type II – Granular Media with Low Heterogeneity and Low Permeability

*Type II settings have porosities that are consistent with typical granular media (e.g., 5 percent to 40 percent), low spatial variation in permeability (less than three orders of magnitude), low permeability consistent with silt or clay deposits (k < $10^{-14}$ $m^2$), and low hydraulic conductivity (K < $10^{-7}$ m/s). An example is a clay deposit with no significant secondary permeability features (such as fractures, root holes, animal borrows, or slickensides). The loess deposit forming the deep road cut in Figure 18 is an example of Type II media. These systems are somewhat uncommon (especially in the near-surface environment where releases typically occur), although some examples include TCE-contaminated clays at the Department of Energy's Savannah River Site in South Carolina. More typically, low-permeability materials contain significant secondary permeability features and thus fit better into the Type V setting description (see below).*

Figure 18 - Example of Type II media (Brian Witzke photo).

In type (II) the entire zone is viewed as hydraulically stagnant. The primary contaminant transport process is diffusion. In general, settings of this nature are difficult to contaminate and are not a common concern.

**Type III – Granular Media with Moderate to High Heterogeneity**

*Type III encompasses systems with moderate to large variations in permeability (greater than three orders of magnitude) and porosities that are consistent with granular media (e.g., 5 percent to 40 percent). Given large spatial variations in permeability (at the scale of centimeters to meters), portions of the zone are comparatively transmissive while others contain mostly stagnant fluids. As an example, an interbedded sandstone and shale is shown in Figure 19. For the purpose of this report, the more transmissive zones in Type III media have a permeability greater than $10^{-14}$ $m^2$ ($K > 10^{-7}$ m/s). Near-surface deposits of this nature are common due to the abundance of alluvium with large spatial variations in permeability and are encountered in either rock or alluvium associated with deltaic, fluvial, alluvial fan, and glacial deposits. Examples include the Garber-Wellington Aquifer in central Oklahoma, the Chicot Aquifer in Texas and Louisiana, and varved sediments near Searchmont, Ontario (Figure 20).*

In Type (III) settings, heterogeneity introduces low permeability groundwater zones to the system. These zones initially attenuate DNAPL constituents that partition into groundwater. After the DNAPL is depleted, the low permeability zones can sustain dissolved phase concentrations in the active flow zones. The low permeability zone may contain fine-grained materials that can have large sorptive capacities. This enhances their ability to sustain dissolved chemical plumes long after the original chemical source (DNAPL) has been depleted.



Figure 19 - Interbedded sandstone and shale, shown as an example of Type III media. SOURCE: Reprinted, with permission, from http://geology.about.com. © 2004 About.com.

Figure 20 - Interbedded sand and silt layers associated with annual depositional cycles from the Varved Sediments, near Searchmont, Ontario, shown as an example of Type III media. SOURCE: Reprinted, with permission, from http://geology.lssu.edu/NS102/images/varves.html. ©2004 Department of Geology and Physics, Lake Superior State University

## Type IV - Fractured Media with Low Matrix Porosity

*Fractured media with low matrix porosity (e.g. Figure 21) are common in crystalline rock including granite, gneiss, and schist. Examples include bedrock in the Piedmont and Blue Ridge Mountain region of the southeastern United States and plutonic cores of mountain ranges in the western United States. The primary transmissive feature in Type IV settings is secondary permeability caused by fractures, because little to no void space exists in the unfractured matrix. The permeability of the unfractured matrix is considered to be less than $10^{-17}$ m$^2$ ($K < 10^{-10}$ m/s). However, the bulk permeability of the media is dependent on the frequency, aperture size, and degree of interconnection of the fractures, such that the anticipated range of bulk permeability values is $10^{-15}$–$10^{-11}$ m$^2$ ($K = 10^{-8}$–$10^{-4}$ m/s). The porosity of both the matrix and the fractures is typically small—less than 1 percent. However, in regions where crystalline rock*

*has been extensively weathered (e.g., at the top of bedrock), the bulk media can behave more like a porous medium than what would be expected from a fractured rock type setting.*

In Type (IV) settings, advection is limited to fractures and there is little mass storage in low permeability zones due to the low matrix porosity. The primary source is likely DNAPL. With time, DNAPL will be depleted from the more transmissive fractures and DNAPL in low flow areas (e.g. dead end fractures) will dominate. Due to the combined effect of low matrix attenuation and low fracture porosity, a common feature in this setting can be high contaminant migration velocity and, consequently, plumes with large dimensions (Sudicky et al., 1993; Parker et al., 1996). A primary challenge in this setting is the complexity of fractures. The fracture frequencies and capacity to transmit fluid can be highly variable. Furthermore, the degree to which sets of fractures are interconnected can be highly variable.
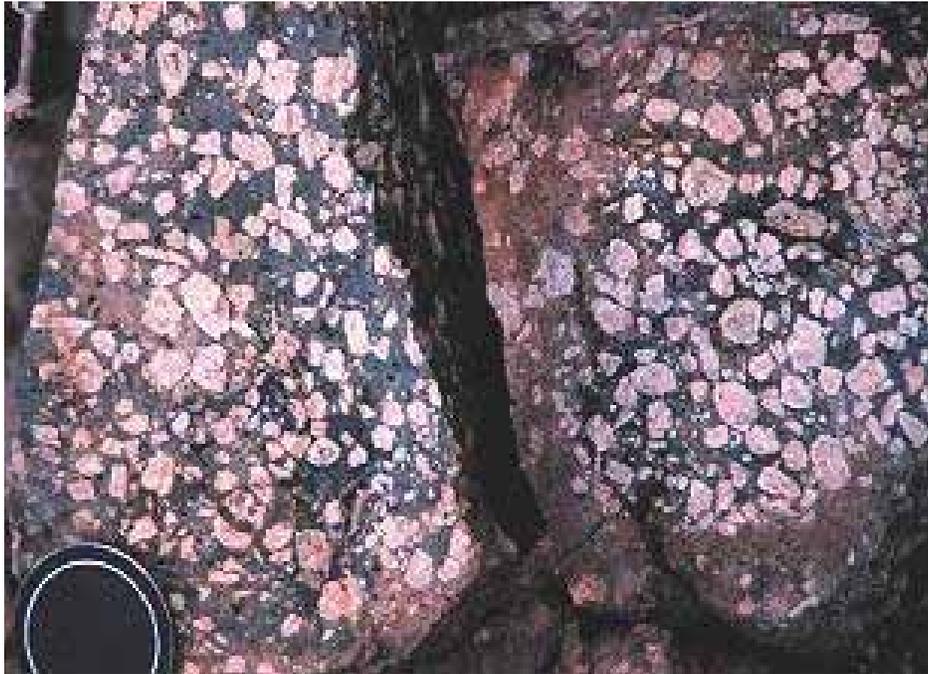
Figure 21 - Fractured crystalline rock shown as an example of Type IV media. Photo taken near Kitt Peak Observatory, Arizona.  SOURCE: Reprinted, with permission, from http://geology.asu.edu/~reynolds/glg103/rock_textures_crystalline.htm. © 2004 Department of Geological Sciences, Arizona State University

### Type V – Fractured Media with High Matrix Porosity

*This setting includes systems where fractures (secondary permeability) are the primary transmissive feature and there is large void space in the matrix. The permeability of the unfractured matrix is considered to be less than $10^{-17}$ $m^2$ (K < $10^{-10}$ m/s). The anticipated range of bulk permeability values is $10^{-16}$–$10^{-13}$ $m^2$ (K = $10^{-9}$–$10^{-6}$ m/s). The porosity of the fractures relative to the total unit volume is small (e.g., <1 percent). However, unlike Type IV, in Type V hydrogeologic settings the porosity of the unfractured matrix is anticipated to fall in the range of 1 percent to 40 percent. Fractured media with high matrix porosity are commonly encountered in sedimentary rock (e.g., limestone, dolomite, shale, and sandstone) and fractured clays. Examples include the Niagara Escarpment in*

46

*the vicinity of the Great Lakes (see Figure 22) and fractured lake-deposited clay in Sarnia, Ontario, Canada.*



Figure 22  - Fractured limestone, Door County, Wisconsin, shown as an example of Type V media.  SOURCE: Reprinted, with permission, from http://www.uwgb.edu/dutchs/GeoPhotoWis/WI-PZ-NE/BayshorePark/bayshcp3.jpg. © 2004 Natural and Applied Sciences, University of Wisconsin-Green Bay.

Setting (V) again introduces low permeability zones to the system.  These zones initially attenuate DNAPL constituents that partition into groundwater by diffusion from the fracture zones into the rock matrix.  After the DNAPL is depleted, reverse diffusion sustains dissolved phase concentrations in groundwater flowing in the fractures.  For systems where the matrix material has large sorptive capacities, the low permeability zones will act as a contaminant sink and accelerate rates of natural DNAPL depletion.  Due to limited mass storage in fractures, rapid depletion of DNAPL may occur via natural processes (e.g. Parker et al., 1997).

An important variant of the Type V setting is karst, which is common in carbonates (e.g., limestone or dolomite).  In this scenario, transmissive zones include sinkholes, caves, and other solution openings that vary widely in aperture and have the potential to store and transport significant contaminant mass (see

Figure 23).  Permeability in karst terrains varies over tens of orders of magnitude from low permeabilities between fractures to open channel flow in channels and caves (Teutsch and Sauter, 1991; White, 1998, 2002).  Karst is characterized by both rapid transport along sparse dissolution features and a high ratio of low permeability to transmissive zones.  As such, it is one of the most challenging hydrogeologic settings to characterize and manage.
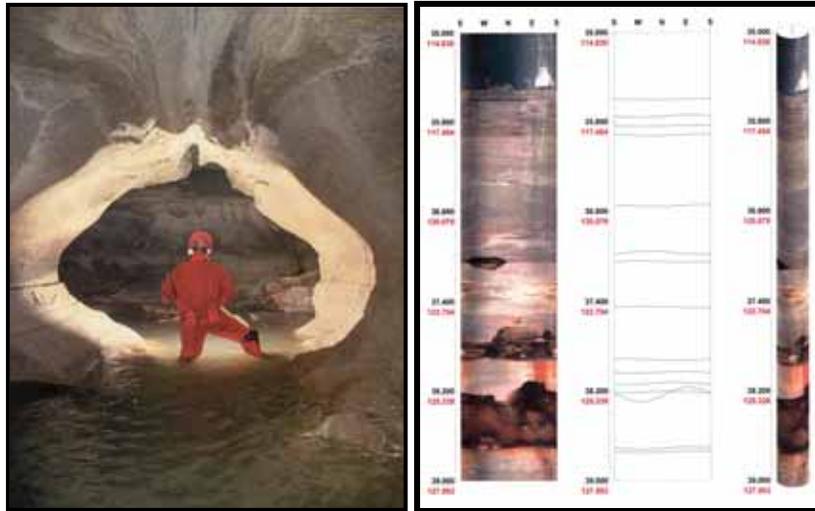


Figure 23 - Large- and small-scale solution features in karst limestone, Redstone Arsenal.  SOURCE: Courtesy of De la Paz and Zondlo, Shaw E&I (2003).

***Source Zones Containing Multiple Type Settings***

*Source zones, especially those above a certain size, may encompass more than one hydrogeologic setting.  This commonly occurs in the instance of shallow alluvium over bedrock.  For example, in the Piedmont of the southeastern United States, one can find fluvial deposits (Type III) and saprolite (Type V) overlying fractured crystalline rock (Type IV) (Figure 24).  Selecting characterization tools and source management technologies is challenging under these conditions, because although contamination may exist throughout, the appropriate tools for one hydrogeologic setting may not work in the adjacent hydrogeologic setting.*
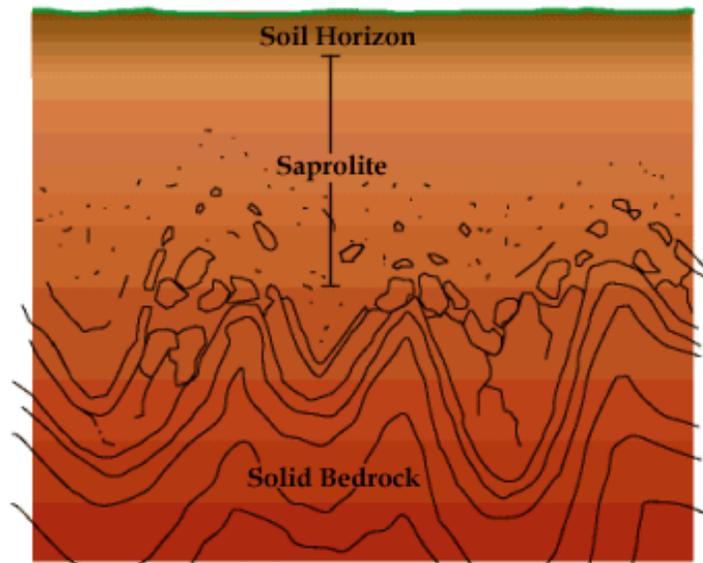
Figure 24- Mixed hydrologic settings of highly weathered saprolite overlying crystalline bedrock. SOURCE: Reprinted, with permission, from http://web.wm.edu/geology/virginia. ©2004 The Geology of Virginia, Department of Geology, College of William and Mary.

## *2.6 Application of Type Setting to Three DoD Field Sites*

F.E. Warren Air Force Base (FEW) is located immediately west of Cheyenne, Wyoming. FEW is underlain by eolian sands, eolian loess (silt), fluvial deposits, and a clayey portion of the Ogallala Formation. These sediments exhibit a large degree of heterogeneity and conform most closely with the Type (II) Setting, that is, Granular Media with Moderate to High Heterogeneity

Interesting aspects of FEW include:

- Relatively small releases of TCE have led to chronic low concentration plumes that have persisted for decades.

- Despite rigorous investigations, no DNAPL has been identified at the plume heads.

- The highest concentrations of TCE in soil and ground water are often encountered in the finer grained (lower permeability sediments).

- Remedies implemented at the site to dates include

  - ➢ Iron permeable reactive barrier

  - ➢ Pump and treat

  - ➢ Soil vapor extraction

  - ➢ Excavation

Further details regard FEW are developed in the Appendix H.

Naval Air Station (NASFtW) Fort Worth and Air Force Plant 4 (AFP4) are adjacent facilities located on the west side of Fort Worth Texas. Alluvium overlies calcareous bedrock. The alluvium is a Type II setting consisting of weathered bedrock commingled with fluvial deposits. The bedrock limestone is a Type IV setting consisting of interbeds of fractured limestone and dolomite. The greatest degree of fracturing is anticipated at the weathered interface between the alluvium and bedrock.

Important aspects of NASFtW/AFP4 include:

- Both small and large releases of TCE and other chlorinated solvents have occurred.
- Plumes have persisted for long periods of time.
- Despite rigorous investigation, including coring and Partitioning Interwell Tracer Test (PITTs), no DNAPL has been found in most of the release areas.
- In one area, DNAPL occurs in wells completed in the fractured bedrock.

- Remedies implemented at NASFtW/AFP4 to date include:

    - Iron permeable reactive barrier
    - Pump and treat
    - Electrical Resistance Heating
    - DNAPL recovery (direct pumping of DNAPL from wells)

Further details regarding NASFtW and AFP4 are presented in Appendix H.


## 2.7  Summary

This section presents a qualitative argument that the source of a chlorinated solvent plume can be sustained by direct dissolution of DNAPL (if any) and/or by reverse diffusion/desorption of dissolved DNAPL constituents from low-permeability zones.  The degree to which either mechanism is the dominant driver depends on numerous factors including the size of the release, the age of the release, and the geologic architecture.  The relevance of recognizing the existence of non-DNAPL source mass is that it can play a major role in the efficacy of source depletion measures.   The following sections quantify processes associated with non-DNAPL sources through laboratory studies and models.


## 2.8  References

Cohen, R. M. and J. W. Mercer (1993). "DNAPL Site Evaluation", C.K. Smokley, CRC Press.

Fountain, J.C, L. Abriola, L. Alvarez-Cohen, M. Baedecker, D. Ellis, T. Harmon, N. Hyaden, P. Kitanidis, J. Mintz, J. Phalean, G. Pope, D. Sabatini, T. Sale, B. Sleep, J. Wilson, J. Young, K. Yuracko (2004), Contaminants in the Subsurface: Source Zone Assessment and Remediation, National Academy Press, Washington, D.C.

Illangasekare, T.H**.**, J. L. Ramsey, K.H. Jensen and M. Butts, (1995). Experimental study of movement and distribution of dense organic contaminants in heterogeneous aquifers, *J. of Contaminant Hydrology*, 20, 1-25.

Kueper, B.H., W. Abbot, and G. Farguhar, (1989). "Experimental Observations of Multiphase Flow in Heterogeneous Porous Media", Journal of Contaminant Hydrology, Vol. 5, pp. 83-95.

Kueper, B.H. and D.B. McWhorter, (1991). " The Behavior of Dense Nonaqueous Phase Liquids in Fractured Clay and Rock. Journal of Ground Water, September-October, Vol. 29, No. 5, pp. 716-728.

Kueper, B.H., D. Redman, R.C. Starr, S. Reistma, and M.Mah (1993). " A field experiment to study the behavior of tetrachloroethylene below the watertable: Spatial distribution of residual and pooled DNAPL" Journal of Ground Water, No. 31, pp. 756-766.

Liu, C. and W.P. Ball (2002), Back Diffusion of Chlorinated Solvent Contamination from a Natural Aquitard to a Remediated Aquifer Under Well-Controlled Field Conditions: Predictions and Measurements, Journal of Groundwater, Vol. 40, No. 2, pp. 175-184.

Parker, B.L., R.W. Gillham, and J. A. Cherry, (1994), Diffusive Disappearance of Immiscible –Phase Organic Liquids in Fractured Geologic Media, Journal of Groundwater, Vol. 32, No.5.

Parker, B.L., J.A. Cherry, and R.W. Gillham (1996) "The effect of Molecular Diffusion on DNAPL Behavior in Fractured Porous Media", Chapter 12 in Dense Chlorinated Solvents and Other DNAPLs in Groundwater, J.F Pankow and J.A. Cherry, Editors. Waterloo Press, pp. 355-393.

Parker, B.L., D.B, McWhorter, and J.A. Cherry (1997) Diffusive Loss of Non-Aqueous Phase Organic Solvents from Idealized Fracture Networks in Geologic Media, Ground Water, Vol. 35, No 6. Pp. 1077-1088

Poulson, Mette, M. and Kueper, Bernard, H. (1992). "A Field Experiment to Study the Behavior of Tetrachloroethylene in Unsaturated Porous Media". Environmental Science and Technology, Volume 26, No. 5, pp. 889-895.

Saenton, S., T.H. Illangasekare, K. Soga and T.A. Saba. 2001. Effects of source zone heterogeneity on surfactant enhanced NAPL dissolution and resulting remediation end-points, *J. of Contaminant Hydrology, 59, 27-44.*

Sale, T and D.B. McWhorter, (2001), Steady-State Mass Transfer from Single Component DNAPLs in Uniform Flow Fields, Water Resources Research, Vol. 37, No. 2, Pp. 393-404.

Sale, T., T. Illangasekare, F. Marinelli, B. Wilking, D. Rodriguez and B. Twitchell. (2004), AFCEE Source Zone Initiative—Year One Progress Report. Colorado State University and Colorado School of Mines, Prepared for the Air Force Center for Environmental Excellence.

Schwarzenbach, Rene, P.M. Gschwend, and Dieter M. Imboden (1993). Environmental Organic Chemistry, John Wiley and Sons, Inc.

Sudicky, E.A., R.W. Gillham, and E.O. Frind (1985), Experimental Investigations of Solute Transport in Stratified Porous Media 1) The Non Reactive Case, Water Resource Research Vol 21, No. 7, pp. 1035-1041.

Sudicky, E.A. (1986), A natural gradient experiment on solute transport in a sand aquifer; Spatial variability of hydraulic conductivity and its role in the dispersion process, Water Resource Research, Vol. 22, No. 13, pp. 2069-2082.

Sudicky, E.A., R.G. McLaren, and J. VanderKwaak (1993) Characterization of contaminant migration processes in fractured geologic media and numerical simulation of pump and treat remediation. Progress Report on Project No. 596G, Ontario Ministry of the Environment, March 8.

Wilson, J.L., S. H. Conrad, W.R. Mason, W. Peplinski, and E. Hafgan, (1990), Laboratory Investigations of Residual Liquid Organics from Spills, Leaks, and the Disposal of Hazardous Wastes in Groundwater. EPA/600/6-90/004. April.

Wilson, J.L., (1997), Removal of aqueous phase dissolved contamination: Non-chemically enhanced pump and treat, Subsurface Remediation Handbook, C.H. Ward, J. Cherry, and M. Scalf (Eds), An Arbor Press, Chelsea, MI, 271-285.

Wilson, J.L., Dueling time constants: Competing processes in aquifer contamination and remediation, Proceedings of 1997 International Conference on Groundwater-Quality Protection: Remedial Technology and Management of NAPL Problems, Taipei, Taiwan, 1997.

# 3.0   Laboratory Studies

In this section, the challenges of complex processes and settings are met by conducting experiments in small, intermediate, and large scale two-dimensional laboratory sand tanks.   Conditions considered including sediment architecture, contaminant sources, and hydraulics are highly idealized.  This provides a basis for quantitative demonstration of the effects of source depletion and/or removal on water quality downgradient of sources.  Through this, the importance of the processes introduced in Section 2 are validated.   Furthermore, experimental results provide an important basis for testing models introduced in Section 6. Studies presented in this section include:


1)  Small-Scale Two Layer Tanks Experiments with Aqueous Point Source
2)  Small-Scale Multiple Layer Tanks Experiments with Uniform Aqueous Sources
3)  Small-Scale Two Layer Tanks Experiments with DNAPL Sources
4)   Intermediate Two Layer Tanks Experiments with DNAPL Sources
5)  Large-Scale Two Layer Tanks Experiments with DNAPL Sources


## 3.1 *Small-Scale Two Layer Tank Experiments with Aqueous Point Source*

The following introduces a set of two layer small-scale tank experiments conducted at Colorado State University using the tanks shown in Figure 25.  The focus is the diffusion process 4 identified in the simplified conceptual model presented in Section 2.  Three of the tanks contained uniform medium sand only. A matching set of three tanks contained the same sand and a layer of uniform well-sorted silt.   Both sediments were acquired from FEW (See Appendix E). Similar point sources of PCE, TCE, MTBE and bromide are imposed on matched pairs of sand only and sand-silt tanks.  Contaminant sources applied as a solute to mimic mass flux from a DNAPL source are active for a period of 25 days.

55

Subsequently, the sources are shut off and water only is flushed through the tanks for an additional 58 days. Through the duration of the experiments contaminant discharge is resolved as a function of time.
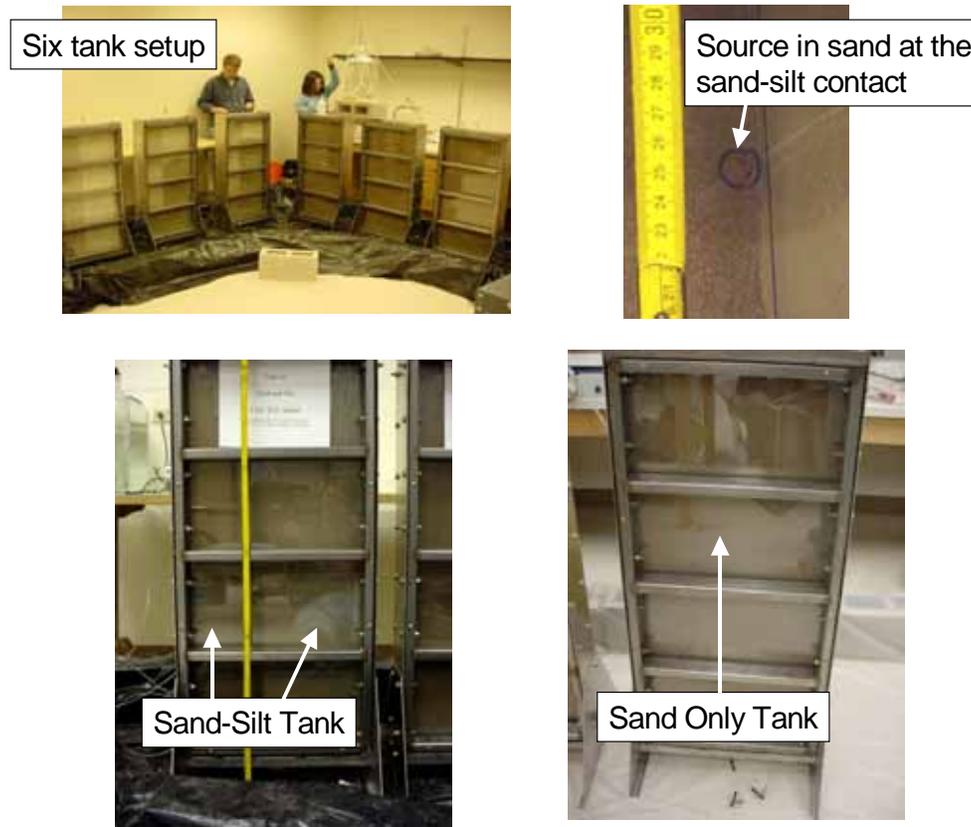


Figure 25 – Two layer small tank experiments (note tanks are run vertically to limit settlement transverse to flow)

Results indicate that even for this short length, the silt layers retain between 15 to 44 percent of the introduced contaminants at the end of the experiment. Upon removal of the contaminant sources, back diffusion sustains contaminant concentrations in the tank effluent at levels two to four orders of magnitude above typical USEPA Maximum Contaminant Levels (MCLs). Considering the mass retained in the silt layers, it appears that extremely long period of time would be required to flush sufficient water through the tank to achieve USEPA MCLs.

Content of this section includes an overview of objectives, methods, and results. Comprehensive documentation of the experiments is provided in Appendix A.

### 3.1.1 Objectives

Primary objectives for this work include:

1) Developing simple experimental illustrations of the significance of contaminant storage and release from hydraulically stagnant zones.

2) Characterizing the role of contaminant concentration and sorption in governing total mass storage in hydraulically stagnant zones.

3) Developing data for testing analytical and numerical models that describe the processes introduced in Section 3.

### 3.1.2 Methods

As noted above, this experiment involves matching sets of sand only and sand-silt tanks with similar point sources of PCE, TCE, MTBE, and bromide. The experimental design and tank dimensions are illustrated in Figure 26. Characteristic of the porous media are presented in Table 1.
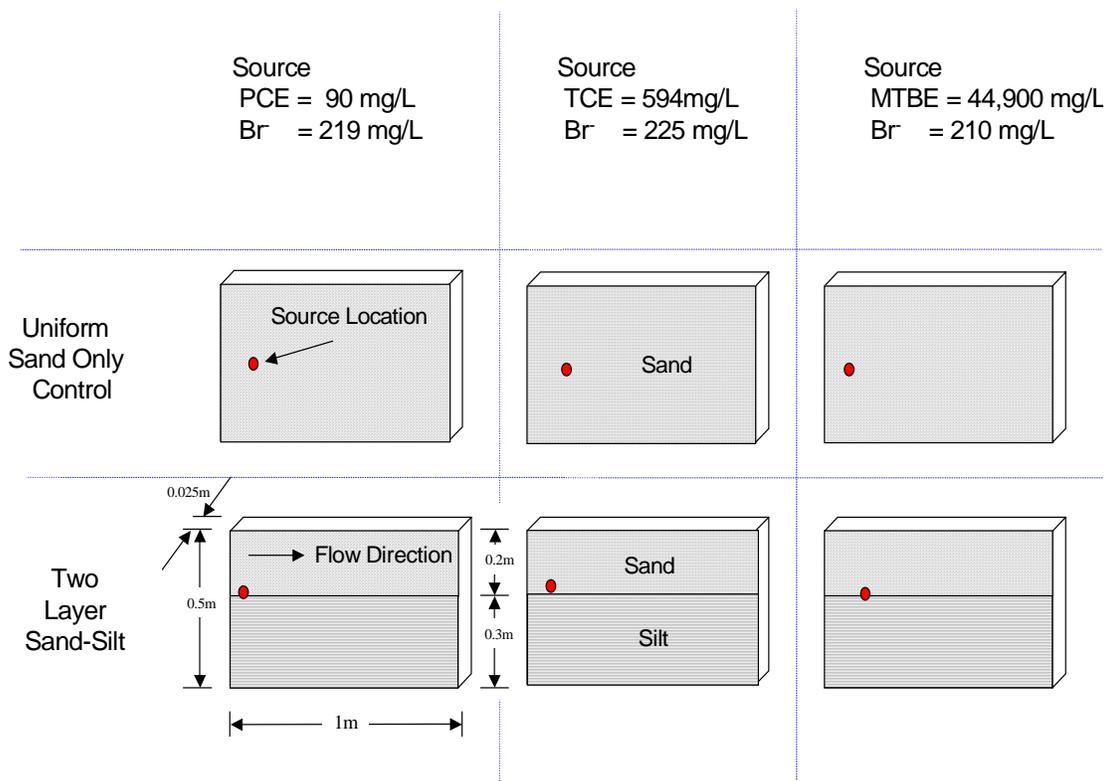
Figure 26 – Experimental design for the two layer small tank experiments

Table 1.  Physical properties of the porous media.

|  | FEW Sand | FEW Silt |
|---|---|---|
| Hydraulic Conductivity | $1.4 \times 10^{-2}$ cm/sec | $1.7 \times 10^{-4}$ cm/sec |
| Porosity | 0.36 | 0.55* |
| Bulk Density | 1.7 gm/cm$^3$ | 1.2 gm/cm$^3$ |
| PCE $K_d$ | 0.2820 (mL/g) | 0.8722 (mL/g) |
| TCE $K_d$ | 0.1673 (mL/g) | 0.5092 (mL/g) |
| MTBE $K_d$ | 0.2150 (mL/g) | 0.4629 (mL/g) |
| Bromide $K_d$ | .0.3650 (mL/g) | 0.1060 (mL/g) |

*Note:  Outside range given by Freeze and Cherry (1979).

Water is delivered to the tanks at two locations.  The primary flow is de-aired City of Fort Collins Colorado tap water.  This is introduced via a head tank on the

upstream side of the tank.  Both the influent, and the identical effluent head tanks, are hydraulically connected with the sand and silt layers.  Thus, no vertical gradients are imposed across the layers.  Flow rates to the tanks result in an average sand seepage velocity of 0.27 m/day.  Based on the hydraulic conductivity values, the average seepage velocity in the silt is estimated at 0.0032 m/day.

Contaminants are introduced to the tanks via ~ 1 cm fritted glass tubes inserted through a stainless steel Swedge Loc$^{TM}$ fitting in the sidewalls of the tank.  The fritted glass pipe fully penetrated the 2.5 cm thickness of the tanks.  In the sand-silt tanks the source is located in the sand immediately adjacent to the sand-silt contact at a distance 13 cm downstream of the influent head tank.  In the sand only tanks, the source is in the same physical position.   Contaminants are introduced at the source points at the concentrations noted in Table 2 at a flow rate of ~5% of the head tank flow.

Table 2 – Two layer experiment source strengths.

| Contaminant | Source Concentration |
|---|---|
| PCE | 90 mg/L |
| TCE | 594 mg/L |
| MTBE | 45,000 mg/L |
| Bromide | 220 mg/L |

The intention of the source configuration is to approximate the concentration profile that would be encountered immediately downgradient of a DNAPL pool perched in the sand above the silt (capillary barrier).  In two prior sets of experiments, an actual NAPL was introduced at the source position.  These experiments failed to meet the experimental objectives.  Problems included:

1) It was difficult to produce identical NAPL sources in the matched sand only and sands-silt tanks.

2) It was difficult to resolve when the NAPL was gone.  This precluded clear resolution of when the back diffusion was driving effluent concentrations.

3) The NAPL source strength was variable with time.  This limited our ability to test the analytical solutions using the laboratory data.

3.1.3 Results

The influent and effluent concentrations and flow rates were measured from each of the six tanks through time during the experiment (see Appendix A).  Based on this data, cumulative contaminant introduced and discharged with the effluent was determined.   The total contaminant mass retained in the tanks was determined as the difference between mass inflow and mass discharge.

Figure 27 presents mass balance results for PCE, TCE, MTBE, and bromide for all of the tanks. This data showed that at the conclusion of the experiment (83 days), only a small percentage of the introduced contaminants were retained in the tanks with sand only.  In dramatic contrast, large fractions of the introduced contaminants (see asterisk data) were retained in the tanks with sand and silt. Since the primary difference is the result of the presence of silt, and there is no transverse advection, enhanced contaminant retention in the sand-silt tanks can only be attributed to transverse diffusion of contaminants at the sand-silt contact. This provided important validation of the significance of transverse diffusion downgradient of the source (Flux 4 introduced in Section 3).
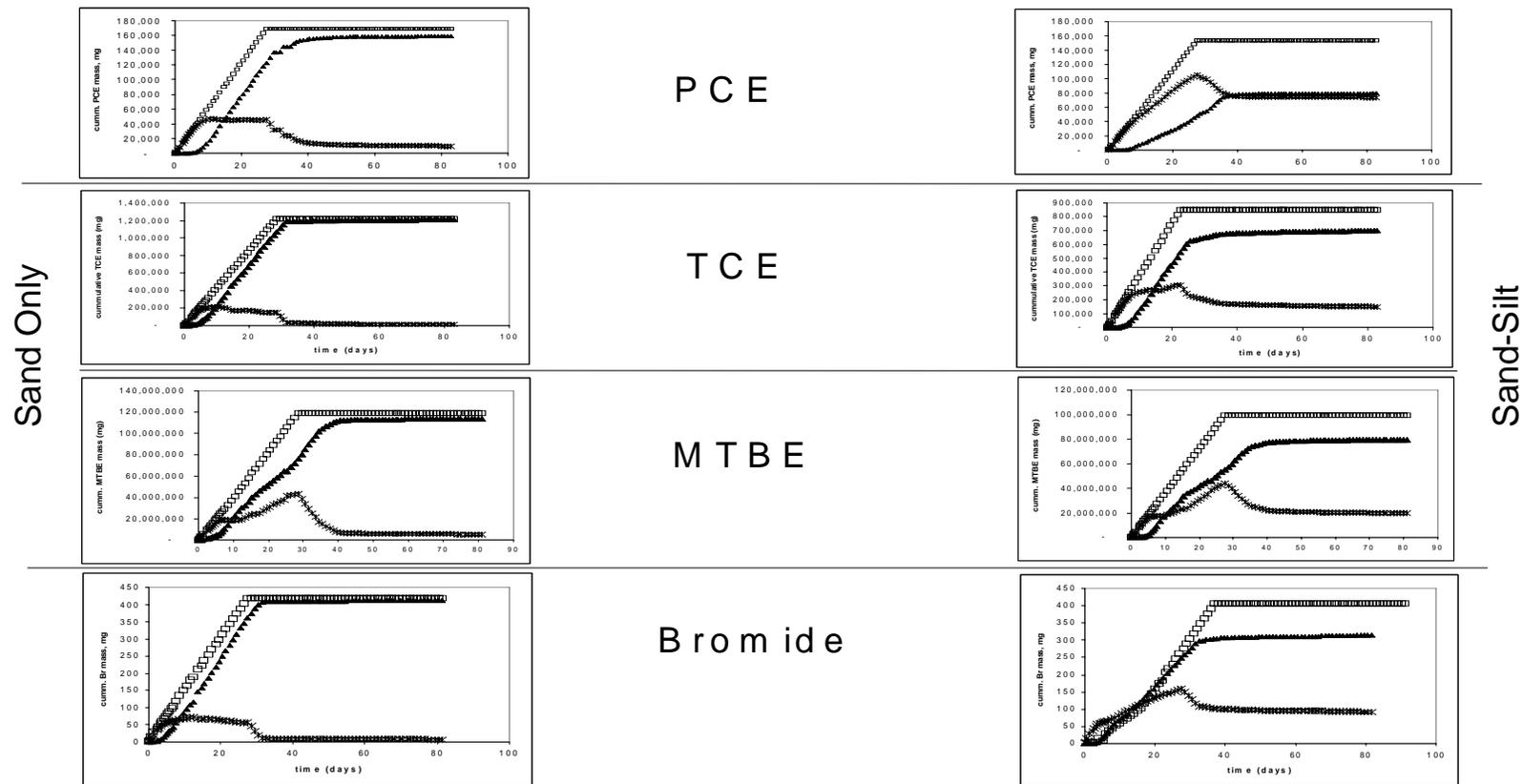
Figure 27 – Mass retained in the tanks based on cumulative influent-effluent mass balances. Mass-in shown as open squares, mass-out as black triangles, and the accumulation within the tank (the difference between mass-in and mass-out) shown as asterisks

More directly, Figure 27 plots contaminant retention in sand tanks, mass retention in sand-silt tanks, and difference in mass retention between tanks using the 83-day data. The difference in mass retention between tanks provides a basis for estimating low-permeability zone mass storage after 83 days. Based on this, mass storage attributable to storage in the silt is between 15 and 44 percent of the introduced contaminant mass depending on the contaminant. The preferential retention of PCE versus other contaminants is attributable to a higher degree of PCE sorption in the silt layer per the $K_d$ values presented in Table 1.

The total amount of contaminant mass storage in the low-permeability zones is also important. Figure 28 presents mass retained on a log scale as a function of the contaminant and tank configuration. The data reveals that sources with larger aqueous concentration result in larger contaminant mass low-permeability zones, given equivalent contact times.
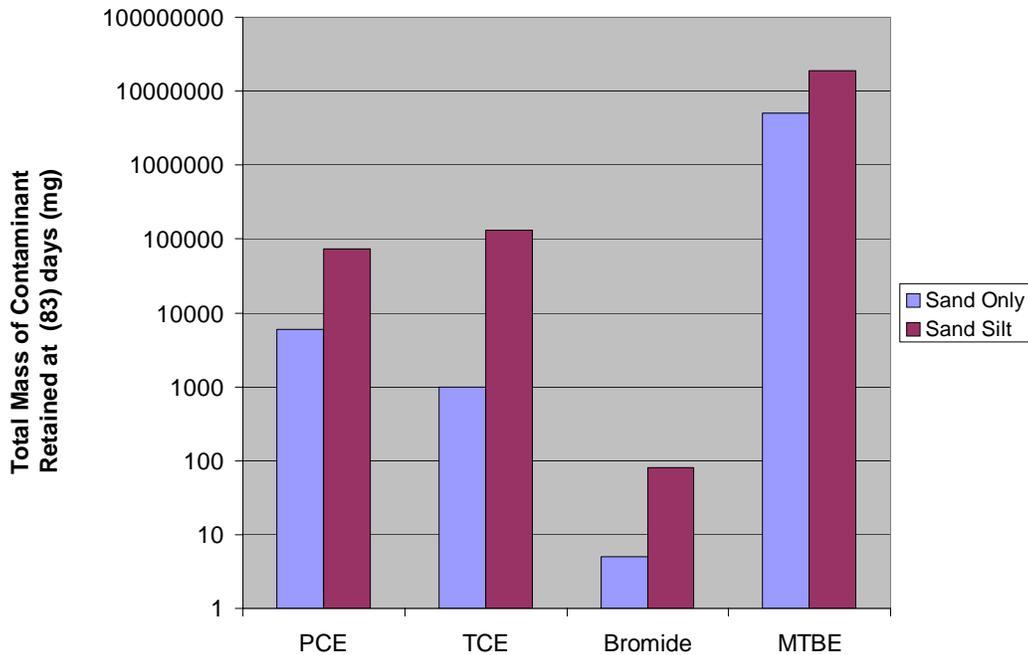


Figure 28 – Total mass of contaminant retained by contaminant

Lastly, consideration is given aqueous concentrations. Figure plots the bulk influent concentration based on tank loading, effluent concentration after the source has been on for 25 days, and the effluent concentrations at 83 days. At 25 days effluent concentrations are lower than loading concentrations due attenuation by the silt layer. Reflecting termination of the source, effluent concentrations at 83 days are approximately 2 orders of magnitude lower than concentration observed with the source on after 25 days. Unfortunately, even with the source off for 53 days, concentrations are still two to four orders of magnitude above typical USEPA MCLs for each of the compounds. Considering the total mass retained in the silt layers, it is likely that these concentrations would be sustained for longer periods of time.
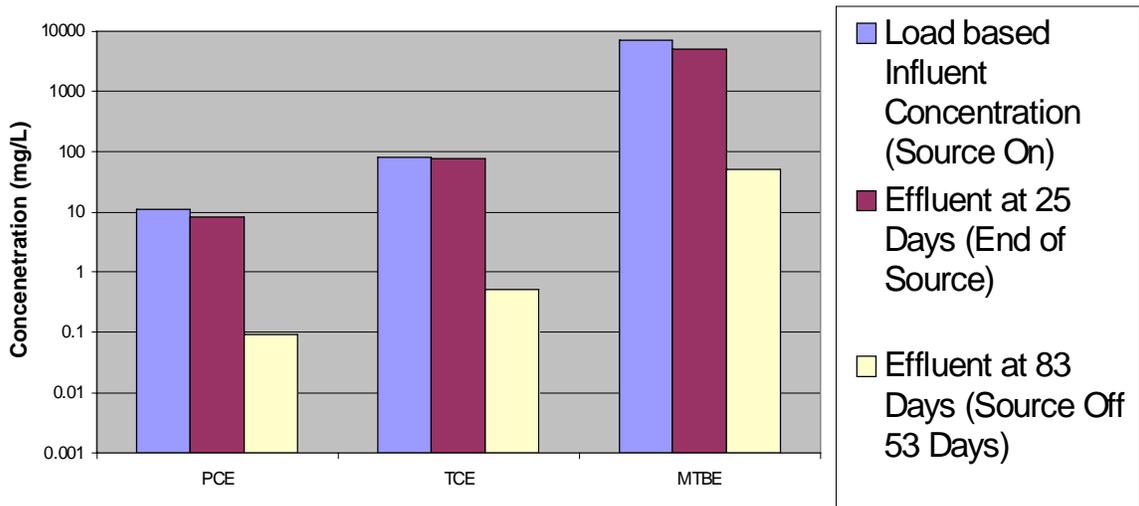


Figure 29 – Concentrations by contaminant based on mass loading of the tanks, observed concentrations at 25 days (end of source on), and 83 day (58 days after source off).

## 3.2 Small-Scale Multiple Layer Tank Experiments with Uniform Aqueous Sources

This section describes a set of small-scale multiple layer tanks experiments conducted at Colorado State University. The experimental setup is illustrated in Figure 30. Six identical tanks containing multiple sand and silt layers were employed. Silt layers in matched pairs of tanks are 1) amended with activated carbon (AC), 2) amended with zero-valent iron (ZVI), and 3) not amended (controls). PCE and TCE amended water (with bromide) were driven through the tanks via an influent head tanks for 28 days. Subsequently, contaminants were removed from influent feed and steady flow is maintained in all of the tanks for an additional 55 days. Influent and effluent contaminant concentrations and flow rates were measured as a function of time. The study demonstrated the effects of adsorption-desorption and degradation of contaminants in low-permeability zones.
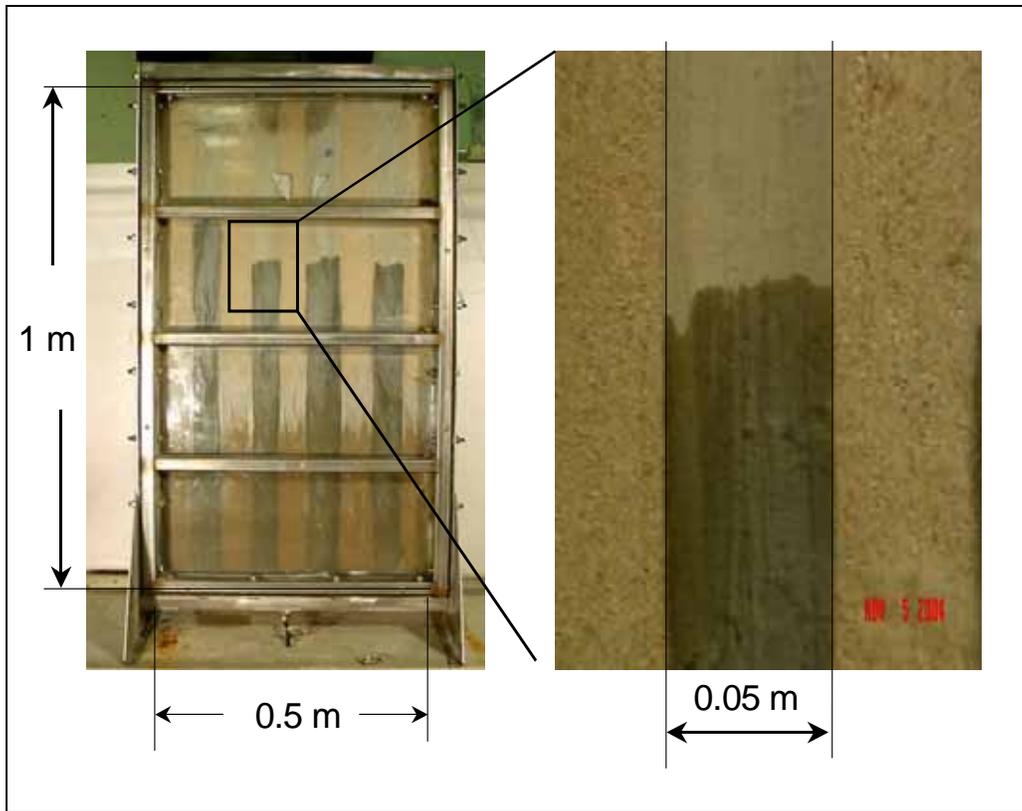
Figure 30 – Multiple layer small tank experiments (Tanks are run vertically to limit settlement transverse to flow, as shown tanks are filling)

Results indicate that 1% activated carbon in the silt layer doubles transverse diffusion and contaminant storage in silt layers for both PCE and TCE. The effects of greater adsorption in low-permeability zones include 1) enhanced plume attenuation while the source is active and 2) sustained back diffusion after the source is off. Furthermore, results indicate that 1% ZVI in the silt layers increases diffusion of PCE and TCE into silt layers by factors of 1.2 and 1.5, respectively. As with activated carbon, ZVI enhances plume attenuation while the source is active. In contrast to activated carbon, ZVI lessened the back diffusion after the source is off. This reflects reactive losses of PCE and TCE in the silt due to the presence of ZVI.

Content of this section includes an overview of objectives, methods, and results. Comprehensive documentation of the study is provided in Appendix A.

3.2.1 Objectives

Primary objectives for this set of experiments included:

1) Developing simple experimental demonstrations of the effects of adsorption-desorption and reactions on contaminant storage in, and release from, hydraulically low permeability zones.

2) Quantitative characterization of the role of adsorption-desorption and reactions on contaminant storage-release from hydraulically stagnant zones.

3) Developing data for testing analytical and numerical models presented in Section 6.

3.2.2 Methods

Each the six tanks contained five 5-cm layers of sand bounded by silt layers. The internal silt layers were 5-cm in thickness. Additional silt layers at the tank margins were 2.5 cm thick. This configuration maintains a diffusion distance from the sand to a no flux boundary in the silt of 2.5 cm. Silt layers in matched sets of tanks were amended with 1% powdered activated carbon and 1% powdered ZVI. In addition, silt layers in two tanks had no amendments. Tanks with no silt amendments provided controls that assisted with decoupling the effects of transverse diffusion, adsorption-desorption, and reactions. The sand and silt were acquired from FEW. Physical properties of the porous media are presented in Table 3. Comprehensive information regarding the sand and silt is presented in Appendix E.

Table 3 - Physical properties of the porous media.

| | FEW Sand | FEW Silt |
|---|---|---|
| Hydraulic Conductivity | $1.4 \times 10^{-2}$ cm/sec | $1.7 \times 10^{-4}$ cm/sec |
| Porosity | 0.36 | 0.46 |
| Bulk Density | 1.4 (gm/cm$^3$) | 1.7 (gm/cm$^3$) |
| PCE $K_d$ | 0.28 (mL/g) | 0.87 (mL/g) |
| TCE $K_d$ | 0.17 (mL/g) | 0.51 (mL/g) |
| Bromide $K_d$ | 0.37 (mL/g) | 0.11 (mL/g) |

De-aired City of Fort Collins tap water was pumped through the sand and silt layers at rates of ~0.3 and 0.004 m/day, respectively. Water was introduced and recovered from head tanks at either end of the tanks that were in full hydraulic connection with the sand and silt layers. With this, no vertical gradients were imposed across the layers in the tanks and transport between the sand and silt is solely due to diffusion.

For the first 28 days of the experiment influent solution were spiked with PCE-bromide or TCE-bromide. Average influent concentrations as a function of time are presented Table 4. The change in average influent TCE concentration at day 7 reflected failure of the reservoir holding the influent TCE solution. TCE concentrations in the replacement reservoir were lower. Bromide was included in the influent to all of the tanks at a similar concentration as means of comparing the performance of each of the tanks and resolving the behavior of a contaminant that was largely unaffected by either the activated carbon or ZVI. Figure illustrates the experimental design.

Table 4 – Averaged Influent Concentrations for Multiple Layer Tank Experiments.

| | Tanks 1-3 | | Tanks 4-6 | |
| --- | --- | --- | --- | --- |
| | PCE | Bromide | TCE | Bromide |
| Day 0 to Day 7 | 110 mg/L | 8 mg/L | 680 mg/L | 8 mg/L |
| Day 7 to Day 29 | 110 mg/L | 8 mg/L | 110 mg/L | 8 mg/L |
| Day 29 to 85 | 0 mg/L | 0 mg/L | 0 mg/L | 0 mg/L |
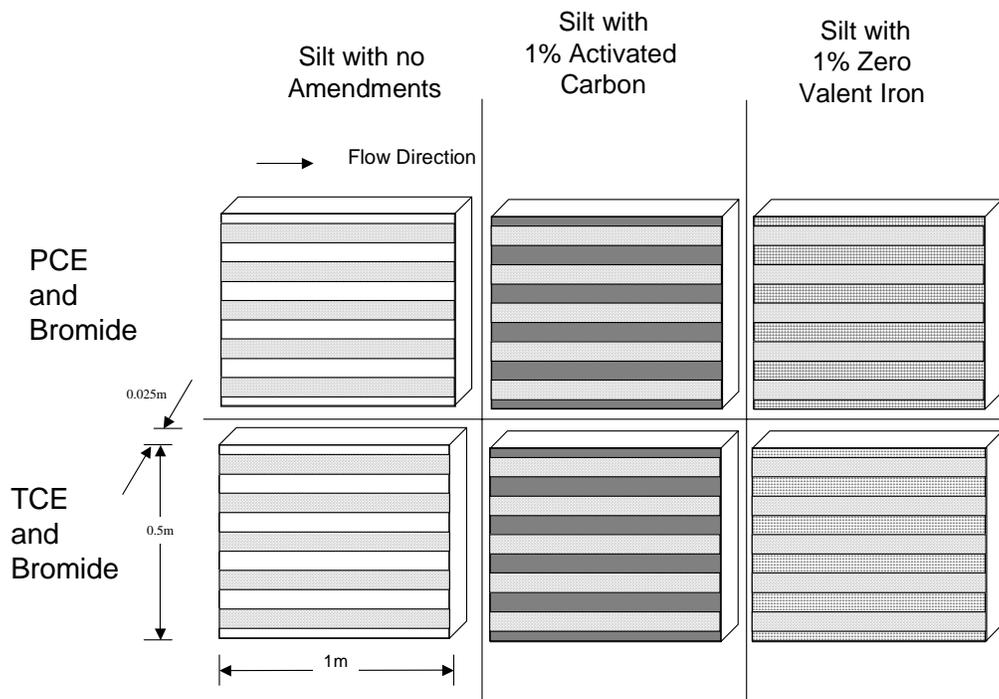


Figure 31 – Experimental design for the two layer small tank experiments

The intention of the source configuration was to approximate the concentration in a well-mixed plume in layered media downgradient of a source zone.

3.2.3 Results

Through the experiment, influent and effluent concentrations and flow rates were measured from each of the six tanks through time (see Appendix A). Based on this data, cumulative contaminant inflow and discharge from the tanks was

determined. The total contaminant mass retained or degraded in the tanks was determined as the difference between contaminant inflow and discharge. Figure presents mass balance results for PCE, TCE, and bromide. Note 1) Bromide data is not provided for the activated carbon tanks due to high background levels of bromide in the activated carbon and 2) Only one set of data for bromide is presented for the PCE and TCE tanks due to similar behavior in the matching tanks.

The differences between influent and effluent mass fluxes from the tanks show large difference between mass loading to the tanks and mass discharge. In all cases this is attributed to transverse diffusion from the sand to the silt layer. For both PCE and TCE adding either a sorptive or reactive sink in the silt zone enhances mass transfer to the silt layer. With it follows that either elevated adsorption or degradation of contaminants in hydraulically stagnant zones can enhance contaminant attenuation in plumes. Contaminants stored in the low permeability zones in either aqueous or sorbed phases will ultimately back diffuse out into adjacent transmissive layers, sustaining contaminant concentrations in plumes. In contrast, contaminants that degrade in hydraulically stagnant zones will not be available for back diffusion.

**TCE**                    **Bromide**
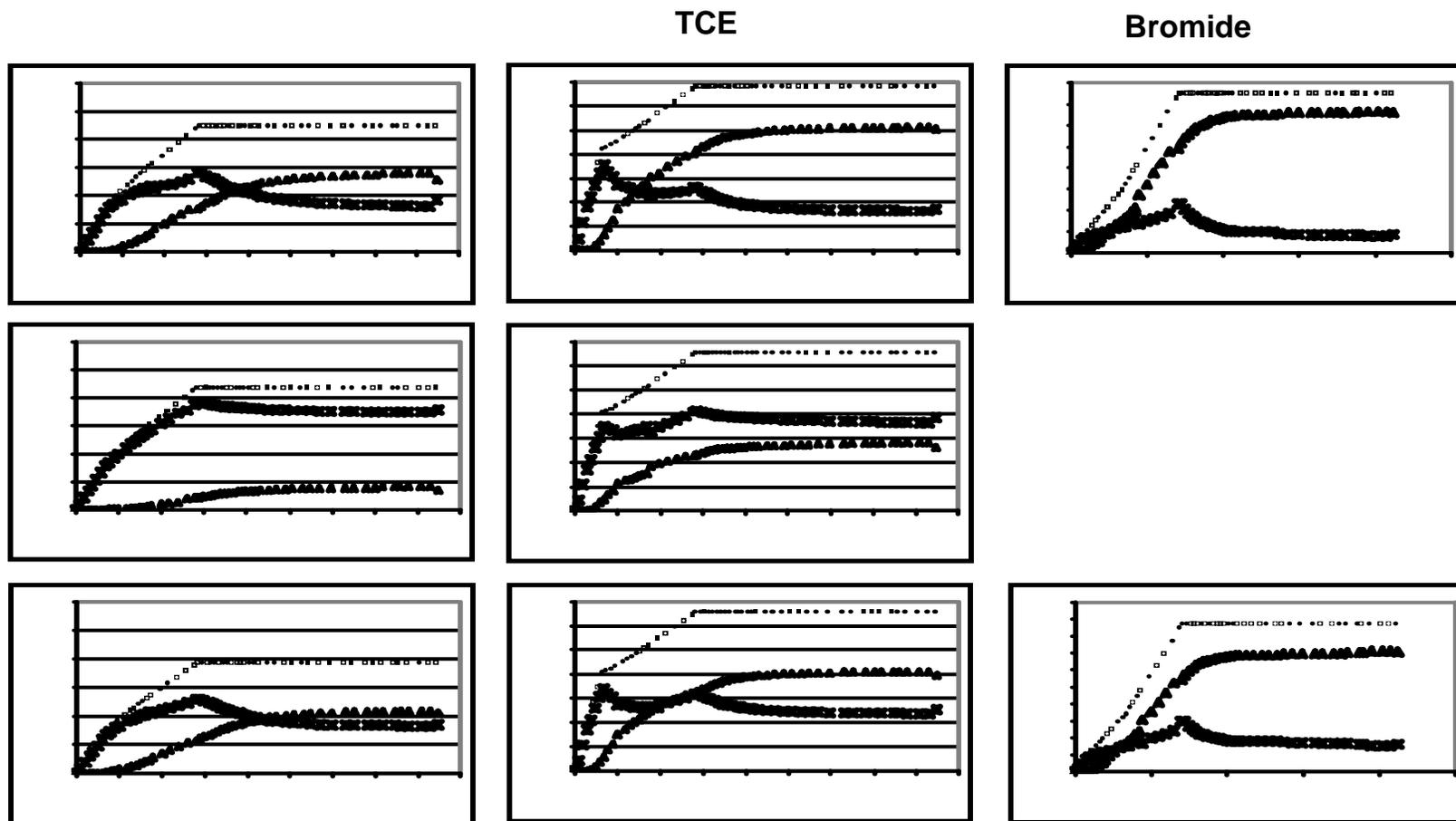


Figure 32 - Mass retained (No amendments or AC) and or degraded (1% ZVI) in the multiple layer tanks based on cumulative influent-effluent mass balances. Mass in shown as open squares, mass out as black triangles, and the difference between mass in and mass out as asterisks

More rigorously, Figure 33 plots the percentages of influent contaminant mass in the silt layers at the end of the experiment.  For PCE and TCE, addition of ZVI increases the fraction of loaded contaminants in the silt by factors 1.2 and 1.5, respectively.  More dramatically, addition of activated carbon increases the fraction PCE and TCE remaining in the silt by factors 2.1 and 2.4, respectively.
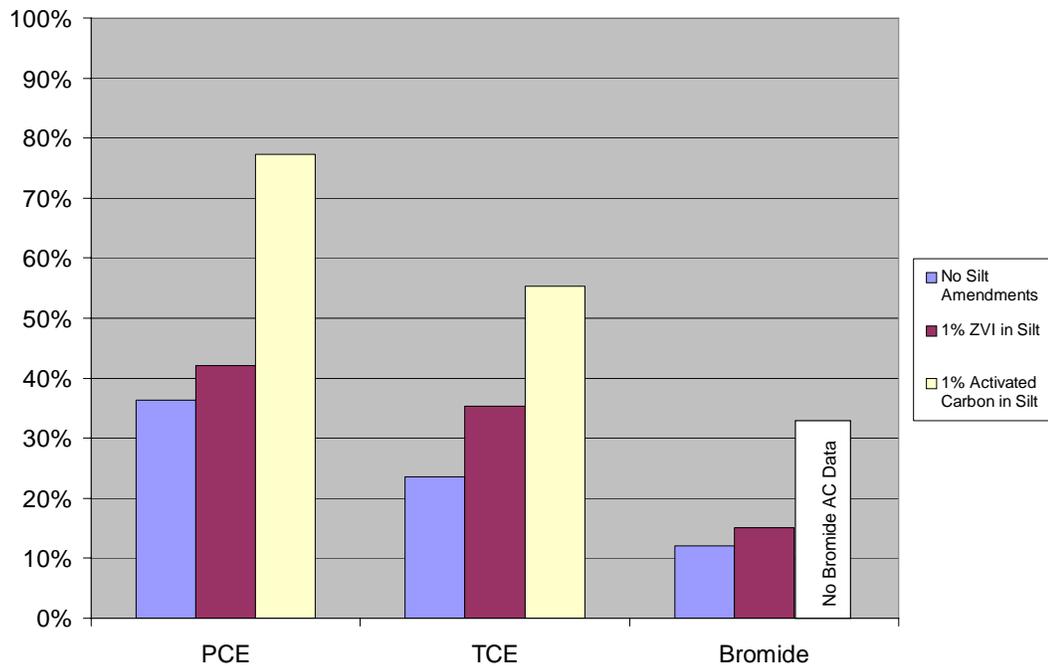


Figure 33 – Percentages of influent contaminant mass driven into the silt layers at the time the source is shut off.

The total amount of contaminant mass driven into the low-permeability zones is also important.  Figure 34 presents mass driven into the low-permeability zones (retained and or degraded) by amendments on a log scale.  The data suggest that both initial contaminant concentrations and adsorption play large roles in governing contaminant mass that is driven into the low-permeability zones.
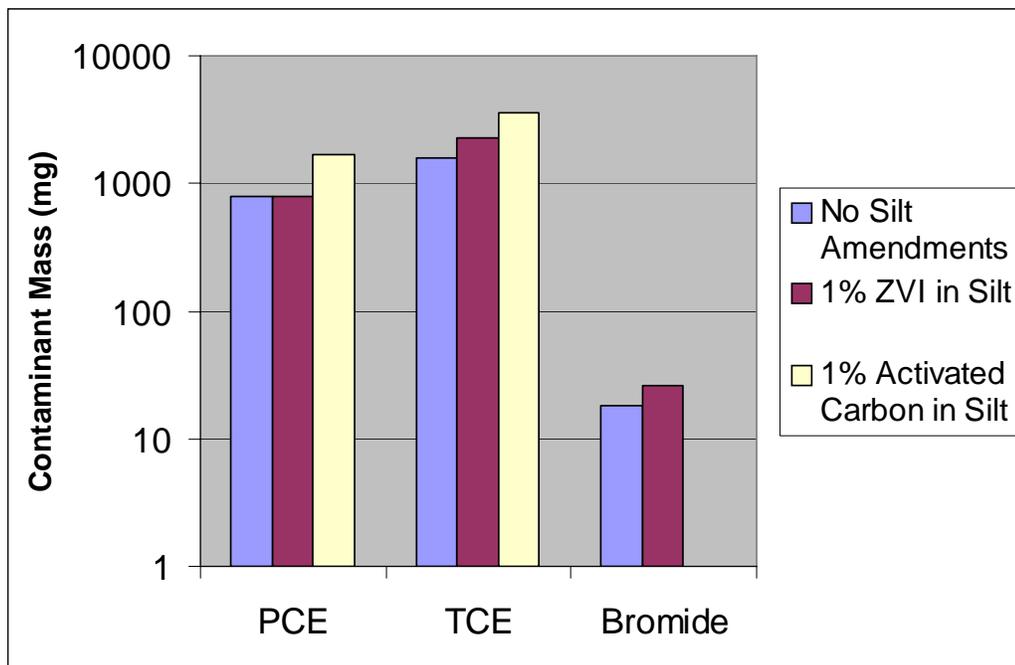
Figure 34 – Total mass retained (No amendments or AC) and/or degraded (1% ZVI) in the multiple layer tanks based on 83-day influent-effluent mass balances.

Lastly, consideration is given aqueous concentrations. Figure 35 plots the bulk influent concentration based on tank loading, effluent concentration after the source has been on for 28 days, and the effluent concentrations at 85 days. At 28 days effluent concentrations are lower than loading concentrations due to attenuation by the silt layers. Reflecting termination of the source, effluent concentrations at 85 days are approximately one to two orders of magnitude lower than concentration observed with the source on after 28 days. Unfortunately, even with the source off for 56 days concentrations are still two to three orders of magnitude above USEPA MCLs for each compound. Considering the total mass retained in the silt layers it is likely that these concentrations can be sustained for long periods of time.
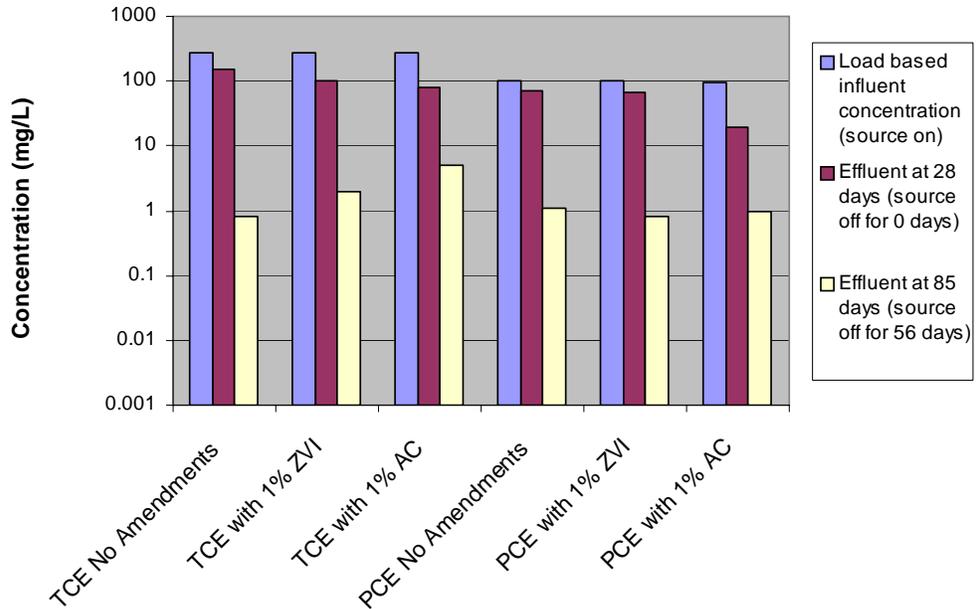
Figure 35 – Concentrations by contaminant based on mass loading to the tanks, observed concentrations at 28 days (end of source on), and 85 day (56 days after source off).

## 3.3  *Small-Scale Two Layer Tank Experiments with DNAPL Sources*

Two layer tank experiments with DNAPL sources were conducted at the Colorado School of Mines (CSM), Golden, Colorado.  DNAPL sources are utilized to study the processes that occur in and in the close vicinity of the DNAPL zone (Fluxes 1, 2, 2` and 3 described in the Summary) and downgradient of the DNAPL zone (Fluxes 4 and 4` described in the Executive Summary, Figure 12).  A simple two layer tank-packing configuration is used with a known amount of DNAPL.  Data from the X-ray attenuation analysis characterizes DNAPL saturations as a function of time.  Effluent water samples are used to resolve the contaminant mass remaining in the tank and the effects of back diffusion after the

DNAPL source is fully dissolved. In addition, at the conclusion of the experiment, soil cores were extracted from the low permeability zones to determine the distribution of the contaminants remaining in the tanks.

The combination of observed DNAPL saturations in the source zone and the post-DNAPL distribution of the dissolved phase mass in the zone of lower permeability enabled conclusions to be drawn on the effect of the degree of DNAPL saturation on contaminant storage in the low flow zones. The details of these experiments are presented in Appendix B and in a MS thesis (Wilking, 2004).

3.3.1 Objectives

Objectives of these experiments were to:

1) Assess the significance of contaminant storage and release from low permeability zones in the presence of a depleting DNAPL source.

2) Determine the effect of DNAPL source zone saturations on the contaminant diffusion within the DNAPL entrapment zone.

3) Develop a basis for testing models described in Section 6.

3.3.2 Methods

Two types of small tanks were used in this series of experiments. These tanks had dimensions of: 2.44 m x 0.60 m x 0.055 m and 0.60 m x 0.40 m x 0.055 m, respectively.

For identification purposes, the first is referred to as "intermediate scale tank" and the second "small tank." The basic setup of the two tanks is similar except for their dimensions. Figure is a photograph of the intermediate scale tank placed on the x-ray platform. Figure 37 shows the schematics of the small tank. The clear polycarbonate walls of the test tank were lined with 3.2 mm (1/8 inch) glass in order to prevent any sorption of the source contaminant to the polycarbonate. The groundwater flow across test aquifer was controlled using constant head reservoirs connected to the upstream and downstream ends of the test tank. Two dissolution experiments were conducted in the intermediate scale tank that was followed by five experiments in the second tank.



Figure 36 - Intermediate scale tank mounted on the x-ray platform.

Figure 37 - Schematic of packing configurations of small tank – side view.

The intermediate scale tanks experiment used a simple layered, heterogeneous configuration. This packing represented a situation where the DNAPL accumulates above the interface between coarse- and fine-sand layers (e.g. a capillary barrier effects at an interface between coarse alluvium and low permeability bedrock). The bottom one third of the tank was packed with a finer #140 sand with a hydraulic conductivity of 4.3 m/day. The top 2/3 of the tank was packed with coarser #30 sand with a hydraulic conductivity of 130 m/day. The top surface of the soil pack was sealed with clay to create confined conditions in the test aquifer and thus create a uniform flow field along its length. The packing architecture and soil types used varied for the five small tank experiments. In addition to the same two sand types #30 and #140 that were used in the intermediate-scale tank experiments, a silt from NASFtW site was used to pack the small tanks. The field silt with a hydraulic conductivity of 69 cm/day is much less permeable that the #140 sand. Therefore, differences in the concentration profiles from cores taken of the silt versus those of the #140 sand

would give insight in to relative significance the advective and diffusive effects of mass transfer when the low-permeability zone characteristics vary.

The source zone for the small tank (2.5 cm x 10 cm x tank width) was much larger than the source zone (1.0 cm x 1.0 cm x tank width) of the intermediate tank experiments, to allow to focus more on the DNAPL entrapment zone process in the small tank experiments.  By increasing the height of the source zone from 1.0 cm to 2.5 cm, a vertical saturation profile could be developed.  The DNAPL source zone was created by injecting the test DNAPL (TCE or TCA) into coarse sand pocket at the interface of the two contrasting soil layers.  The DNAPL was colored with Sudan IV red dye at a ratio of 0.0005 mg Sudan IV to 1.0mg DNAPL for visualization through the transparent tanks walls.  The exact mass of DNAPL that was placed was carefully monitored to determine the initial saturation and contaminant mass present.

In the intermediate scale tank, a head drop of 2.5 cm over the flow distance of 244 cm length was used to create the approximate range of flow velocities observed at the NASFtW (1.5-2.0 ft/day).  The key attributes and the flow rates in the small tank experiments are summarized in Table 5.

In all experiments the effluent concentrations during the dissolution of the emplaced DNAPL source were measured.  Aqueous samples were collected at the downstream end and analyzed using a gas chromatograph (GC) to determine solute concentrations in the tank effluent.  During dissolution, the DNAPL mass depletion rate in the source zone was accurately monitored using an automated X-ray attenuation system. In order to gather the data required to evaluate effluent aqueous concentration versus time from the DNAPL dissolution and to calculate the DNAPL mass that had dissolved and migrated out of the tank, many samples of the effluent had to be taken.

Table 5 - Key attributes of small tank packing configurations.

| EXPERIMENT | SMALL TANK NUMBER | COARSE | FINE | X – DISTANCE FROM INLET TO SOURCE ZONE (CM) | DNAPL | FLOW RATE (L/D) |
|---|---|---|---|---|---|---|
| BST1 | 1 | #30 | #140 | 14.5 | TCE | 5.7 |
| BST2 | 2 | #30 | #140 | 14.0 | 1,1,2-TCA | 5.7 |
| BST3 | 2 | #30 | #140 | 13.0 | 1,1,2-TCA | 5.1 |
| BST4 | 2 | #30 | Field Silt | 10.0 | 1,1,2-TCA | 5.1-7.5 |
| BST5 | 2 | #30 | Field Silt | 9.5 | 1,1,2-TCA | 3.4-11.3 |

3.3.3 Results

The key results from the intermediate-scale and small-scale tanks are presented in the following section. First the results from the two intermediate-scale tank experiments are presented. This is followed by the results from the five small-tank experiments. After the presentation of the results specific to each type of experiment, a summary discussion on how the findings contributed to achieving the stated objectives is presented.

*Experiment 1: Intermediate Tank Experiment 1 with 1,1,2-TCA as the test DNAPL*

In this experiment, 4.24 grams of 1,1,2-TCA were injected into the coarse inclusion to create the DNAPL source at the coarse/fine sand interface. Figure 38 shows the DNAPL mass depletion as a function of time as measured using the X-ray system. A hardware failure caused a gap in the X-ray data from day 2 until day 7. However, the data indicate complete depletion of the DNAPL in the source zone in 7.5 days.

**1,1,2-TCA Mass Removal from the Source Zone**
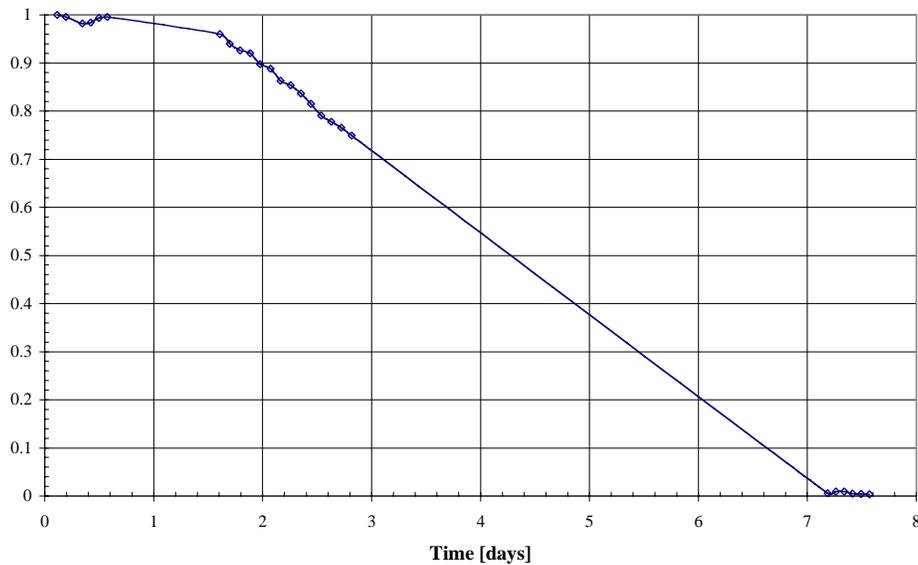


Figure 38 - 1,1,2-TCA source dissolution as measured by X-ray analysis

Figure 39 shows the breakthrough of the aqueous 1,1,2-TCA in the effluent from the time of DNAPL injection. Figure 40 illustrates the depletion of the DNAPL in the source zone as well as the cumulative 1,1,2-TCA mass in the effluent. As can be seen, 102 percent of the 1,1,2-TCA that was injected in the source zone was recovered in the effluent. The mass recovered was greater than the mass injected because of the errors in the hexane extraction sampling protocol. During the course of the experiment, the groundwater flow rate was measured to vary between 15.0 and 16.5 L/day.
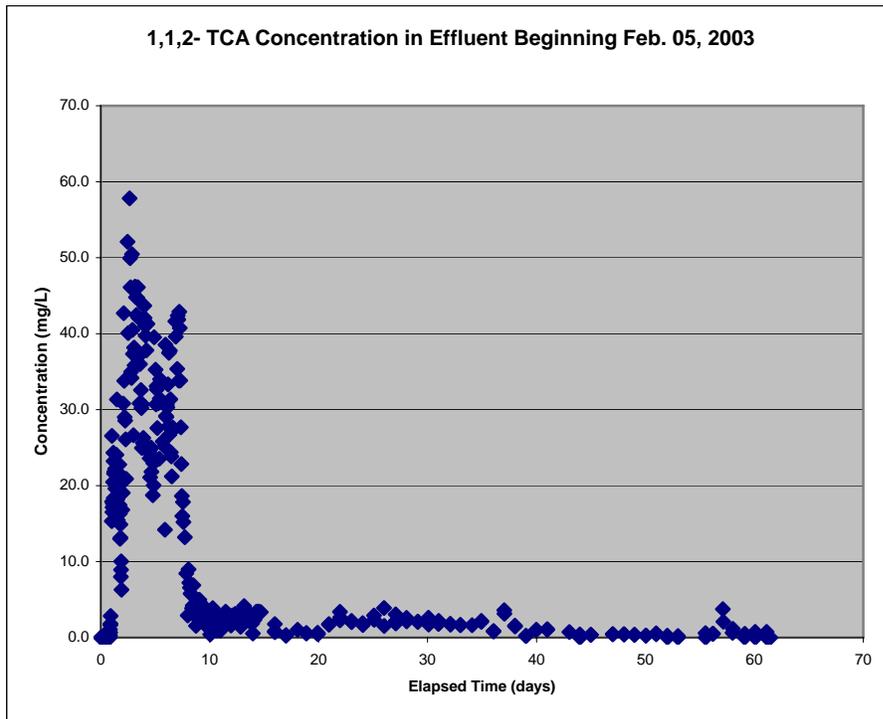
Figure 39 - 1,1,2- TCA concentration in effluent for intermediate tank

**Cumulative 1,1,2-TCA Mass vs. Elapsed Time**
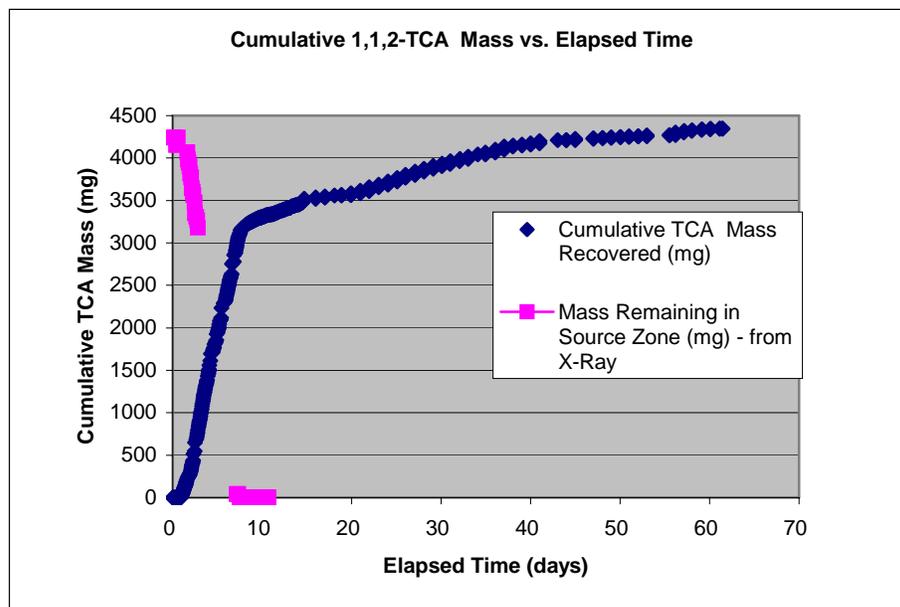
Figure 40 - Cumulative 1,1,2-TCA mass removed / recovered for the intermediate tank

Even though the DNAPL source was fully depleted in 7.5 days, it took 61 days for the effluent concentrations to reach non-detectable levels. This suggests that the process of matrix storage was significant. At the time of DNAPL depletion, 73 percent of the 1,1,2-TCA mass had been recovered, indicating, 27 percent of the mass was still in the tank stored in the soil. Extending the effluent sampling an additional 24 hours for the dissolved fraction to exit the tank, it was observed that 24 percent of the initial injected mass still remained in the tank. Thus, nearly a quarter of the contaminant mass was being stored in the soil matrix. It required 53 days, nearly six times longer than the time required to dissolve the DNAPL, for the stored contaminant to exit the tank at non-detectable levels. These results clearly suggest that storage in the low permeability layer can be a key contributor to long-term site contamination (objective 1).

*Experiment 2: Intermediate Tank Experiment 2 with TCE as the test DNAPL.*

Due to the lower solubility of TCE than 1,1,2-TCA, a smaller mass (1.53 grams) was injected into the source zone. Figure 41 shows plots of DNAPL mass depletion as a function of time as measured using the X-ray system.

Figure  also shows the mass depletion of non-aqueous TCE from source zone monitored with the X-ray system. Complete dissolution of the DNAPL was observed after 11 days.  For this source zone architecture, the depletion followed a nearly linear trend.
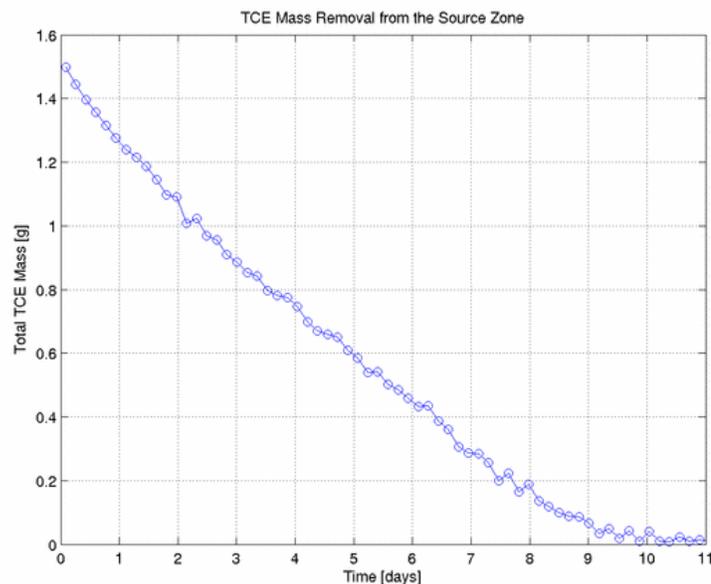


Figure 41 - TCE source dissolution as measured by X-ray analysis

The effluent was sampled and directly measured in the aqueous phase using GC techniques.  Two experimental difficulties arose that prevented the development of the effluent contaminant breakthrough versus time curve.  First, the sampling protocol allowed for the sealed sample vials to be exposed to the air via a thin gauge needle used for venting purposes.  This led to loss of TCE to the air and reduced the observed concentrations to a level much below the anticipated

concentrations.  Second, the filters in the tank became clogged and the flow rate dropped dramatically to approximately one third of the original flow rate.  The flow rate was not measured on a daily basis during this experiment.  Therefore, the effects of the flow-rate change on the dissolution and migration of the TCE in the tank could not be determined.  For these two reasons, the effluent data from this experiment could not be used and are not presented here. However, this experiment provided useful information to validate the experimental methods that were used in the subsequent experiments.

Despite the relatively rapid depletion of DNAPL pools and residuals (<10 days), downstream concentrations remained well above USEPA MCLs for weeks to months.  The contradiction between relatively quick DNAPL dissolution and long-term effluent concentration tails is best explained by contaminant storage in the low-permeability layer.  Thus, it appears contaminant storage and release from the low-permeability layer is relevant per the introductory discussion in Section 2.

 *Experiment 3: Small Tank Experiment with TCE source (BST1)*

This experiment utilized Small Tank 1 that is shown in Figure 42 (note: negative numbers were used on the x-axis due to the nature of the X-ray analytical programs).   7.47 grams of TCE were injected into the coarse inclusion. Unfortunately, the same issues relating to losses of TCE that hindered intermediate scale tank Experiment 2  were also present here, causing an erratic breakthrough curve with large variations in concentrations between aqueous samples.  The experiment was continued for 144 days before a pump failure caused termination.  Even though no useful results were obtained from this experiment, it confirmed the impracticability of using the highly volatile TCE in the experiments where the maintenance of mass balance becomes critical. The use of TCE as the test DNAPL was discontinued because of these experimental difficulties.
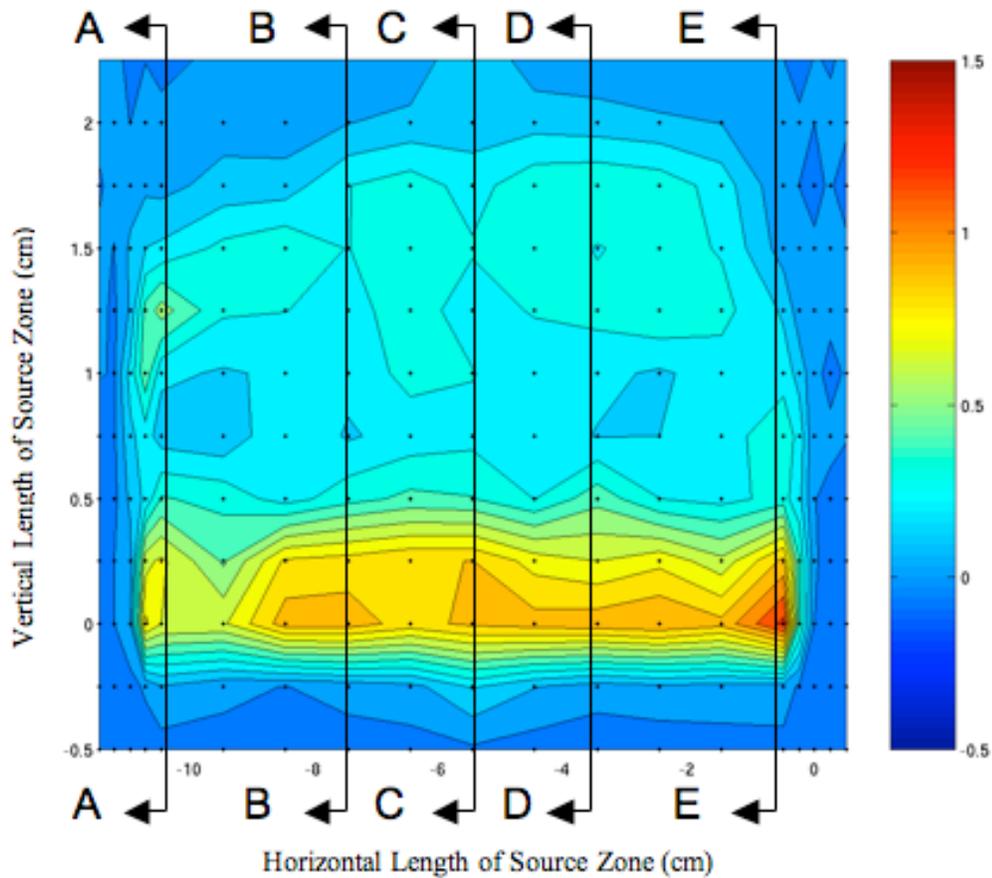
Figure 42 - DNAPL distribution after injection during BST2.

*Experiment 4: Small Tank Experiment 2 with 1,1,2-TCA (BST2)*

Focusing on the second objective to evaluate the effect of source zone DNAPL saturation distribution on matrix diffusion into the low-permeability layer, the injection was controlled to create a known saturation profile in the vertical direction. The DNAPL was injected until the entire coarse sand inclusion was fully saturated. Then, DNAPL was withdrawn out of the inclusion back until the vertical profile of the entrapment zone contained distinct sections of DNAPL at

higher saturation and transitions zone with variable saturation. The resulting DNAPL saturation distribution within the source zone, as depicted in contours via X-ray analysis, is shown in Figure 42.

In Figure 42, the contours represent the cumulative length of DNAPL within the pores spaces that was encountered by the photons of the X-ray beam. The zero position on the vertical axis represents the interface between the coarse inclusion and the fine layer. For this experiment, a maximum DNAPL saturation (path length divided by the product of tank width and porosity) of 0.55 was observed near the right edge of the source zone. The X-ray scanning continued throughout the duration of DNAPL dissolution to monitor the variations in DNAPL saturation. Also, effluent sampling was performed beginning after the DNAPL injection, and it continued until 2.6 days after the DNAPL source had been completely depleted. The breakthrough curve is shown in Figure 43 and the corresponding source zone mass monitored with the x-ray system is shown in Figure 44.
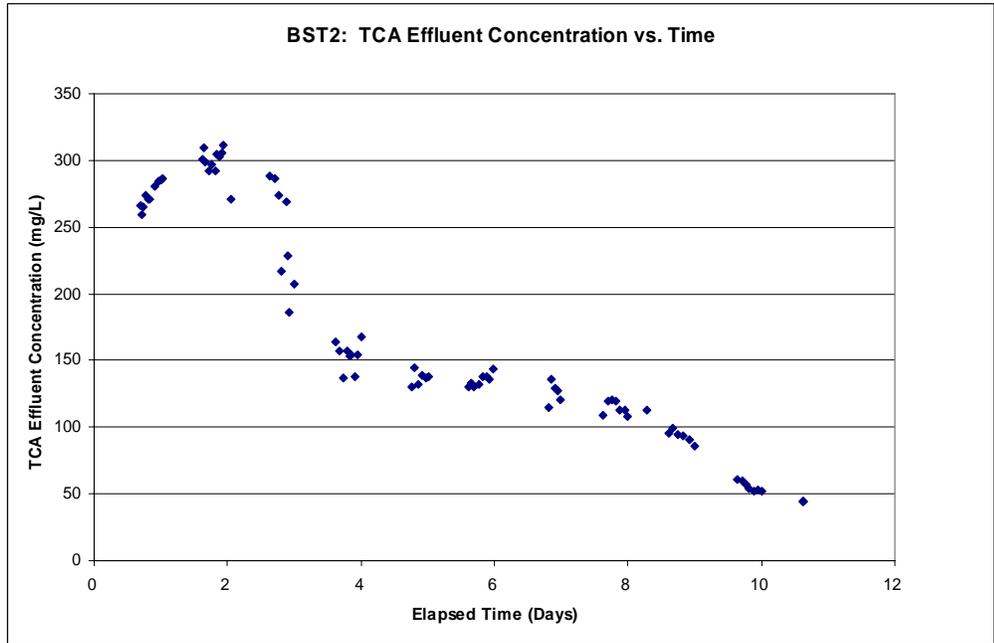
Figure 43 - Contaminant breakthrough in effluent versus time for BST2.
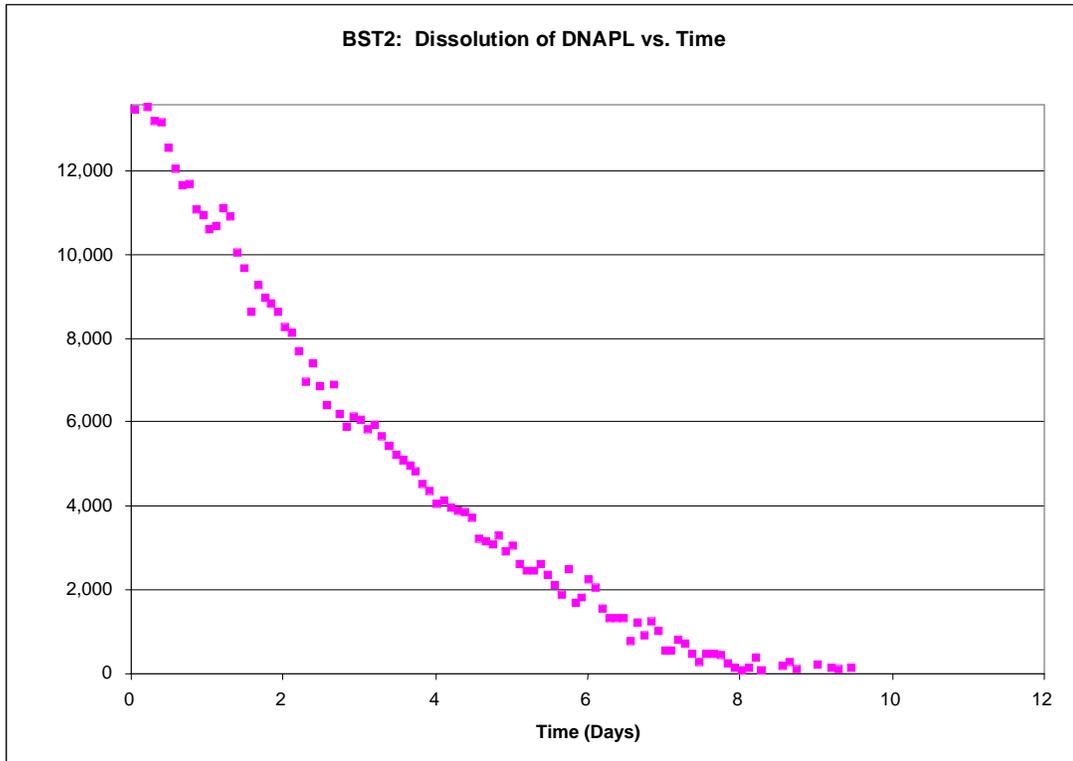
Figure 44 - Results of DNAPL dissolution for BST2 as depicted by X-ray.

Although the mass recovery of the 1,1,2-TCA only totaled 67 percent of the injected mass, the majority of the losses are assumed to have occurred in the excavation procedure as explained later. Figure 44 shows several interesting occurrences in the breakthrough curve. For instance, there is a peak concentration of approximately 300 mg/L observed at two days of elapsed time from the DNAPL injection. Then, there is a noticeable, abrupt drop in concentration at three days elapsed time. After the sharp drop, the concentration declines very slowly until eight days have elapsed. Finally, after eight days, the concentration decreases again at a more rapid pace. A closer examination of Figure 43 and Figure 44 reveals a relationship between the DNAPL distribution in the source zone and these occurrences in the breakthrough curve. The DNAPL saturation levels near the bottom of the source zone are sufficiently high to

reduce the aqueous phase relative permeability such that only limited flow occurs in this area. The flow bypasses this area in favor of a more permeable zone, which is located in the upper sections of the source zone. Thus, the upper part of the source zone has an increased rate of flow through it. Therefore, the dissolution of the DNAPL during the first three days occurs primarily from the upper source zone area.

In addition to the effluent results, this experiment yielded other data that are important to understand the processes that govern matrix storage. These data were acquired during the excavation and coring of the tank that occurred 2.5 days after complete DNAPL dissolution. The procedure used for excavation and coring is discussed in Appendix A. The distribution of the dissolved contaminant in the low-permeability layer is shown Figure 45.
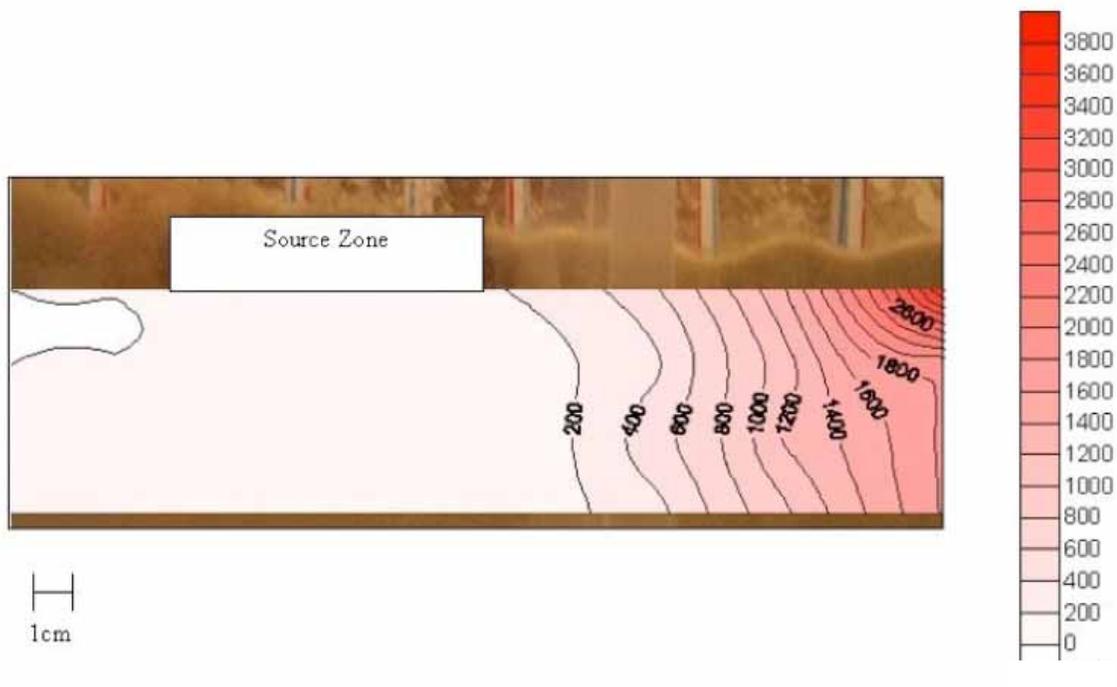


Figure 45 - Distribution of 1,1,2-TCA concentrations dissolved from DNAPL in the low permeability layer

This was the first attempt for the coring procedure. Although good data were obtained for a small volume of the low permeability layer, the cores did not cover the full lateral or vertical extent of the tank because it was not known how many cores would provide a representative data set. Specifically, the cores covered only 22.2 cm laterally and only 6 cm vertically in the low permeability layer. For subsequent tanks, steps were taken to ensure full coverage of the low permeability layer. Although the coring did not provide full coverage of the #140 sand in the tank, the results revealed an important factor. The highest concentrations (nearly 3000 mg/L) were observed at the top of the #140 sand layer. This suggests that the primary mode of contaminant transport into the #140 sand layer was diffusion from the source zone and the coarse layer above it. The peak concentrations were observed downgradient from the source zone. This was due to the small degree of advection that occurred in the #140 sand layer. Since the cores were taken 2.5 days after DNAPL dissolution ceased, the peak concentrations of the diffused mass had been transported toward the downgradient section of the tank.

*Experiment 5: Small Tank Experiment 3 (BST3) with 1,1,2-TCA*

The injection resulted in the placement of 14.2 grams of 1,1,2-TCA in the coarse inclusion. The DNAPL distribution within the source zone, as measured using X-ray analysis, is shown in Figure 46. This shows some heterogeneity in the levels of DNAPL saturation through the source zone, although it is less pronounced than for BST2. The maximum DNAPL saturation level is 0.40 - 0.42 for section E and section A and less than 0.30 for all other sections. Additionally, due to the DNAPL withdrawal procedure, the maximum DNAPL saturation level is observed at 0.5 cm above the interface with the low permeability layer.
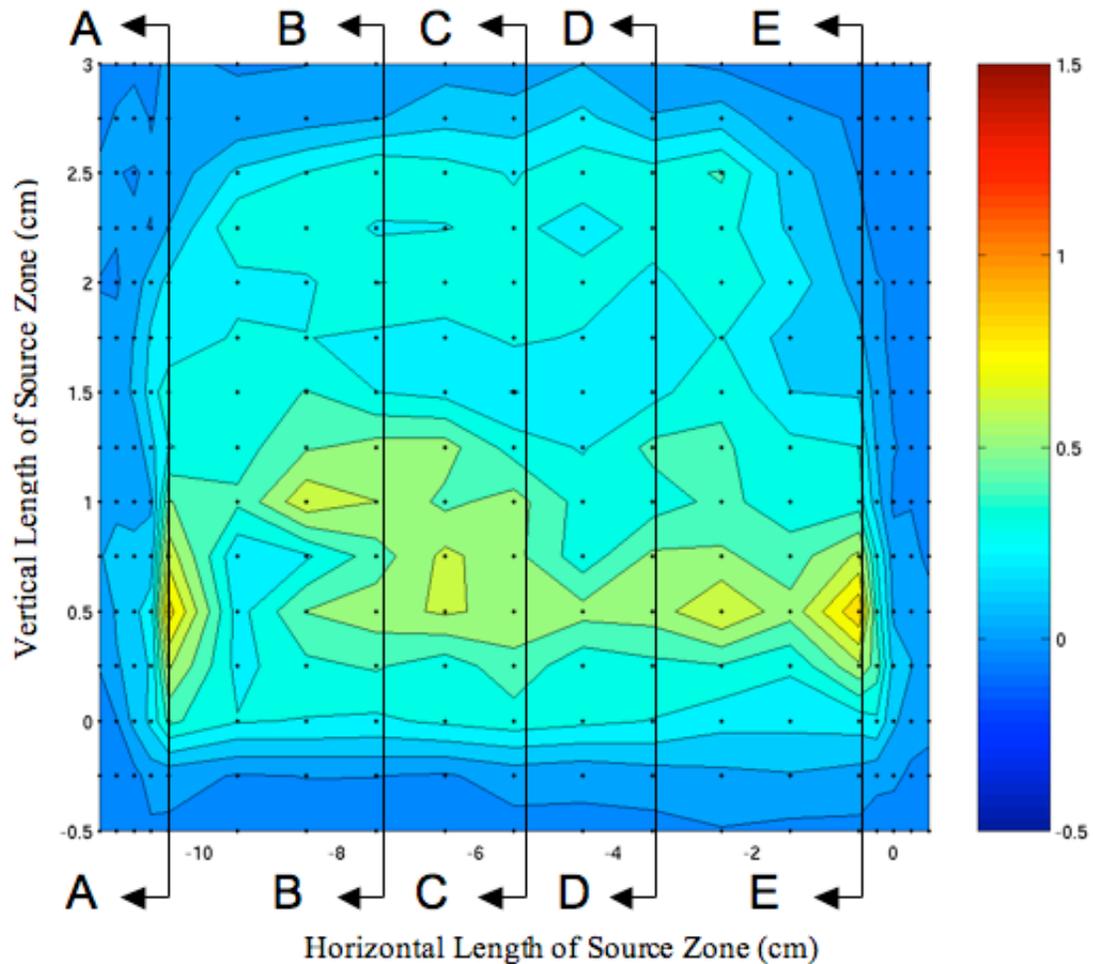
Figure 46 - DNAPL distribution after injection during BST3.

The dissolution experiment was performed for 9 days. Effluent sampling and soil coring for BST3 achieved recovery of 94 percent of the 1,1,2-TCA mass injected into the tank. Analysis of X-ray data indicated that the DNAPL had completely dissolved after 5.5 days. The effluent contaminant breakthrough curve is shown in Figure 47.
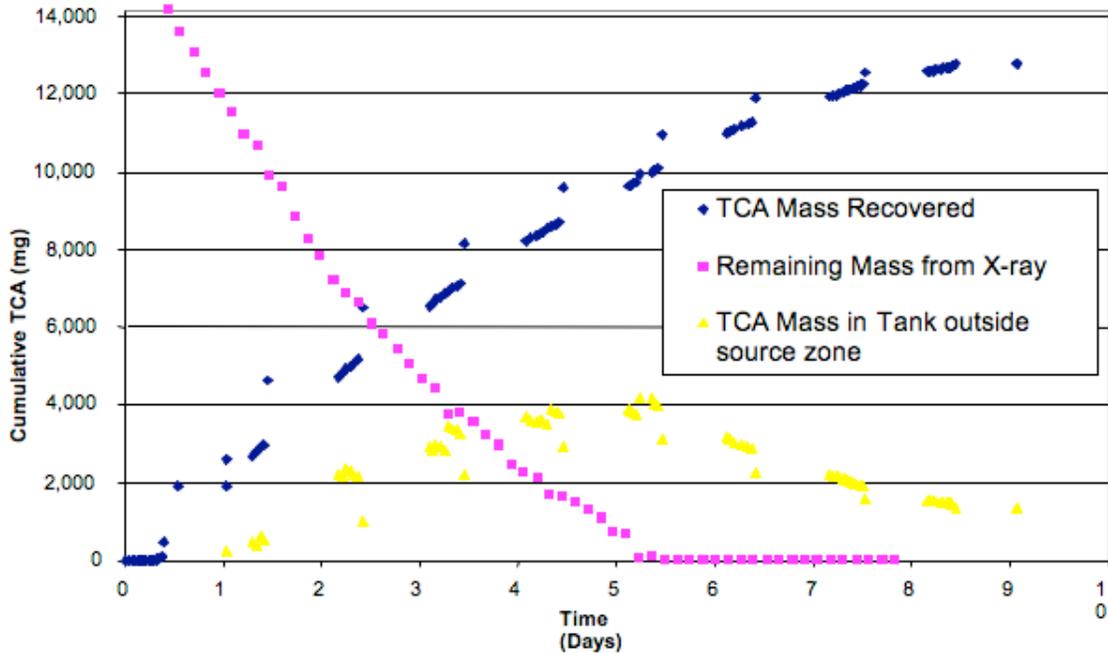
Figure 47 - Distribution and recovery of 1,1,2-TCA mass for BST3.

A comparison of Figure  and Figure 43 (the breakthrough curve for BST2) identifies three differences between the two curves.  First, the peak concentration for BST2 was approximately 300 mg/L, but the peak concentration for BST3 was greater than 500 mg/L.  Second, after the initial peak, BST2 displayed an abrupt drop in concentration that was not present in the same magnitude in BST3.  Third, a greater amount of DNAPL (14.2 grams) was injected during BST3 compared to 13.6 grams for BST2, yet BST3 dissolved in a shorter period of time (5.5 days compared to 8.3 days).

**BST3: TCA Effluent Concentration vs. Time**
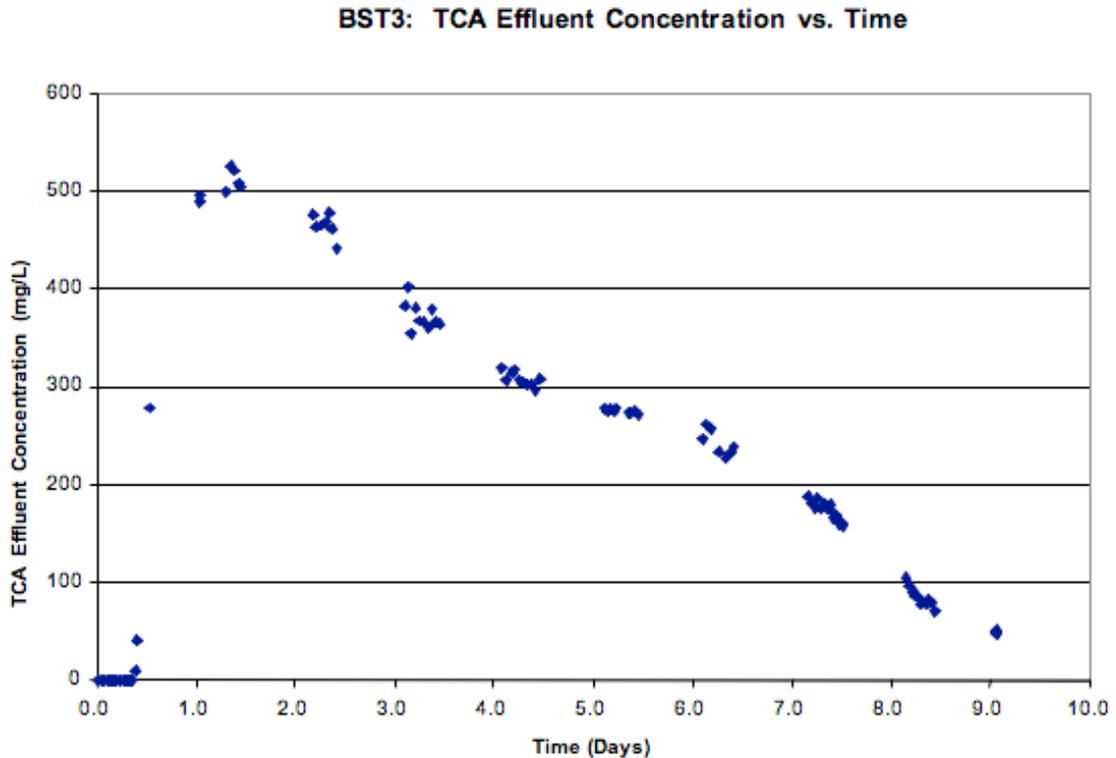
Figure 48 - Contaminant breakthrough in effluent versus time for BST3.

These differences demonstrate that different phenomena were controlling the dissolution and/ or the solute transport during the experiments. The flow rate and packing were similar between the two experiments. The only major difference between the two tanks was the distribution of the DNAPL in the source zones. BST3 did not contain a highly saturated area near the bottom of the source zone (at the interface between the high and low-permeability layers). Additionally, it did not contain as wide a range of levels of DNAPL saturation as BST2. These factors caused a different flow field to develop through the source zone within BST3. BST3 did not exhibit the degree of flow bypassing that occurred in BST2. Therefore, the entire source zone experienced flow through it that enabled dissolution of DNAPL from all parts of the source zone to occur throughout the duration of the experiment. This observation is supported by the breakthrough

curves.  The DNAPL in BST3 was more exposed to the flow, which increased the dissolution rate generating higher peak concentrations.   Also, because flow bypassing was minimal in BST3, the abrupt drop after the initial peak seen in BST2 was not present in BST3.  Moreover, the DNAPL in BST3 dissolved more quickly because of the enhanced flow throughout the source zone whereas DNAPL in the lower area of the BST2 source zone had minimal exposure to the water causing a lower dissolution rate.

Coring of the low-permeability layer upon termination of the experiment was performed over the entire lateral distribution of the tank.  Additionally, the cores were driven into low-permeability layer to a maximum depth ranging from 9-14 cm.  This provided comprehensive coverage of the distribution of the dissolved-contaminant mass in the low-permeability layer at 3.5 days after dissolution had ended. Figure 49 shows a contour plot of the aqueous concentrations that were observed in the low-permeability layer.
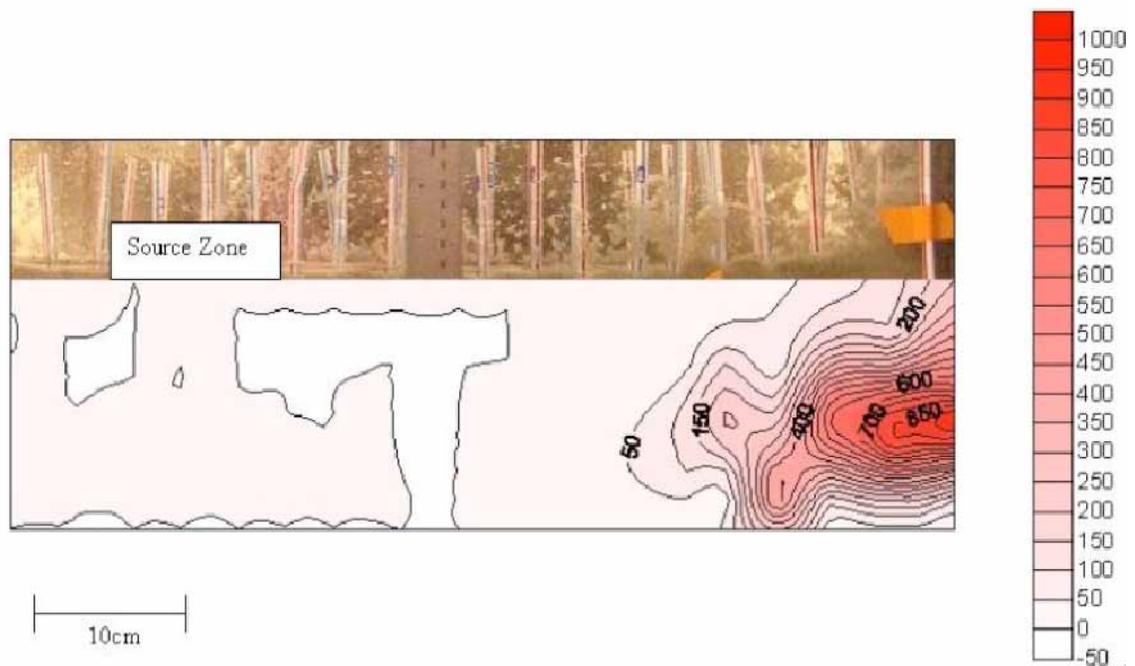


Figure 49 - Diffused mass in the low permeability layer in experiment BST 3.

The peak concentrations were observed once again downgradient of the former source zone because of the small degree of advection in the #140 sand layer. However, the depth of the peak concentration was from 5.5 – 7.0 cm below the interface of the two soils, whereas the peak concentration in BST2 was at the interface of the soils. This result suggests that diffusion was not the key transport mechanism for contaminant mass into the #140 sand layer. Instead, a vertical component of the flow field had been introduced causing advective transport into the low-permeability layer. Inspection of the source zone from Figure 49 suggests that DNAPL distribution caused aqueous phase relative permeability changes. As a result, the flow field was modified in the source zone and became two-dimensional (with a flow component normal to the layer interface). Additionally, since the level of DNAPL saturation at the interface was not as high as 0.5 cm above the interface, flow was encouraged downward toward the low-permeability layer. As water flowed through the source zone, it reached dissolved phase concentrations near or at the maximum solubility. Thus, when it entered the low permeability layer, it was laden with contaminant mass. The vertical flow was met by the horizontal flow within the low-permeability layer, and eventually the vertical component was stopped from transporting flow any deeper into the low-permeability layer. After this point, the mass was transported horizontally downgradient in the low permeability layer.

It is important to note that although diffusion did not dominate the contaminant transport in this experiment, its effects were still seen. Detectable concentrations were observed at depths up to 13 cm from the soil interface. Thus, while advection transported the highest concentrations 5.5 – 7.0 cm deep into the low-permeability layer, diffusion was responsible for the transporting the contaminant deeper. Greater depths than 13 cm may have reached if the DNAPL had persisted for a longer period of time.

*Experiment 6: Small Tank Experiment 4 (BST4)*

In this experiment the field silt (NAS Fort Worth sample) was used in the low-permeability layer. The desired flow rate for this experiment was 5.1 L/day. However, due to partial clogging of the fiberglass filters at the ends of the tank, a constant flow rate could not be obtained. The flow rate was monitored daily, and it is shown in Figure 50 along with the effluent breakthrough curve.
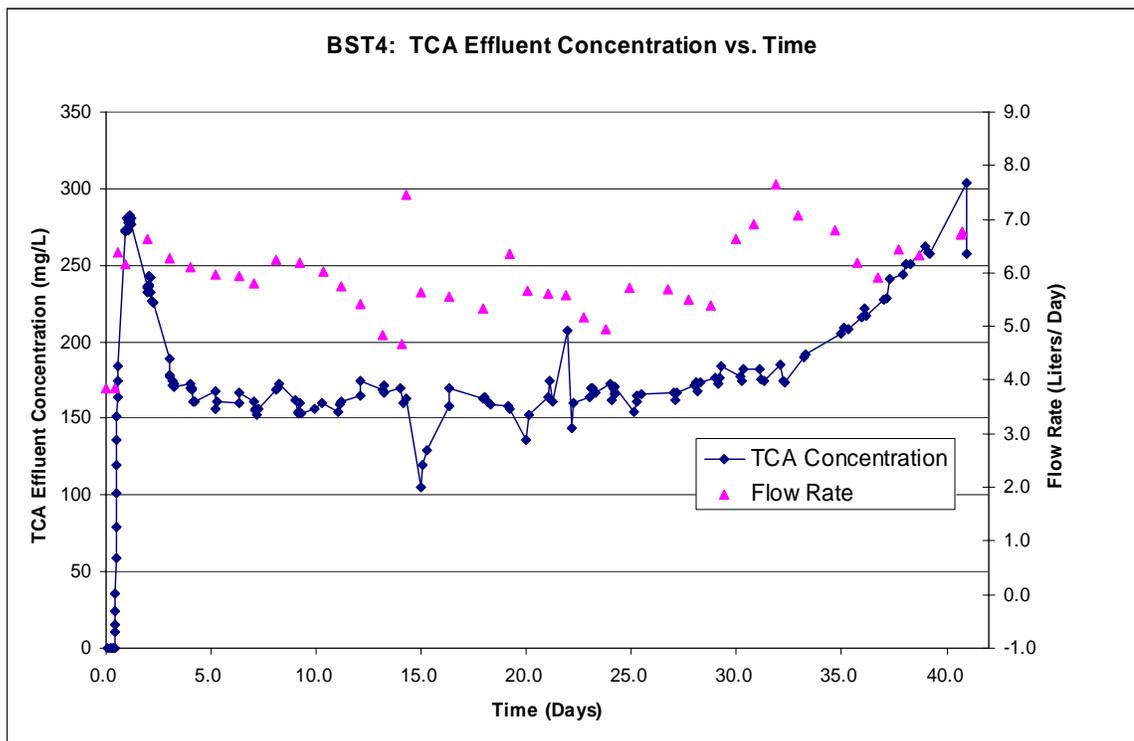


Figure 50 - Contaminant breakthrough (mg/L of TCA) and water flow rate (L/day) for BST4.

The DNAPL distribution within the source zone, as depicted via X-ray analysis, is shown in Figure 51. The highest levels of DNAPL saturation were in the bottom

portion of the source zone.  The excess DNAPL in the source zone caused higher saturation levels than for the other small tank experiments.
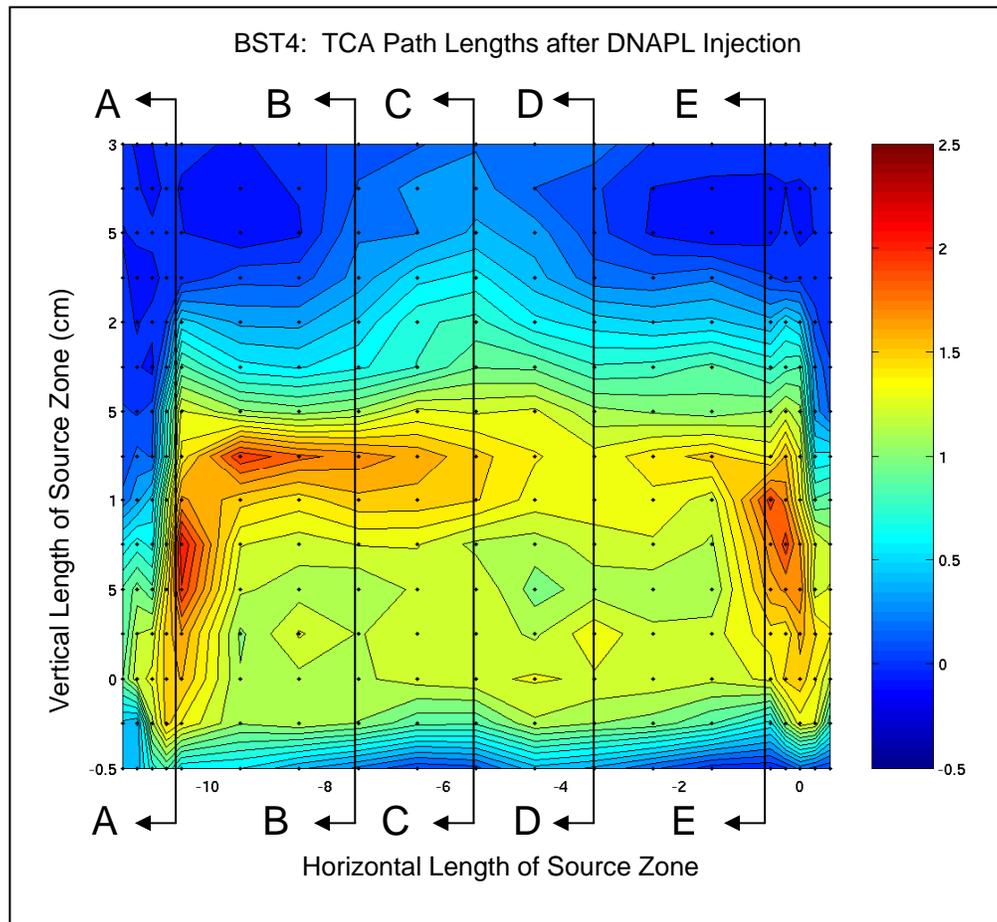


Figure 51 - DNAPL distribution after injection of 1,1,2-TCA during BST4.

The experiment was conducted for 41 days.  Effluent sampling and soil coring for BST4 achieved recovery of 87 percent of the 1,1,2-TCA mass injected into the tank.  Analysis of X-ray data indicated that the DNAPL had completely dissolved after 40 days (see Figure 52).  Due to the extended duration of the experiment, X-ray scanning was discontinued during days 14 – 36, and it resumed from day 37 until day 41 when the analysis showed that the DNAPL had dissolved.
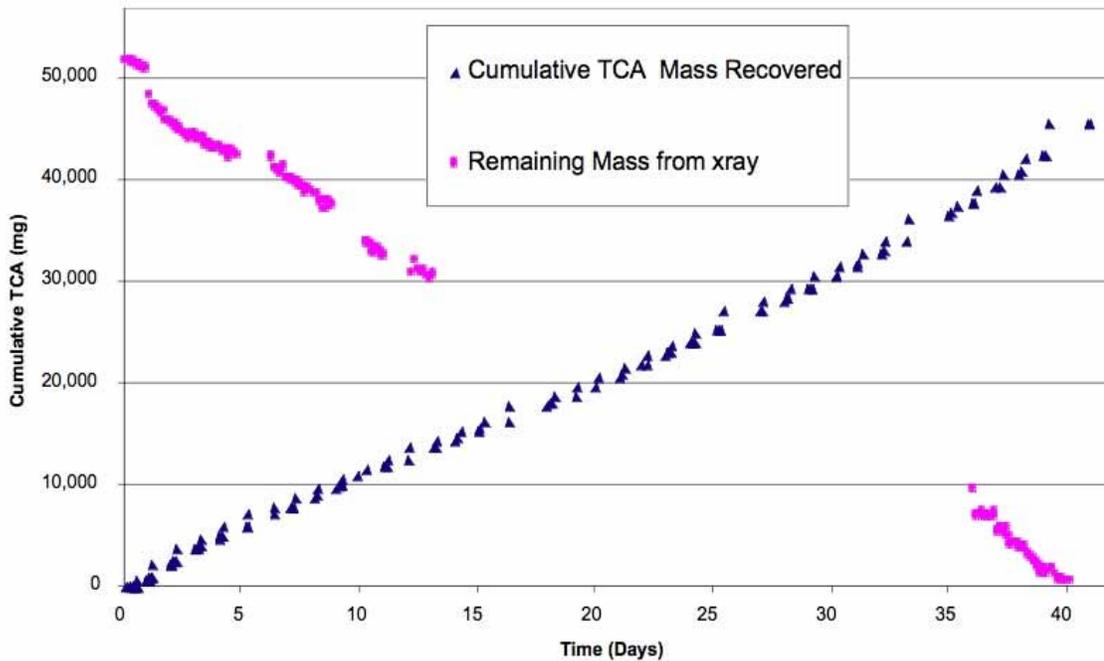
Figure 52 - DNAPL and recovered TCA versus time for BST4.

The breakthrough curve (shown earlier in Figure 50) indicates that the expected initial peak, which occurred at 1.2 days of elapsed time, was followed by a sharp decline in concentration from two to four days of elapsed time. Then, a period of constant concentrations was observed from four days to 26 days. This followed the pattern that was observed in BST2. The higher levels of DNAPL saturation on the bottom of the source pool forced flow bypassing. Thus, after the dissolution of the upper section of the source zone, only dissolution from the edges of the lower section of DNAPL occurred thereby lowering the effluent concentration significantly.

Unlike BST2, though, the breakthrough curve of BST4 indicates a rebounding effect after day 26 that continued until the experiment was terminated. The

highest concentration observed at any time during the experiment was seen on the last day of sampling.

The results of the coring procedure are show in Figure 53. During batch testing, the field silt was observed to exhibit appreciable sorptive characteristics. Its sorption coefficient was measured to be 0.6 L/kg. Thus, the observed concentrations from the soil coring include both dissolved and sorbed phases.
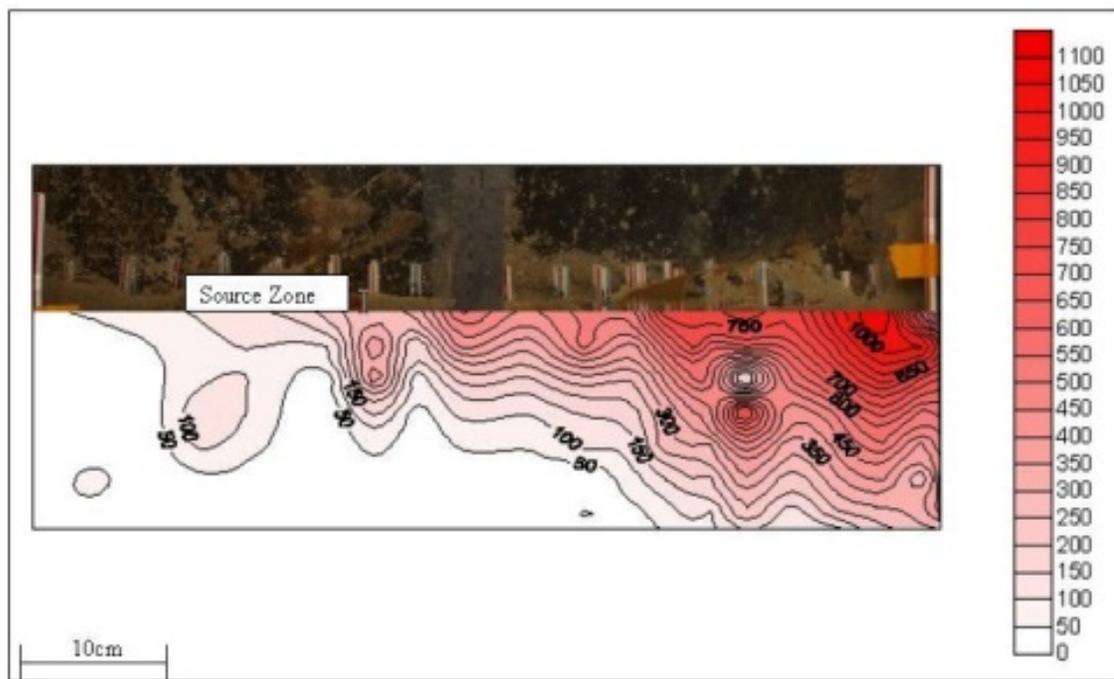


Figure 53 - Contours of dissolved 1,1,2-TCA concentration in the low permeability silt layer (experiment BST 4)

Due to the extended duration of the experiment, the residence time of DNAPL exposure to the low permeability layer was much longer than in previous experiments. The elongated residence time is the primary reason why the contaminant has reached a greater lateral and vertical extent than in previous experiments. Also, the hydraulic conductivity of the NASFtW silt is only one-third of the #140 sand. Thus, the decreased flow allowed for dissolved contaminant

within the silt layer to diffuse into a larger portion of the layer. Concentrations reaching 200 mg/L were observed at the extreme upgradient edge of the tank signifying that diffusion rivaled advection in the low permeability layer.

An examination of the peak concentration shows that the greatest concentrations remained near the interface of the two soils. This suggests that transport into the low-permeability layer was dominated by diffusion. Also, because of the small flow velocity that existed in the low-permeability layer and because the cores were taken after DNAPL dissolution was complete, advection had carried the peak concentrations downgradient. As with BST2, the high levels of DNAPL saturation near the soil interface had occluded flow from that region. Thus, flow bypassing had occurred into the upper section of the source zone. Since there was no flow between the two soil layers, diffusion was the key transport mechanism for contaminant mass into the low-permeability layer. The highest saturation levels occurred between 0.75 cm and 1.5 cm above the soil interface. This contradicts the results from BST3 where this distribution of DNAPL seemed to encourage flow into the low permeability layer. However, the absolute values of the levels of DNAPL saturation at the soil interface were very different between BST3 and BST4. BST3 saturation levels ranged from 0.1 – 0.2, but BST4 levels ranged from 0.55 – 0.72. This suggests that the absolute level of DNAPL saturation at the soil interface is important to determining the transport mechanism into the low-permeability layer as well as the relative levels of DNAPL saturation throughout the source zone.

*Experiment 7: Small Tank Experiment 5 (BST5)*

This experiment used the same packing configuration and soil types as BST4. The goal of this experiment was to create a different distribution of DNAPL in the source zone, and then compare the results to BST4. A constant flow rate was desired. However, similar filter clogging issues as occurred with BST4 made this unattainable. Figure 54 shows the flow rate and effluent concentration versus elapsed time. Between three days and seven days after DNAPL injection, the flow rate varied from 3.43 L/day to 11.25 L/day. The head gradient was adjusted during this time in order to compensate for the clogging. Unfortunately, the adjustments to the head gradient over compensated for the clogging issue causing the wide range of flow velocities observed during this time. After seven days, the flow rate remained steady. The experiment was conducted for 14 days. Effluent sampling and soil coring for BST5 achieved recovery of 86 percent of the 1,1,2-TCA mass injected into the tank.
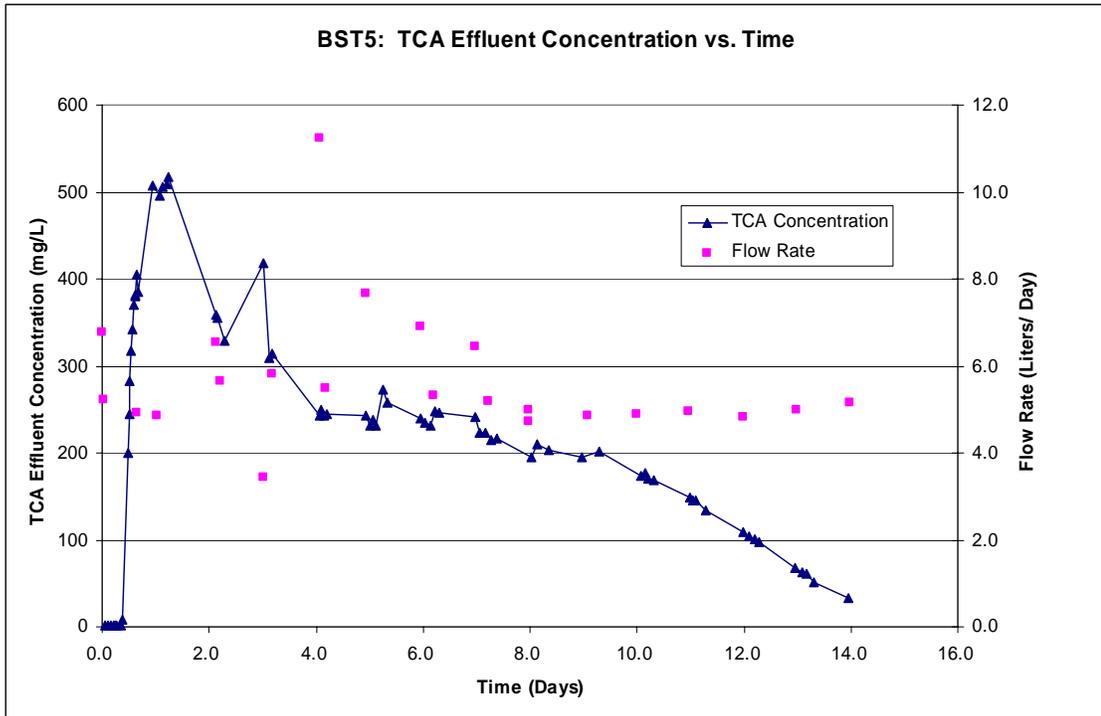
Figure 54 - Contaminant breakthrough and water flow rate for BST5

The DNAPL infusion and withdrawal procedure resulted in 19.32 grams of 1,1,2-TCA being injected in the tank. The DNAPL distribution within the source zone, as depicted via X-ray analysis, is shown in Figure 55. The level of saturation at the soil interface (between 0.40 – 0.54) was much greater than in the upper sections of the source zone.

The short transition zone between high levels of saturation and low levels of saturation suggests that flow bypassing of the lower source zone area may have been encouraged in this experiment. Indeed, that is what is shown in Figure where the effluent concentrations reached an initial peak during the bypassing of flow into the upper source zone area causing an enhanced dissolution rate. Then, after the upper source zone area was depleted of DNAPL, the effluent

concentrations declined quickly until day four when a slow decrease in concentration occurred. At day nine, the concentrations dropped more rapidly again signaling the approach of complete dissolution of DNAPL in the tank. For BST5, due to X-ray equipment problems, only an initial scan of the tank was performed. In order to determine when the DNAPL had dissolved completely, the breakthrough curve was examined as mentioned previously.
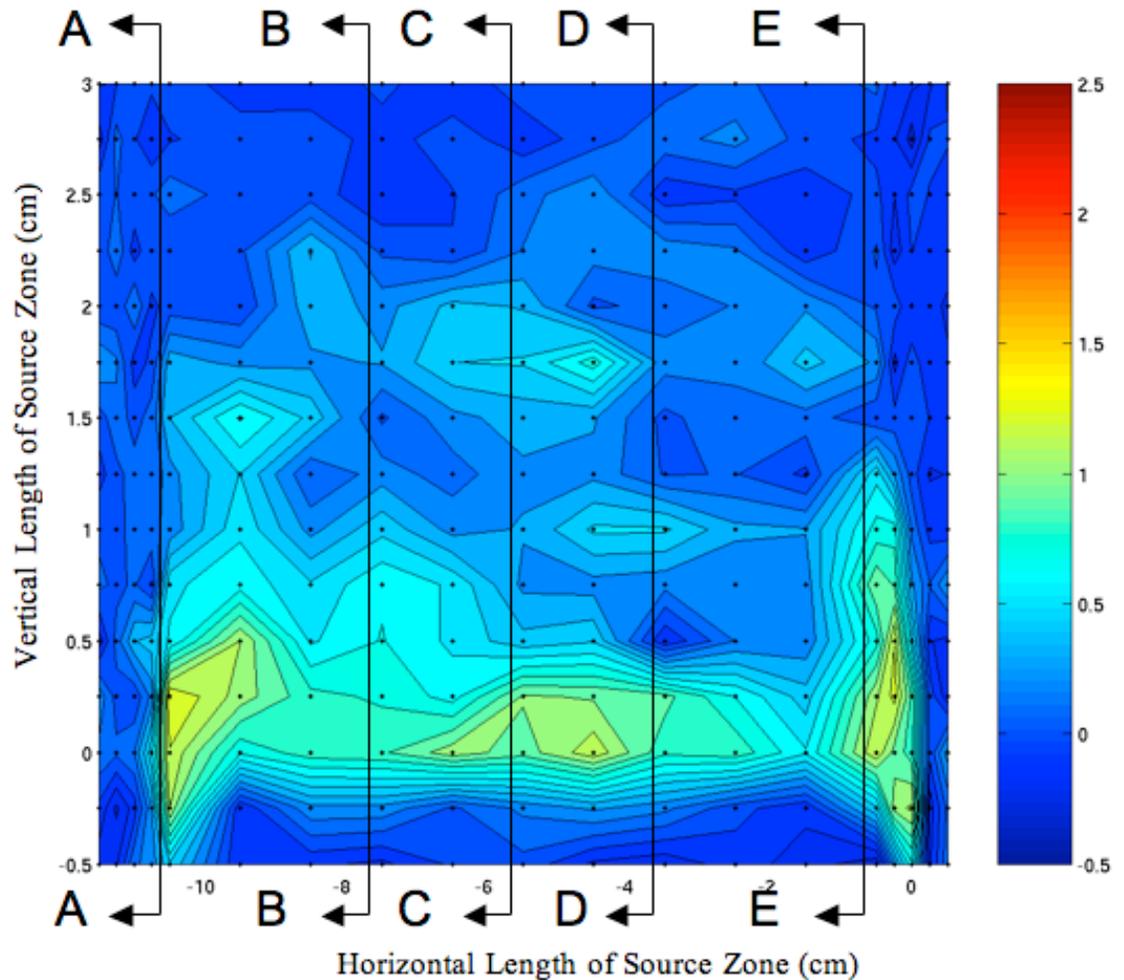


Figure 55 - DNAPL distribution after injection during BST5.

The DNAPL distribution for BST5 showed similarities to BST2 and BST4 with respect to the highest levels occurring at the bottom of the source zone and a wide range of saturation levels from top to bottom. However, BST5 also showed similarities to BST3 regarding the absolute levels of DNAPL saturation in the tank being lower than in BST2 and BST4. In order to analyze how both the relative and absolute levels of DNAPL saturation affected matrix storage, soil cores were taken. The results of the coring are shown in Figure 56.

The highest concentrations were seen at depths from 4.4 – 6.6 cm below the soil interface. This suggests that advection from the source zone into the low permeability layer played a key role in the contaminant transport. This is a similar observation to BST3. Therefore, this data suggest that the absolute levels of DNAPL saturation controlled the flow from the source zone into the low permeability layer. While the relative levels of DNAPL saturation were important regarding the flow field through the source zone, if high enough levels of saturation occurred at the soil interface, flow was not permitted to enter the low permeability layer. This was observed in BST2 and BST4.

Additionally, it is noted that the penetration depth within the low permeability layer of the peak concentration was lower (4.4 – 6.6 cm) in BST5 than in BST3 (5.5 – 7.0 cm). This may correspond to the lower permeability of the silt used in BST5 than the #140 sand used in BST3. However, the DNAPL distribution was complex and tank specific, so it is difficult to isolate and quantify the causes of the differences in vertical flow velocities through the source zone. Thus, only qualitative assessments can be made about the role of the hydraulic conductivities of the soils. However, the expected result was observed.
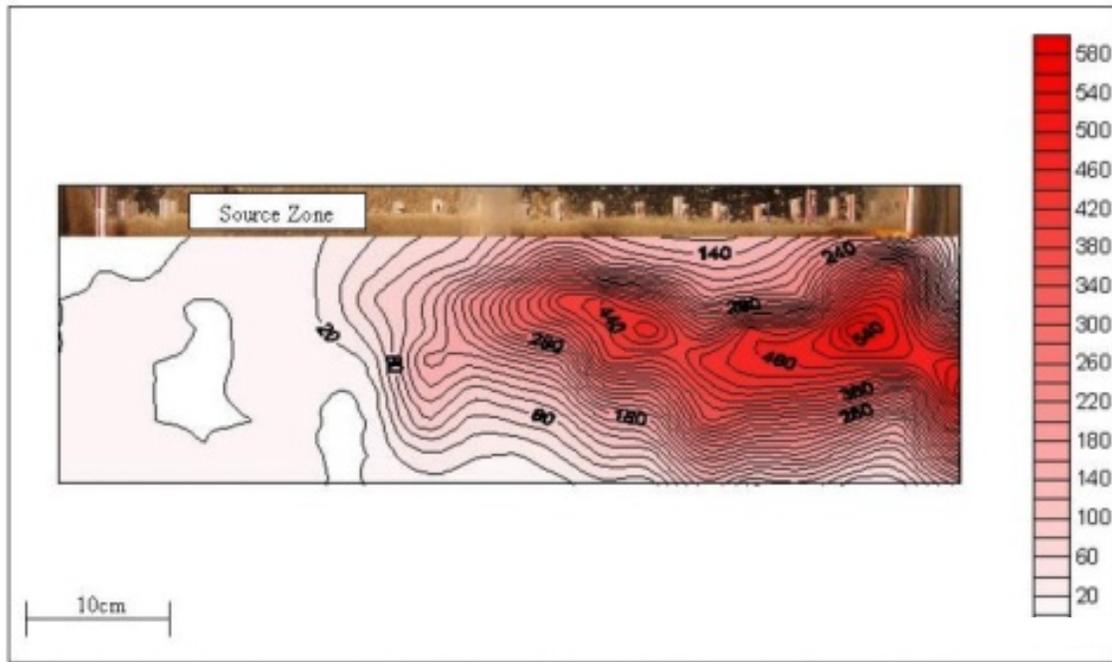
Figure 56 - Contoured results of concentrations (mg/L) from soil coring in NASFtW silt for BST5.  Note:  area shown is full extent of NASFtW silt in tank.

Powers et al. (1991) determined that the assumption of local equilibrium is valid for DNAPL dissolution for groundwater velocity in the range of 0.1 to 1.0 m/d.  In the small tanks, the flow velocity in the layer of low permeability near the source zone was much less than in the coarse layer (hydraulic conductivity of the NAS silt and #140 sand expressed as a fraction of hydraulic conductivity of #30 sand is 0.0055 and 0.0144, respectively.).  Thus, for the small flow velocities in the low permeability layer, it can be concluded that the local equilibrium assumption was valid for the dissolution of DNAPL from the source zone into the layer of low permeability.  An extension of this assumption is that the aqueous phase in the layer of low permeability at the interface with the source zone maintains a level of maximum solubility during the period of DNAPL persistence regardless of the DNAPL distribution in the source zone.  Therefore, although the four small tank experiments exhibited different DNAPL distributions, maximum solubility in the aqueous phase was achieved for all of them.  Excluding differences in DNAPL depletion times and the #140 sand versus the NASFtW silt, this condition of universal maximum solubility should have led to equivalent distributions of

104

dissolved contaminant in the layer of low permeability for each of the four experimental tanks.

However, the small tank studies provided experimental evidence that the distribution of DNAPL within the source zone impacted both the amount of contaminant mass that entered the low-permeability zone and the distribution of the contaminant mass within the zone.  Thus, it can be concluded that another transport process, advection, contributed to the distribution of the mass. Figure 57 compares the expected concentrations in the low-permeability layer estimated by solving the diffusion equation and the observations from coring in test BST3. The concentration in the low-permeability zone were estimated from soil cores extracted from a vertical plane 39.5 cm downgradient from the leading edge of the source zone, three days after DNAPL depletion.   Coring was done downgradient of the source as horizontal advection transported the contaminant within the low permeability layer.
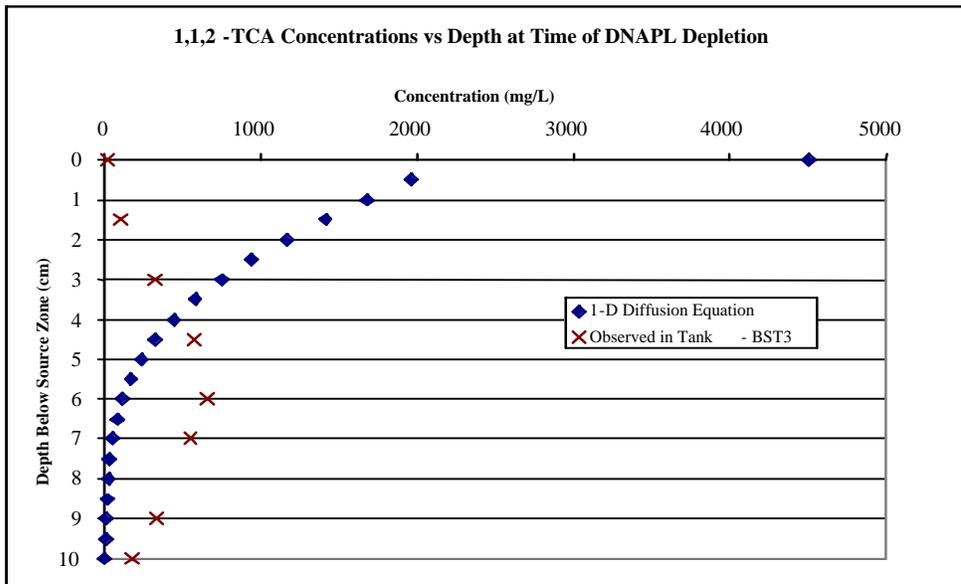


Figure 57  - Comparison of concentrations in low permeability layer for diffusion transport only versus observed results from one of the small tank experiments.

The observed concentrations deviated substantially from the theoretically determined values based on the assumption of diffusion-only transport due to the

contribution of advection that occur in the low permeability layer.  In BST3, the highest concentrations were observed 5.5 – 7.0 cm below the soil interface.  At this depth, the observed concentrations were five to six times greater than the predicted values providing additional verification that advection was occurring in the low permeability layer.  At greater depths, diffusion was the controlling transport mode, as can be seen from the data from both experiments.  The observed concentrations were still much higher than the predicted values because the increased concentrations at middle depths for the observed data produced a higher concentration gradient than for the hypothetical data.  The data also suggests that the dissolved mass transferring into the low permeability zone is influenced by advection in the low-permeability layer.

This supports the conceptual argument that changes in water relative permeability in the source zone caused by the presence of the DNAPL influenced the flow fields through the source zone, and hence the mass transfer to the low permeability zone.  The flow fields within the DNAPL entrapment zones created unique situations within each tank test settings that affected advection differently.

Areas of high DNAPL saturation caused flow bypassing, resulting in decreased dissolution.  Additionally as the DNAPL saturations within the DNAPL-entrapment zone is highest at the interface between the two, layers, resulting in transport into the low-permeability zone primarily by diffusion.  Conversely, a source zone that did not contain zones with sufficiently high DNAPL saturations to cause flow bypassing resulted in increased dissolution and advective transport of contaminant mass into the low permeability zone.

The dissolved mass transfer by advection into the layer of low-permeability layer was also limited by the low hydraulic conductivity of that layer.  The NASFtW silt had a hydraulic conductivity of approximately one-third of the #140 sand. Thus, it was more difficult for advection to transport contaminant as deeply into the silt as into the #140 sand.  This was validated by a comparison of the BST3 and BST5 soil coring data.   The BST3 (#140 sand experiment) produced higher

106

concentrations at depths 1.0 – 2.0 cm in the low-permeability zone than did BST5. Therefore, the hydraulic conductivity of the low-permeability layer is a key factor that determines how the dissolved contaminant is distributed. Zones with extremely low hydraulic conductivities such as clays or bedrock may prohibit advective transport. Conversely, fine sands or silts may allow for increased advection to occur, and thus may present a different dissolved mass distribution. Under real field conditions, additional factors, such as desorption rates and size and distribution of fractures would also need to be considered.

It is beyond the scope of the small tanks experiments to quantify the effects of the downstream back diffusion. This process is studied in the up-scaled experiments in the large tanks. Liu and Ball (2002) provided some similar data that frames the significance of this effect. In that study, plots similar to Figure 57 were presented that depicted sorbed concentrations of PCE versus depth for soil cores taken from two locations. One core showed no back diffusion effects, and the highest concentrations were observed at the interface with the aquifer. The other core displayed the effects of back diffusion. The peak concentrations in that core were observed at 10 cm below the interface with the coarse layer. However, at the Dover Air Force Base, DE, where the study was performed, the DNAPL source had been excavated 10 years prior to the coring. The peak concentrations had only shifted from the interface to a depth of 10 cm over a period of 10 years. In the research presented here, only three days had elapsed from DNAPL depletion to soil coring. Therefore, it is unlikely that back diffusion played a substantial role in the effluent contamination of the small tank experiments with the exception of the contaminant contained within the uppermost few millimeters of the low permeability layer. This is reinforced by the results of BST2 and BST4 where the peak concentrations were observed at the soil interface.

## 3.4 *Intermediate Two Layer Tank Experiments with DNAPL Sources*

The following describes intermediate scale experiments conducted at Colorado School of Mines.  The objective of intermediate scale tank experiments was to evaluate the phenomenon of matrix diffusion in a smaller test domain before the use of the Large Tank, thereby allowing preliminary experiments to be executed in less time, with less generation of waste, and with more accurate source zone characterization.  Two in-situ techniques are used to monitor DNAPL mass depletion from source zone during dissolution.  The first method uses gamma energy attenuation.  The second uses X-ray attenuation. In our past work, we have shown that the X-ray methods provide more accurate measurements compared to gamma.  As the goal of the experiments was to obtain accurate data on the source depletion and diffusion at the source (flux 2), the DNAPL mass depletion measurements in the intermediate-scale tanks were performed using the X-ray method.  The ability to accurately monitor the DNAPL mass remaining in the source zone provides us with a valuable experimental tool to keep track of the distribution of mass between DNAPL and dissolved phase within the test system.  The Intermediate Tank allowed for the testing and possible validation of a numeric model to be used for subsequent Large Tank experiments.

The clear polycarbonate walls of the test tank were lined with 3.2 mm (1/8 inch) glass in order to prevent any sorption of the source contaminant to the polycarbonate.  The groundwater flow across test aquifer was controlled using constant head reservoirs connected to the upstream and downstream ends of the test tank.  For the experiments performed, a head drop of 2.5 cm across the length of the tank was maintained to approximate groundwater flow velocities at the NASFtW site.

The first packing was a simple layered, heterogeneous configuration. This packing represented a situation where the DNAPL accumulates above the interface between coarse- and fine-sand layers due to capillary barrier effects or a pool formed at the aquifer-bedrock (or aquitard) interface. The bottom one third of the tank was packed with a finer #140 sand with a hydraulic conductivity of 4.32 m/day. The top two thirds of the tank was packed with coarser #30 sand with a hydraulic conductivity of 125 m/day. The top surface of the soil pack was sealed with clay to create confined conditions in the test aquifer and thus create a uniform flow field along its length.

The DNAPL source zone was created by injecting the test DNAPL (TCE or TCA) into coarse sand pocket at the interface of the two soil layers. The DNAPL was colored with Sudan IV red dye at a ratio of 0.0005 mg Sudan IV to 1.0 mg DNAPL for visualization through the transparent tanks walls. The exact mass of DNAPL that was placed was carefully monitored to determine the initial saturation.

The experiment involved measurement of effluent concentration during the dissolution of the emplaced DNAPL source. Aqueous samples were collected at the downstream end and analyzed using a gas chromatograph (GC) to determine solute concentrations in the tank effluent. During dissolution, the DNAPL mass depletion rate in the source zone was accurately monitored using an automated X-ray attenuation system. In order to obtain the data required to evaluate effluent aqueous concentration versus time from the DNAPL injection and to calculate the DNAPL mass that had dissolved and migrated out of the tank, many samples of the effluent had to be taken. Moreover, since the focus of the research was on the matrix storage capability of the soil under the packed test configuration (heterogeneity), each experiment was performed for many weeks in order to capture the data necessary to evaluate the significance of this process as represented by low concentrations in the long tail of the effluent breakthrough curve. Initially, a sample was taken every 20 minutes. This frequency continued for several days and was performed so that the initial breakthrough curve of the

dissolved contaminant could be well characterized. After the initial breakthrough curve was captured, sampling frequency decreased over a period of seven to ten days until samples were only taken two or three times a day. The low sampling frequency was sufficient to capture the slow, relatively steady, effluent concentrations that were observed during the long process of the release of the contaminant mass that had been stored in the low permeability region of the soil matrix.

The data on mass depletion in the source zone and the cumulative effluent mass as determined from the solute breakthrough curves were used to determine the mass that remained within the test system. As the sandy soils used in these experiments were non-sorptive, the long-term mass accumulation within the test system was fully attributed to matrix diffusion.

## 3.5   *Large-Scale Two Layer Tank Experiments with DNAPL Sources*

The large tank experiments are a continuation of the small tank work by Wilking, 2004, adding further analysis of the processes that occur downstream of the source zone as the plume develops. The work performed by (Wilking, 2004) allowed for an accurate description of the processes that were occurring at and around the source zone. It must be noted, that the goal of the large tank studies is not to mimic field conditions, but rather to create conditions to capture the governing processes that occur in the field that contribute to plume loading and longevity. Once the basic mechanisms first studied in small test systems and then up-scaled to large-scale laboratory setting are understood and quantified, it is then possible to incorporate this knowledge into numerical models that may then be applied to field setting. In the field, much more complex manifestations of these processes occur as controlled by site specific spill conditions, entrapment architecture of the DNAPLs, and the natural geologic heterogeneity.

3.5.1 Objectives

Based on a review of the field lithology by Parsons (1998) (example shown on Figure 58 [Cross Section A-A, East Parking Lot Model]) three dominant subsurface morphologies to define the low-permeability zone geometries in large tank testing were identified (see Figure 59): (1) a sand layer overlaying a horizontal low-permeability layer of silt, (2) a mound of silty soil within a sandy formation that intercepts the dissolved plume, and (3) an inclined layer of silty soil that produces a converging flow field within a sandy layer.
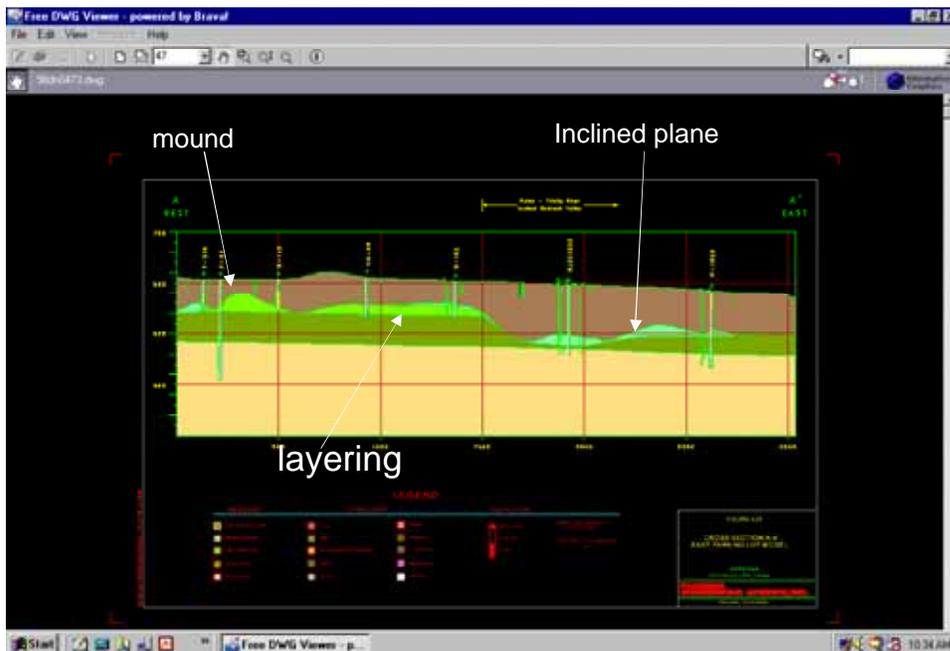


Figure 58 - Example morphologies observed in the field.
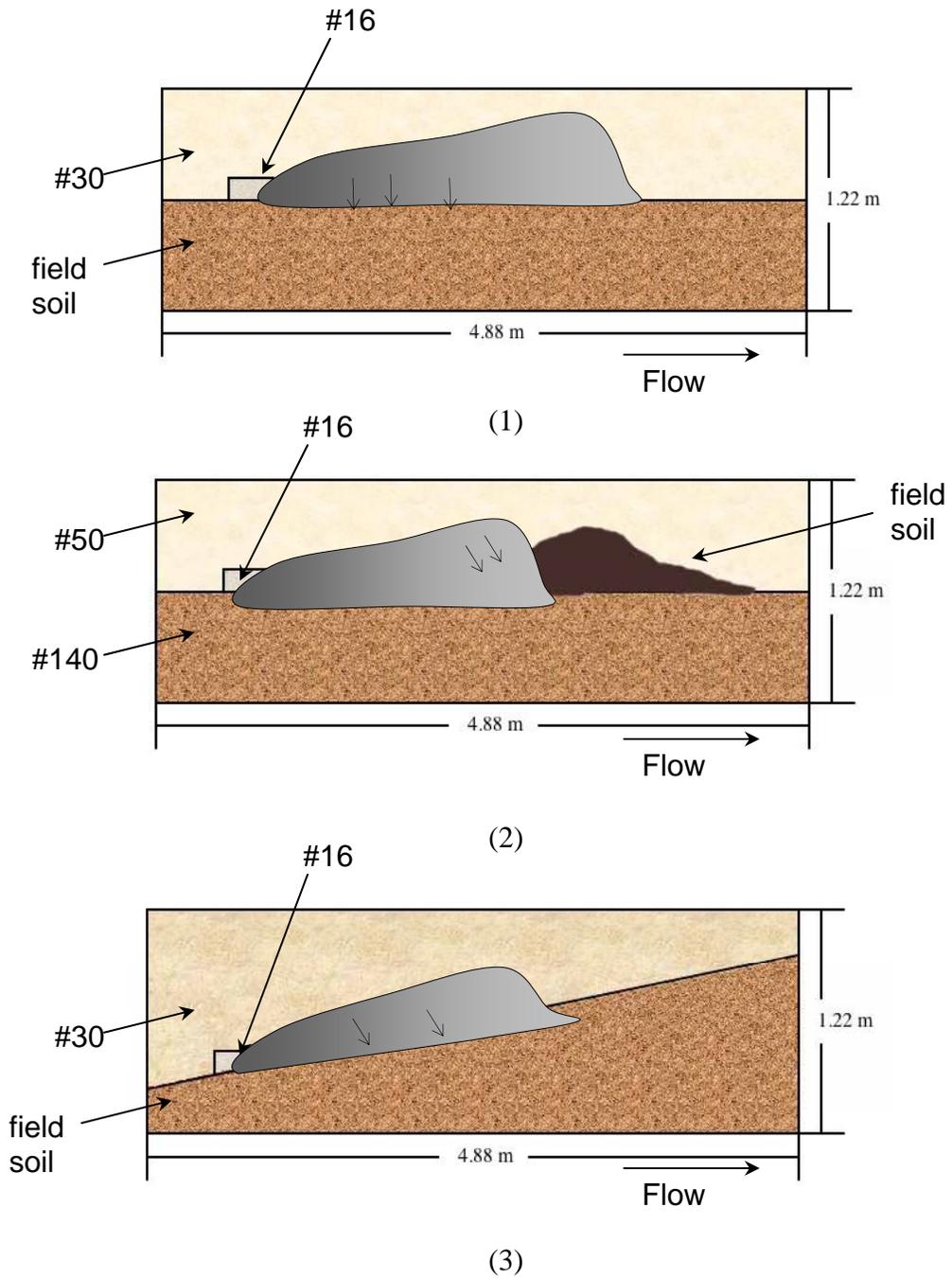
Figure 59 - Intermediate scale tank configurations: (1) a sand layer overlaying a horizontal low permeability layer of silt, (2) a mound of silty soil within a sandy formation that intercepts the dissolved plume, and (3) an inclined layer of silty soil that produces a converging flow field within a sandy layer.

In the first packing configuration, the primary mechanism through which the dissolved mass enters the low permeability horizontal layer is through molecular diffusion only, as there is no velocity component normal to the interface that produces advective flux. In the second case, the mound intercepts the plume and as there is a velocity component normal to the interface between sand and silt, both molecular diffusion and advection contributes to mass transfer into the silt. The final configuration captures the mechanisms associated with a case where a non-uniform velocity field in the sand layer resulting in both advective and diffusive flux contributing to the mass transfer into the low permeability formation. This case will capture the process of mass transfer into low permeability zones when the plume migrates preferential through high permeability zones while interacting with the low permeability formations.

These three distinct morphologies were studied independently in three separate large-scale tank experiments. The goal is to generate data sets to validate numerical models simulating these three distinct morphologies could be combined at a field scale and incorporated into the domain of a three-dimensional numerical model.

In order to best understand the fundamental processes that were occurring in each experiment, it was critical to obtain a complete and accurate mass balance. Mass balance was evaluated by monitoring the following: (1) the mass leaving the tank with the effluent (2) the total DNAPL mass placed in the source zone and the time at which the total emplaced mass has dissipated through dissolution and (3) the mass of dissolved contaminant from the plume absorbing into silt.

### 3.5.2 Methods

The large-scale tank with a total length of 4.8 m (16 ft) used in the experiments was constructed using four pre-fabricated wall units. Each section measured 2.4 m in length by 1.2 m in height. The tank walls were lined with plate glass to prevent DNAPL chemically interacting with the polycarbonate wall surface. Two

water supply reservoirs connected to the upstream and downstream ends of the tank were used to control the groundwater flow gradient across the tank.

The tank was dry packed in 7.6 cm lifts with a 7.6 cm bentonite layer placed on the bottom and top of the permeable soils to create confined flow conditions in the tank. A coarse sand inclusion to inject the DNAPL to create a source was packed by placing aluminum plates spaced apart to obtain the exact dimensions of the source. After placing the coarse sand, the spacers were lifted slowly allowing the surrounding finer soil to settle around the inclusion. The sharp transition between the coarse and the fine sand was used to create a capillary barrier to contain the DNAPL.

### 3.5.2.1 Creation of DNAPL source zone

An injection line for DNAPL placement was installed at the midpoint of each coarse inclusion. The injection line consisted of a thin diameter glass tube attached to thin-walled GC capillary tubing that was inserted through the top soil surface (this avoided the need to drill holes on the glass wall). The tank was saturated for approximately two to three weeks to achieve steady-state flow conditions prior to DNAPL injection.

The same process of DNAPL injection was used in all large tank experiments, irrespective of the size and location of the source. A 10 ml syringe attached to the end of the capillary tubing through a three-way valve was used to extract 2 ml of water from the source area in order to completely fill the GC tubing with water. A known volume of the test DNAPL (1,1,2-TCA) dyed with 0.05% Sudan IV dye was placed in the source zone using the injection tube. The injection was done at very low rates at approximately two-minute time steps to prevent unstable fingering developing at the capillary barriers containing the DNAPL source within the coarse sand inclusion. Water was injected into the tubing to purge any remaining 1,1,2-TCA in the injection line. By keeping track of the volumes of total injection and withdrawal it is possible to determine the exact initial saturation

of DNAPL within the source zone.  After the placement of the source and during the experiment the DNAPL source zone was continuously scanned with the X-ray system to monitor the DNAPL source depletion through dissolution.

### 3.5.2.2    Effluent Sampling and Discharge Measurement

Effluent samples were gathered to determine the dissolved mass flux leaving the tank.  Once an injection occurred, the effluent end of the tank was sampled on a daily basis.  The required frequency was determined after the conclusion of the first large scale tank experiment. The time variation of breakthrough concentrations suggested that one sample per day was adequate to capture the plume behavior and to conduct mass balance analysis.  The dissolved DNAPL concentrations in the effluent were determined using a gas chromatograph with flame ionization detector.   The groundwater discharge through the tank was estimated by collecting the effluent in a 5-gallon bucket, and recording the weight accumulation as a function of time.

### 3.5.2.3 Soil Excavation and Coring

Upon the conclusion of each tank experiment, the low permeability formation created using the field soil was cored and analyzed to determine solute mass using a hexane extraction technique, similar to that performed by (Wilking, 2004).  After the effluent concentrations had reached a value that was determined to be low enough to conclude the transport experiment, the water level in the tank was lowered to be above the elevation where the cores were to be extracted.   The goal was to keep the core saturated without draining the dissolved mass.  A 5.0 cm deep layer of soil was then removed using a spade to reach the sampling location.  An aluminum plate with evenly spaced 1 cm holes was placed on the excavated soil surface to use as a template for sampling.   Drinking straws (approximately 20.3 cm long and with a 3 mm internal diameter) were then inserted through the holes on the template to penetrate the soil.  A spade was then used to dig under the straws and carefully remove them in pairs, care taken not to disturb the soil core contained in the straws. This method of sampling was

continued until the required depth of sampling was reached. After each layer excavation, the straws were kept frozen until testing to avoid mobilization of the water within the straw.

Once the material in the straws had been frozen, the straws were removed from the freezer and cut into 1 cm lengths. The field material was then extracted from each 1 cm section of the straw into a 3 ml vial that contained 2 ml of hexane. The samples stayed in the hexane for a period of 24 hrs in the refrigerator, where then a 2 ml aliquot was taken and injected into a 2 ml gas chromatograph vial with zero headspace. The extracted samples were then analyzed using the electron capture detector on a gas chromatograph for 1,1,2-TCA content. Knowing the mass of hexane and the mass of soil and assuming a density of water, calculations of the total mass (liquid + adsorbed) of 1,1,2-TCA in each sample were performed.

### 3.5.2.4    Methodology Specific for each Large Tank Experiment

Because of the differences in the packing configuration in each of the three tank experiments, some of the testing methods had to be varied from tank to tank. The specific methods that were used are presented below.

**Large Tank Experiment #1 -** As shown in Figure 60, the packing configuration in this tank consisted of horizontal layers of #30 white silica sand overlying a field soil obtained from the NASFtW Site (See Table 6 for properties).

Figure 60 - Large Tank Experiment #1- horizontal layers.

Table 6 - Soil properties.

| Media Type | Hydraulic conductivity (cm/day) | Retardation factor | Mean grain size (mm) | Uniformity coefficient |
|---|---|---|---|---|
| #30 sand | 15,000 | 1.0 | 0.49 | 1.5 |
| Field soil | 2,000 | 1.4 | 0.38 | 3.0 |

As is shown in Table 6, the contrast in hydraulic conductivities of the two soils was approximately one order of magnitude. The tank was packed with a 5.1 cm bentonite layer to seal the tank bottom, followed by a 30.5 cm layer of the field soil and a 71.1 cm layer of #30 sand. A 5.0 cm thick bentonite clay layer was packed at the top of the tank to establish confined aquifer conditions and to prevent volatilization of contaminants. The emplaced DNAPL source zone consisted of a 5.1 cm x 5.1 cm x 5.1 cm coarse inclusion of #16 silica sand.

After achieving steady-state flow conditions along the tank length, approximately 14.82 g of Sudan IV dyed 1,1,2-TCA was injected into the source zone. The emplaced saturation of the DNAPL in the source zone was estimated to be 34%, by gravimetric analysis. Liquid samples were collected from the effluent end of the tank until no significant change in concentration occurred (8 ppm +/- 2.5 was observed for 40 days). Flow to the tank was then stopped and the field soil layer was cored and approximately 400 samples were analyzed.

**Large Tank Experiment #2 -** The second experiment was conducted in the same tank used in the first large-scale tank experiment. The packing configuration consisted of a low permeability mound (field soil) embedded in a high permeability matrix (#50 sand). The high permeability formation overlaid a lower permeability #140 sand layer. The source was created in a #16 sand inclusion placed upstream of the silt mound, at the interface of the #140 sand layer (see Figure 61).



Figure 61 - Large Tank Experiment #2.

The material properties of the soils used in this experiment are shown below in Table 7.

Table 7 - - Soil properties

| Media Type | Hydraulic conductivity (cm/day) | Retardation factor | Mean grain size (mm) | Uniformity coefficient |
|---|---|---|---|---|
| #140 sand | 389 | 1.0 | 0.10 | 1.86 |
| #50 sand | 3,480 | 1.0 | 0.31 | 1.94 |
| #16 sand | 50,900 | 1.0 | 0.96 | 1.73 |
| Field soil | 2,000 | 1.4 | 0.38 | 3.0 |

The tank was packed in the same manner as what was done for the first experiment. The flow in the tank was allowed to reach steady-state conditions prior to injection. Approximately 59.6 g of 1,1,2-TCA were injected into a #16

sand inclusion with the same dimension source zone as was used for the first experiment. The resulting average 1,1,2-TCA saturation was estimated to be 42%.

**Large Tank Experiment #3 -** For the final large scale tank experiment, a second tank was constructed to be placed on the testing platform of the X-ray machine. The X-ray system was used for the in-situ monitoring of the source during dissolution. The packing configuration included an inclined low permeability layer (field soil) beneath a high permeability (#30 sand) layer (see Figure 62).



Figure 62 - Large Tank Experiment #3

The soil properties were the same as for what was described for the large tank experiment #2. The field soil was packed at a 12% incline from the upstream end of the tank to the downstream end. The #30 sand was packed on top of the incline. The #16 coarse sand inclusion for the DNAPL emplacement was created at the inclined interface of the #30 sand and low permeability layer

After achieving steady-state flow conditions, approximately 35.43 g of 1,1,2-TCA was injected into the tank. The 1,1,2-TCA saturation in the source zone was estimated to be 22%. Immediately after injecting the 1,1,2-TCA into the tank, the X-ray scanning was started. For approximately 26 days (24 hours a day, 7 days a week), the source was scanned over 750 points. Five pressure readings were

also taken from the tank over a period of 24 hrs at various locations within the domain with the goal of calibrating a flow model.

3.5.3 Results

*3.5.3.1 Large Scale Tank Experiment #1*

An in-situ source monitoring system was not available for this experiment. Hence, as a similar DNAPL source configuration was used, results of the small tank by (Wilking 2004) were used to assume that the source zone had completely dissolved after approximately 14 days.  The measured concentrations of dissolved DNAPL in the effluent are shown in Figure 63.  The breakthrough concentrations display long tailing, indicating non-ideal behavior, i.e., a non-constant value of dispersivity.  It is also interesting to note that in this simple test configuration, even after 80 days, the 1,1,2-TCA concentration in the effluent is at 8 ppm, which is significantly higher than the USEPA maximum contaminant level (MCL) for 1,1,2-TCA of 5 ppb.
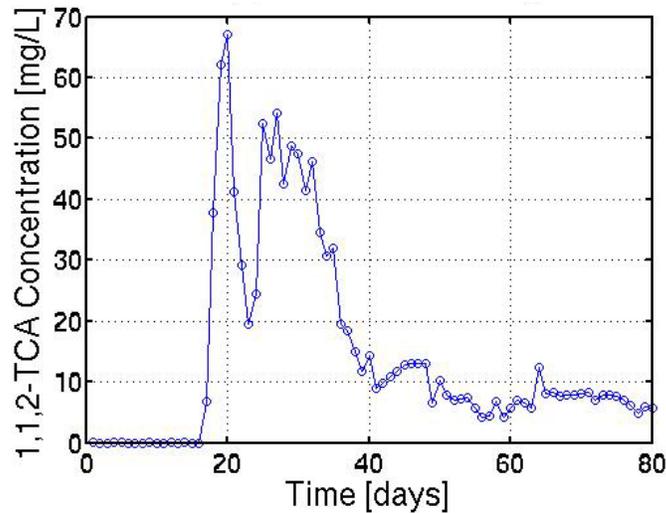


Figure 63 -Tank #1 1,1,2-TCA effluent curve.

As is shown in Figure 64, at 80 days, 80% of the emplaced 1,1,2-TCA mass appeared in the effluent, leaving 20% of the mass still within the soils.
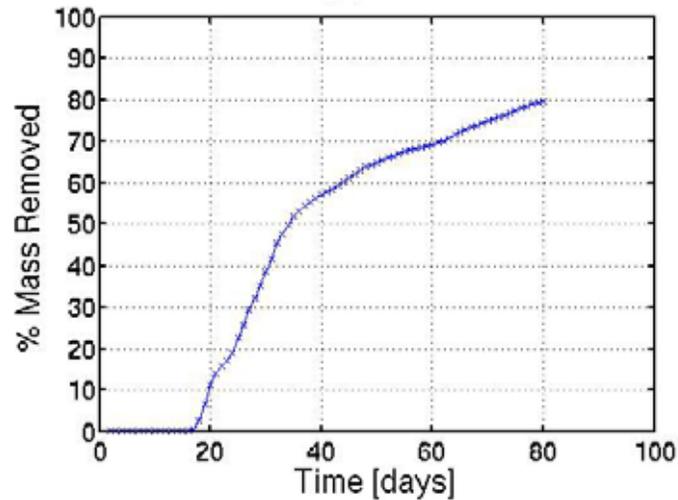
Figure 64 - Tank #1 -1,1,2-TCA mass removed from tank through the effluent.

A contour map of the concentration of dissolved TCA in the silt layer determined through coring as given on Figure 65 shows how the mass that remained in the soil is distributed. The center of mass of concentration distribution is located towards the end of the tank, indicating the dissolved mass has advected through the silt. It is also possible that the lower concentrations close to the source is due to some of the mass diffusing back into the sand. The data supports the hypothesis that the lower conducting layer will act as a new contaminant source acting over the length of the entire layer. The longer tank lengths allowed for the up-scaling of this back diffusion process to larger scales where the plume length becomes a factor that contributes to matrix storage and back diffusion. The findings of this test answer the question on why contamination in groundwater wells at field sites is still observed, even after the source is known to have been depleted or removed (see Section 2.6).
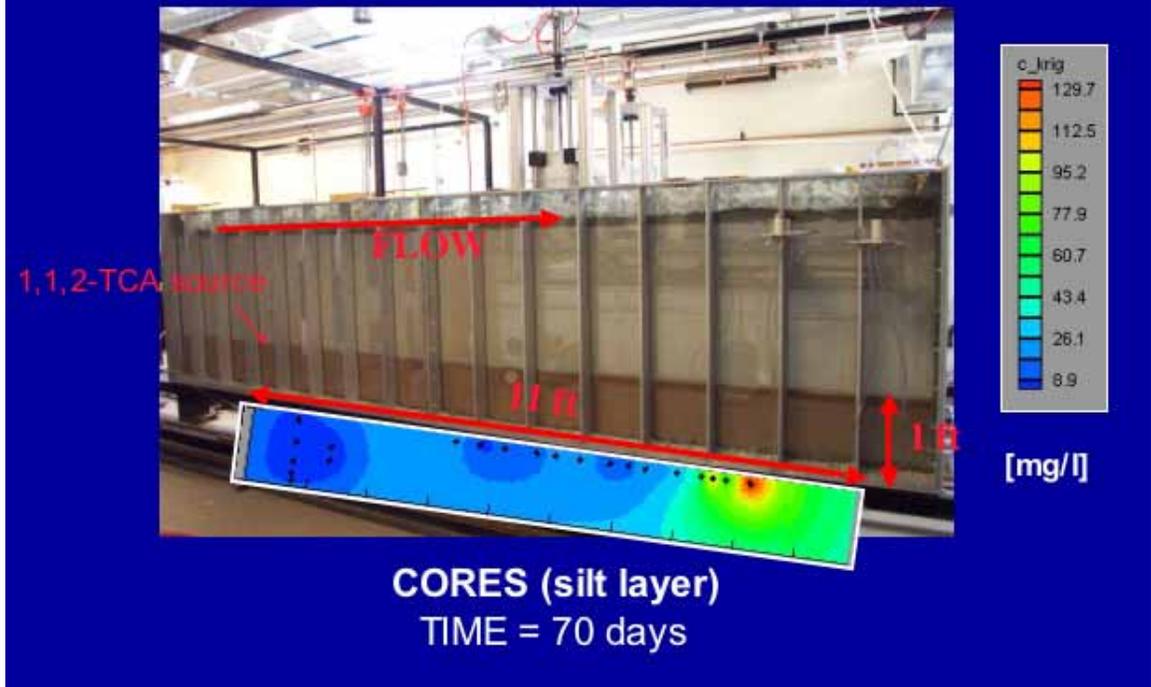
Figure 65 - Tank #1 1,1,2-TCA soil core results.

### 3.5.3.2.  Large Scale Tank Experiment #2

In this experiment, the process of mass transfer into low permeability zones and rebound both through molecular diffusion and advection was evaluated. Figure 66 shows the breakthrough curve of the effluent concentration after approximately 80 days into the dissolution experiment.  The area of the interface between the high and low permeability formations in this experiment was 550 $cm^2$, that is much lower than the value of 1680 $cm^2$ in the first experiment.  A comparison of the breakthrough curve of this experiment with that of the first experiment suggests high attenuation of the dissolved mass.  Hence, this increased mass attenuation even with a lower interface area can be attributed to the advection contributing to the mass transfer into the silt.
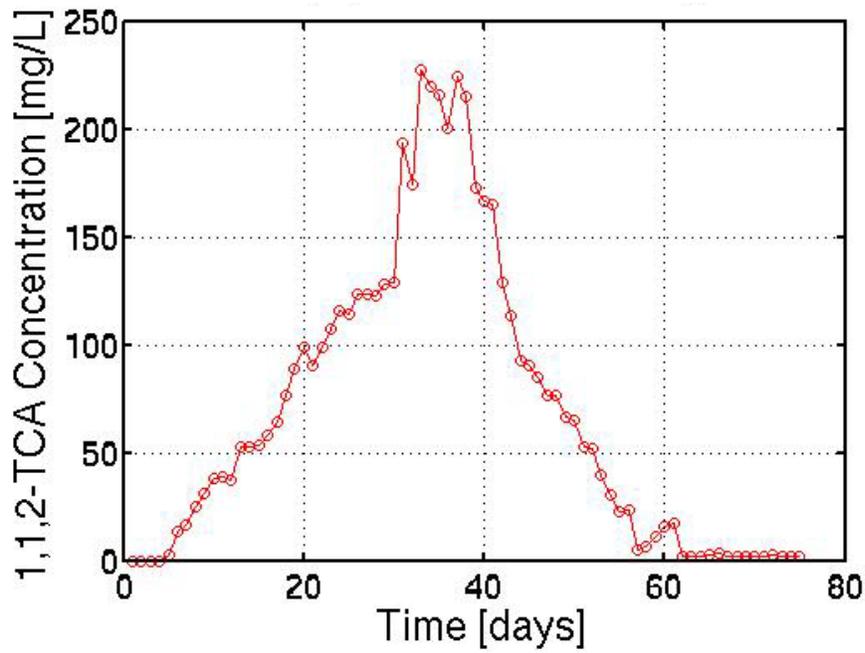
Figure 66 - Tank #2 1,1,2-TCA effluent curve.
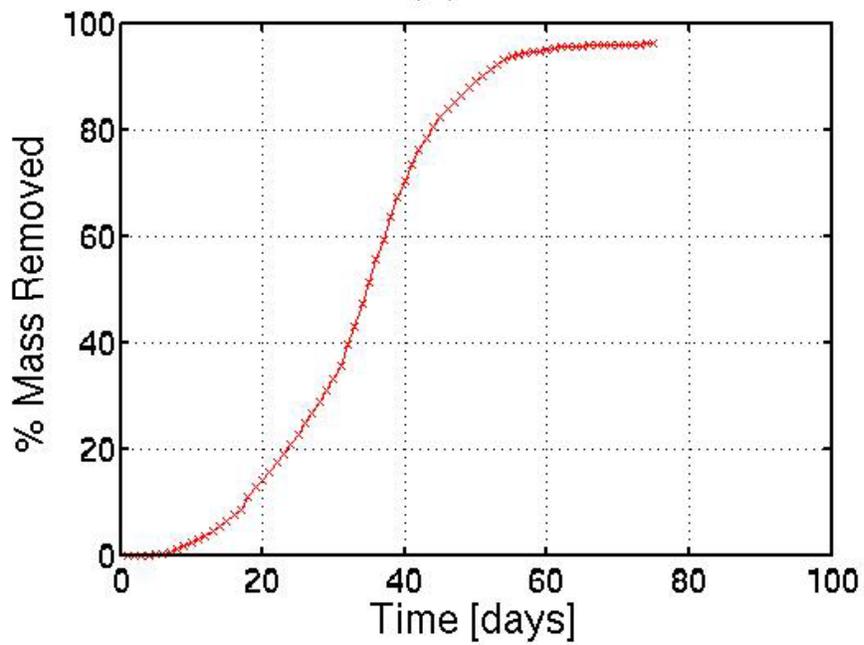


Figure 67 - Tank #2 1,1,2-TCA mass removed from tank through the effluent.

A plot of cumulative mass removal (Figure 67) shows almost 97% mass was removed from the system at the completion of the experiment. This data again suggests that the advection contributes to efficient removal of mass from the low permeability silt formation. In summary, this experiment showed that even a small fraction of low hydraulic conductivity material could affect the low permeability zone mass storage and rebound. In addition, these results suggest that the morphology of distribution of the low permeability material with respect to the source location has an impact on the plume longevity.

*3.5.3.3 Large Scale Tank Experiment #3*

The setting of this experiment introduces much more complex flow configuration and larger interface area between the two high and low conductivity zones. The X-ray system also provided accurate data on the dynamics of the source during dissolution. Figure 68 a and b show the configuration of the source zone immediately after injection of 1,1,2-TCA and at day 28, as monitored using the X-ray system. The figure shows the saturation of the DNAPL as captured by the X-ray. The source was not completely dissolved at 26 days, but the X-ray scanning had to be stopped due to a leaking roof near the X-ray power supply. Extrapolation of the data provided an estimate of complete mass depletion at 28 days.
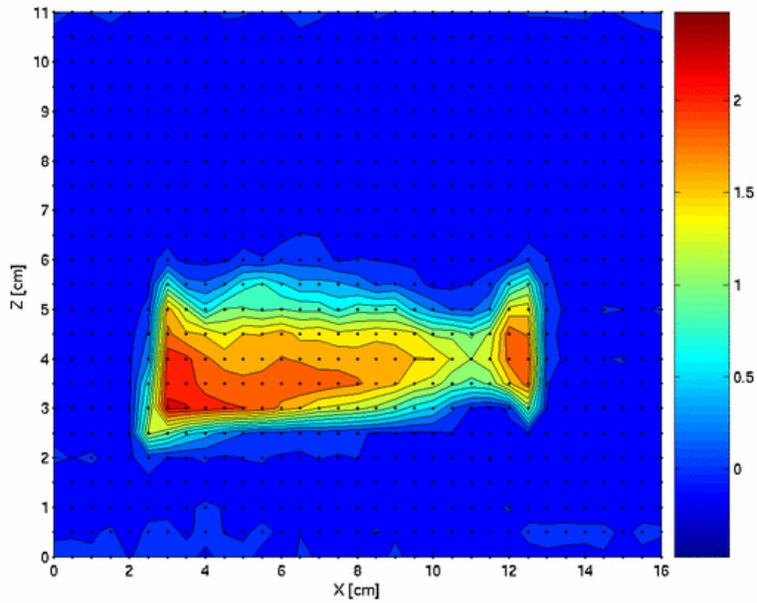
(a)
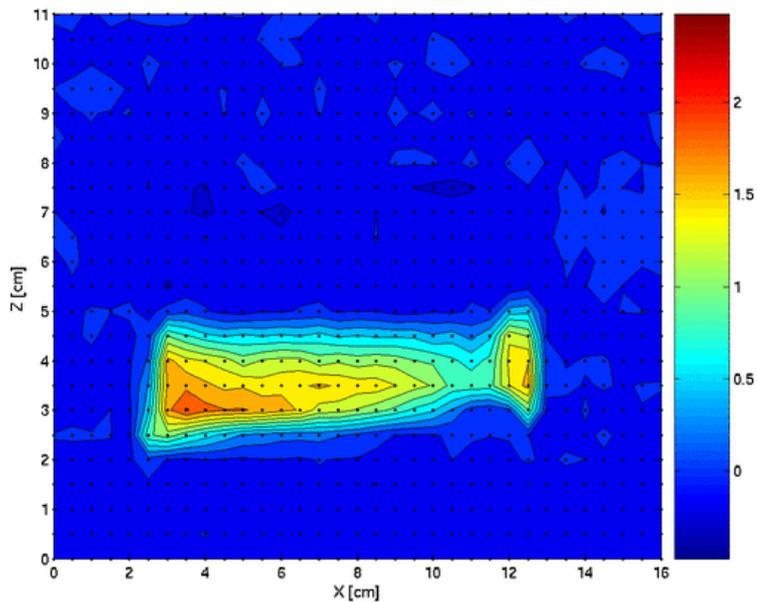


Figure 68 - a and b show the saturation of the source zone at day 1 (a) and day 28 (b). The higher the path length, the greater the saturation of 1,1,2-TCA. Flow is from left to right

The breakthrough concentrations in the effluent are shown in Figure 69. The inclined interface between the high and low permeability layers has a pronounced effect on the shape of the breakthrough curve. The significant effect

of how the low permeability formation affects the plume is demonstrated again in this experiment. Even though the DNAPL source was completely depleted in 28 days, even after 165 days, the concentrations are still at relatively high values (from maximum of 22 mg/L to 12 mg/L). The cumulative mass removal as a function of time is shown in Figure 70. Approximately 96% of the mass was removed for the duration of this experiment. It is interesting to note the amount of attenuation that has occurred due to the inclined plane in comparison with the first two experiments. The field soil layer that constituted the inclined plane for this experiment has been cored and the analyses are underway.
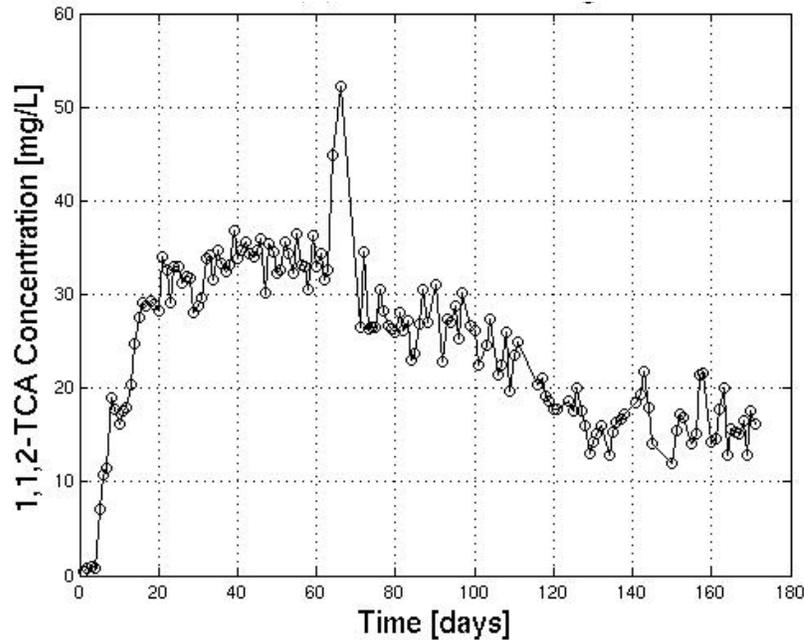


Figure 69 - Tank #3 1,1,2-TCA effluent curve.
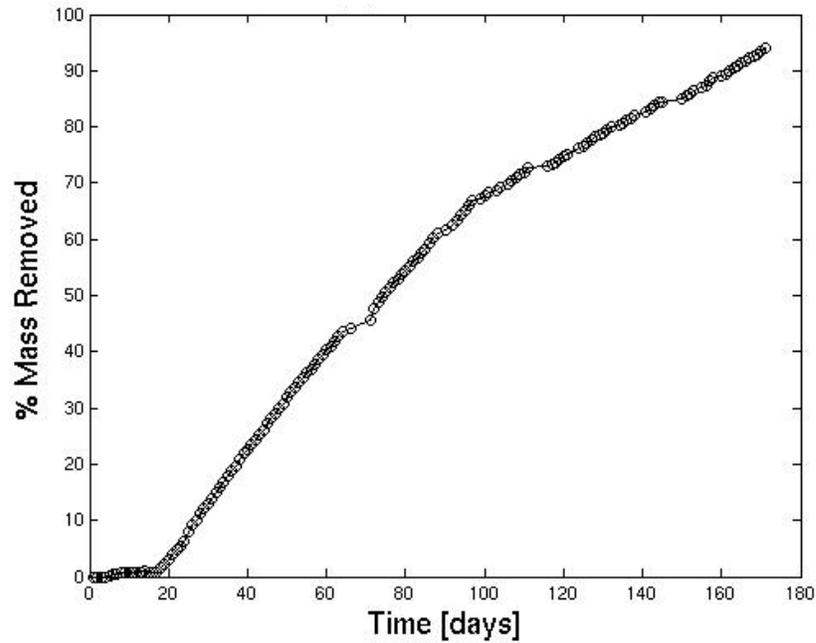
Figure 70 - Cumulative 1,1,2-TCA mass removed from Tank #3.

In order to compare and contrast the effects that each morphology had on the amount of mass released from the system, the mass remaining in each domain from all three large tanks experiments was normalized and plotted in Figure 71.

**Normalized 1,1,2-TCA Mass in Domain for all Large Tank Experiments**
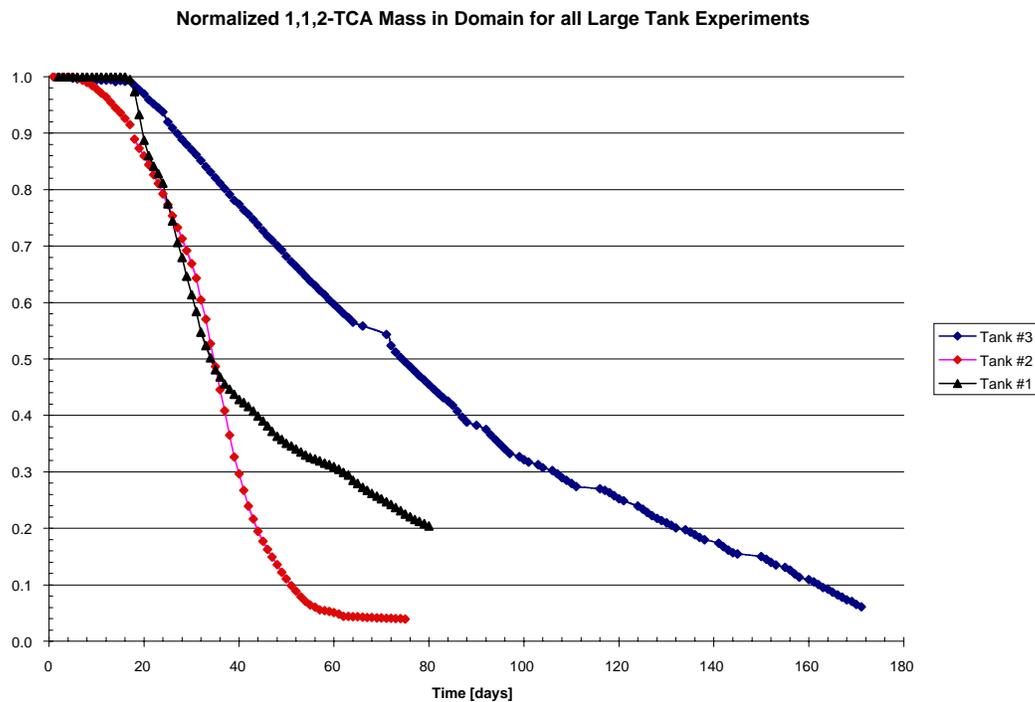


Figure 71 - Normalized Mass in Domain for Large Scale Experiments.

In Tank #1 the 1,1,2-TCA in the source zone had completely depleted in 14 days. Both in Tanks #2 and #3, the source depleted in approximately 30 days. These are important points on these graphs, as they represent the transition time before which most of the dissolved mass in the plume is generated in the source zone. After this time, the mass observed in the each tank is a result of the stored mass in the plume.

## 3.6 Summary of Results from Laboratory Studies

The results suggest that the processes identified in Section 2 are critical to understanding the benefits of DNAPL source control measures. The completion of the tank studies has provided data needed to rigorously document governing processes and test our methods (models) for a priori analyses of the benefits of source control measures.

## 3.7 References

Illangasekare, T. H., E. J. Armbruster III, and D. N. Yates, 1995. Nonaqueous phase fluids in heterogeneous aquifers – experimental study. *J. Environ. Eng.*, 121(8): 571-579.

Liu, C., and W. P. Ball, 2002. Back diffusion of chlorinated solvent contaminants from a natural aquitard to a remediated aquifer under well-controlled field conditions: predictions and measurements. *Groundwater,* 40(2): 175-184.

Parker, B.L., R.W. Gillham, and J. A. Cherry, (1994), Diffusive Disappearance of Immiscible –Phase Organic Liquids in Fractured Geologic Media, Journal of Groundwater, Vol. 32, No.5.

Parker, B.L., J.A. Cherry, and R.W. Gillham (1996) "The effect of Molecular Diffusion on DNAPL Behavior in Fractured Porous Media", Chapter 12 in <u>Dense Chlorinated Solvents and Other DNAPLs in Groundwater</u>, J.F Pankow and J.A. Cherry, Editors. Waterloo Press, pp. 355-393.

Parker, B.L., D.B, McWhorter, and J.A. Cherry (1997) Diffusive Loss of Non-Aqueous Phase Organic Solvents from Idealized Fracture Networks in Geologic Media, Ground Water, Vol. 35, No 6. Pp. 1077-1088.

Parsons Engineering Science, Inc. Report on the Geology of Air Force Plant 4 and Naval Air Station Fort Worth Joint Reserve Base Fort Worth, Texas. 1998.

Poulson, Mette, M. and Kueper, Bernard, H. (1992). "A Field Experiment to Study the Behavior of Tetrachloroethylene in Unsaturated Porous Media". Environmental Science and Technology, Volume 26, No. 5, pp. 889-895.

Powers, S. E., C. O. Loureiro, L. M. Abriola, and W. J. Weber Jr., 1991. Theoretical study of the significance of nonequilibrium dissolution of nonaqueous phase liquids in subsurface systems. *Water Resour. Res.*, 27(4): 463–477.

Sale, T and D.B. McWhorter, (2001), Steady-State Mass Transfer from Single Component DNAPLs in Uniform Flow Fields, Water Resources Research, Vol. 37, No. 2, Pp. 393-404.

Sudicky, E.A., R.W. Gillham, and E.O. Frind (1985), Experimental Investigations of Solute Transport in Stratified Porous Media 1) The Non Reactive Case, Water Resource Research Vol 21, No. 7, pp. 1035-1041.

Sudicky, E.A., R.G. McLaren, and J. VanderKwaak (1993) Characterization of contaminant migration processes in fractured geologic media and numerical simulation of pump and treat remediation. Progress Report on Project No. 596G, Ontario Ministry of the Environment, March 8.

Wilking, B.T. 2004. Factors controlling matrix storage during DNAPL mass depletion in heterogeneous porous media. Master's Thesis. Colorado School of Mines.

Wilson, J.L., S. H. Conrad, W.R. Mason, W. Peplinski, and E. Hafgan, (1990), Laboratory Investigations of Residual Liquid Organics from Spills, Leaks, and the Disposal of Hazardous Wastes in Groundwater. EPA/600/6-90/004. April.

# 4.0    Modeling

The following describes models developed through this project to describe processes governing emissions from subsurface sources.   This builds on the concepts introduced in Section 2 and the laboratory studies described in Section 3.  This work constitutes a critical step in developing tools for *a priori* analyses of the efficacy of source treatment.

Section 4.1 describes analytical methods. Analytical solutions are a good starting point in that they provide exact solutions and, in general, are computationally simple to apply.  Results provide an important expansion of our understanding of processes introduced in Section 2 and a basis for proceeding to numerical models.   In addition, exact analytical models provide a basis for testing approximate solution models that are based on numerical solutions. The primary limitation of analytical solutions is that they can only be applied to highly idealized situations that often fall short of true field conditions.

Section 4.2 describes numerical methods.   Numerical methods provide approximate solutions to governing equations with the advantage that they can be applied to more complex systems.   Although, data and computational requirements of traditional numerical methods for field scale problems may be prohibitive.  Both the advantages and limitations of numerical method models are considered in this section.

Section 4.3 describes the multiple layer developments.  Detailed discussion on the topic is covered in Appendix C.

## 4.1    Analytical Solutions

The following presents quantitative estimates of the "Simple Case" contaminant fluxes introduced in Section 3.  These fluxes are reintroduced in Figure 72 and described below.
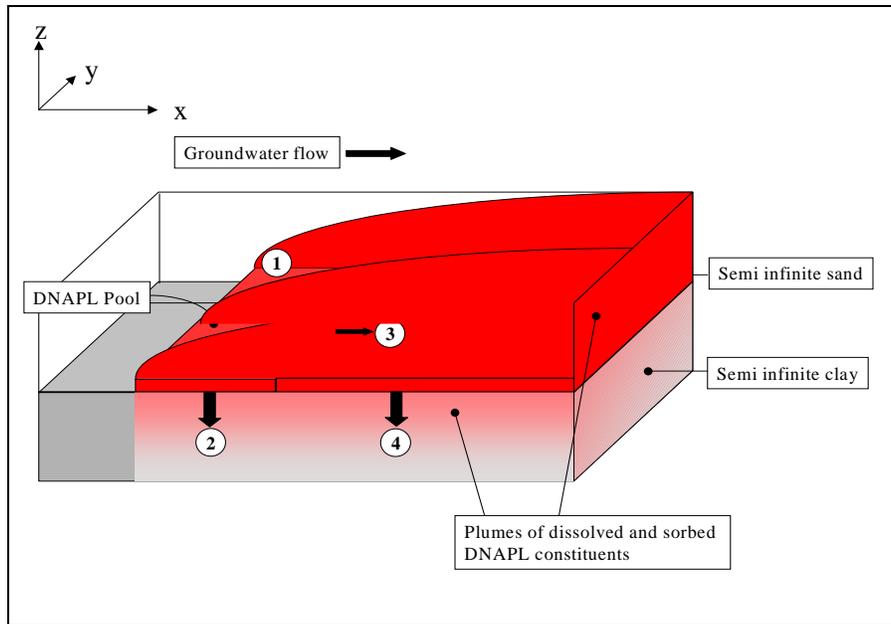
Figure 72 - The simple case – DNAPL perched on a capillary barrier

## 4.1.1 Fluxes 1, 2, and 3

Table 8 presents analytical solutions for fluxes 1, 2 and 3 where:

$\dot{M}_{1-3}$ = mass flux per unit of pool width (M/T-L)

$\phi_{sand}$ = porosity of sand

$\phi_{silt}$ = porosity of silt

$C_s$ = effective solubility of the DNAPL (M/L$^3$)

$L$ = length of the pool (parallel to flow) (L)

$V_w$ = groundwater seepage velocity (L/T)

$D_{TSand}$ = effective transverse diffusion coefficient for the sand (L$^2$/T)

$D_{TSilt}$ = effective transverse diffusion coefficient for the silt (L$^2$/T)

$D_{LSand}$ = longitudinal dispersion coefficient for the sand (L$^2$/T)

$R_{Silt}$ = contaminant retardation coefficient for the silt

$t$ = time since pool was introduced (T)

$t\grave{}$ = time at which the pool/source is removed (T)

$K_l$ = pores-scale mass transfer rate coefficient (1/T)

132

Table 8 - Analytical solutions for fluxes 1, 2, and 3

| FLUX | MASS DISCHARGE PER UNIT OF POOL WIDTH | SOLUTION TYPE | REFERENCES |
|---|---|---|---|
| 1 | $$\dot{M}_1 = 2\phi_{sand}C_s\sqrt{\frac{LV_wD_{TSand}}{\pi}}$$ | Steady State | Adapted from Bird, et al., (1960), Sale (1998) |
| 2 | $$\dot{M}_2(t) = \phi_{silt}C_sL\sqrt{\frac{R_{Silt}D_{TSilt}}{\pi t}}$$ | Transient | Adapted from Parker et al., (1994) |
| 2` | $$\dot{M}_{2`}(t,t`) = \phi_{silt}C_sL\left[\sqrt{\frac{R_{Silt}D_{eSilt}}{\pi t}} - \sqrt{\frac{R_{Silt}D_{eSilt}}{\pi(t-t`)}}\right]$$ | Transient | Adapted from Parker et al., (1994) |
| 3 | $$\dot{M}_3 = C_sh_{pool}V_w\phi_{sand}\left[1 - \exp((\frac{L}{2D_L})(V_w - \sqrt{V_w^2 + \frac{4D_{LSand}K_l}{\phi}}))\right]$$ | Steady State | Adapted from Miller et al., (1990), Sale (1998) |

**Flux 1** reflects transverse diffusion of contaminants into the groundwater passing over the top of the pool.  A primary assumption used in developing this solution is steady state conditions.  Available data suggests that steady state conditions are achieved in a short time frame relative to the longevity of the pool (Schwille 1988, Gellar and Hunt 1993, Sale 1998).  Based on this, the assumption of steady sate conditions is not seen as a major limitation in our applications that follow.

**Flux 2** reflects transverse diffusion of contaminants into the silt underlying the pool.  This solution considers transient conditions and the effect of contaminant adsorption onto the silt.  Adsorption in the silt can be substantially greater than the sand due to greater surface area and higher carbon content associated with a more quiescent depositional environment.  The primary assumptions in this solution are that groundwater is stagnant in the silt layer and that transport occurs solely in the vertical (z) direction.

**Flux 2`** describes reverse diffusion from the silt into the sand that is initiated at time t' when the DNAPL is completely depleted along the contact.  This solution

provides an important opportunity to study the effects of mass stored in low permeability zones after complete DNAPL depletion. The key assumption employed in this solution is the concentration at the sand-silt boundary is uniformly and instantaneously decreased from $C_s$ to 0 at time t`. In reality this is not strictly true. Nevertheless, this solution provides a useful a starting point.

**Flux 3** describes discharge of contaminants at the end of the pool, due to flow through the pool. A main assumption here is that the DNAPL does not reduce the flow of groundwater through the pool. In fact this is typically not true because some of the pore space is occupied by DNAPL and not water. Fortunately, flux 3 is typically small relative to fluxes 1 and 2. Consequently, the error associated with the assumption is not considered critical. Another assumption is that of steady state conditions. Available data suggests that steady state conditions are achieved in a short period relative to the longevity of the DNAPL (Imhoff et al., 1993, Powers et al., 1994). Based on this, the assumption of steady state conditions is not seen as a major limitation to our applications that follow. Note that for almost all conditions of interest, the bracketed term in the equation for flux 3 is very close to 1. Thus, flux 3 can be approximated as

$$\dot{M}_3 = C_s h_{pool} V_w \phi_{sand}$$

4.1.2  Application of Table 8 Equations

The following explores key questions through applications of the solutions presented in Table 8. This is achieved by considering the "base case" conditions introduced in Figure 73.
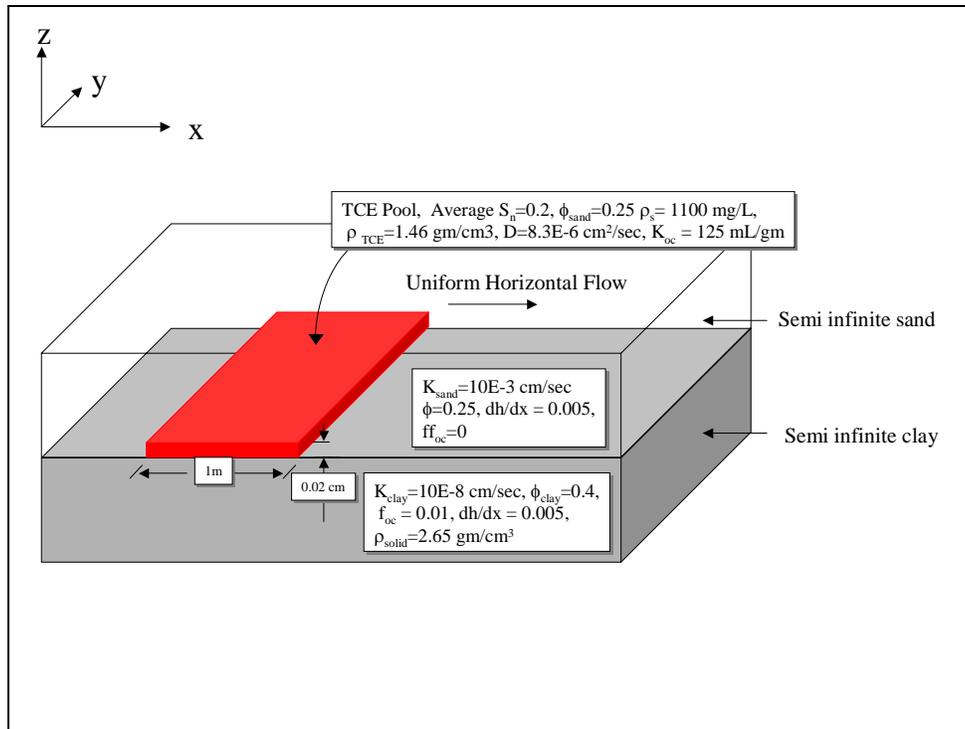
Figure 73 - Base case conditions

Figure 74 shows the cumulative mass discharges (kg/meter of pool width) from
the DNAPL zone as a function of time.   Specifically, cumulative mass discharge
to the sand above, to the silt below, to the sand downstream is developed.  Total
cumulative discharge is also presented. The results were obtained by integrating
the Table 8 solutions with respect to time and assuming that the length of the
DNAPL zone remains constant.   Supporting calculations are presented in
Appendix D.   Figure 74 results are a first-order approximation that should be
valid provided that the mass removed remains small relative to the initial mass in
place.
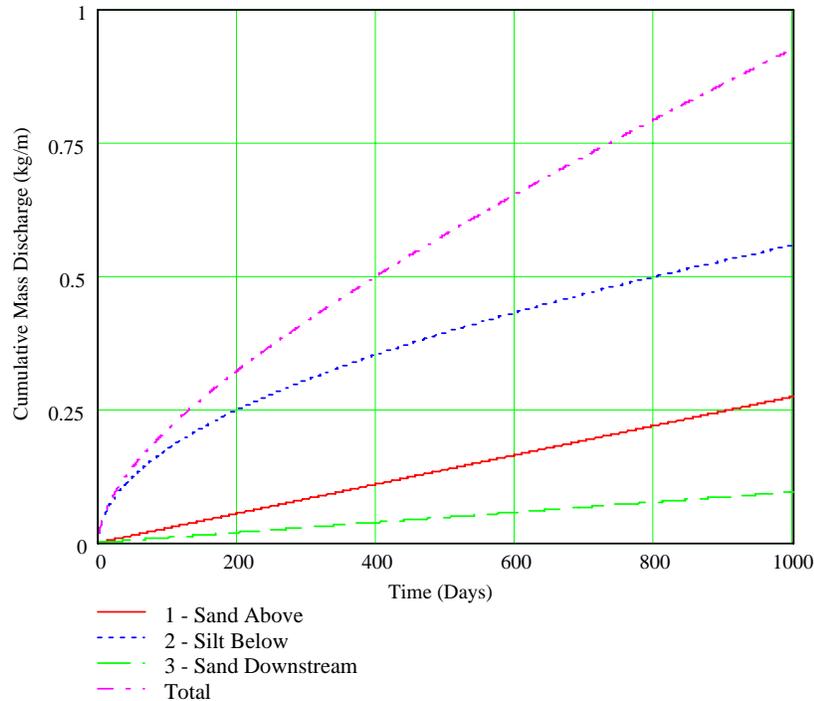
Figure 74 - Cumulative contaminant discharges

The base case solution can be used to evaluate the following two questions.

**Considering fluxes 1, 2 and 3, how much contaminant mass ends up in the silt layer?** Inspection of Figure 74 reveals that the majority of the dissolved contaminant mass released from the DNAPL zone (61%) ends up in the silt after 1000 days. Also, at 1000 days, 64% of the initial TCE DNAPL has been depleted. The fact that flux 2 is larger than 1 reflects the importance of contaminant diffusion and adsorption in the silt layer. Observations related to Figure 74 include:

- The large magnitude of flux 2 indicates that (1) the presence of the low permeability zone accelerates the rate of DNAPL dissolution (i.e., depletion) and (2) large amounts of mass can be stored in low permeability zones.

136

- The overall longevity of the DNAPL is relatively short (on the order of a decade)

The process of low permeability zone mass storage provides a plausible explanation as to why it is often difficult to find DNAPL at the heads of plumes (e.g., F.E. Warren AFB, select locations at AFP4). Furthermore, chemical mass in low permeability zones is a likely explanation of contaminant rebound that is commonly observed when employing flushing technologies, such as pump-and-treat, that only remove contaminants in transmissive zones.

**What happens when all the DNAPL is gone?**

Ultimately, all of the DNAPL will be depleted. Once this happens, contaminants will begin to diffuse back out of the low permeability silt layer and into the transmissive sand layer. This will sustain contaminant concentration in the sand after the DNAPL is gone. Analysis of this problem is ongoing. An approximate solution is developed by integrating the 2` solution in Table 8 and assuming that concentrations along the contact is instantaneously reduced from $C_s$ to 0 at time t`, that is, when the DNAPL is completely depleted.

Building on this, Figure 75 estimates cumulative contaminant discharge to the sand layer, from the silt, for 1000 days after removal of the DNAPL. It is assumed that the DNAPL had been present at the sand-silt contact for 1000 days per Figure 74. The total loading to the sand in the 1000 days after the removal of the DNAPL is approximately one third of the loading that occurred during the 1000 (previous) days when the DNAPL was present. This suggests that complete removal of DNAPL can have only a moderate effect on downgradient water quality.
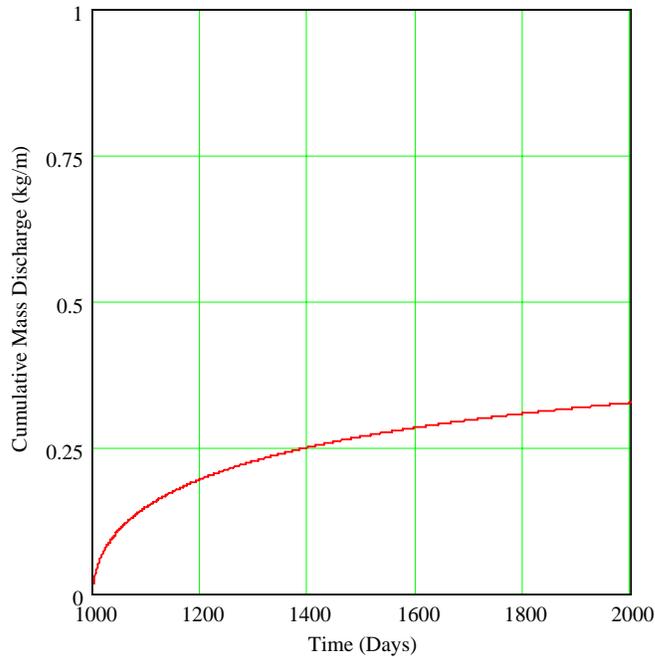
Figure 75 – Cumulative mass discharge to the transmissive zone (2') after the DNAPL is completely depleted.

### 4.1.3  Flux 4 and 4'

Contaminant transfer from the dissolved plume in the transmissive sand layer to the low permeability silt layer also occurs downstream of the DNAPL zone.  This has two important effects.  First, it attenuates (reduces) aqueous phase concentrations in the downgradient plume while the DNAPL is present. Second, it sustains aqueous phase concentrations after the DNAPL is gone. This is conceptualized in Figure 76.  Also shown in Figure 76 is a hypothetical monitoring well located downgradient of the DNAPL zone.  Ultimately, methods developed in this subsection are used to predict concentrations in downgradient wells.  This is an important development in that groundwater samples from wells are the primary means for evaluating the performance of field remedies.
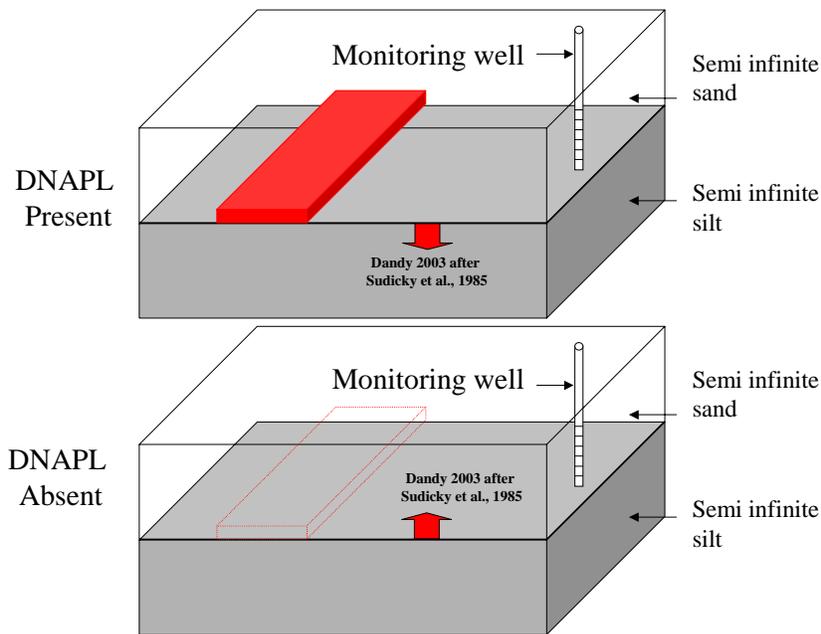
Figure 76- Conceptualization of flux 4

In attempting to model flux 4, Dr. David McWhorter (professor emeritus Colorado State University) led us to Sudicky et al., (1985). Although nearly 20 years old, this remarkable paper challenges many of the current conventions regarding contaminant transport in porous media. In Sudicky et al., (1995), a sand tank experiment is described in which a sand layer is constructed between thick silt layers as shown in panel (a) of Figure 77. A chloride solution is pumped though the sand and effluent concentrations are measured. Panel (b) illustrates the observed effluent concentrations (dots) and analytical model results (lines). The isolated line on the left of panel (b) illustrates predicted effluent concentration if there is no diffusive transport into the silts. The other results (lower right corner) show large contaminant attenuations associated with diffusion of contaminants into the silt. Panel (c) illustrates an experiment with a higher seepage velocity where the chloride source is turned off at some point during the experiment. Concentration after nine days illustrates that diffusion (from the silt into the sand) sustains contaminant concentrations in the sand layer. If there were no diffusion, the concentration would have rapidly decreased to near zero before the end of the experiment.
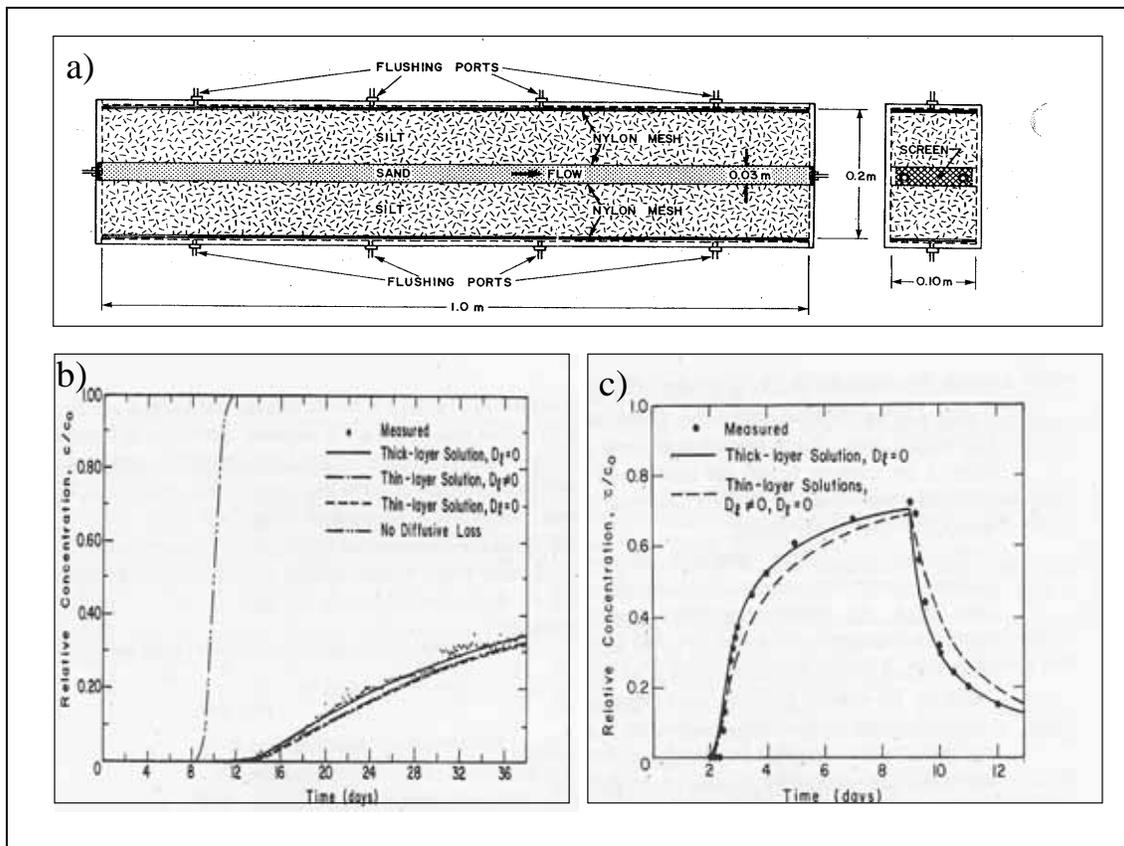
Figure 77 - Excerpt from Sudicky et al, 1985

Through the analytical solutions presented in Sudicky et al., (1985), we found that theoretical results are consistent with our hypotheses regarding governing processes (Section 2) and experimental observations (Section 3). Unfortunately, the solutions are limited (relative to our needs) in the following ways:

- The solutions involve summations and numerical integrations to infinity that have to be approximated. Dealing with these, with computational accuracy, is challenging.

- No solution is presented for concentrations in the silt layer(s).

- A uniform influent concentration is assumed in the sand layer.  This is inconsistent with the concentration profile that occurs with a DNAPL zone at the sand-silt contact.

- The solutions do not account for adsorption in the silt layer.

- The solutions do not account for degradation in the sand and silt layers

## 4.2 Two Layer Developments

To address limitations Dr. David Dandy, Professor of Chemical Engineering, Colorado State University, updated the Sudicky et al., (1985) solutions. Specifically, Dr. Dandy developed three unique analytical solutions for the two layer cases described in Table 9 and Figure 78.  Detailed derivations of the solutions are presented in Appendix C.   The advantage of the less rigorous solutions (Versions 1 and 2 respectively) is that they are computationally less complex.

Table 9 - Simple Case Models

| | Sand Processes | Silt Processes |
|---|---|---|
| Version 1 - Two layer base case | Longitudinal advection and transverse diffusion | Transverse diffusion |
| Version 2 - Two layer base case with sorption | Longitudinal advection and transverse diffusion with retardation | Transverse diffusion with retardation |
| Version 3 - Two layer base case with sorption and reaction | Longitudinal advection and transverse diffusion with retardation and reaction | Transverse diffusion with retardation and reaction |

Additional parameters introduced in Figure 78 include:

$R$ = Contaminant retardation coefficient for the sand

$k$ = First order reaction rate coefficient for the sand

$k^`$ = First order reaction rate coefficient for the silt
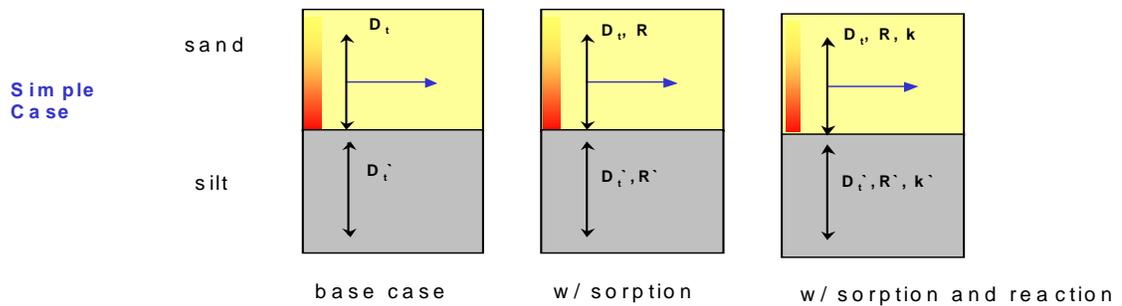


Figure 78 – Illustration of two layer simple case models

## 4.2.1 Model Testing

After developing Versions 1-3 of the analytical solutions for the two-layer scenario (Table 9), the models were tested to see if plausible output was generated and model results were compared to laboratory data introduced in Section 3.2 and Appendix A. Test calculations indicate that the solutions are stable so long as the calculations are conducted for portion of the solution domain where concentrations were not ultra low (far below typical concentrations of concern. The second step indicates that a close match to the laboratory data can be achieved given the experimental conditions introduced as inputs and a reasonable value (fitted) for transverse diffusion. Figure 79 compares laboratory data for bromide, PCE, and TCE to Version Two model output.
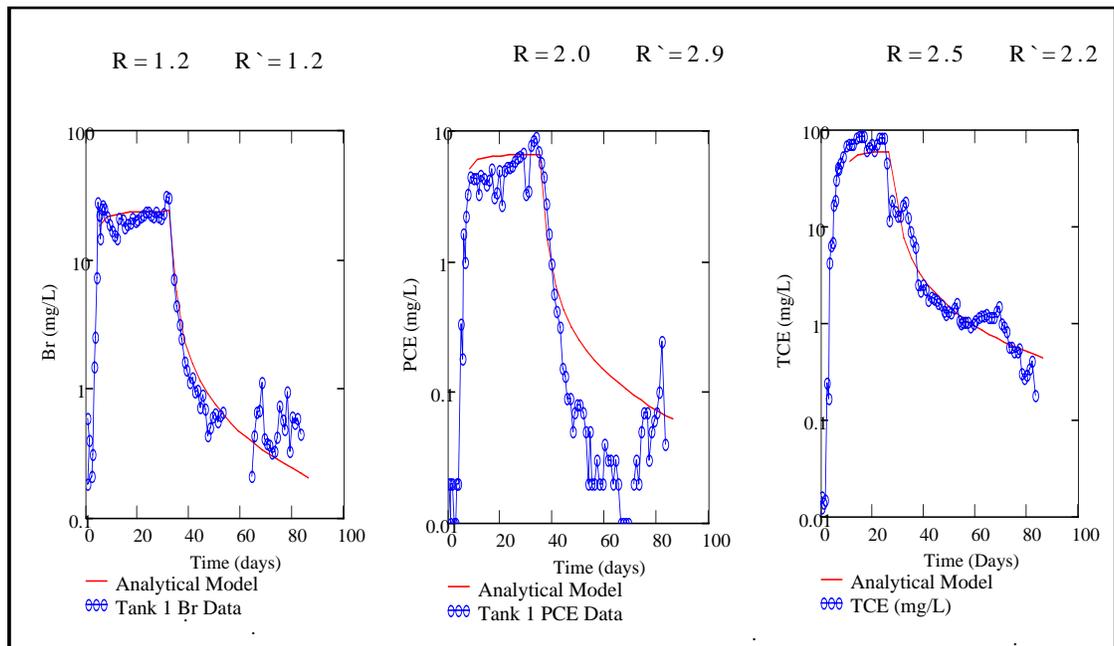


Figure 79 - Comparison of model and laboratory results (Laboratory conditions with $D_{TSand}$ = 8.0 E-8 and $D_{TSilt}$ =1.3E-9 m$^2$/sec, retardation values are based on laboratory measurements using noted contaminants and soils)

In general, Figure 79 indicates favorable agreement between the model and laboratory data.  This supports the validity of the model.  The most notable exception is the late time PCE data.  Our current opinion is that the less than perfect fit at late time reflects error in the experimental measurements as opposed to significant flaws in the model.  Note that no data was developed during our laboratory studies to test the reaction component of the Version 3 of the two-layer model.  The value of adding a reaction term to the model was recognized after the completion of the two layer tank experiments.  Subsequent multiple layer laboratory tank studies and analytical models provide a basis for testing our approach to modeling reactions.

4.2.2 Applications of the Two-Layer Analytical Solutions

As a next step, we have applied Version 1-3 of the two-layer model to advance our understanding of how plumes are impacted by transverse transport, adsorption, and reactions. This is reviewed in the following text.

**Version 1** – Figure 80 presents normalized concentration ($C/C_s$) as a function of position for the simple case with a source (analog DNAPL pool) on for a period of 1000 days using Version 1 of the two-layer model. Physical conditions are those identified for the base case in Figure 73 with the exceptions that the seepage velocity in the sand is 0.3 m/day and there is no adsorption of contaminants in the silt layer. (Note that these differences simply reflect calculation conducted at different times). Figure 80 illustrates attenuation of the aqueous phase plume in the sand and significant mass storage in the silt. Note, per Figure 80, the contamination is only introduced in the sand. Based on this, contaminants in the silt are solely due to transverse diffusion from the sand.



**Elapsed Time = 1000 days – Source on for 1000 days**

$V_w$ = 0.3m/day, R=1, Dimensions in m
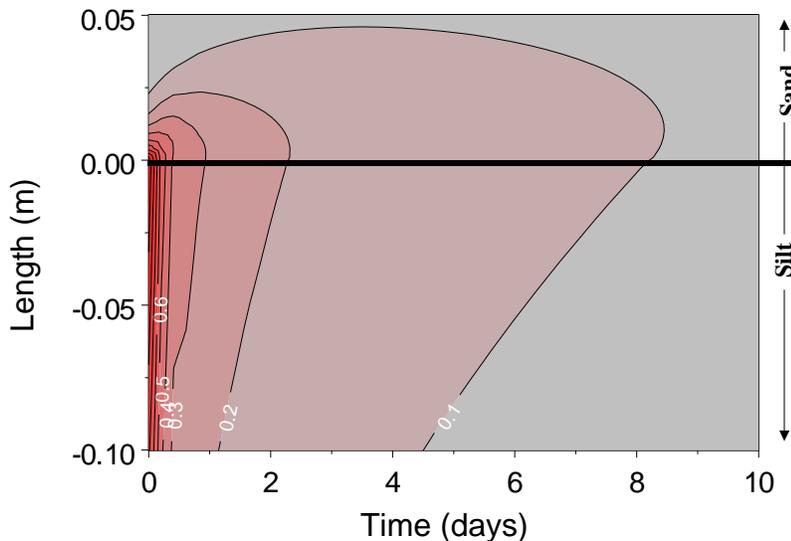
Figure 80 - Normalized aqueous concentrations in the sand and silt after 1000 days

Figure 81 illustrates concentrations at 1010 days assuming that the source is removed at 1000 days.  At distances of less than 3 m, contaminants near the contact are diffusing upward from the silt to the sand.  At greater than 3 m the opposite is occurring; contaminants are diffusing downward from the sand into the silt.  Considering plumes of large dimensions (e.g., field-scale), inward and outward diffusion at the sand-silt contact is likely occurring at all times, at some point in space.  This process is not typically described in conventional numerical models due to coarse spatial discretization of the solution domain.  At best, conventional numerical transport models lump this process into dispersion coefficients.

**Elapsed Time = 1010 days  – Source off for 10 days**

$V_w = 0.3$m/day, R=1, Dimensions in m



Figure 81 - Normalized aqueous concentrations in the sand and silt after 1010 days
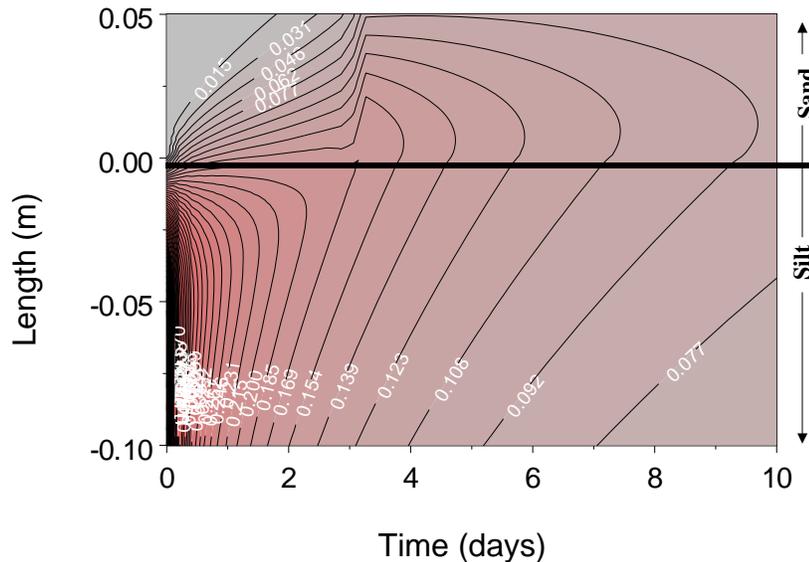
At depth, downward diffusion of contaminants continues to occur in the silt. This will occur for long periods of time after elimination of the original chemical source. Following Feenstra et al. (1996), a consequence is that the time for the contaminants to diffuse from the silt into the sand will be much larger than the time required to drive the contaminants into the silt. Another way to say this is that there is a hysteretic nature to the way in which contaminants are stored and released in source zones and plumes. This is consistent with a number of the observations including:

- Tailing (or persistent) contaminant concentrations in laboratory studies when sources are turned off

- Rebound of contaminant concentrations in plumes and source zones after they have been depleted from transmissive zones (e.g., after pump and treat or in-situ chemical oxidation)

- Persistence of plume head in the absence of any visual evidence of DNAPL

Figure 82 and Figure 83 show the dissolved concentration distribution at 1100 and 2000 days, respectively. Through this period, outward diffusion sustains contaminant levels in the transmissive sand layer.

**Elapsed Time = 1100 days – Source off for 100days**

V$_w$ = 0.3m/day, R=1, Dimensions in m
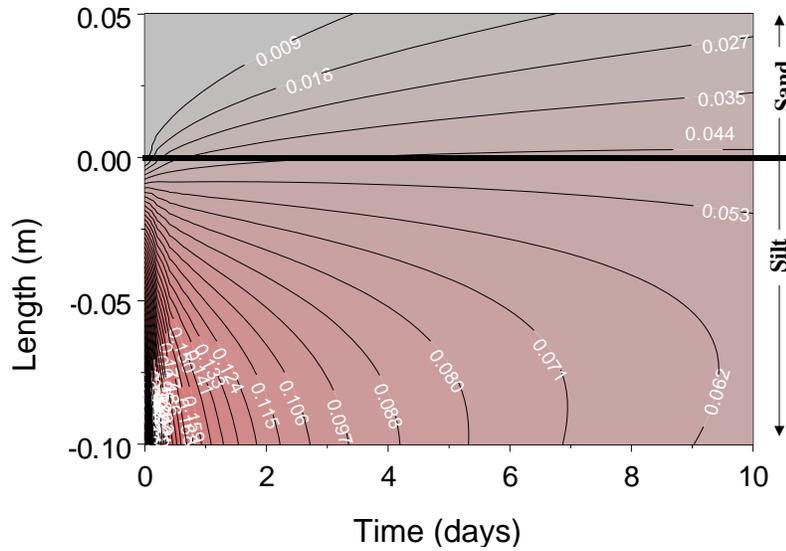


Figure 82 - Normalized aqueous concentrations in the sand and silt after 1100 days


**Elapsed Time = 2000 days – Source off for 1000 days**

V$_w$ = 0.3m/day, R=1, Dimensions in m
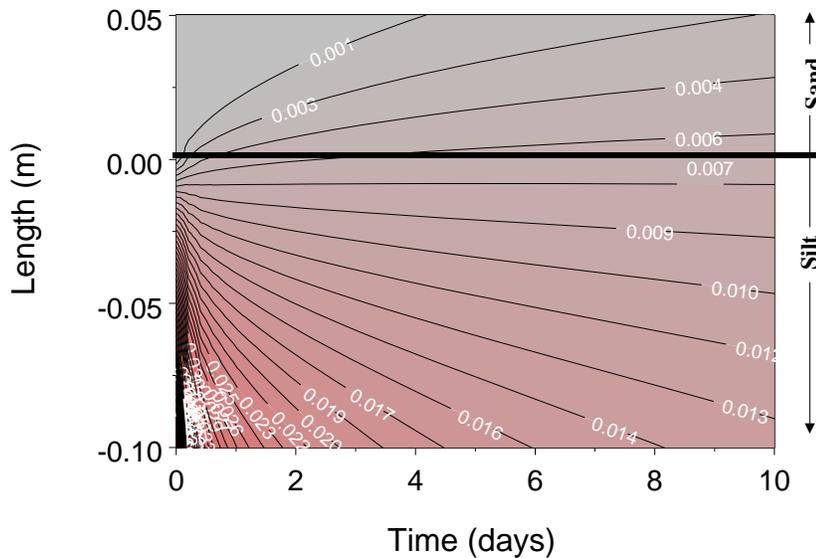


Figure 83 - Normalized aqueous concentrations in the sand and silt after 2000 days

148

**Version 2** - As noted in Section 3.2, sorption also governs contaminant storage and release. The following illustrates the significance of sorption using Version 2 of the two layer analytical solutions introduced in Table 9. In addition, the following illustrates applications in a field-scale domain, concentration output in mg/L, and a higher seepage velocity of 1 m/day.

Figure 84 and Figure 85 consider a PCE source that has been on for 1000 days with organic carbon fraction of 0 in both the sand and silt layers. This results in no adsorption in either layer. Figure 84 presents aqueous contour intervals between 0 and 1500 mg/L. This illustrates that the highest concentrations remain local to the source even after 1000 days. The large upper bound provides a basis for subsequent comparison in which sorption is added and total contaminant concentrations are mapped.

## Base Case – Aqueous Conc. (mg/L)
Contour Interval 0-1500 mg/L
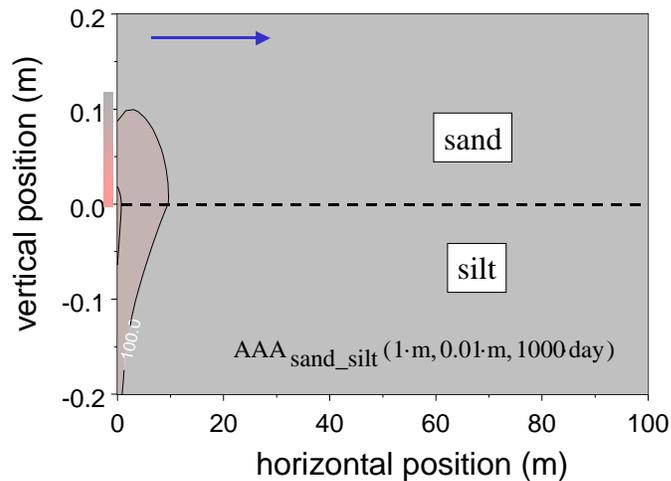


Figure 84 - Aqueous PCE Concentrations with a 0-1500 mg/L contour range

## Base Case

### Aqueous Conc (mg/L)

Contour Interval 0-150 mg/L

$$\text{AAA}_{\text{sand\_silt}} (1{\cdot}\text{m}, 0.01{\cdot}\text{m}, 1000\,\text{day})$$

.
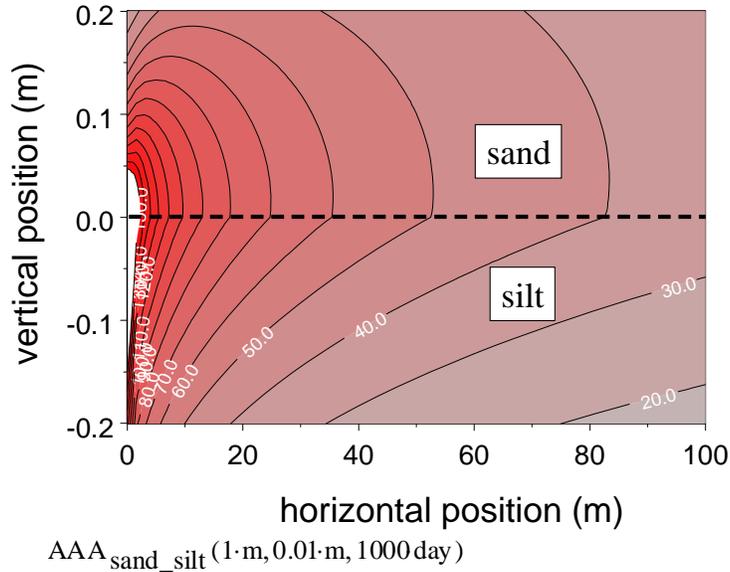
Figure 85 - Aqueous PCE Concentrations with a 0-150 mg/L contour range

Unfortunately, the large contour interval of Figure 84 misses the details of downgradient contaminant concentrations. To address this, Figure 85 is presented with contour intervals between 0 and 150 mg/L. This illustrates the broad distribution of aqueous contaminants throughout the solution domain. As with the Version 1 calculations, contaminants in the silt layer are solely attributable to transverse diffusion from the transmissive sand layer.

Figure 86 presents aqueous concentration with sand and silt fraction of organic carbon of 0.001 and 0.01, respectively. The difference from the aqueous concentrations conditions shown in Figure 84 is that the area of large concentration, local to the source, is smaller.

## With Adsorption

Aqueous Conc. (mg/L)
Contour Interval 0-1500 mg/L
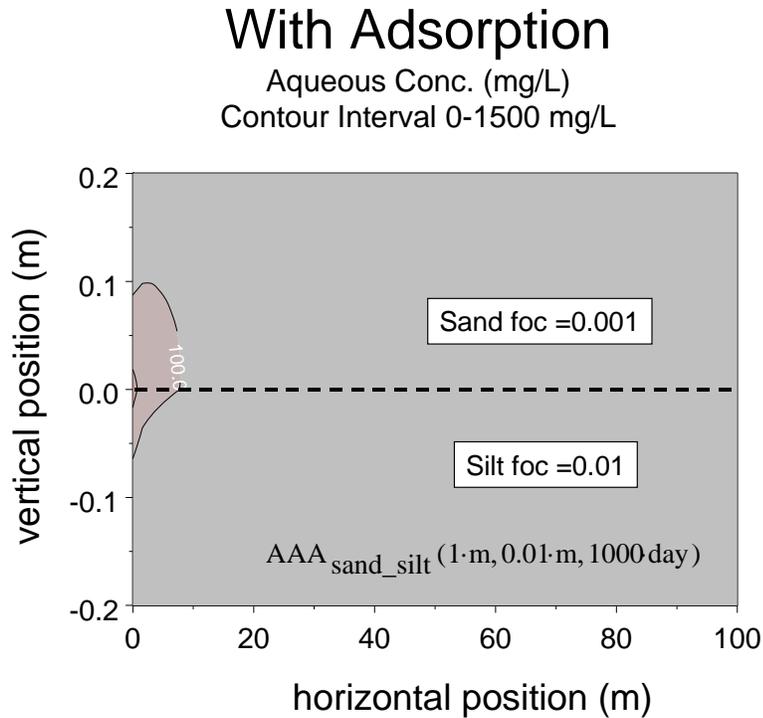


Figure 86 - Aqueous PCE Concentrations with a 0-1500 mg/L contour range with adsorption

Unfortunately, Figure 86 is misleading in that it fails to depict the mass of contaminants present as a sorbed phase. To address this limitation, Figure 87 presents total contaminant concentration (sorbed and dissolved) per 1000 $cm^3$ of porous media. This presents a dramatically different picture than that seen when only aqueous concentrations are considered. Specifically, as compared to Figure 87:

- Most of the contaminant mass is in the silt layer,
- Contamination in the silt layer is present in excess of 100 m downgradient of the source
- Magnitudes of total contaminant concentrations are dramatically larger in the silt

-

An important observation that can be drawn from the comparison of Figures 87 and 88 is that characterizing contaminant distribution solely on water-quality data can be misleading.

## With Adsorption

Total Conc. (mg/ 1000cm³ porous media)
Contour Interval 0-1500 mg/1000 cm³
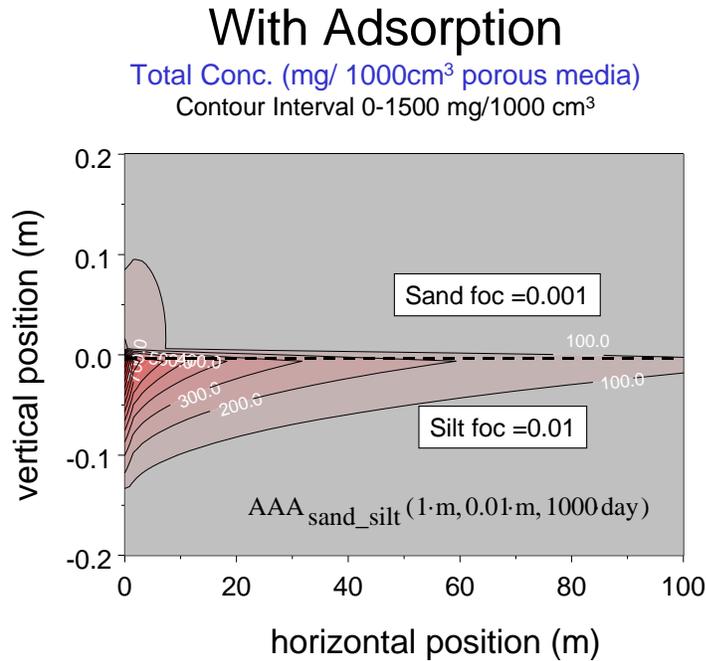


Figure 87 - Total PCE Concentrations with a 0-1500 mg/L contour range with adsorption

Finally, using model Version 2, Figure 88 presents conditions 200 days after the source was turned off.  In this case the combined processes of desorption and back diffusion will sustain contaminant concentrations in the transmissive sand layer.

# Back Diffusion With Adsorption

Total Conc. (mg/1000 cm$^3$ porous media)

Contour Interval 0-1500 mg/L



$$AAAx_{sand\_silt}(1{\cdot}m, 0.01{\cdot}m, 1200\,day, 1000\,day)$$
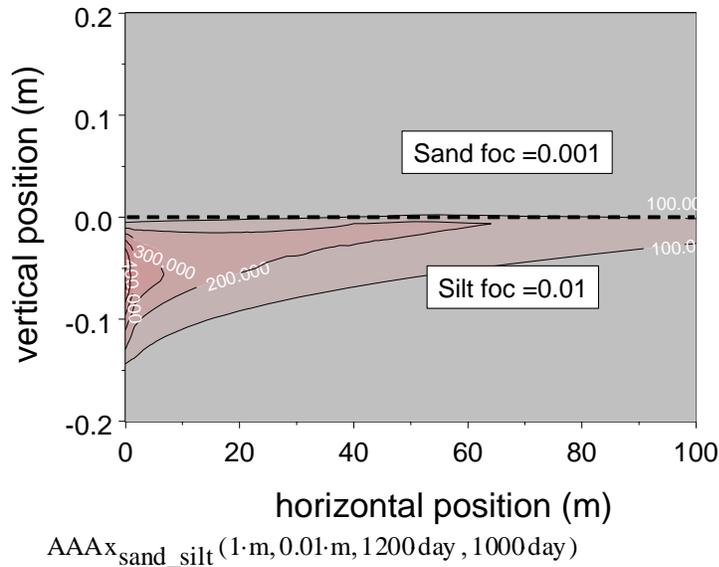
Figure 88 - Total PCE Concentrations with a 0-1500 mg/L contour range with adsorption 200 days after the source is turned off

**Version 3 -** In addition to advection (sand only), transverse diffusion, and adsorption, Version 3 also addresses first-order degradation of the contaminant in both the sand and silt.   Inclusion degradation builds on the observations that chlorinated solvents can degrade in plumes and source zones via either biotic (e.g. Wiedemeier et al., 1999) and/or biotic (e.g. Lee, and Batchelor. 2002) processes.   Version 3 of the two-layer model is demonstrated in Figure 89.  In this case, the model is used to estimate the aqueous concentrations in wells with 3 m screens that are completed immediately above the silt in the sand. Locations considered are 1, 10, and 100 m immediately downgradient of the source.  Integrating the concentrations in the sand over the vertical interval of concern and dividing the result by the length of the vertical interval determine aqueous concentrations in wells.
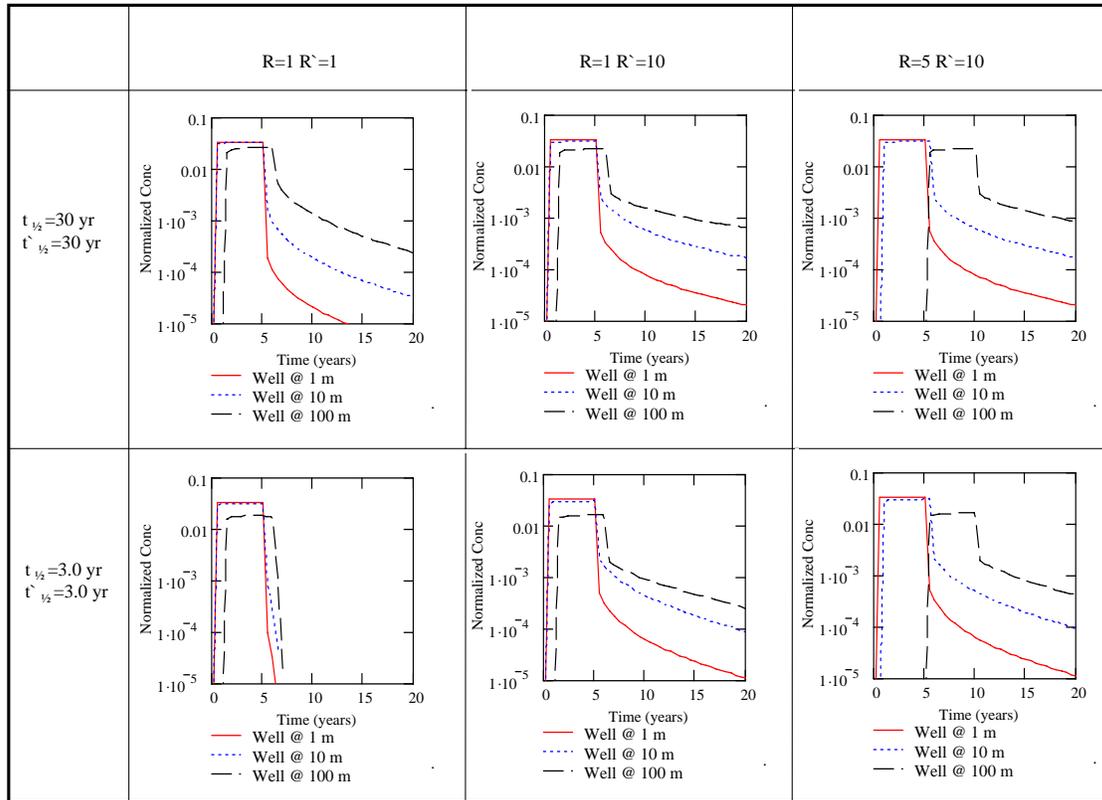
Figure 89 - Sensitivity of Version 3 output to contaminant half-life, retardation coefficient and downgradient distance from source. (Seepage rate is 0.3 m/day, the source is on from 0 to 5 years, and the wells have 3-m screens that are completed immediately above the sand-silt contact)

A number of important observations can be drawn from Figure 89 including:

1)  After removing the source, water quality improve far quicker close to the source than distant from the source.

2)  Increasing retardation coefficient delays the initial arrival of the contaminants and while the source is on and sustains aqueous concentrations after the source is off.

3)  Shorter contaminant half lives lead to lower concentrations at all times and a reduced significance of back diffusion.

154

4) In terms of sustained concentrations downgradient, post source removal, the worst-case scenario (upper right hand corner) is that an approximate one-order-of-magnitude improvement in water quality is observed 100 m downgradient of the source 15 years after the source is removed.

5) The above point suggests that, for the noted conditions, high retardation and low reaction rates for the time frame in which one would see improvements in downgradient water quality may be large.

6) In terms of sustained concentrations downgradient, post source removal, the best-case scenario (lower left), is that an approximate four-order-of-magnitude improvement is achieved almost immediately after the source is removed.

7) The above point suggests that the time frame in which one would see improvements in downgradient water quality can be small when retardation is low and reaction rates are moderately fast.

Field scale behavior similar to the behavior noted in items 5 and 7 is presented in Section 5, which describes results from zero-valent iron permeable reactive barriers at FEW and NASFtW.

## 4.3 Multiple Layer Developments

An analytical solution was also developed for the multiple-layer case. Detailed derivations of the solutions are presented in Appendix C. Unfortunately, a practical way to apply this solution was not found during this project.

## 4.4 Numerical Modeling

4.4.1 Objectives

Models based on closed-form analytical solutions such as the ones presented in the previous section have the limitations that they could only be used to simulate idealized conditions that involve simple aquifer geometries, homogenous aquifer properties and one-dimensional flow conditions. Numerical models allow for the simulation of more realistic conditions that are encountered in the laboratory and the field. An existing numerical code, after appropriate modifications, was evaluated for its ability to capture the basic processes that are of relevance to this work. The data generated in the laboratory test tanks was used in this evaluation. Part of this study also involved the demonstration of the limitation of existing advection-dispersion models for their ability to capture the diffusive processes into the low permeability stagnant zones. It is not the goal in this task to calibrate or validate the model, as all parameters required for this purpose were not available.

The specifications of the model have been developed based on the processes described in Section 2. The model needs to have the capabilities to simulate the following processes:

(1) dissolution from an entrapped NAPL source at residual saturations and pools of high saturation,

(2) advection, dispersion and diffusion that transport the soluble constituents of the DNAPL in the vicinity of entrapment zones and in the aquifer downgradient of the source zone,

(3) diffusion that occurs through the interfaces where the continuous DNAPL is in direct contact with low permeability materials in the aquifer,

(4) diffusion from the solute plume into the low permeability zones that are encountered during its migration,

(5) reverse diffusion (or rebound) that occurs from the low permeability zones to flowing groundwater, and

(6) adsorption that occurs in the material contained both in the low permeability zone and the transmissive portion of the aquifer.

4.4.2 Methodology

4.4.2.1    Limitations of Advection/Dispersion Based Models

It was our hypothesis that conventional transport models that simulate the advection-dispersion processes do not capture the process of mass diffusion into the low permeability zones of aquifers.  To test this, a model based on the groundwater flow code MODFLOW and the transport code MT3D was selected to simulate the advection, dispersion and diffusive processes.  The DNAPL dissolution in this preliminary model was simulated using SEAM3D (Waddill and Widdowson, et al, 2000) that is integrated into MT3D.  All of the model packages (MODLFOW, MT3D, and SEAM3D) were integrated within the US Department of Defense's Groundwater Modeling System (GMS) software, Version 4.0.

The test simulations demonstrated that the model was able to capture the advection process adequately but with an optimum grid size selected (to conduct the simulations with reasonable computational cost and time), the diffusion processes were not modeled with acceptable accuracy.  The details of this test are given in Appendix E.

4.4.2.2 Dual-Porosity Based Models

Based on the simulations described in Appendix E, an alternative model was required that captured both the advective and diffusion processes that were observed in the experiments.  The numerical model named Finite Element Heat and Mass transfer (FEHM) from the Los Alamos National Laboratory was investigated and selected, based on the discussions in the following text.  The FEHM model has the ability to model multiphase, multicomponent, reactive and nonisothermal flow and transport in three-dimensions.    Although    this

157

comprehensive simulator has many capabilities, the primary feature of FEHM required by this project was its ability to capture back and reverse-diffusion through the utilization of its dual-porosity module. Based on previous modeling work on matrix diffusion presented in the validation test plan of FEHM (Dash 2003), it was hypothesized that the dual-porosity code would provide the ability to model the back diffusion that was observed in the experiments. In addition, FEHM includes the ability to model the standard advective contaminant transport component. The major drawback to FEHM is that it does not model rate-limited mass transfer from pure phase material; the model assumes equilibrium. Calculating the dissolved mass flux rate from the X-ray mass depletion data and inputting these values as a transient source function curve into the model domain helped to overcome this limitation. A general description of how the dual-porosity module works in FEHM is presented in the following section, followed by a simple example of how the dual-porosity module simulations compare to an analytical solution given by Tang et al. (1981).

A dual-porosity system is a porous media system that contains two media that have contrasting values of porosity. Figure  illustrates such a system. In both (a) and (b), the yellow layer, N1, contains a material with a high permeability and a porosity of 0.3. N1 represents the #30 test sand from the tank experiments. The orange layer, N2, contains a lower permeable layer and has a porosity of 0.5. The N2 layer represents the field soil mix of sand and silt. The boundaries in (a) and (b) represent a simple node-centered model domain. Figure  (a) illustrates how a typical model domain would be constructed for this system, without using dual-porosity. The nodes for N1 and N2 would be assigned the corresponding material properties, initial conditions, and appropriate boundary values. The flow and transport equations for the model domain would then be solved at the nodes.
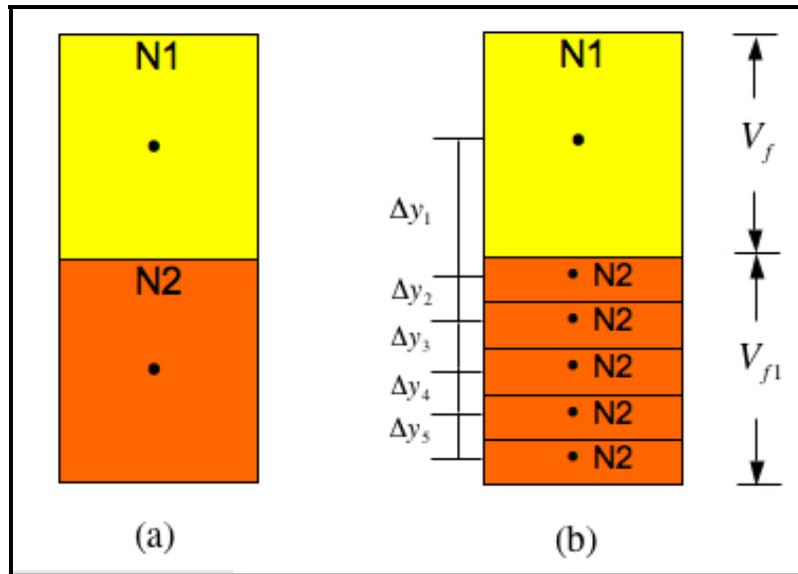
Figure 90 - Simple layered domain (a) without dual-porosity nodes and (b) with dual-porosity nodes.

In order to apply the dual-porosity concept to the simple system in Figure 90 (a), the model domain must be reconstructed as shown in Figure 90 (b). The structure of this model domain follows the requirements of the generalized dual-porosity macro (gdpm) that is included in FEHM. First, the node in N1 is defined as being a dual-porosity node. Second, the user-defined discretization of the N2 layer is applied to the node at N1, starting with the first layer at an increment of $\Delta y_1$ and ending with the last increment of $\Delta y_5$. These layers are referred to as the matrix layers in the model and their node spacing is not required to be uniform. The number of required matrix layers is dependent upon each model domain and is iteratively adjusted according to the user's requirements of the model. The volume fraction of the primary porosity, N1, is designated as $V_f$. The volume fraction of the matrix nodes, defined as $1-V_f$, is equally distributed to the matrix nodes. The material properties, initial conditions and boundary conditions are defined for the N1 and N2 nodes the same as was the case for the system in Figure 90 (a).

Using the volume fractions; $V_f$ and $1-V_f$, and the length scales; $\Delta y_1$ through $\Delta y_5$ allows the dual-porosity system to be solved in a one-dimensional fashion. The volume fraction of the matrix nodes, $1-V_f$, is represented by $V_{f1}$, thereby allowing a simple definition of

$$V_f + V_{f1} = V_T = 1 \qquad (1)$$

The length scale of the primary porosity volume (N1) is defined as

$$L_f = L_{f0}V_f \qquad (2)$$

where $L_{f0}$ represents the nodal spacing between the primary porosity node and the first matrix node ($\Delta y_1$ in Figure 90). The length scale of the first matrix volume is defined in a similar way as

$$L_{f1} = L_{f0}V_{f1} \qquad (3)$$

The length scale between the matrix nodes is defined as

$$L_{f2} = L_{f0}V_{f2} \qquad (4)$$

where $V_{f2}$ is the fraction of the second matrix volume. A geometric factor representing the spatial differencing of the one-dimensional flow between the primary porosity node and the first matrix node is given as (Zyvoloski 1995)

$$T_{ff1} = \frac{V_T}{L_{f1}(L_F + L_{f1})} \qquad (4)$$

using the terms defined in (1) through (3). The geometric factor representing flow between the matrix nodes is given by

$$T_{f1f2} = \frac{V_T}{L_{f2}(L_{f1} + L_{f2})} \qquad (5)$$

Equations (4) and (5) are incorporated into a mass balance equation as additional flux terms using the following equations (Zyvoloski 1995) with $m$ referring to the matrix and $f$ refers to the primary porosity

$$T_{f1f2}\left(\frac{k\rho_v}{\mu_v}\left(P_{m,v} - P_{f,v}\right) + \frac{k\rho_l}{\mu_l}\left(P_{m,l} - P_{f,l}\right) + D(C_{m,v} - C_{f,v}) + D(C_{m,l} - C_{f,l})\right) \qquad (6)$$

The parameters to equation (6) are defined in Table 10.

Table 10.  Symbol definitions for Equation (6).

| Symbol | Definition | Units |
|--------|------------|-------|
| $k$ | Intrinsic permeability | $L^2$ |
| $\rho$ | Density | $M/L^3$ |
| $\mu$ | Viscosity | $M/LT$ |
| $P$ | Pressure | $M/LT^2$ |
| $h$ | Enthalpy | $L^2/T^2$ |
| $\eta$ | Mass fraction of air | [-] |
| $T_{f1f2}$ | Transfer term | [-] |
| $D$ | Matrix Diffusion Coefficient | $L^2/T$ |
| C | Concentration of solute | $M/L^3$ |
| $v$ | Subscript representing vapor phase | |
| $l$ | Subscript representing liquid phase | |

Eqn. (6) is solved in one-dimension for each user defined dual-porosity nodes, thereby greatly increasing the speed and efficiency of the overall numerical solution.  The left side of Eqn. (6) is the Darcy flux into and out of the dual-porosity nodes and the right side of Eqn. (6) is the contaminant flux into and out of the dual-porosity nodes.  In summary, the dual-porosity macro of FEHM is solved in one-dimension for flow and transport going into and out of the defined dual-porosity nodes.  This solution may be embedded into a model domain that contains advective/dispersive transport and an example of this is presented in the following section.

## 4.4.2.3 FEHM Code Verification with Analytical Solution

To demonstrate that the dual-porosity module of FEHM was working properly, a code verification study (Dash 2003) that has been reported in literature is presented here. The transport module of FEHM with equilibrium sorption has been tested against two-dimensional analytical solutions that assume equilibrium sorption. The test case involves a two-dimensional grid (see Figure 91) with a permeability field set up to simulate one-dimensional flow in a fracture. Fluid in the surrounding matrix is stagnant. Tracers are injected into the flowing fluid in the fracture and are transported into the matrix via molecular diffusion. Sorption may occur in either the fracture, the matrix, or both the fracture and the matrix.
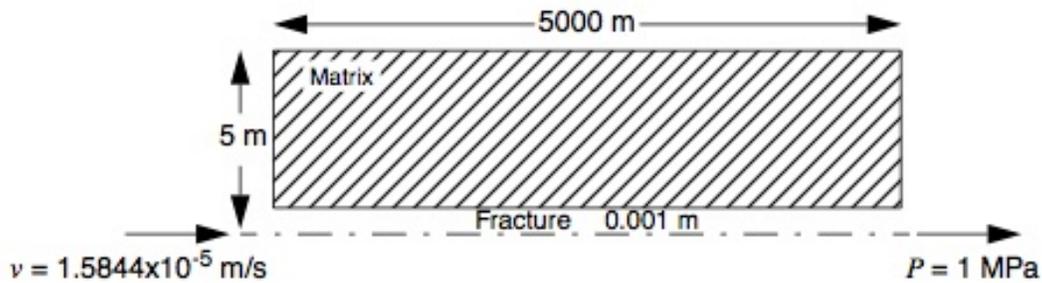


Figure 91 - Geometry and boundary conditions for the validation problem (Dash 2003).

An analytical solution has been provided by Tang et al., (1981) for the case of one-dimensional axial dispersion in a fracture, coupled to diffusion into an infinite medium. This solution is given by:

$$\frac{C}{C_{in}} = \frac{2 \cdot \exp\left(\frac{L}{2\alpha}\right)}{\pi^{1/2}} \int_{l}^{\infty} \exp\left[-\xi^2 - \frac{L^2}{4\alpha^2\xi^2}\right] erfc\left(\frac{Y}{2T}\right) d\xi \qquad (9)$$

where $\xi$ is the integration variable, $l$, the lower integration bound is given by

$$l = \frac{L}{2}\left(\frac{R_f}{\alpha vt}\right)^{1/2} \qquad (10)$$

162

and the lumped parameters *Y, T*, and *A* are given by

$$Y = \frac{R_f L \tau}{4 \alpha A \xi^2},$$
(11)

$$T = \sqrt{t - \frac{R_f L^2}{4 D \xi^2}},$$
(12)

and

$$A = \frac{b R_f}{\phi (R_m D_{mol})^{1/2}}.$$
(13)

The retardation factor on the fracture is given by $R_f$, the mean residence time of the fluid through the column is $\tau$, $\alpha$ is the dispersivity, $\nu$ is the fluid velocity, t is time, b is the half-width of the fracture aperture, $\phi$ is the porosity of the matrix, $R_m$ is the retardation factor in the matrix and $D_{mol}$ is the molecular diffusion coefficient of the solute. The analytical solution is given in terms of retardation factors for the fracture and matrix in order to model sorption. For FEHM, the equation used to give a retardation factor for a saturated medium is given by

$$R_f = 1 + \frac{\rho_b K_d}{\phi \rho_f}$$
(14)

where $K_d$ is the sorption distribution coefficient.

The inputs for the model runs are given in Table 11.

Table 11.  Model inputs for the fracture transport with matrix diffusion test problem (Dash 2003).

| Parameter | Symbol | Value |
|---|---|---|
| Flow Path Length (x) | L | 5000 m |
| Node spacing along flow path | $\Delta x$ | 100 m |
| Model width | Y | 5 m |
| Node spacings into the matrix | $\Delta y$ | 0.001 – 0.5 m |
| Fluid Density | $\rho_f$ | 1000 kg/m$^3$ |
| Bulk Rock Density | $\rho_b$ | 2700 kg/m$^3$ |
| Matrix Porosity | $\phi$ | 0.05 |
| Pore Water Velocity | $\nu$ | 1.58 x 10$^{-5}$ m/s |
| Dispersivity in fracture | $\alpha$ | 500 m |
| Matrix Diffusion Coefficient | D$_{mol}$ | 1.5 x 10$^{-12}$ m$^2$/s |
| Time step (tracer) | $\Delta t$ | 0.001 – 5000 days |
| Total elapsed time | t | 1500 years |
| Pressure | P$_0$ | 1.0 MPa |
| Initial concentration | C$_0$ | 0.0 |
| Inlet concentration | C$_{in}$ | 1 |

The boundary conditions for the problem are as follows:

At $l$ = 0 m, $q = v\rho_f \phi_f A_f$ = 7.922 x 10$^{-6}$ kg/s

At l = 5000 m, P = 1 MPa

The cross-sectional area of the fracture is A$_f$ and the fracture porosity is given by $\phi_f$. The parameters that were varied for these simulations are given in Table 12.

Table 12. Adsorption Parameters for the Fracture Transport Problem (Dash 2003).

| Test | Medium | $\alpha_1$ | $\alpha_2$ | $\beta$ | R |
|---|---|---|---|---|---|
| Transport with Matrix Diffusion, No Sorption | fracture | 0.0 | 0.0 | 1.0 | 1.0 |
| | matrix | 0.0 | 0.0 | 1.0 | 1.0 |
| Transport with Matrix Diffusion, Sorption (linear) in the Matrix | fracture | 0.0 | 0.0 | 1.0 | 1.0 |
| | matrix | $7.4074(10^{-2})$ | 0.0 | 1.0 | 5.0 |
| Transport with Matrix Diffusion, Sorption in the Fracture and matrix | fracture | 8.88889 | 0.0 | 1.0 | 25.0 |
| | matrix | $7.4074(10^{-2})$ | 0.0 | 1.0 | 5.0 |

As is seen in Figure 92, FEHM has correctly implemented the solute transport solution with equilibrium sorption in two dimensions. The slight discrepancies are probably due to numerical errors associated with insufficiently small grid spacing adjacent to the fracture (Dash 2003).
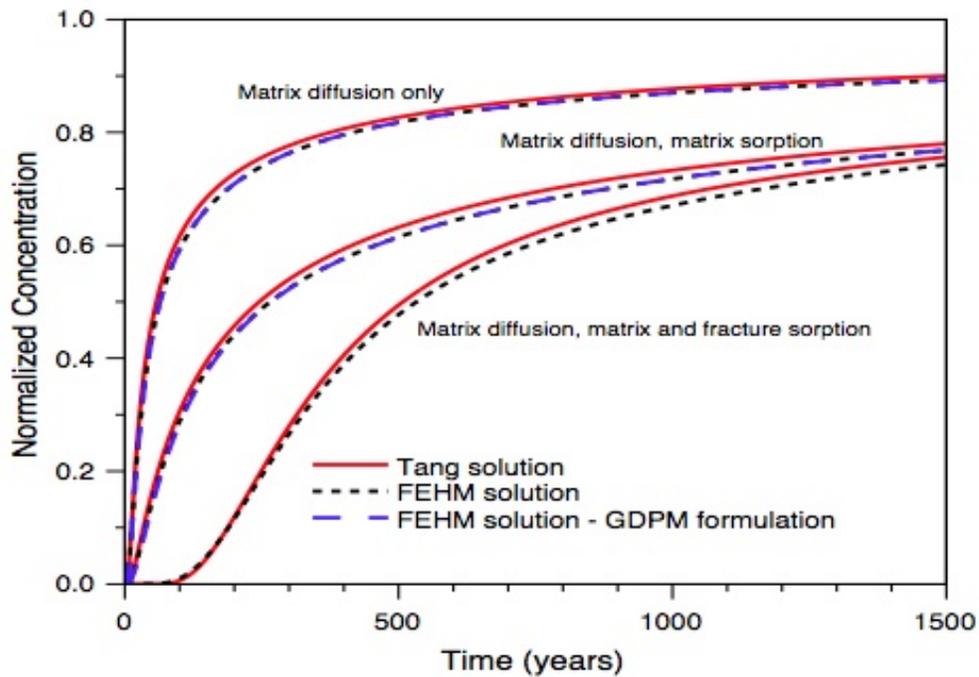


Figure 92  - Comparison of FEHM and Tang analytical solution for concentration versus time for the matrix diffusion model (Dash 2003).

## 4.4.2.4 FEHM Experimental Modeling

After successful application of FEHM to model the Tang et al. (1981) analytical solution, the ability of FEHM to capture the dominant features of the experimental data collected from the three intermediate-scale experiments was evaluated. The primary purpose of this modeling exercise was not to validate FEHM using the experimental data, but rather to use FEHM to explain the experimental observations. It would be difficult to validate FEHM with the data obtained from these experiments due to the fact that the sampling of the generated plume was only conducted at the effluent end of the tank. Sampling the length of the domain of the tank during the experiment may have affected the shape of the effluent plume and as such, it was decided only to collect samples at the effluent. It was hypothesized that if FEHM was able to qualitatively (or semi-quantitatively) match the experimental observations, then FEHM was capable of capturing the fundamental processes that were identified in the conceptual model, and that were not able to be simulated using the conventional advection-dispersion models. In this introductory outline, the common parameters that are needed in simulating the experiments are presented.

The overall approach used in these modeling exercises was to conduct two-dimensional numerical simulations of the first two tank experiments and then, using the information gathered from these model simulations, determine if FEHM could predict the experimental results of the third tank experiment. The physical properties of the materials used in the experiments were determined in the laboratory and are listed in Table 13.

Table 13.  Physical properties of experimental materials measured in CESEP lab.

| Name | Value | Units |
| --- | --- | --- |
| #16 bulk density | 1620 | kg/m$^3$ |
| #16 hydraulic conductivity | 6e-3 | m/sec |
| #16 porosity | 4e-1 | [-] |
| #16 sorption partition coefficient | 0 | L/kg |
| | | |
| #30 bulk density | 1610 | kg/m$^3$ |
| #30 hydraulic conductivity | 2e-3 | m/sec |
| #30 porosity | 4e-1 | [-] |
| #30 sorption partition coefficient | 0 | L/kg |
| #30 longitudinal dispersivity | 2.5e-1 | m |
| #30 transverse dispersivity | 2.5e-2 | m |
| | | |
| #50 bulk density | 1850 | kg/m$^3$ |
| #50 hydraulic conductivity | 3e-4 | m/sec |
| #50 porosity | 4e-1 | [-] |
| #50 sorption partition coefficient | 0 | L/kg |
| #50 longitudinal dispersivity | 2.5e-1 | m |
| #50 transverse dispersivity | 2.5e-2 | m |
| | | |
| #140 bulk density | 1740 | kg/m$^3$ |
| #140 hydraulic conductivity | 3e-5 | m/sec |
| #140 porosity | 4e-1 | [-] |
| #140 sorption partition coefficient | 0 | L/kg |
| | | |
| Field soil bulk density | 1430 | kg/m$^3$ |
| Field soil hydraulic conductivity | 2e-5 | m/sec |
| Field soil porosity | 5e-1 | [-] |
| Field soil sorption partition coefficient | 1.2e-1 | L/kg |

The measured potentiometric head values recorded in each tank experiment were used as boundary fluxes (inflow/outflow) for each numerical simulation.  All of the flow simulations representing the conditions in the tanks (referred to as tank models) were conducted for 20 days prior to dissolved DNAPL injecting, in order to allow the flow rate in each model to achieve steady-state conditions, as recommended by FEHM developers.  The measured dissolved mass flux rates were calculated from the mass depletion data that was measured in the source zone using X-ray analyses (Wilking 2004).  This transient dissolved mass flux was used as input for the DNAPL source node in each model.  In each model

domain, a 5 cm x 5 cm x 10 cm coarse inclusion with the DNAPL was represented by a single node. Due to the difficultly of experimentally determining the value of the matrix diffusion coefficient, the value of the molecular diffusion coefficient of 1,1,2-TCA in water was first used and then sensitivity analyses were performed. Sensitivity analysis helped in determining the appropriate value for this parameter as compared to the shape of the experimentally obtained breakthrough curve.

4.4.2.4.1    Numerical Modeling Simulations for Experimental Tank #1

The model domain for the first intermediate-scale tank experiment was described in detail in Section 3.  In summary, the tank packing consisted of a #30 test sand overlying a layer of the field soil.  Constant head end reservoirs were used to keep the flow in the tank steady.  Approximately 14.82 g of pure phase 1,1,2-TCA was injected into a coarse inclusion of #16 test sand located close to the upstream end of the tank.  As was discussed previously, FEHM does not currently have the capability to model rate-limited mass dissolution, so the dissolved phase mass flux values were calculated from measured X-ray data and used as input to the model.  The model domain for the simulation is shown in Figure 93.
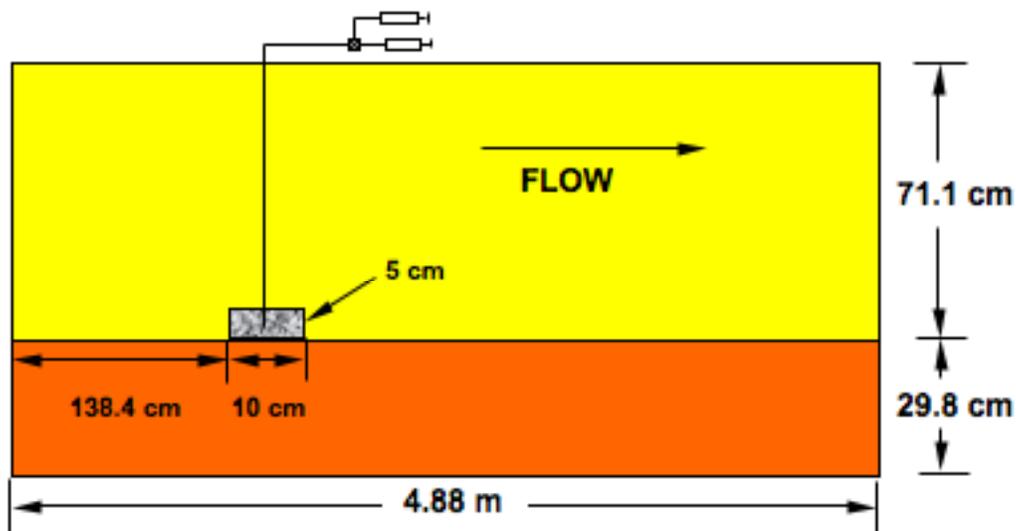


Figure 93 -  Model domain for experimental tank #1.

The mesh consisted of 2,550 nodes and 2,450 elements.  The spacing of the nodes in the #30 sand layer was 6.25e-3 m in the y-direction and 1e-1 m in the x-direction.  The spacing of the nodes in the field soil layer was reduced to 1e-3 m in the y-direction and 1e-1 m in the x-direction.  The injection node was located at [3.5 m, -0.625 m] and was assigned the material properties of #16 test sand.  For

the boundary heads provided, the flow is from the right end of the tanks to the left end.  All the nodes in the #30 sand layer that were located along the length of the sand/field-soil interface were designated as dual-porosity nodes.    Figure displays the velocity vectors for the numerical modeling simulations.  The larger arrows in the upper region of the figure show high values of velocity through the #30 test sand and the small arrows in the lower portion of the figure indicate smaller velocities through the field layer.  Table 14 summarizes the model input values and boundary heads.
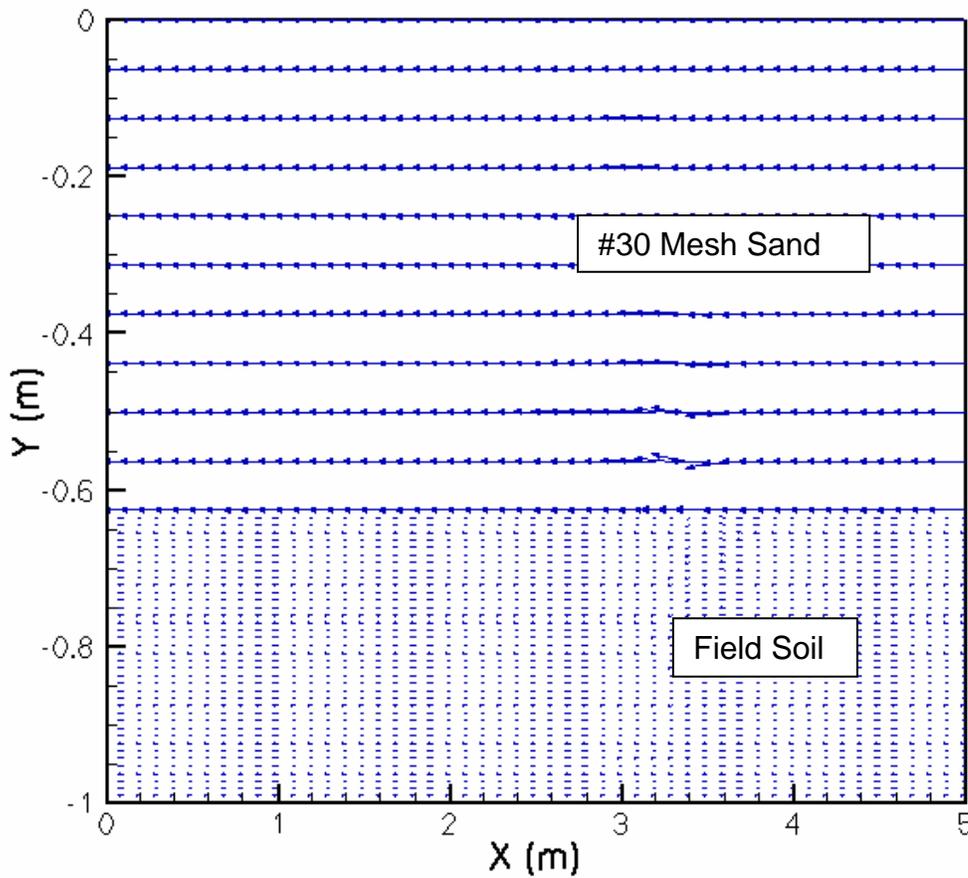


Figure 94 - Velocity vectors for experimental tank #1.

Table 14. Model inputs for large tank experiment #1.

| Name | Value | Units |
|---|---|---|
| Domain length (x) | 5 | m |
| Domain height (y) | 1 | m |
| #30 node spacing in the x-direction | 1e-1 | m |
| #30 node spacing in the y-direction | 6.25e-2 | m |
| Field node spacing in the x-direction | 1e-1 | m |
| Field node spacing in the y-direction | 1e-3 | m |
| Volume fraction assigned to primary porosity in gdpm macro | 8e-1 | [-] |
| Number of gdpm layers at each dual-porosity node | 10 | [-] |
| Water density | 1000 | kg/m$^3$ |
| Boundary head at inlet | 1.473 | M |
| Boundary head at effluent | 1.435 | M |
| Water temperature | 20 | C |
| #16/#30 x-direction dispersivity | 2.5e-1 | M |
| #16/#30 y-direction dispersivity | 2.5e-2 | M |
| #16/#30 effective molecular diffusion coefficient | 8e-10 | m$^2$/sec |
| Field x-direction dispersivity | 1e-3 | M |
| Field y-direction dispersivity | 1e-4 | M |
| Field effective molecular diffusion coefficient | 9e-9 | m$^2$/s |
| Field sorption partition coefficient | 1.2e-1 | L/kg |

Initially, the source zone was modeled to have a constant input concentration at the solubility limit, over a time interval that was consistent with what was observed with the corresponding X-ray analysis. Although this method was able to produce a near exact mass balance comparable to what was measured in the experiment, the resultant breakthrough curve did not match the experimental data. A second attempt at modeling the source zone involved calculating transient, dissolved mass flux values based on the measured mass depletion values in the source zone from the X-ray analysis. A transient dissolved mass flux curve was then generated and entered into FEHM for the source condition over the time of injection.
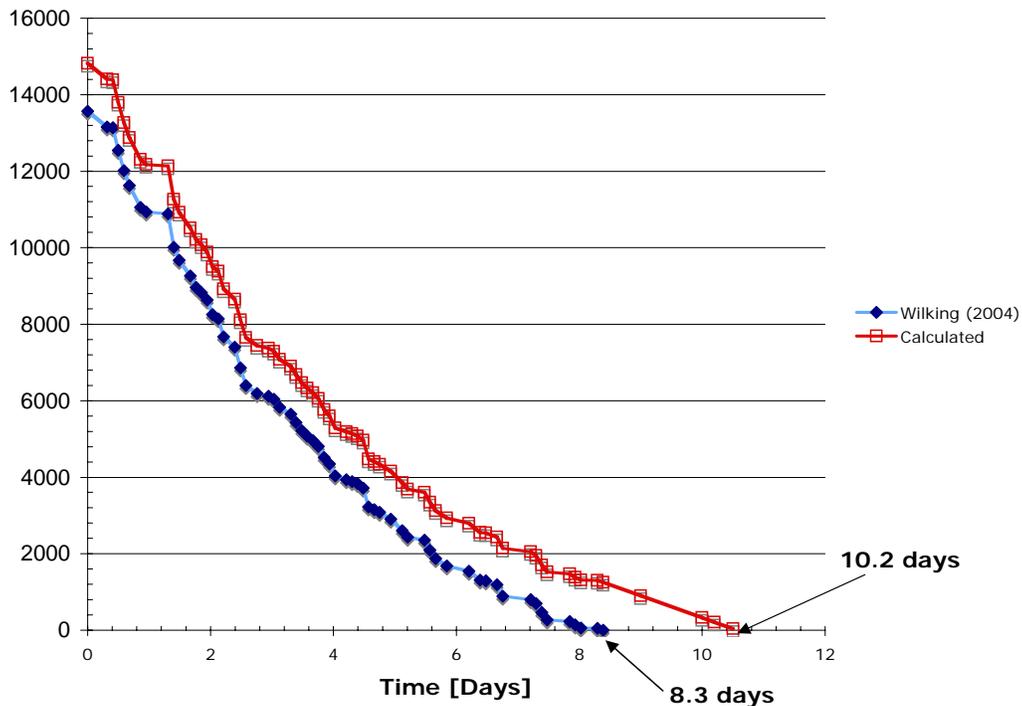
Figure 95 - Comparison of 1,1,2-TCA mass depletion in the source zone as measured by X-ray analysis for Wilking (2004) and the calculated values used for the numerical model for intermediate-scale experiment #1.

Figure 95 compares the exact data that was measured by (Wilking 2004) and the calculated mass depletion curve for the first intermediate-scale experiment. Additional calculations had to be performed in order to account for differences in the total mass injected between the intermediate-scale experiments and those performed by Wilking (2004). The additional calculations were done in the following manner. First, the rate values in Figure 95 obtained from the Wilking (2004) data were applied to the initial injected mass of the intermediate-scale experiment, which was a somewhat higher mass value than what was injected for the Wilking (2004) experiment. Therefore, at approximately 8.3 days, the mass in the Wilking (2004) experiment was depleted, while in the intermediate-scale experiment there was some amount of remaining mass. The rate value corresponding to the same mass remaining from the Wilking (2004) experiment was then incrementally applied to the remaining mass in the intermediate-scale

172

tank until the mass was depleted.  For example, if there were 1000 mg remaining in the intermediate-scale experiment, then the calculated rate value corresponding to 1000 mg remaining in the Wilking (2004) data was used to dissolve the remaining mass.  The time increment used was 0.1 days, in order to coincide with the measurement increment of the X-ray system.  Extending the rate obtained from the Wilking (2004) data over 0.1-day increments yielded a total time to mass depletion of 10.2 days for the intermediate-scale tank.
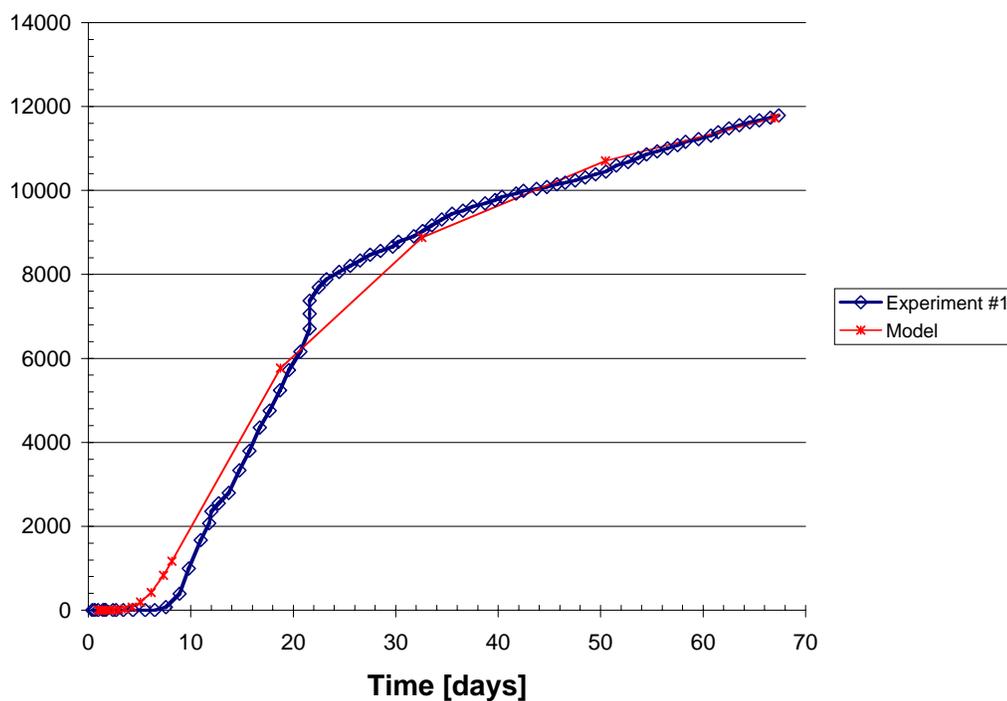


Figure 96 - Cumulative mass-depletion comparisons from experiment #1 and the numerical model.  Note:  The source is depleted at 10.2 days.

The transient flux curve was input to the numerical model and the mass removed from the model domain was plotted against the amount of mass removed during the course of the first experiment.  The model curve shown in Figure 96 does not capture the initial peak of the experimental data.  The tailing of the curve does follow the trend of the experimental data.  It was hypothesized at this point, that the source zone architecture was more complicated than originally assumed.  It

was thought that there might be two distinct dissolving source zones of 1,1,2-TCA in the coarse inclusion. The X-ray saturation profile for this source was re-examined to determine if the source zone had two separate dissolving sources. Figure 97 confirms that there may have been two separate masses in the source zone thought to be a direct result of the low amount of 1,1,2-TCA free-phase mass initially injected. The injection method for this experiment was conducted in the same manner as for experiments #2 and #3, although it is thought that due to the small amount of mass injected, there wasn't enough pressure to push the 1,1,2-TCA to the bottom of the coarse inclusion. This resulted in a dispersed architecture that contained two sources of 1,1,2-TCA in the coarse inclusion (see Figure 97). The first source, Region 1 in Figure 97, would dissolve quickly and would not have contact with the field soil layer, thereby allowing faster dissolution in the #30 sand layer. The second source, Region 2 in Figure 97, would contain the majority of the 1,1,2-TCA mass and would be in direct contact with the interface between the #30 sand layer and the field soil layer.
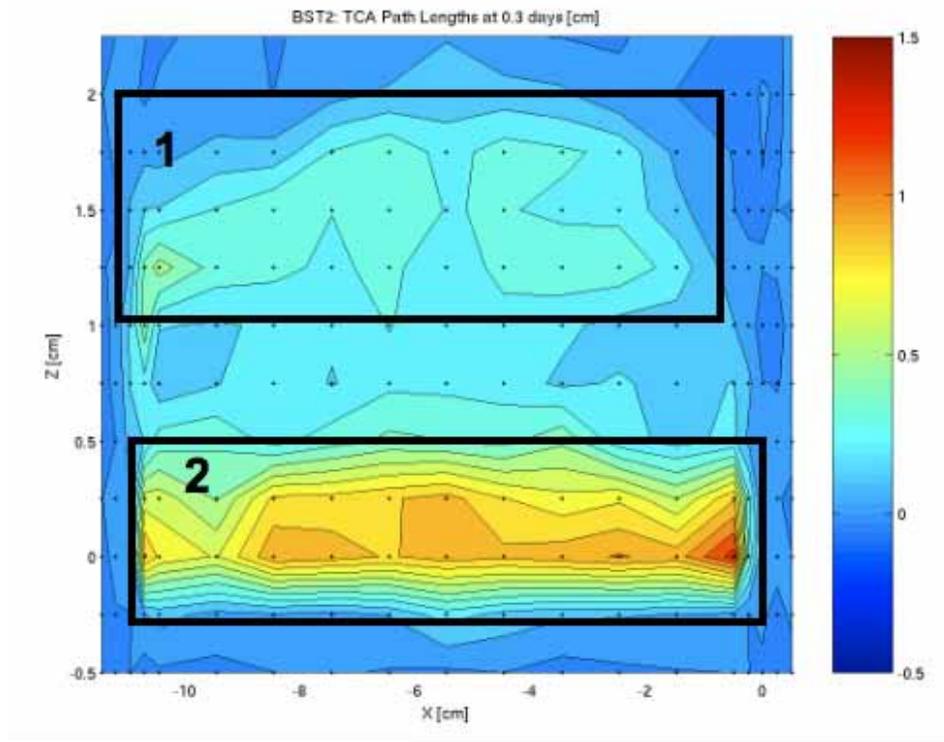
Figure 97 - X-ray saturation profile of BST-2 (Wilking 2004).  Region 1 represents a lower saturation source zone, while Region 2 represents a separate, higher saturation source zone.

Based on the hypothesis of a dual-source zone, the numerical simulations were revisited.  Several attempts were made to capture the initial peak of the experimental data using a separate source zone in the #30 sand layer, but it was determined that there was some degree of interconnectivity between the two sources that was not being captured by the model.

Sensitivity analyses were then conducted to determine which parameters had the strongest influence on the shape of the resulting breakthrough curve.  The first sensitivity test was performed by varying the number of matrix layers located at each dual-porosity node.  It was found that increasing the number of layers affected the breakthrough curve by increasing the peak height of the curve. From these analyses, it was determined that 110 layers best represented the system to the depth of the tank.  Sensitivity analyses were also performed on the

volume fraction assigned to the primary porosity at the dual-porosity node.  As discussed previously, this means that the volume fraction assigned to the #30 sand and field soil in the dual-porosity nodes was varied.  For example, if the volume fraction input was 0.01, then 0.01 of the total volume at a node was assigned to the #30 sand and 1 – 0.01, or 0.99 was assigned to the field soil.  It was determined that a value of 8e-1 best represented the experimental data.

The sensitivity results of varying the matrix diffusion coefficient determined that the matrix diffusion coefficient was the most sensitive parameter in the numerical model and represented the degree to which mass diffuses into and out of the field soil layer.  A higher value of the coefficient results in more mass entering the field layer.  The following figures display kriged 1,1,2-TCA dissolved mass concentrations within the model domain over time.  Flow is from right to left in all figures.  The highest concentration of dissolved 1,1,2-TCA is represented in red, while a zero concentration is indicated by blue.  The orange horizontal line on the figures illustrates the interface between the #30 test sand and the field soil.  The orange vertical line in the figures represents the starting point of the dissolved 1,1,2-TCA injection.
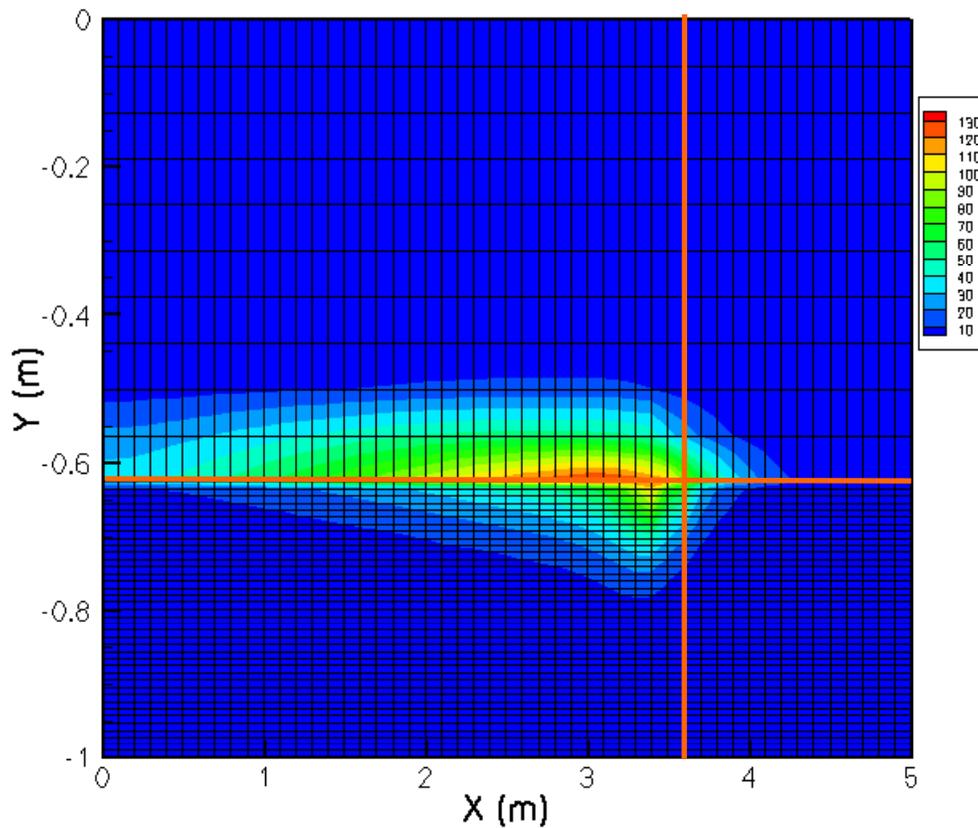
Figure 98 – Distribution of 1,1,2-TCA concentrations, Experiment #1, time = 8.16 day

In Figure 98, the majority of the plume is being advectively transported through the #30 test sand layer, although some of the mass is diffusing into the field soil layer at the interface between the two materials.

In Figure 99, the mass in the source zone has completely dissolved, as measured through X-ray analysis. At this point, the plume continues to separate into an upper portion, located in the #30 sand layer, and a lower portion, located in the field soil layer.
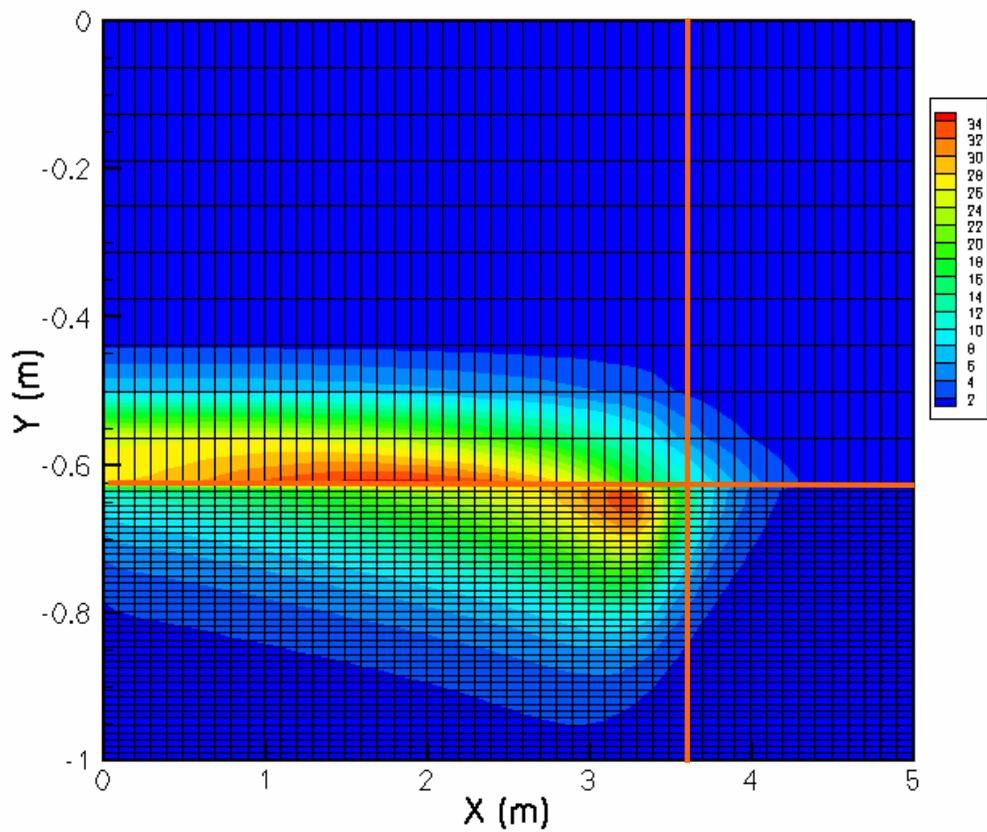
Figure 99 - Distribution of 1,1,2-TCA concentrations, Experiment #1, time = 18.76 days
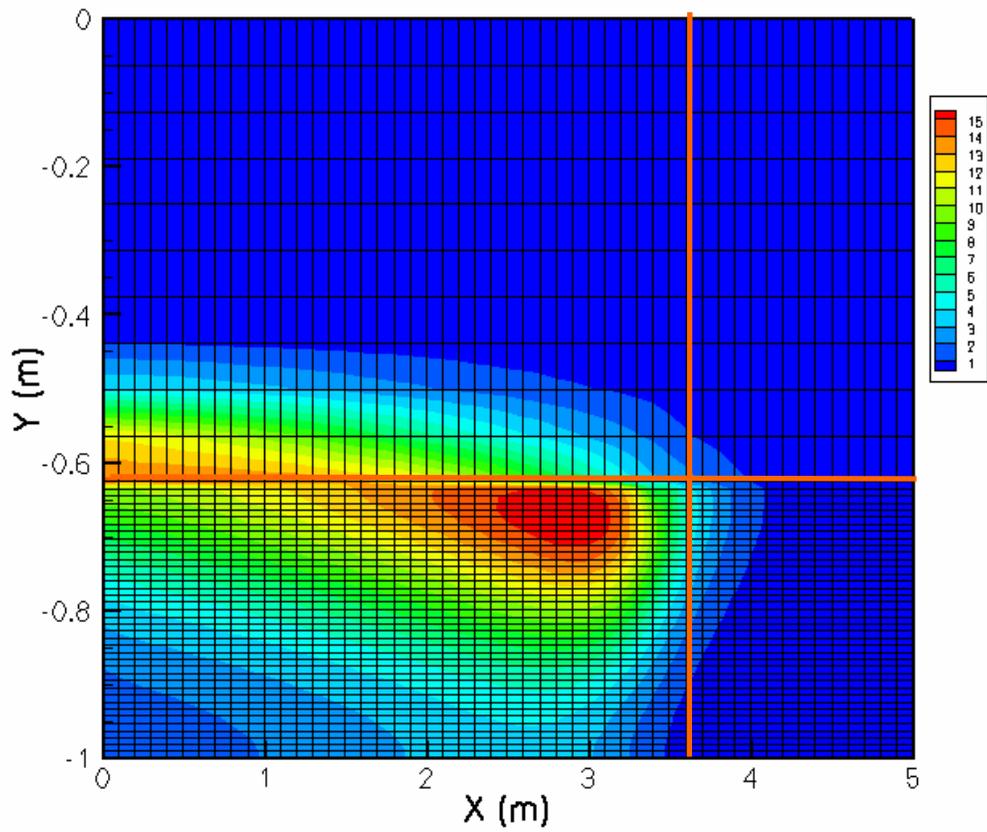
Figure 100 - Distribution of 1,1,2-TCA concentrations, Experiment #1, Time = 32.55 days
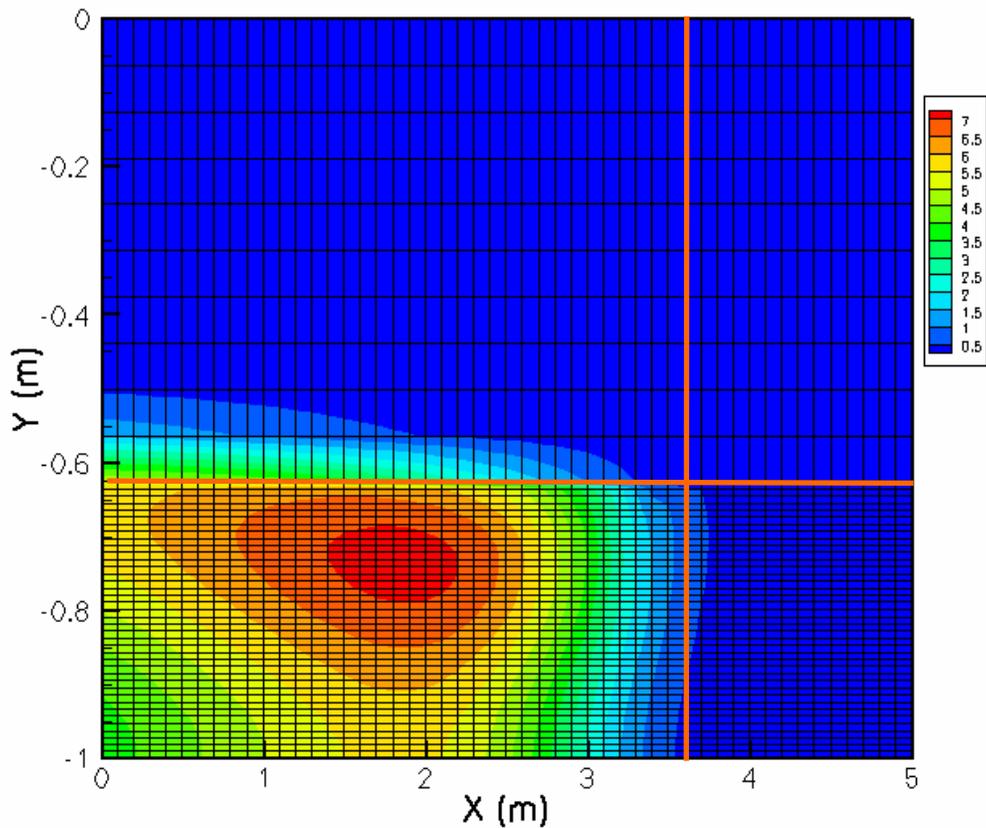
Figure 101 - Distribution of 1,1,2-TCA concentrations, Experiment #1, Time = 67 days

The final state of the experiment in Figure 101 is similar to what was found when destructive sampling was performed on the field layer (see Section 3). At this stage, the dissolved 1,1,2-TCA is contained in the silt layer as a result of the transverse diffusion from the sand layer and slow advective transport through the field layer. The field layer was not cored to the bottom of the tank, but the measured data was kriged in order to generate what may have been one interpretation. The kriged data shows a hotspot downstream of the injection point, near the effluent end of the tank, similar to what is shown in Figure 101.

The initial hypothesis of the numerical simulations for experiment #1 was to determine if FEHM could explain the experimental data. Due to the complexity of the initial source zone architecture, it was concluded that FEHM was not able to capture the complexity of the initial source condition for this experiment. FEHM did simulate the processes that were contributing to the shape of the breakthrough curve, namely the strong contribution of the matrix diffusion coefficient and transfer of mass between the immobile and mobile dual-porosity defined nodes at the interface.

It was unfortunate that such a small amount of mass was injected into the source, but it was not known at the time of execution of the experiment how much mass was needed in order to generate a "predictable" source zone. Although this experiment was the easiest to conduct in the laboratory, it was the most difficult to numerically simulate. The next sections provide discussions on experiments #2 and #3 which where much more complex to execute in the lab, but proved to be easier to simulate due to a more uniform initial block structure of the injected pure phase 1,1,2-TCA in the source zone.

4.4.2.4.2      Numerical Modeling Simulations for Experimental Tank #2.

The model domain for the second intermediate-scale tank experiment was described in detail in Section 3. In summary, the main feature of intermediate-scale experiment #2 was a mound of field soil located downstream of the injection point. The purpose of the mound was to simulate both diffusion and
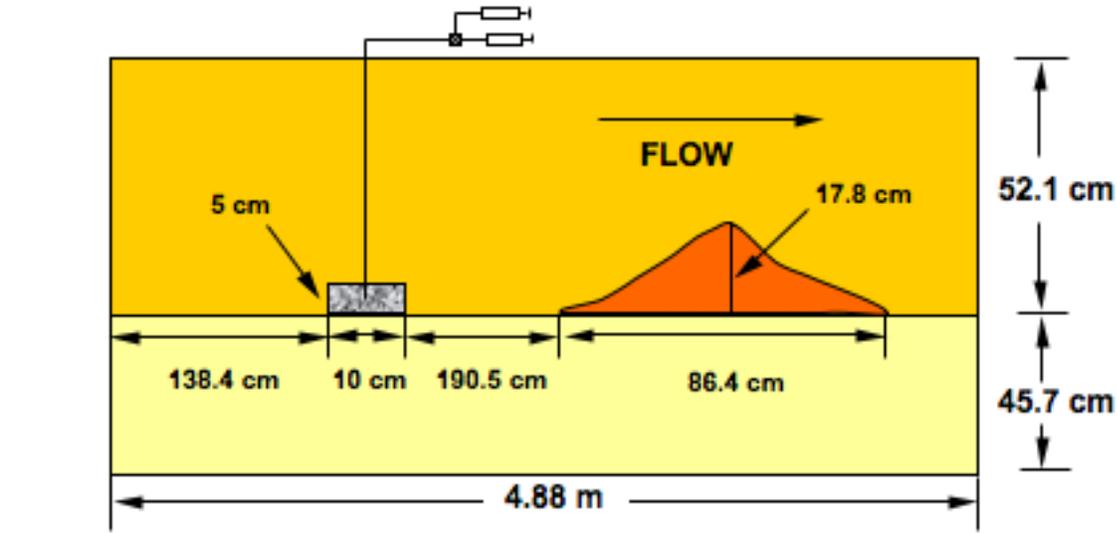
Figure 102 - Model domain for experimental tank #2.

advection contributing to stagnant zone storage. The layered system consisted of a #50 test sand overlying a #140 test sand. The model domain consisted of 2,541 nodes and 2,432 elements (see Figure 102). The injection node was located at [3.6 m, -0.521 m] and was assigned the material properties of #16 test sand. For the boundary head provided, the flow in Figure is from the right end of the tank to the left end. All of the nodes in the #50 sand layer that were located along the length of the sand/field-soil interface layer were designated as dual-porosity nodes.

Figure 103 illustrates the velocities vectors in the area immediately surrounding the coarse inclusion of a #16 test sand used for the source zone. The lengths of the vectors are proportional to the magnitude of the velocity. The streamlines that enter and are directly above the higher permeability material diverge from the lower permeable #30 sand material and pass through the coarse material at a higher velocity. The smaller arrows in the lower half of the figure indicate the smaller velocities through the #140 sand layer. Figure 104 illustrates the velocity vectors into and around the mound of field material. As the streamlines approach the incline of the field soil mound, the velocity increases and some of

the streamlines pass through the mound, while many are forced to converge over the top of the mound. The velocity vectors that enter the mound are at a reduced velocity as indicated by the smaller arrows and are directed downwards into the mound. The streamlines exit the left side of the mound and are at the same angle that they entered the mound at the right side. The small arrows in the lower half of Figure 104 show the reduced velocities through the #140 sand.
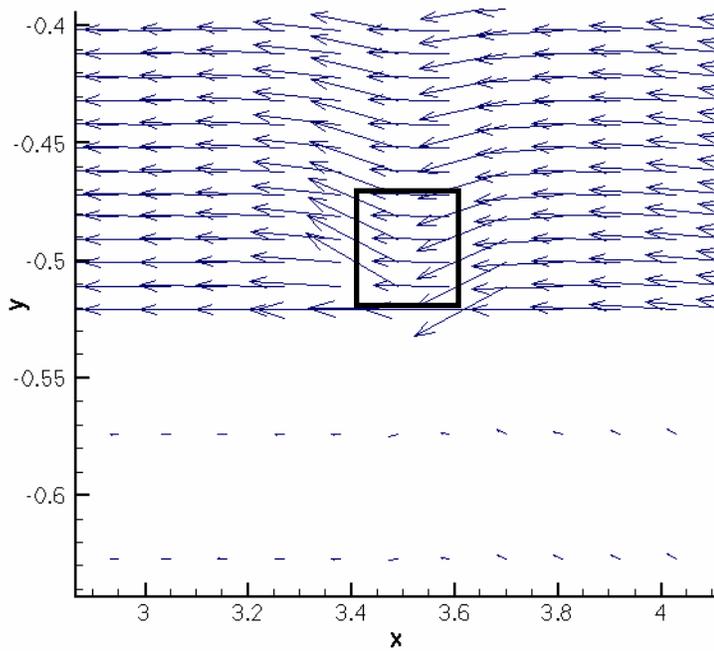


Figure 103 - Velocity vectors for the source zone area in the domain of experiment #2.
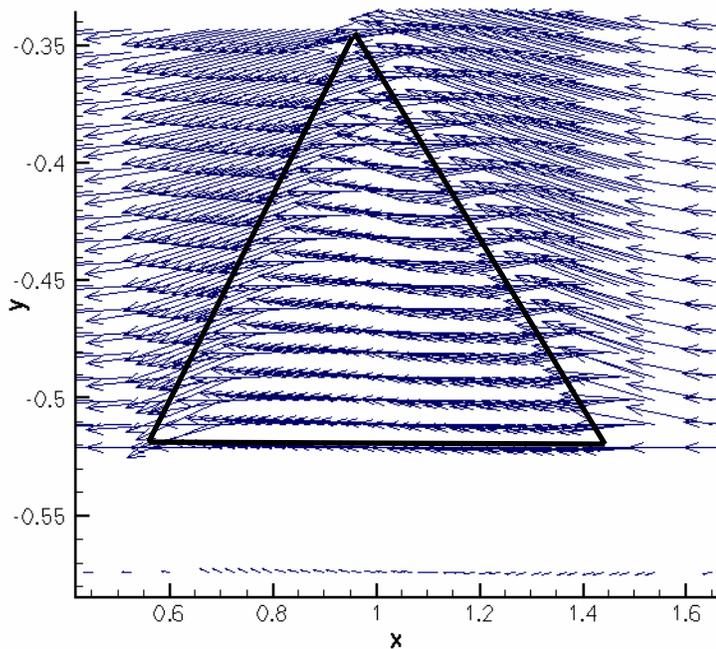
Figure 104 - Velocity vectors for the mound area in the domain of experiment #2.

The same methods used for the experimental tank #1 simulations were used for the experimental tank #2 simulations. The rate of mass depletion obtained from the X-ray data obtained by (Wilking 2004) was applied to a somewhat higher total mass injected for the second intermediate-scale experiment (see Figure 105). For this X-ray data set, scans on the source zone were not performed for approximately 20 days from day 15 to day 35. Therefore, an average mass depletion rate was assumed for this time period.
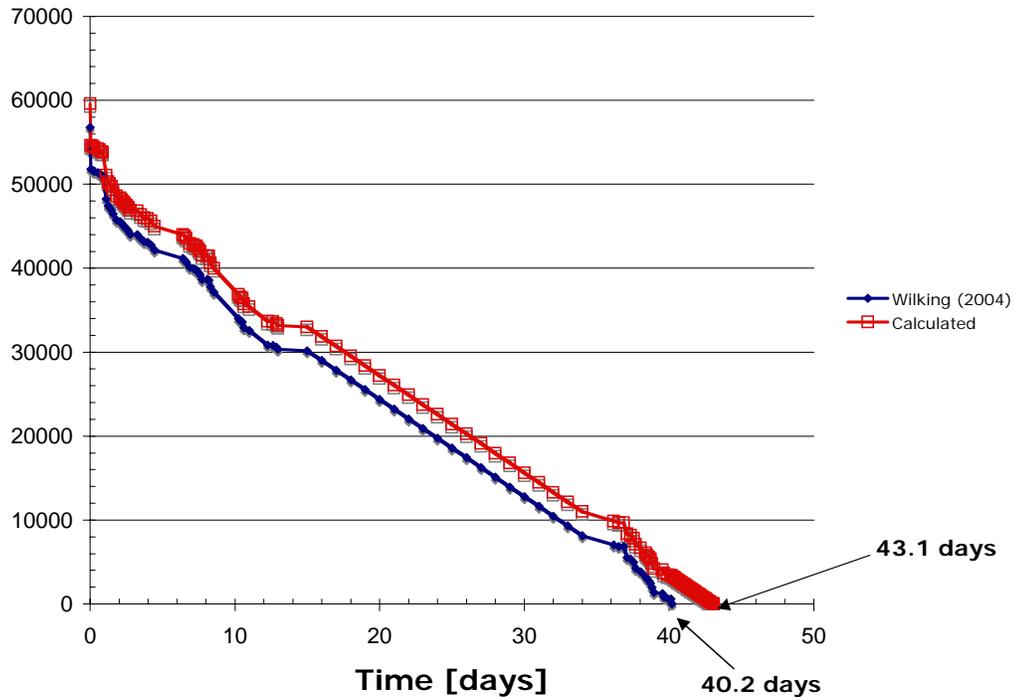
Figure 105 - Comparison of 1,1,2-TCA mass depletion in the source zone as measured by x-ray analysis for Wilking (2004) and the calculated values for the second intermediate-scale experiment.

Table 15 lists the model inputs for experiment #2. The matrix diffusion coefficient determined from the simulations for the first experiment was used as a starting point for the second experiment simulations. The volume fraction of the primary porosity assigned to the dual-porosity node from the first experiment was used as a staring point for the second experiment. Due to the nature of the geometry of the domain (the depth of the field material in experiment #2 was much less than experiment #1), the number of matrix layers used in the field soil mound was reduced from the number used in the first experiment. An initial value of eight layers was used as a starting point, which is equal to the minimum value recommended by the model developers.

Table 15.  Model inputs for large tank experiment #2.

| Name | Value | Units |
|---|:---:|:---:|
| Domain length (x) | 5 | m |
| Domain height (y) | 1 | m |
| #50 node spacing in the x-direction above mound | 7.5e-2 | m |
| #50 node spacing in the y-direction above mound | 6.9e-2 | m |
| #50 node spacing in the x-direction with the mound | 2.5e-2 | m |
| #50 node spacing in the y-direction with the mound | 1e-2 | m |
| Field node spacing in the x-direction | 2.5e-2 | m |
| Field node spacing in the y-direction | 1e-2 | m |
| Volume fraction assigned to primary porosity in gdpm macro | 8e-1 | [-] |
| Number of gdpm layers at each dual-porosity node | 8 | [-] |
| Water density | 1000 | $kg/m^3$ |
| Boundary head at inlet | 1.543 | m |
| Boundary head at effluent | 1.505 | m |
| Water temperature | 20 | C |
| #16/#50/#140 x-direction dispersivity | 1e-2 | m |
| #16/#50/#140 y-direction dispersivity | 1e-3 | m |
| #16/#50/#140 effective molecular diffusion coefficient | 8e-10 | $m^2/sec$ |
| Field x-direction dispersivity | 1e-3 | m |
| Field y-direction dispersivity | 1e-4 | m |
| Field effective molecular diffusion coefficient | 8e-10 | $m^2/s$ |
| Field sorption partition coefficient | 1.2e-1 | L/kg |

Figure 106 illustrates the numerical mass removal curve compared to the mass removal curve measured in the experiment.  The numerical curve does not exactly match all the features of the experimental data.  The discrepancy in the curves is directly attributable to the calculated transient source function used as input to the numerical model.  X-ray data was not captured from days 15 to 35 by Wilking (2004) and therefore the average value used may both underestimate or overestimate the transient source curve depending on what time interval is observed.
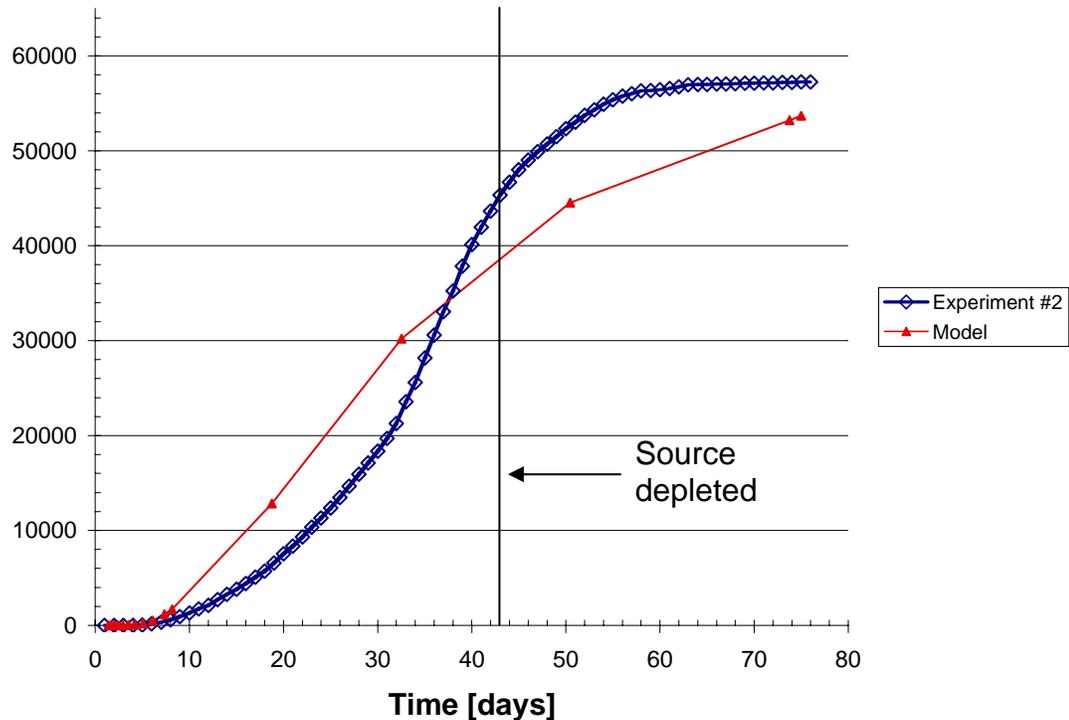
Figure 106 - Comparison of model-simulated total mass removed with mass removed in the experiment.

Sensitivity analyses were performed similar to what was done for experimental tank #1. The major difference for this experiment compared to the first experiment, was that the dual-porosity macro had a reduced effect on the resultant breakthrough curve. This was thought to be the result of (1) the available interfacial area between the #50 sand material and the field soil was much less than what was available between the #30 sand layers and the field layer in the first experiment and (2) the mound created a situation that caused advective transport to dominate. Although the dual-porosity macro did not have as great effect on the breakthrough curve, mass was still entering the mound. Further sensitivity analyses showed that the sorption process occurring in the mound had little to no effect on the resultant breakthrough curve. Overall, the sensitivity analyses showed a strong advective dominance occurring in the domain of experiment #2. The interfacial area between the field soil and the #50 test sand available for molecular diffusion was limited to the incline side of the

mound, as the mass exiting the decline side was a result of the mass being forced downward by the velocity profile (discussed previously in Figure 104).  As a direct result, changes in the matrix diffusion coefficient had little effect on the breakthrough curve.

In summary, the two driving factors for experiment #2 were (1) the transient mass flux curve generated as a result of a higher saturated source zone and (2) the velocity profile generated as a result of the downstream mound.  The influence of the transient mass flux curve determined most of the shape of the curve up to its maximum peak value in the breakthrough curve.  The mound in the domain of the experiment attenuated the advective transport of dissolved mass not only through the mound, but also over the top of the mound and directly beneath the mound.  The following figures are snap shots of the kriged concentrations of the dissolved 1,1,2-TCA mass being transported through the domain during the time interval of the experiment.  For all figures, the red color represents the highest concentration value and the blue represents a zero concentration value.  Flow in the figures is from right to left.  The orange horizontal line indicates the interface between the #50 test sand and the #140 test sand.  The orange vertical line indicates the location of the injection point.
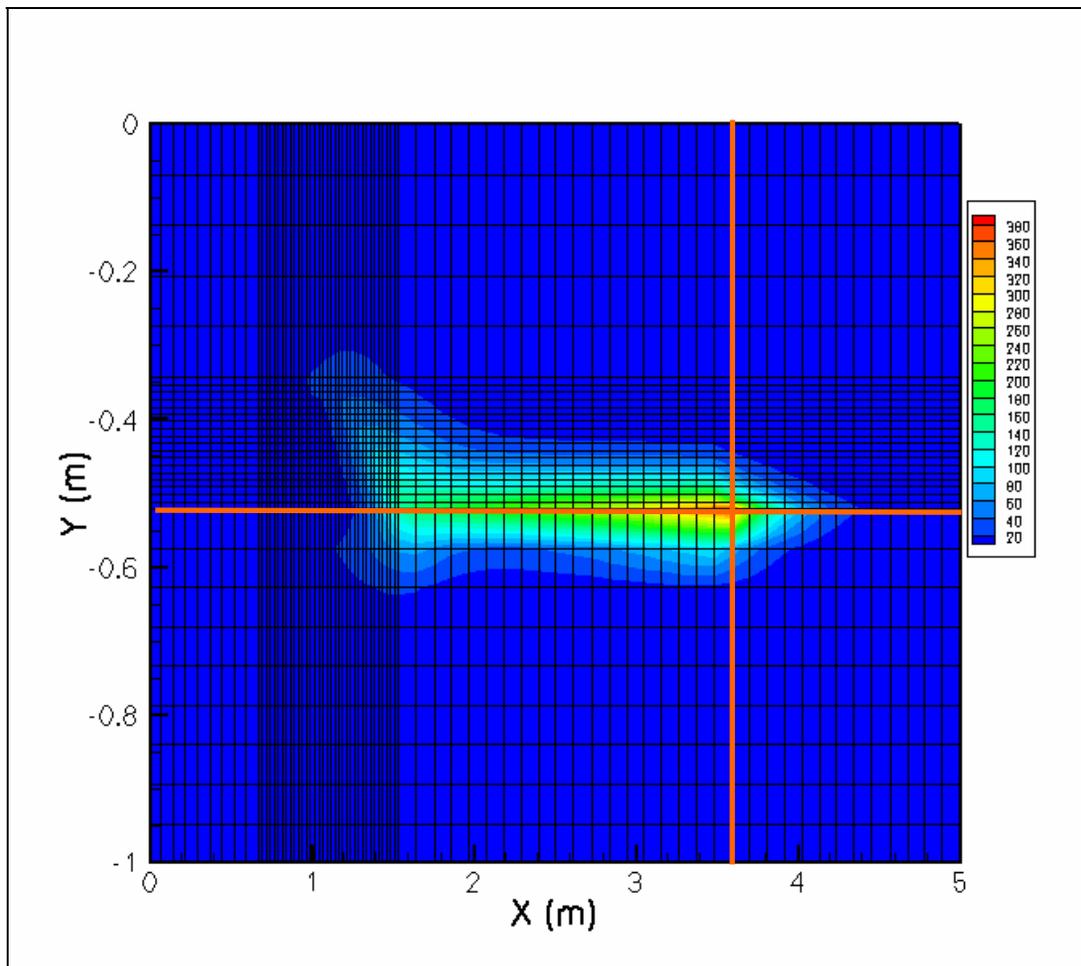
Figure 107 - Distribution of 1,1,2-TCA concentrations, Experiment #2, Time = Day 8.16.
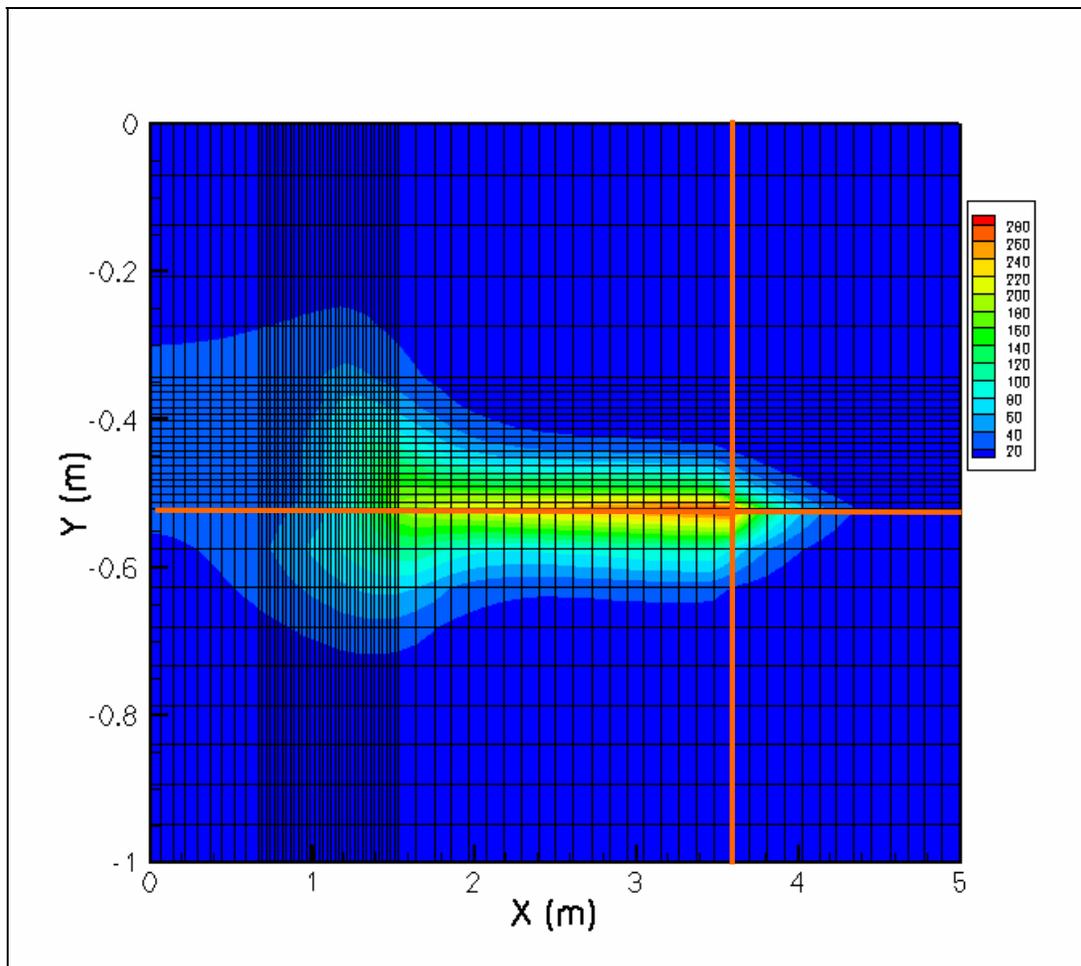
Figure 108 - Distribution of 1,1,2-TCA concentrations, Experiment #2, Time = Day 32.55

As shown in Figure , all of the pure phase mass has dissolved from the source zone.
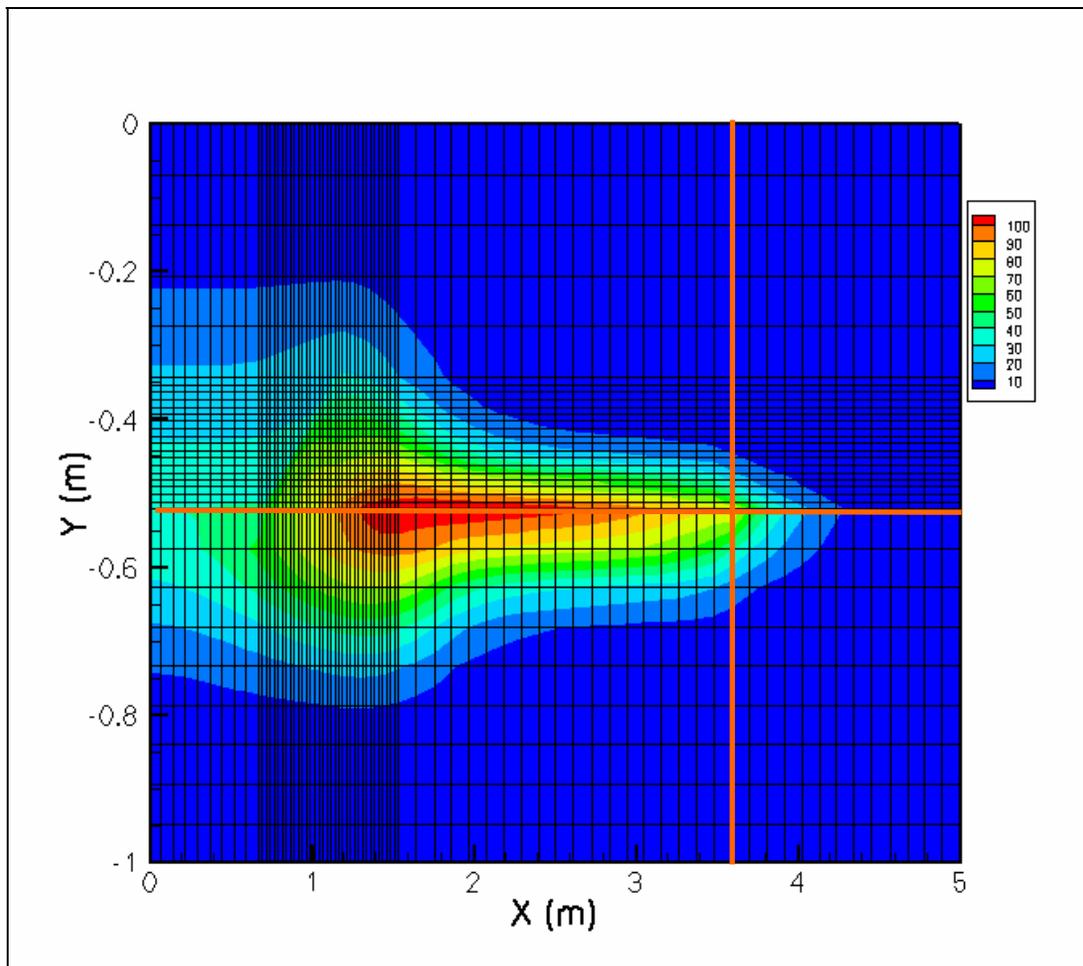
Figure 109 - Distribution of 1,1,2-TCA concentrations, Experiment #2, Time = Day 50.47.
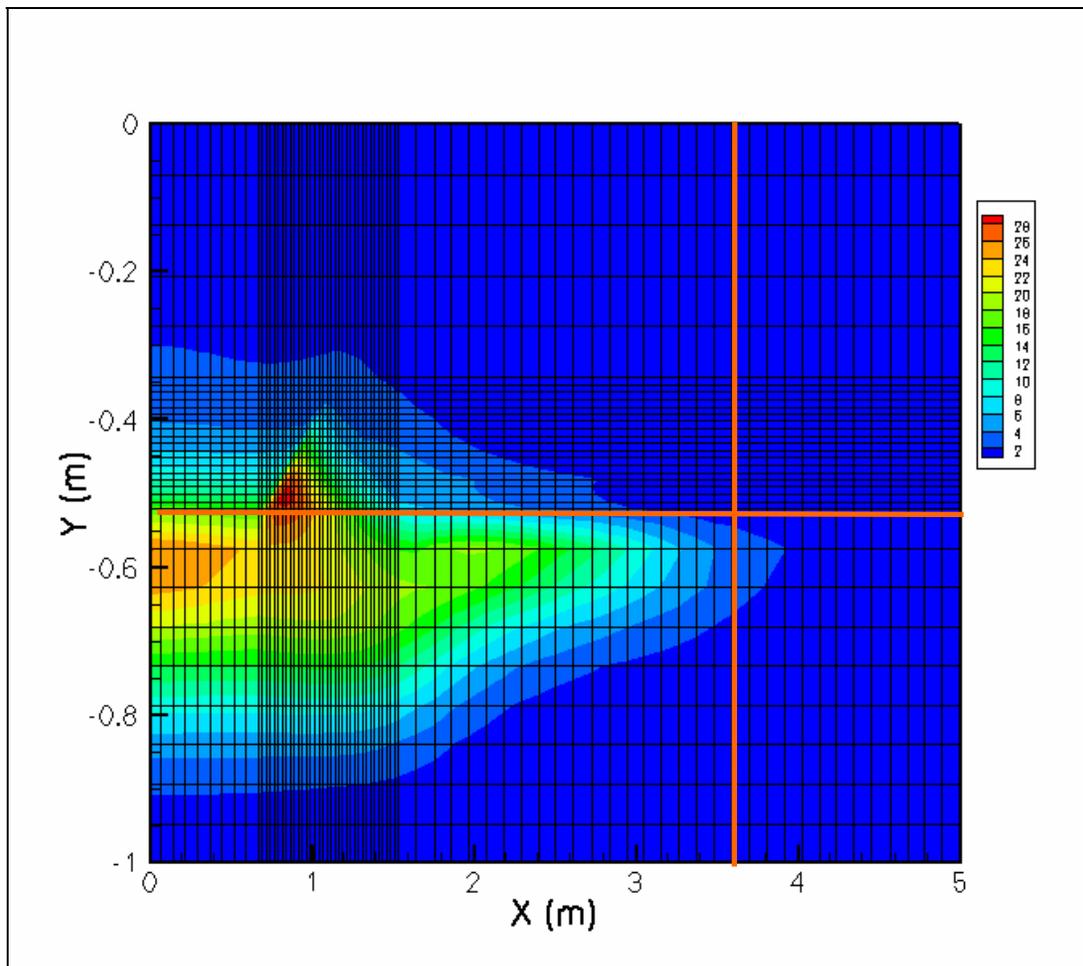
Figure 110 - Distribution of 1,1,2-TCA concentrations, Experiment #2, Time = Day 75.

### 4.4.2.4.3 Numerical Modeling Simulations for Experimental Tank #3

The model domain for the third intermediate-scale tank experiment was described in detail in Section 3. In summary, the main feature of intermediate-scale experiment #3 was an inclined plane of field soil overlaying a layer of #30 test sand. The model domain consisted of 3,050 nodes and 2,940 elements. The injection node was located at [4.29 m, -0.65 m] and was assigned the material properties of a #16 test sand. For the boundary head provided, the flow in Figure 111 is from right to left. All of the nodes in the #30 sand layer, with the exception of nodes 2921, 2983, and 3045, that were located along the length of the sand/field interface were designated as dual-porosity nodes.
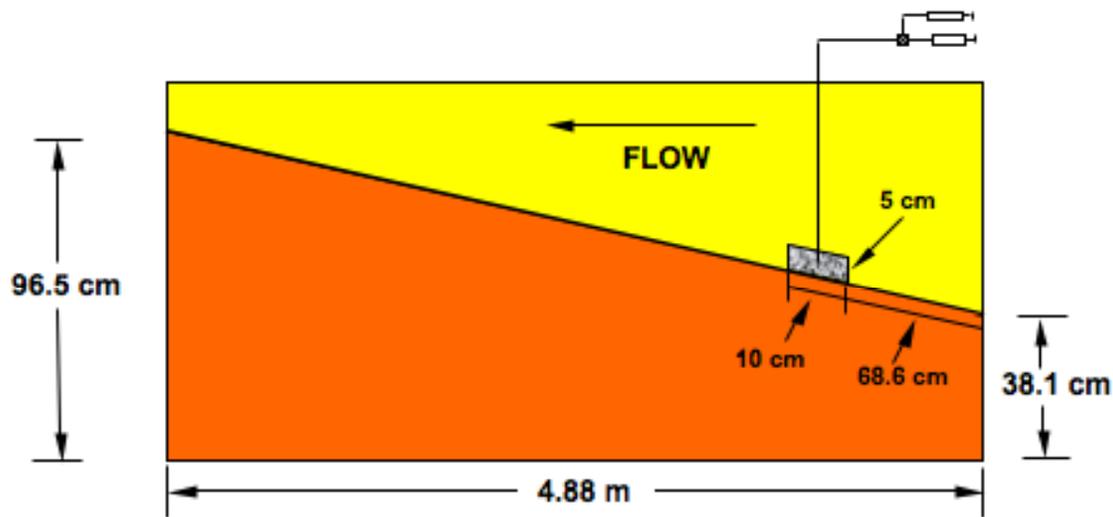


Figure 111 - Model domain for Experiment #3

The heterogeneity representation used in the packing produced a complex flow field as shown in Figure 112 and Figure 113. As was the case for the flow field near the incline side of the mound in experiment #2, the velocity vectors at the interface between the field layer and the #30 sand layer are directed downwards into the mound. The vectors that approach the top of the mound start to converge and the velocity is increased. The size of the arrow is proportional to the magnitude of the vector.
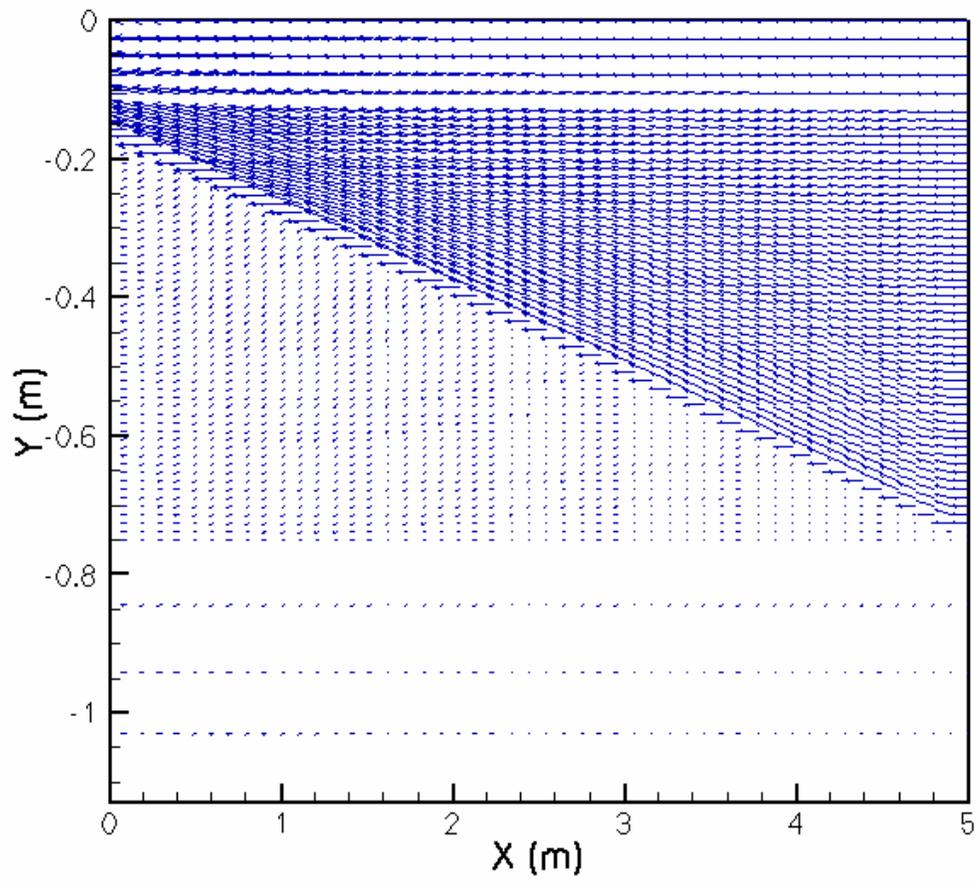
Figure 112 - Velocity vectors for experiment #3.
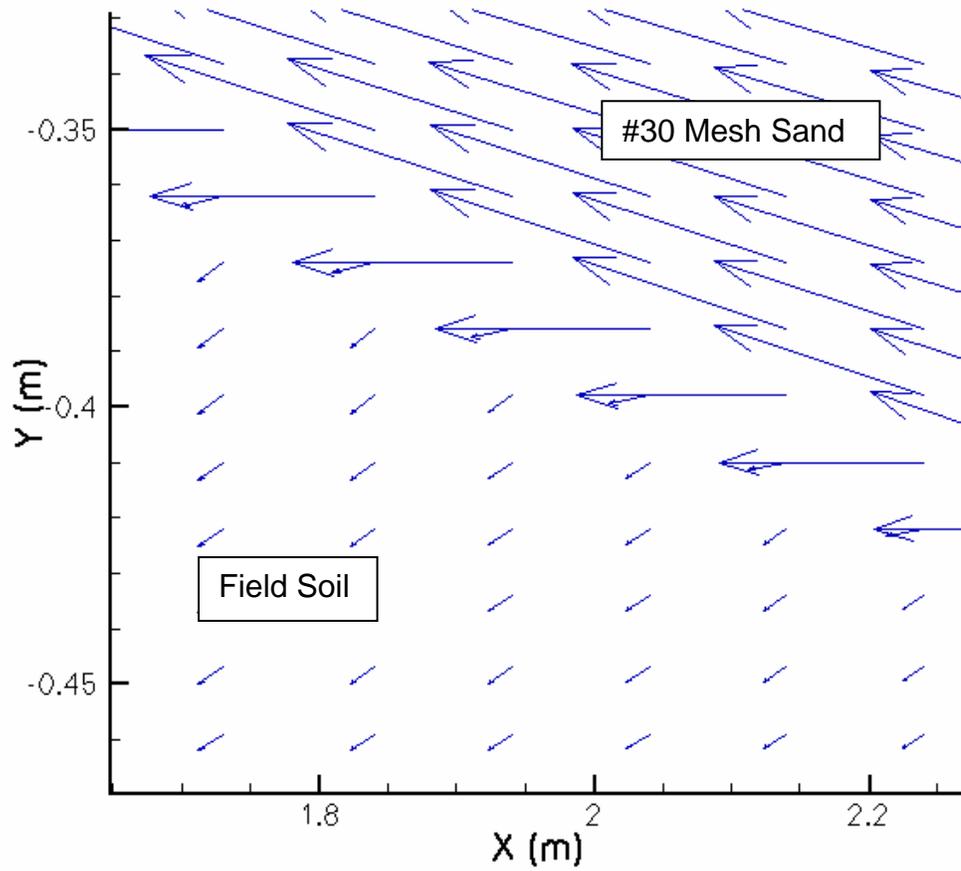
Figure 113 -Magnified section of velocity vectors for Experiment #3 at the interface between the #30 sand layer and the field-soil layer on the incline.
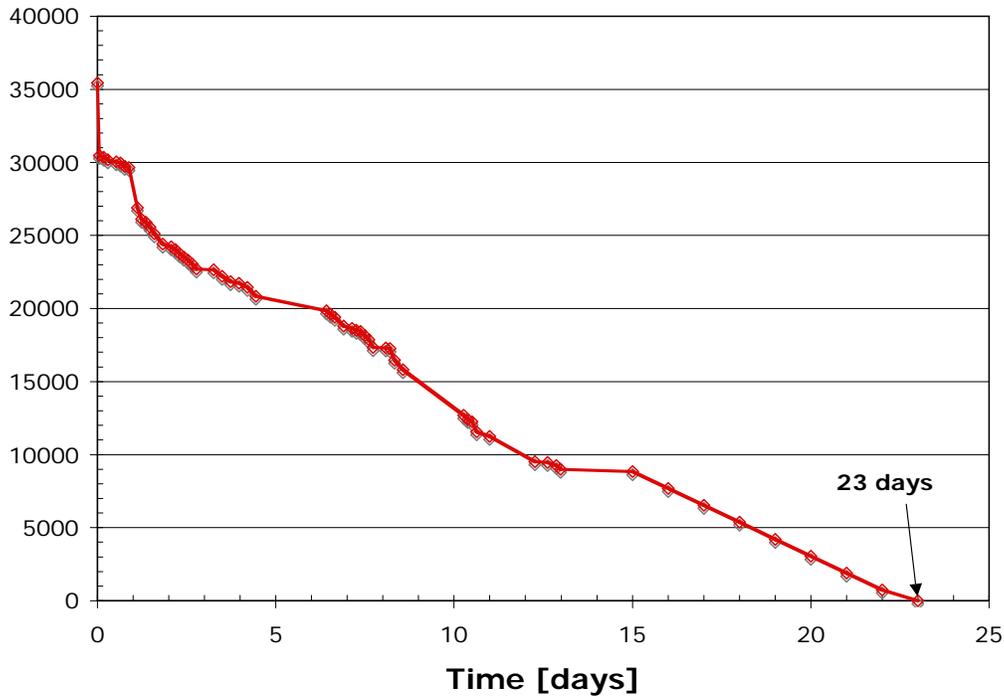
Figure 114 - Calculated values for 1,1,2-TCA mass depletion in the source zone. Obtained from X-ray analysis by Wilking (2004) for the third intermediate-scale experiment.

The same rate values used for the calculation of the mass depletion curve in experiment #2 were used for experiment #3 (see Figure 114). As was the case for the first two experiments, the measured rate values were applied to the initial starting mass of the actual intermediate-scale experiment. Table 16 lists the model inputs for the simulations of experiment #3. As was discussed in the introduction section of the modeling work, the objective of modeling experiment #3 was to predict the experimental breakthrough curve using the knowledge gathered from the simulations of experiments #1 and #2. With this in mind, the matrix diffusion coefficient, number of matrix layers used at the dual-porosity nodes, and volume fraction assigned to the primary porosity of the dual-porosity nodes obtained in the simulation of the first experiment were used as input.

Table 16. Model Inputs for large tank experiment #3

| Name | Value | Units |
|---|---|---|
| Domain length (x) | 5 | m |
| Domain height (y) | 1.2 | m |
| #30/Field node spacing in the x-direction | 1e-1 | m |
| #30 node spacing in the y-direction above incline | 2.6e-2 | m |
| #30/Field node spacing in the y-direction (incline) | 1.2e-2 | m |
| #30/Field node spacing in the y-direction below the incline | 9.5e-2 | m |
| Volume fraction assigned to primary porosity in gdpm macro | 8e-1 | [-] |
| Number of gdpm layers at each dual-porosity node | 10 | [-] |
| Water density | 1000 | kg/m$^3$ |
| Boundary head at inlet | 1.470 | m |
| Boundary head at effluent | 1.468 | m |
| Water temperature | 20 | C |
| #16/#30 x-direction dispersivity | 1e-2 | m |
| #16/#30 y-direction dispersivity | 1e-3 | m |
| #16/#30 effective molecular diffusion coefficient | 8e-10 | m$^2$/sec |
| Field x-direction dispersivity | 1e-2 | m |
| Field y-direction dispersivity | 1e-3 | m |
| Field effective molecular diffusion coefficient | 8e-10 | m$^2$/s |
| Field sorption partition coefficient | 1.2e-1 | L/kg |

The initial simulation run did not predict the measured experimental breakthrough curve data. Although, after performing sensitivity analyses, it was determined that increasing the value of the matrix diffusion coefficient generated a closer match to the mass removal curve as shown in Figure 115. The spike in the effluent data was caused by a spike in the influent feed water from the facility.

Sensitivity analyses were performed in similar fashion to what was done in the first two experiments and the value of the matrix diffusion coefficient had the greatest effect on the amount of mass removed from the model domain.
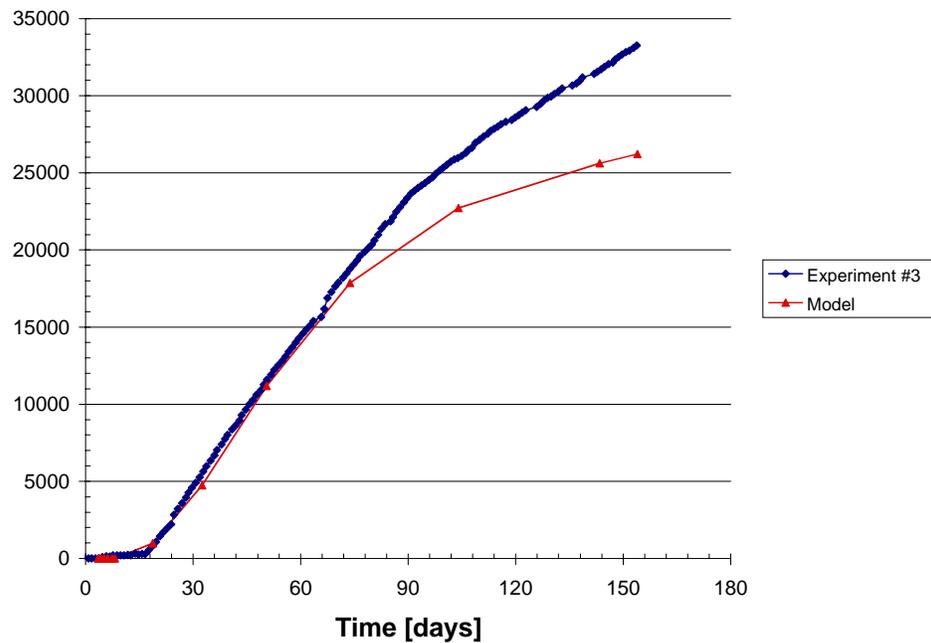
Figure 115 - Cumulative mass-depletion comparison between experiment #3 and the numerical model results.

The discrepancy in the curves in Figure 115 at approximately day 70, is directly attributable to two major spikes in the influent water to the experimental tank system from the facility water supply. A spike occurred at days 74 and at 104 that coincide with the increased in mass removed on the experimental curve. From day 104 onward, the flow rate in the system saw an overall increase, possibly a result from the spikes to the system causing some clogged material to unclog. A transient flow simulation was also executed using the daily measured flow rate values obtained from the experimental system. The following figures provide snapshots for the perturbations in the 1,1,2-TCA dissolved contaminant plume over the duration of the experiment. The red color in the legend indicates the highest concentration, while the dark blue color indicates zero concentration.

Flow is right to left in all figures. The orange vertical line indicates the starting point of the injection and the orange inclined line, represents the interface between the #30 test sand and the field soil layer.

In the following figures, the source zone has almost completely dissolved. Although, due to both transverse advection into the field soil layer and diffusion into the field soil layer, the majority of the plume is being displaced into the field material. The remaining figures will illustrate these concepts.



.
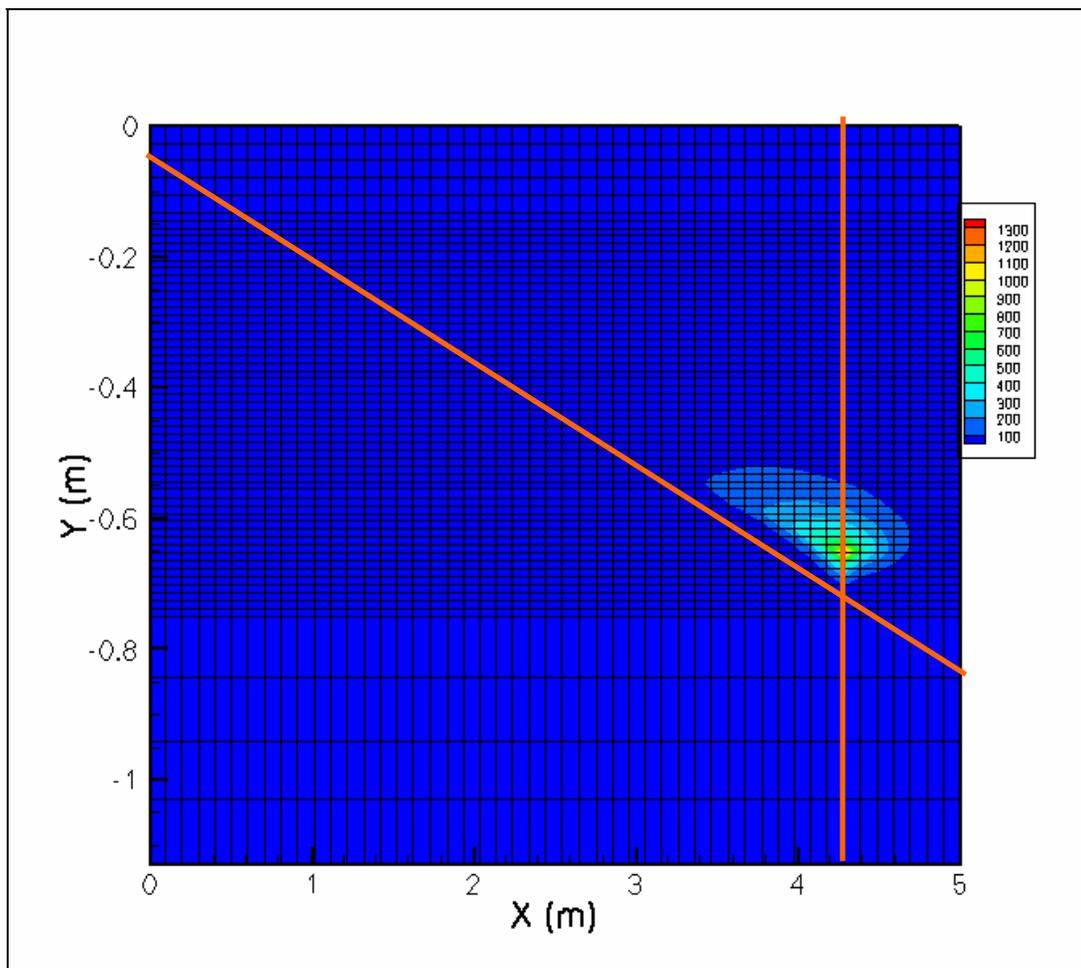
Figure 186 - Distribution of 1,1,2-TCA concentrations, Experiment #3, Time = Day 8.2.
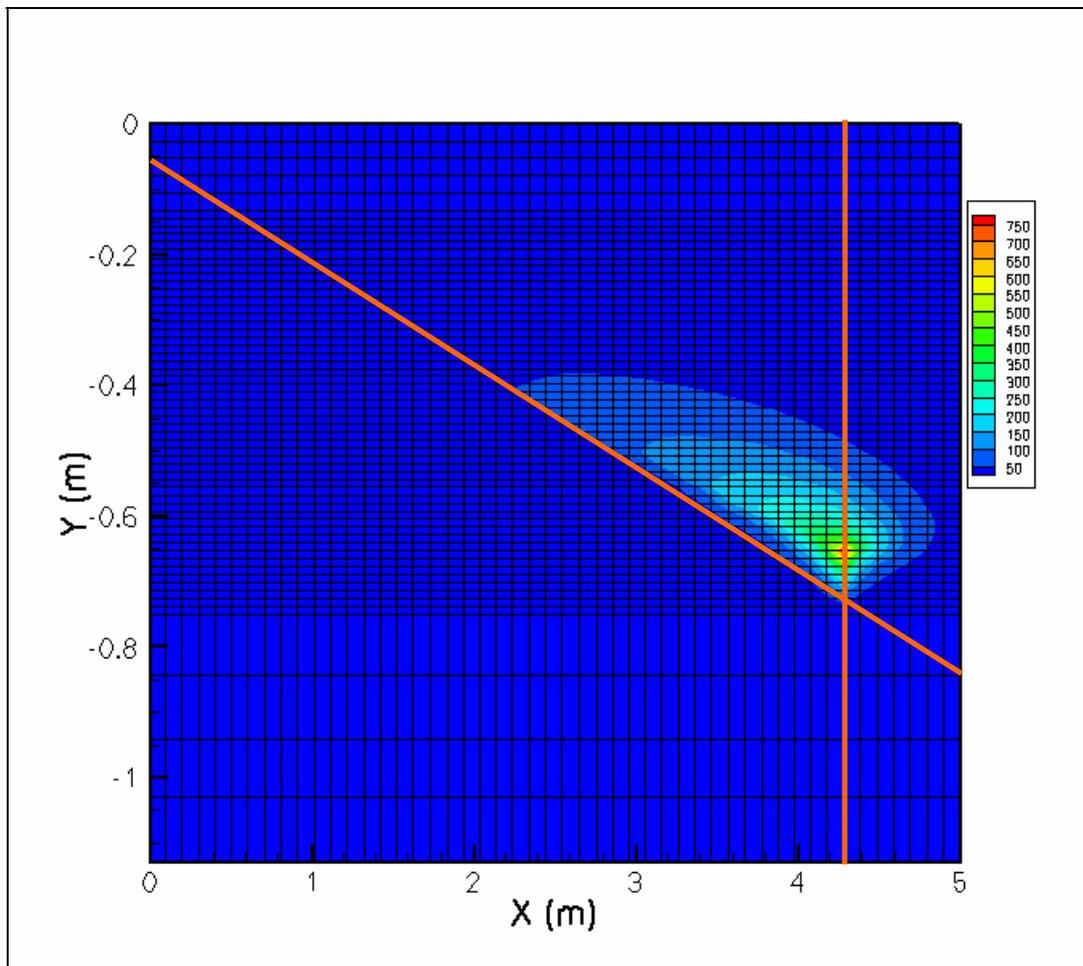
Figure 19 Distribution of 1,1,2-TCA concentrations, Experiment #3, Time = Day 18.8.
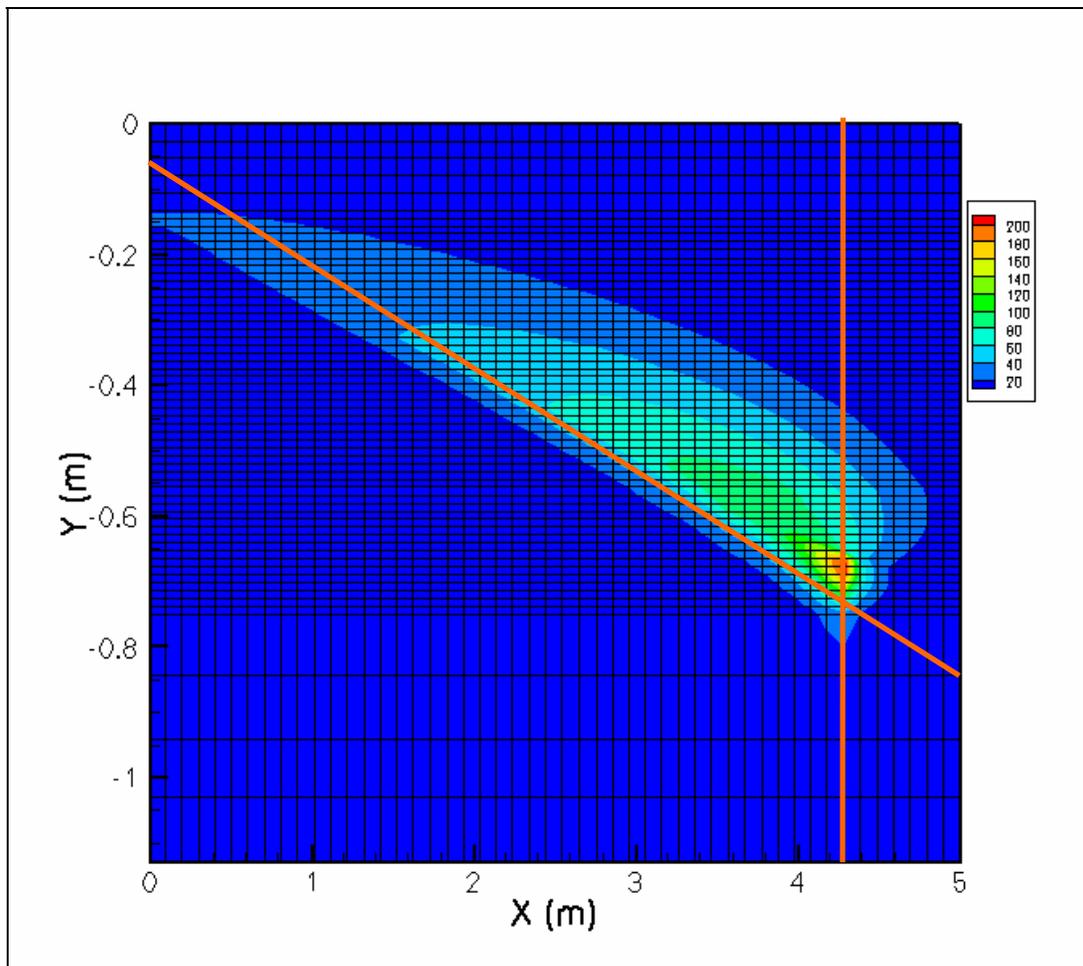
Figure 118 - Distribution of 1,1,2-TCA concentrations, Experiment #3, Time = Day 32.5.
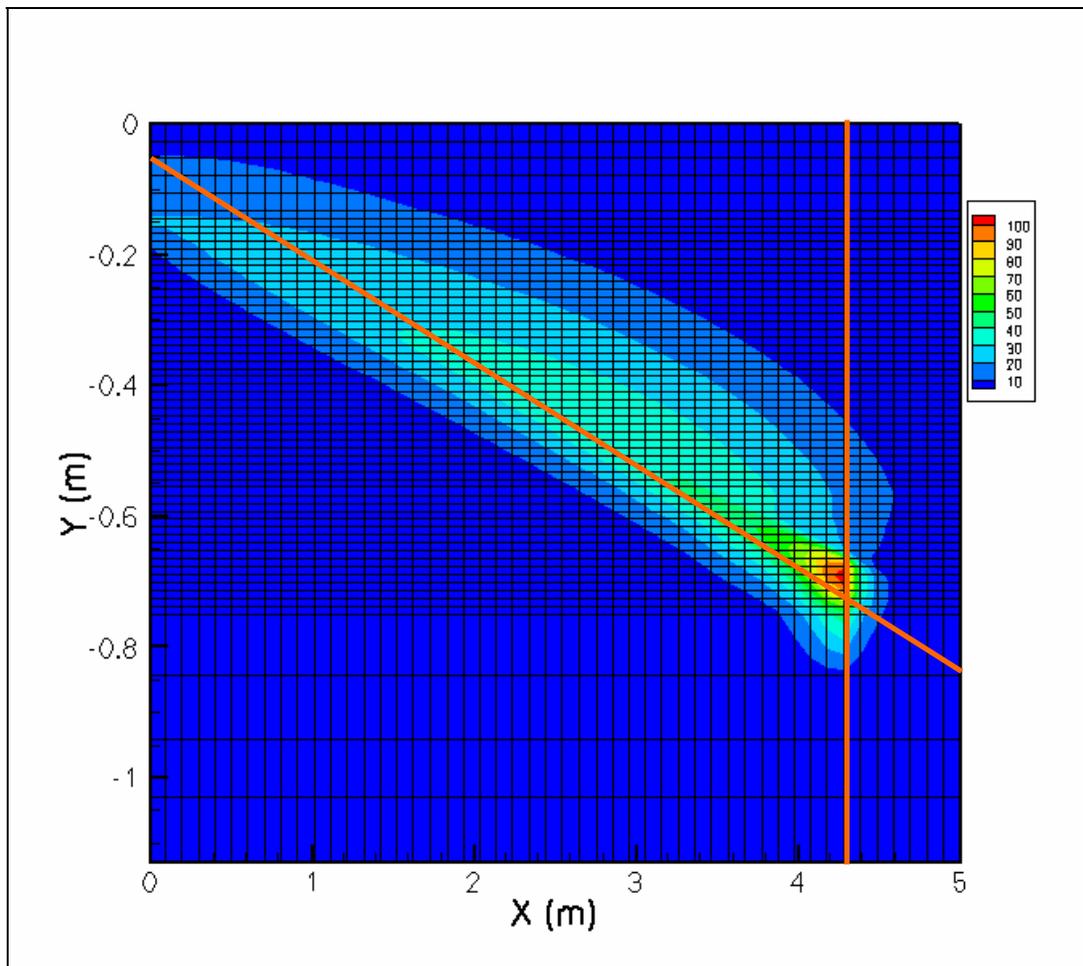
Figure 119 - Distribution of 1,1,2-TCA concentrations, Experiment #3, Time = Day 50.5.
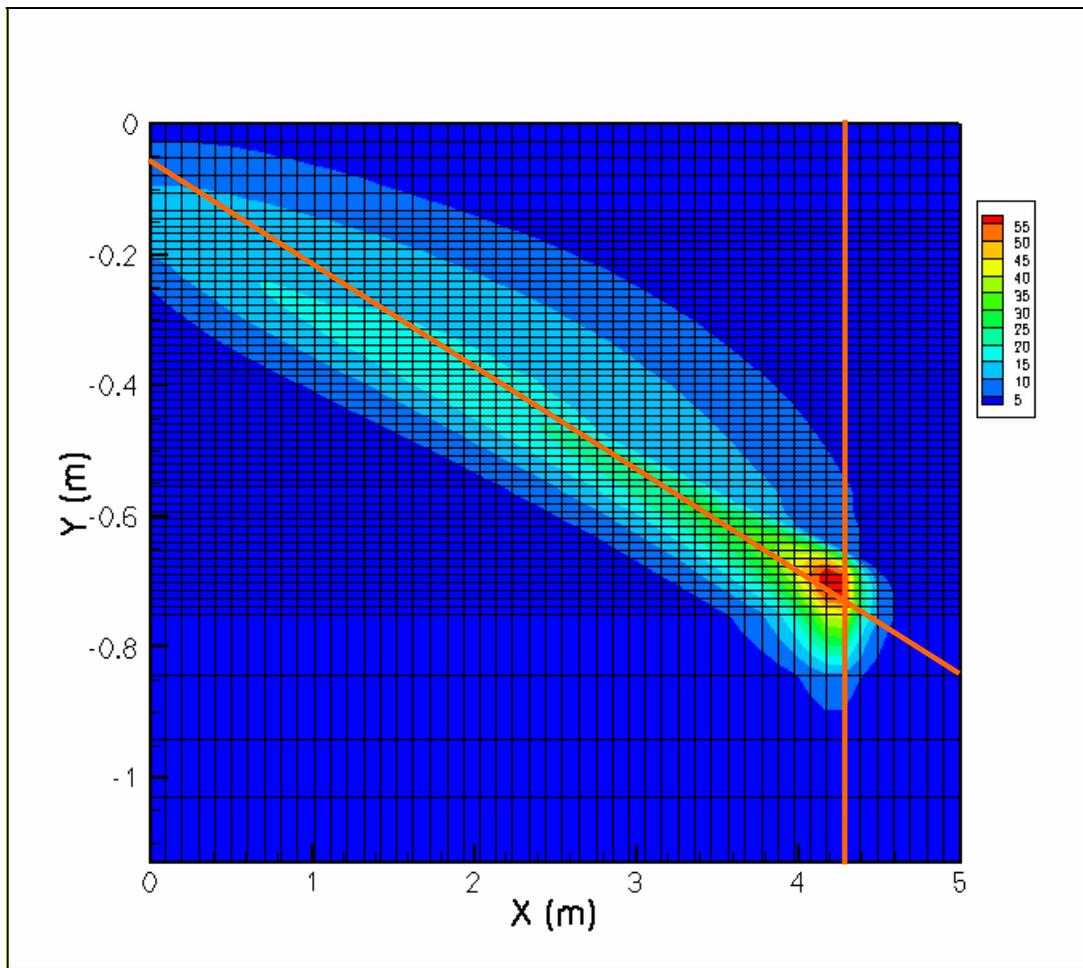
Figure 120 - Distribution of 1,1,2-TCA concentrations, Experiment #3, Time = Day 73.8.
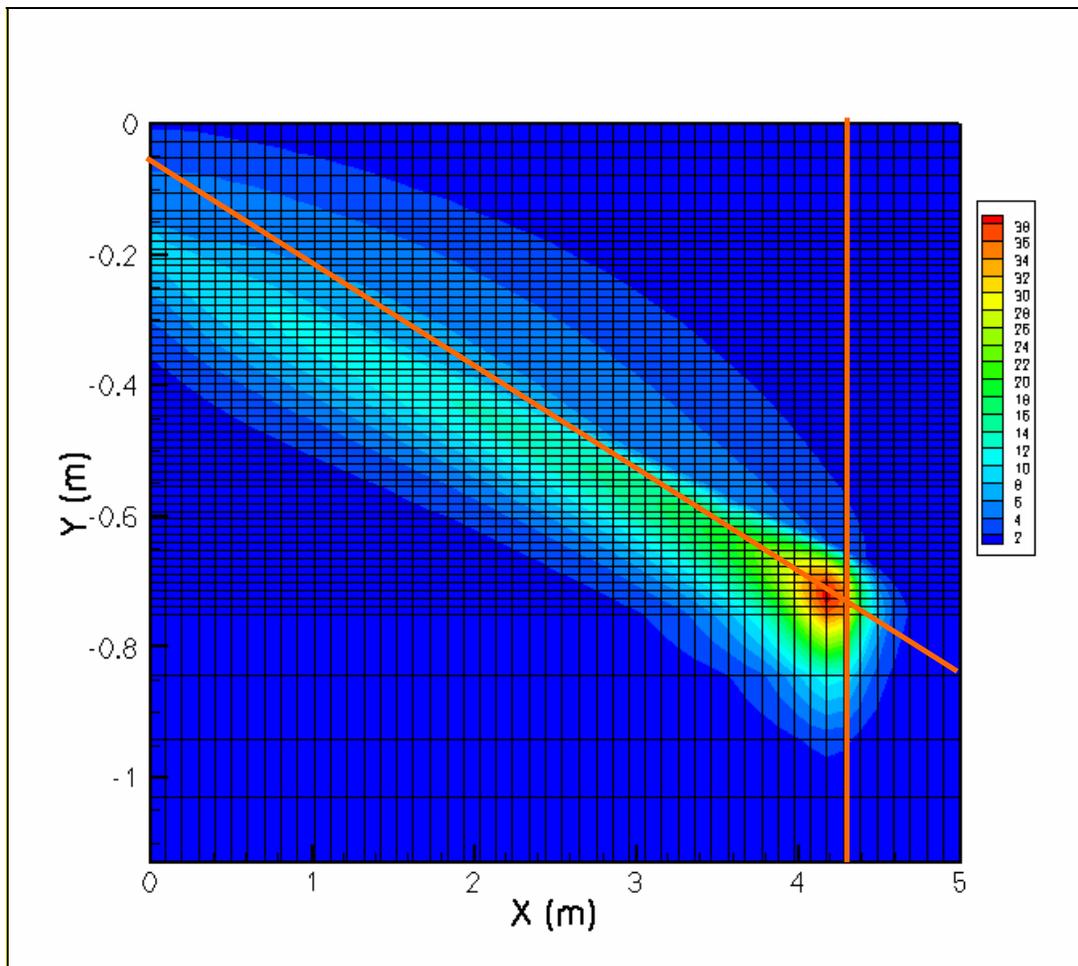
Figure 121 - Distribution of 1,1,2-TCA concentrations, Experiment #3, Time = Day 104.1.
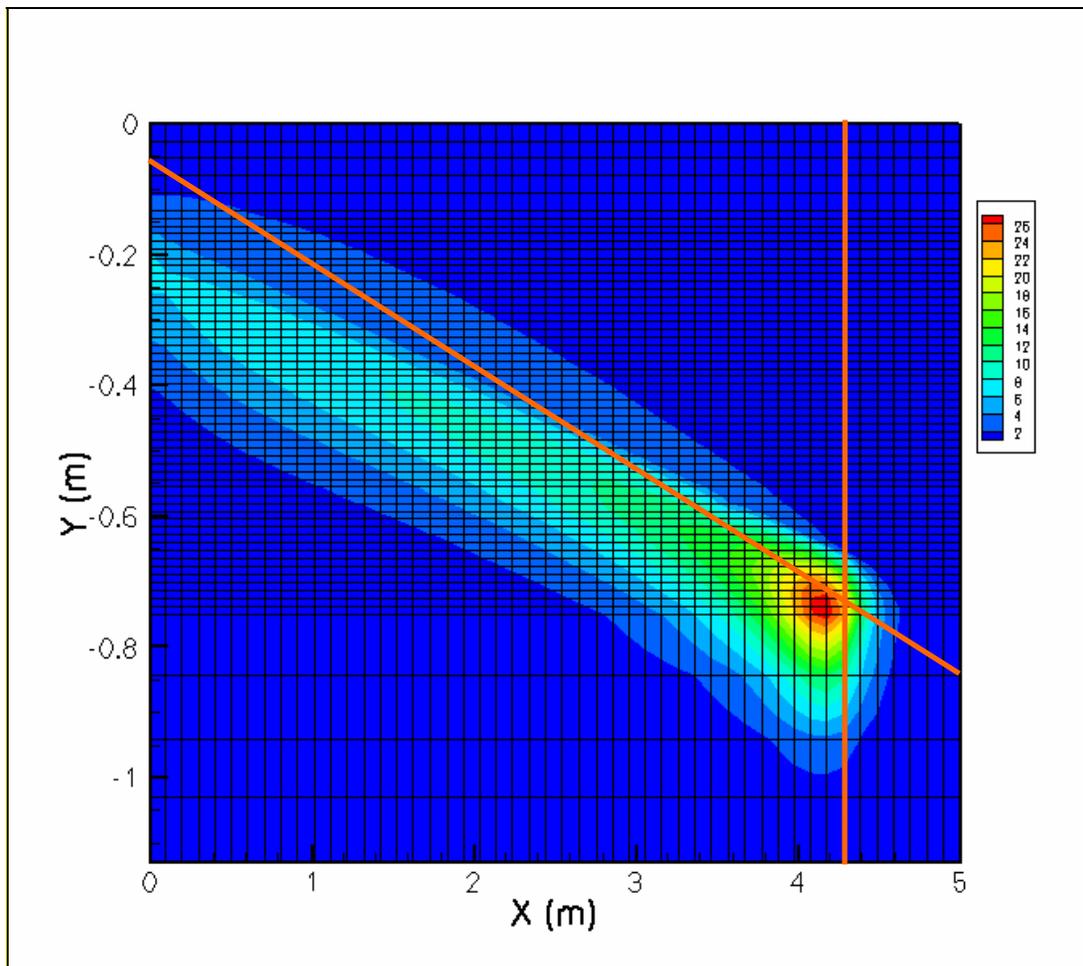
Figure 122 - Distribution of 1,1,2-TCA concentrations, Experiment #3, Time = Day 143.4.
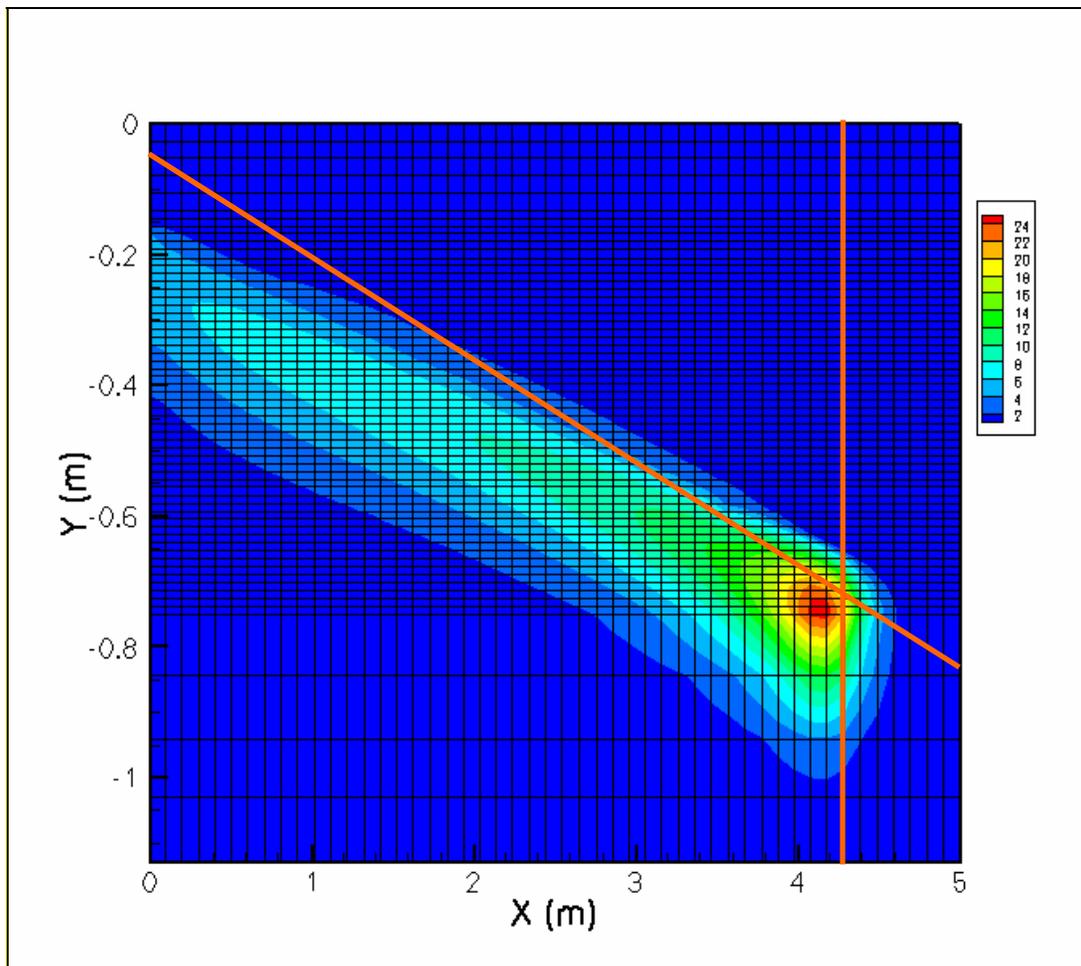
Figure 123  -  Distribution of 1,1,2-TCA concentrations, Experiment #3, Time = Day 154

## 4.5 Summary

This section documents our progress in developing tools that can be used to resolve the benefits of source management measures.  Overall, the analytical and numerical solutions indicate that:

1)  Diffusion of contaminants into hydraulically low permeability zone can be a significant factor driving depletion of source DNAPL.  This is consistent with the relatively brief longevity of the DNAPL sources observed in the laboratory studies.

2) Due to back diffusion from low permeability zones, dissolved-phase plumes can persist for long periods after the DNAPL has been depleted. Again this is supported by laboratory studies that indicate persistent dissolved-phase plumes after DNAPL depletion.

Building on this it seems plausible that field plumes (older, relatively small releases, in heterogeneous materials) may be sustained by non-DNAPL source material. In these instances technologies that only address DNAPL may have limited efficacy.

The numerical modeling work has shown that a dual-porosity numerical solution that incorporates adsorption and matrix diffusion may be used to capture the experimental data that was generated to understand the dominant mechanisms described throughout this report. Now that the numerical solution has been shown to be able to capture the important processes at a laboratory-scale for these specific domains, further work should be performed at a field-scale with synthetically generated domains.

## 4.6 References Cited

Berkowitz, B., Scher, H., and Cortis, A. 2004. (http://www.weizmann.ac.il/ESER/People/Brian/CTRW/)

Bird, R, B., W.E. Stewart and E.N. Lightfoot. 1960. *Transport Phenomena*, John Wiley and Sons, Inc.

Cortis, A., Claudio, G., Scher, H., and Berkowitz, B. 2004. Numerical Simulation of Non-Fickian Transport in Geological Formations with Multiple-Scale Heterogeneities, *Water Resour. Res., 40.*

Dash, Z. V. 2003. Validation Test Plan for the FEHM Application Version 2.21. Revision 0. STN: 10086-2.21-00. Document ID: 10086-VTP-2.2.1-00.

Dentz, M., Cortis, A., Scher, H., and Berkowitz, B., 2004. Time behavior of solute transport in heterogeneous media: transition from anomalous to normal transport, Advances in Water Resources, 27, 155-173.

Feenstra, S., J.A. Cherry and B.L. Parker. 1996. Conceptual Models for the Behavior of Dense Nonaqueous Phase Liquids (DNAPLs) in the Subsurface. In: *Chapter 2, Dense Chlorinated Solvents and Other DNAPLs in Groundwater*, J.F. Pankow and J.A. Cherry, Editors, Waterloo Press, pp. 53-88.

Gellar, J.T. and J.R. Hunt. 1993. Mass Transfer From Nonaqueous Phase Organic Liquids in Water Saturated Porous Media. *Water Resources Research*, vol. 29, no. 4, pp. 833-845.

Hinton, E. and Owen, D. R. J. 1979. An Introduction to Finite Element Computations. Pineridge Press, Swansea, Wales.

Imhoff, P.T., P.R. Jaffe and G.F. Pinder. 1993. An experimental study of complete dissolution of a nonaqueous phase liquid in saturated porous media. *Water Resources Research*, vol. 30, no. 2, pp. 307-320.

Lee and Batchelor. 2002. Abiotic Reductive Dechlorination of Chlorinated Ethylenes by Iron-Bearing Soil Minerals. 1. Pyrite and Magnetite. Environ. Sci. Technol. 36(23). 5147-5154.

Levy, M., and Berkowitz, B. 2003. Measurement and analysis of non-Fickian dispersion in heterogeneous porous media. Water Resources Research, 32, 583-593.

Liu, H. H., Bodvarsson, G.S., and Zhang, G. 2004a. Scale Dependency of the Effective Matrix Diffusion Coefficient. Vadose Zone Journal, vol. 3, 312-315.

Liu, H.H., Salve, R., Wang, J. S. Y., Bodvarsson, G. S., and Hudson, D. 2004b. Field investigation into unsaturated flow and transport in a fault: Model analysis. J. Contam. Hydrol. 74. 39-59.

Liu, H. H., Haukwa, C. B., Ahlers, F., Bodvarsson, G. S., Flint, A. L., and Guertal, W. B. 2003b. Modeling flow and transport in unsaturated fractured rocks: An evaluation of the continuum approach. J. Contam. Hydrol. 62-63: 173-188.

Miller, C.T., M.M. Poirier-McNeill and A.S. Mayer. 1990. Dissolution of trapped nonaqueous phase liquids; mass transfer characteristics. *Water Resources Research*, vol. 26, no.11, pp. 2783-2796.

Parker, B.L., R.W. Gillham and J.A. Cherry. 1994. Diffusive disappearance of immiscible–phase organic liquids in fractured geologic media. *Groundwater*, vol. 32, no.5.

Parker, B.L. 1999-2003. Unpublished presentations at Solvents-in-Groundwater Research Consortium Meeting

Powers, S.E., Abriola, Linda, M. and W.J. Weber. 1994. An experimental investigation of nonaqueous phase liquid dissolution in saturated subsurface systems: transient mass transfer rates. *Water Resource Research*, vol. 30, no.2, pp. 321-332.

Saenton S., Illangasekare, T.H. Soga, K., Saba, T.A. 2002. Effects of source zone heterogeneity on surfactant-enhanced NAPL dissolution and resulting remediation end-points. *Journal of Contaminant Hydrology*, vol. 59, pp. 27– 44.

Sale, T.C. 1998. *Interphase Mass Transfer from Single Component DNAPLs.* Ph.D. Dissertation, Department of Chemical and Bioresource Engineering, Colorado State University, Fort Collins, Colorado.

Schwille, F. 1988. *Dense Chlorinated Solvents in Porous and Fractured Media*, Translated by J. F. Pankow, Lewis Publishers, Boca Raton, Florida.

Smith, I. M. and Griffiths, D. V. 1998. Programming the Finite Element Method, 3$^{rd}$ edition. John Wiley & Sons.

Tang, D. H., E. O. Frind, and E. A. Sudicky. 1981. Contaminant Transport in Fractured Porous Media: An Analytical Solution for a Single Fracture. Water Resources Research 17(3), 555-564.

Waddill, D. W. and M.A. Widdowson. 2000. *SEAM3D: A numerical model for three-dimensional solute transport and sequential electron acceptor-based bioremediation in groundwater*. ERDC/EL TR-00-18, prepared for U.S. Army Engineer Research and Development Center, Vicksburg, MS.

Wiedemeir, T.H., H.S. Rafai, C.H. Newell, and J.T. Wilson, (1999), Natural Attenuation of Fuels and Chlorinated Solvents in the Subsurface. John Wiley and Sons, Inc. New York.

Zheng, C. and Bennett, G. D. 1995. *Applied Contaminant Transport Modeling: Theory and Practice*. Van Nostrand Reinhold.

Zyvoloski, G. A., Robinson, B. A., Dash, Z. V. and Trease, L. L.  1995.  Models and Methods Summary for the FEHMN Application.  Document ID: LA-UR-94-3787, Revision 1.

## 5.0    Field-scale Evaluations

A primary challenge of the project is extrapolating laboratory results to field-scale source zones.  The two critical elements are: (1) determining whether we are capturing the relevant field-scale processes and (2) understanding field-scale performance of source control measures.  To build a basis for moving from the laboratory to the field scale, we reviewed the performance of source control measures at FEW, NASFtW, and AFP4.  The following documents our progress through July 2003 on this task.

## 5.1    Remedial Technology Overview

Groundwater remedial technologies performed at FEW, NASFtW, and AFP4 were identified based on published technical reports and personal communication with site investigators.  The identified remedial actions are summarized in Table 17.

| | | | | | | |
|---|---|---|---|---|---|---|
| | | Table 17 | | Remedial actions at FEW, NASFtW, and AFP4 | | |
| **TECHNOLOGY Name** | **SOURCE** | **FACILITY Name** | **SITE Name** | **COMMENTS** | **TARGET Compounds** |
| Pump and Treat | Earth Tech, March 2002 | FEW | Spill Site 7 | Treatability study; Operated April 1995 to march 1996 | TCE |
| | | | | Operational problems; Design limitations; Premature shut-down | |
| | | | | Intercepted shallow groundwater; Incomplete capture | |
| **Passive Reactive Barrier (PRB)** | Earth Tech, March 2002 Quarterly Reports | FEW | Spill Site 7 | Interim remedial action | TCE |
| | | | | Partially penetrating; Intercepted upper 15 ft of aquifer | |
| | | | | Completed April 1999 | |
| Excavation | Earth Tech, January 2001 | FEW | Spill Site 7 | Sludge removal from grease trap | TCE |
| | | | Grease trap area | Excavation of 285 tons of adjacent hazardous soils | trans 1,2 DCE |
| | | | | Not all impacted soils were removed | |
| Excavation | Earth Tech, January 2001 | FEW | Spill Site 7 | 1200 cy excavated as of January 2001 | TPH |
| | | | Landfill 2 | Additional impacted soils present | |
| | | | | | |
| Excavation | EE/CA | FEW | Spill Site 7 | Being considered | VOC |
| | | | | | |
| | | | | | |
| 2-Phase Vapor Extraction | Personal communication with site investigators | FEW | Plume B | Treatability study | VOC |
| | | | | | |
| Electrolytic Barrier | Tom Sale | FEW | Plume C | Installed 2003 | VOC |
| | | | | Currently operating and being evaluation | |
| | | | | | |
| Monitored Natural | Personal communication | FEW | Zone A | | VOC |

212

| | | | | Table 17 | Remedial actions at FEW, NASFtW, and AFP4 | | |
|---|---|---|---|---|---|---|
| Attenuation (MNA) | with site investigators | | | | | |
| | | | | | | |
| Pump and Treat | Personal communication | FEW | Zone C | Low permeability materials | VOC |
| | with site investigators | | Landfill LF3 | | |
| | | | | | |
| ISOC | Personal communication | FEW | URS treatability area | | VOC |
| | with site investigators | | | | |
| | | | | | |
| IMOX | Personal communication | FEW | URS treatability area | | VOC |
| | with site investigators | | | | |
| | | | | | |
| Permanganate | Personal communication | FEW | URS treatability area | Concern with elevated arsenic | VOC |
| | with site investigators | | | | |
| | | | | | |
| **Electrical Resistance Heating (ERH)** | Final report fall 2003 | AFP4 | Building 181 | 0.5 acres.  Problems with nonuniform heating. 1200 lb TCE removed. | TCE |
| | | | | Many downgradient wells,  One well 50 ft downgradient.  One well | |
| | | | | within footprint area.  System now shutdown. | |
| 2-Phase Vapor Extraction | "Final remedial process optimization | AFP4 | Landfill 3 | 16 ft DNAPL in one well. System turned off 2 years ago.  Very little | TCE |
| | report". | | | water produced. Vapor extraction was no longer effective.  No | |
| | | | | landfill cap. Conc up to 180000 ppb.   Fractured bedrock. | |
| Excavation | Limited reporting.  Some pictures. | AFP4 | Landfill 1 | Excavate 14000 cy in early 1980s. Missed DNAPL. | TCE |
| | | | | | |

| | Table 17 | Remedial actions at FEW, NASFtW, and AFP4 | | | | |
|---|---|---|---|---|---|---|
| | | | | | | |
| Pump and Treat | "Final remedial report; east parking lot | AFP4 | East Parking Lot Area | Downgradient of Building 181. $ 7 M. 60 extraction wells. 32 MG water. | TCE |
| | area", March 2002. | | | 1000 (?) lb TCE. Problem with treatment plant. Many wells not working. | |
| | | | | Upper sand 5000 ppb TCE. | |
| Pump and Treat | Personal communication | AFP4 | West site of building | Small system. | TCE |
| | with site investigators | | | | |
| | | | | | |
| Natural Attenuation | Personal communication | AFP4 | General | | VOC |
| | with site personnel | | | | |
| | | | | | |
| **Free Product (DNAPL) Recovery** | Paper: "Enhanced DNAPL Recovery | AFP4 | West site of building | | TCE |
| | from Fractured Limestone, AFP4, | | | | |
| | Fort Worth, Texas | | | | |
| Free Product (LNAPL) Recovery | Personal communication with site investigators | AFP4 | Fuel saturation area #3 | Bailing wells. Some LNAPL. At one time, couple feet of free product in wells. No further action. | TPH |
| | | | | | |
| **Permeable Reactive Barrier (PRB)** | New report by HydroGeologic | NASFtW | Landfill 4-5 area | Installed 2002 | TCE |
| | | | | | cis-1,2-DCE |
| | | | | | VC |
| Pump and Treat | "Landfill 4-5 O&M report" | NASFtW | Landfill 4-5 area | TCE conc. never decreased during pump & treat. Not working well. | TCE |
| | | | | Drums removed from area. An interim action. | |
| | | | | Shut down with reactive barrier construction. | |

214

| | | | | | |
|---|---|---|---|---|---|
| Drum Removal | Personal communication with site personnel | NASFtW | Landfill 4-5 Area | | VOC |
| | | | | | |
| Other Interim Measures | Personal communication with site investigators | NASFtW | | Scrape soils. Remove drain. Remove tanks. | VOC |
| | | | | | |
| Pump and Treat | Personal communication with site investigators | NASFtW | AOC-1 Fuel area. | Pump & treat to be installed near creek. | Benzene Fuel |
| | | | | | |
| **Notes:** | | | | | |
| | Technologies in bold print are retained for further evaluation | | | | |
| FEW | F. E. Warren Air Force Base, Cheyenne, Wyoming | | | | |
| AFP4 | Air Force Plant 4, Fort Worth, Texas | | | | |
| NASFtW | Naval Air Station, Fort Worth, Texas | | | | |
| VOC | Volatile organic compounds | | | | |
| TPH | Total petroleum hydrocarbons | | | | |
| ISOC | In situ Submerged Oxygen Curtain | | | | |
| IMOX | In situ co-Metabolic Oxidation | | | | |

Table 17      Remedial actions at FEW, NASFtW, and AFP4

Table 17 indicates that many different technologies have been utilized including both standard and innovative methods.  A summary of the remedial technologies is provided in Table 18.

Table 18        Summary of remedial technologies

| Remedial Technology | Chemical Phase | Source Depletion vs. Plume Control | Technical Approach |
|---|---|---|---|
| Pump and treat | Dissolved in saturated zone | Plume control (cutoff). Sometimes used for source depletion | Extraction of contaminated groundwater by wells or drains.  Aquifer is "flushed' by induced flow of uncontaminated groundwater. |
| **Permeable reactive barrier (PRB)** | Dissolved in saturated zone | Plume control (cutoff) | In situ chemical/biological degradation of chlorinated solvents within a permeable trench.  Provides a zero chemical flux boundary within the plume.  Downgradient portion of plume is "flushed' by natural flow of uncontaminated groundwater. |
| Excavation | DNAPL and/or chemicals sorbed to soil | Source depletion | Removal of soils containing DNAPL or sorbed chemicals. |
| 2-phase vapor extraction | Dissolved in saturated and unsaturated zones. DNAPL | Source depletion | A combination of pump-and-treat and soil vapor extraction.  Volatile chemicals are vaporized and then collected in the unsaturated zone. |
| Electrolytic barrier | Dissolved in saturated zone | Plume control (cutoff) | In situ chemical degradation of chlorinated solvents within a permeable trench.  Provides a zero chemical flux boundary within the plume.  Downgradient portion of plume is "flushed' by natural flow of uncontaminated groundwater. |
| Monitored natural attenuation (MNA) | All phases | Plume control (dissipation) | Natural (primarily biological) degradation of contaminants to nontoxic compounds. |
| ISOC, IMOX, permanganate | All phases | Source depletion | Chemical oxidation of contaminants to nontoxic compounds. |
| **Electrical resistance heating** | Dissolved in saturated and unsaturated zones. DNAPL | Source depletion | Volatile chemicals are vaporized and then collected in the unsaturated zone. Heating used to enhance vaporization. |
| **Free product recovery** | DNAPL | Source depletion | Physical removal of DNAPL from below the water table |
| Drum removal | DNAPL | Source depletion | Physical removal of DNAPL |

Table 18 technologies are generally categorized as source depletion or plume control.  Source depletion attempts to reduce the amount of chemicals that create and sustain a dissolved groundwater plume.  If these chemical sources are depleted, it is presumed

that subsequent flow of uncontaminated groundwater through the area will eventually "flush" residual contaminants from the aquifer. Plume control involves removing or treating affected groundwater contaminated with dissolved chemicals occurring outside a source area. Flushing is assumed to improve water quality downgradient of the remedial facility, but no attempt is made to improve water quality upgradient of the facility (that is between the source and the facility).

Of those remedial technologies listed in Table 18, four actions (three technologies) were retained for further evaluation. These are summarized in Table 19.

Table 19    Remedial actions retained for further evaluation

| Technology | Facility | Description | Comments |
|---|---|---|---|
| Permeable Reactive Barrier (PRB) | NASFtW | Trench excavated in the aquifer. Backfilled with sand and zero valent iron. Degrades chlorinated solvents to nontoxic compounds. | Barrier fully penetrates the aquifer. Provides a zero chemical flux boundary. Useful for evaluating downgradient processes. |
| Permeable Reactive Barrier (PRB) | FEW | Trench excavated in the aquifer. Backfilled with sand and zero-valent iron. Degrades chlorinated solvents to nontoxic compounds. | Barrier partially penetrates the aquifer. Provides a zero chemical flux boundary in the upper (most contaminated) portion of the aquifer. Useful for evaluating downgradient processes. |
| Electrical Resistance Heating (ERH) | AFP4 | Electrodes used to heat unsaturated soils and volatilize chlorinated solvents. Soil vapor extraction (SVE) system collects vapors. | Innovative technology for reducing chemical mass in a source area. Useful for evaluating the effects of source depletion. |
| Free Product (DNAPL) Recovery | AFP4 | Opportunistic pumping of free product from monitoring wells | Extracts significant quantities of DNAPL from the source area. Useful for evaluating the effects of source depletion. |

The retained remedial actions have adequate levels of chemical monitoring, are well documented, and are useful for evaluating either downgradient transport processes or the direct effects of source depletion. In this report, evaluations focused on the PRBs at NASFtW and FEW. These facilities provided very good data for evaluating the effects of matrix diffusion on plume migration. The ERH project has been completed and the Free Product Recovery project is still ongoing at AFP4.

## 5.2 Remedial Action Descriptions

The following sections provide brief descriptions of the retained remedial actions.

### 5.2.1 NASFtW Permeable Reactive Barrier

The, Naval Air Station (NAS) Fort Worth (FtW) Joint Reserve Base (JRB), formerly Carswell Air Force Base, is located southeast of a large manufacturing facility know as Air Force Plant 4 (AFP4). AFP4 is a known source of chlorinated solvents that has contaminated an extensive area of groundwater including portions of the NASFtW. A site map is shown on Figure .
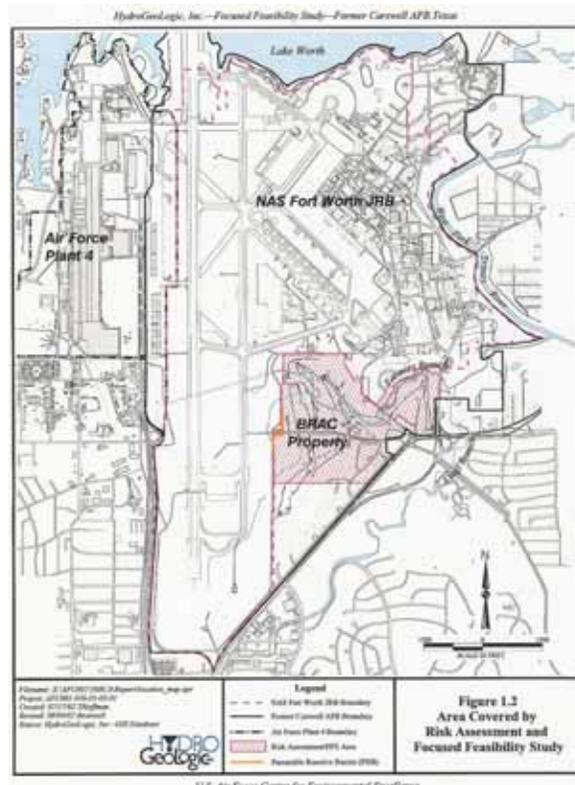


Figure 124 - NASFtW site map

An east-southeast-trending groundwater contaminant plume has been mapped from the southern portion of AFP4. In the downgradient (southeast) direction, the plume extends from AFP4, across the southern portion of the NASFtW, and into an adjacent area known as the Base Realignment and Closure (BRAC) property. The primary chemicals of concern (COCs) within the plume are TCE, cis-1,2-DCE, and vinyl chloride (VC). The groundwater plume exists within a shallow unconfined aquifer with a maximum depth of

about 35 feet below ground surface. The aquifer is of fluvial origin and contains a heterogeneous mixture of sand, silt, clay and some gravel. Several solid waste management units (SWMUs) exist along the boundary between the NAS and BRAC properties. These SWMUs have been investigated and have received regulatory approval for no further action required.

A focused feasibility study (FFS) was performed to evaluate alternatives for reducing contaminant concentrations in the groundwater within the BRAC property. In developing remedial alternatives, it was presumed that all contaminants where in the dissolved phase, and that there were no known occurrences of DNAPLs east of the NASFtW/BRAC property boundary. The selected alternative was a PRB installed along the boundary. The PRB consisted of a trench, excavated using conventional equipment and degradable biopolymer slurry, which was backfilled with a mixture of 50 percent sand and 50 percent zero-valent iron. Previously conducted bench-scale tests indicated that when contaminated groundwater interacted with the zero-valent iron, abiotic degradation would reduce the dissolved concentrations of TCE, cis-1,2-DCE, and VC to below Federal drinking water standards. The bench-scale tests, however, did not consider the effect of the biopolymer slurry that was ultimately used during construction.

The 1,126-foot long PRB was constructed between March and April, 2002. Its alignment is approximately perpendicular to the groundwater flow direction and it extends across most of the contaminant plume. The monitoring network consists of new groundwater sampling wells installed just upgradient and downgradient of the wall, new wells installed directly into the wall, and pre-existing upgradient and downgradient wells located at various distances from the wall. Of these, only the pre-existing wells had been sampled prior to PRB construction. Since construction, there have been four groundwater-sampling events (summer, fall, and winter 2002 and spring 2003). The results from these events can be used to assess the short-term performance of the PRB. Sampling over a longer time frame will be required to assess the effect of the PRB on more distant downgradient water quality.

## 5.2.2 FEW Permeable Reactive Barrier

F.E. Warren Air Force Base (FEW) is located near Cheyenne, Wyoming. Identified within the Base boundaries are several areas with contaminated soils and groundwater. These are illustrated in Figure 125. A primary area of interest is Spill Site 7 (SS-7). Figure provides a more detailed delineation of Spill Site 7.
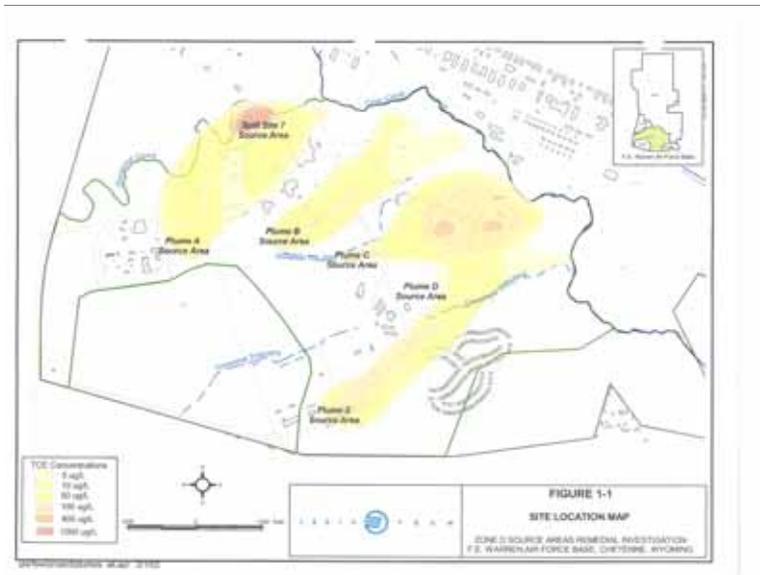


Figure 125 - Plume map for F.E. Warren AFB
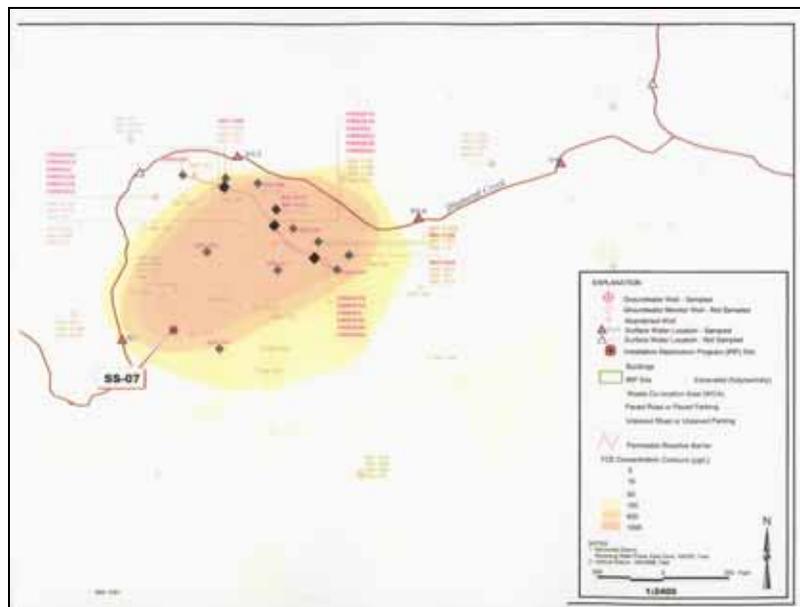


Figure 126 - FEW Spill Site 7 map

The SS-7 plume is located within a shallow unconfined aquifer composed of a heterogeneous mixture of clay, silt, and sand. The highest TCE concentrations are detected in the uppermost portion of the groundwater flow system; that is, within 10 to 30 feet below the water table. From SS-7, the plume migrates to the northeast and discharges to Diamond Creek, a perennial stream. It is interpreted that most affected groundwater within the chemical plume discharges to the creek. However, there are detections of contaminants in wells north of the stream channel, suggesting that some groundwater flows under the creek and continues north.

In 1999, a PRB was constructed between SS-7 and Diamond Creek to intercept and treat affected groundwater prior to creek discharge. The wall contains a mixture of zero valent iron and sand. The PRB is about 550 feet long and extends across the portions of the plume with high TCE concentrations. Although the saturated thickness of the aquifer can be greater than 70 feet, the PRB only penetrates to a depth of about 15 feet below the water table, an interval known to have the highest TCE concentrations. Thus, the PRB intercepts only the upper portion of the groundwater system.

5.2.3   AFP4 Electrical Resistance Heating

Chemical releases have occurred below Building 181 at the industrial complex known as Air Force Plant 4 (AFP4) located near Fort Worth, Texas (see Figure 126). Chemicals below the building are a continuing source that has created a groundwater contaminant plume that extends approximately 1400 feet east-southeast of the building. The primary chemical of concern within the plume is TCE. The chemicals are contained in saturated and unsaturated fill composed of gravel and silty clay, alluvial deposits composed of sand, silt, and clay with some gravel, and bedrock composed of limestone interbedded with silt/clay layers. Some of the underlying bedrock is either fractured or not present at all. The missing bedrock confining layer areas have been eroded by "paleochannels" that are interpreted as originating from abandoned fluvial channels of the ancient West Fork Trinity River. The areas where the bedrock confining layer has been eroded are called the "Window Area." Maximum soil TCE concentrations are about 2800 mg/kg and dissolved TCE groundwater concentration range between 20,500 to 100,000 mg/L.

A source depletion action was initiated during 2002 using a combination of soil vapor extraction (SVE) and electrical resistance heating (ERH). Regularly spaced electrodes were used to heat soil in the unsaturated zone above the water table. This led to vaporization of volatile organic compounds (VOC) as well as existing soil moisture. The VOC vapors were then collected using SVE and processed above ground. The system was installed over an area of about ½ acre below the Building 181 concrete floor.

A construction report for the ERH system is currently in progress. The following description of the ERH system is based on the Draft Work Plan dated October 2001. The proposed characteristics of the ERH system are summarized in Table 20.

Table 20 - Characteristics of ERH system

| Item | Description |
|---|---|
| Average electrode spacing | 19 feet |
| Un-insulate (heating) depth | 6 to 32 feet below floor (or to top of rock) |
| Volume of treated soil | 23200 yd$^3$ (2 to 32 feet over 0.5 acres) |
| Soil temperature | 100 °C |
| Power consumption | 1200 to 1300 kW |
| SVE | 64 wells co-located with electrodes |
| Aboveground hardware | Blowers, piping, tanks, and condensers for converting vapors to (contaminated) water and free product (mainly TCE) |

It is our understanding that the final system was constructed to these specifications.

The ERH/SVE system was operated between May 2002 and January 2003

### 5.2.4  DNAPL Recovery at AFP4

Two former waste disposal areas (Landfills 1 and 3) are situated west of a large government manufacturing facility known as Air Force Plant 4 (AFP4), located near Fort Worth, Texas (see Figure 126).  Apparently, chlorinated solvents were disposed at one or both of these landfills over an uncertain period.  Site investigations have indicated that DNAPLs are present in the subsurface below the landfills.  The general area containing the landfills is also referred to as the West Parking Lot Area.

Significant thicknesses of DNAPL have historically accumulated in monitoring well W5.  Since June 2000, accumulated DNAPL has been pumped from the well on a regular basis.  Between June 2000 and December 2002, a total of 460 gallons of pure DNAPL was recovered.

From ground surface downward, the geology of the site consists of fill and Terrace Alluvium, with a combined thickness of 2 to 20 feet, and the underlying Goodland/Walnut Formation.  The Goodland/Walnut Formation is a 20 to 30 foot thick limestone with interbedded clay layers.  The base of the Walnut is better cemented and appears to act as a confining unit.  The upper portion of the Goodland/Walnut is

generally weathered and fractured, and in some areas has been eroded completely by paleochannels, leaving the underlying drinking-water aquifer (upper Paluxy Formation) in direct contact with contaminants originating from releases above .

The West Parking Lot Area clearly contains significant quantities of DNAPL. A maximum thickness of 18 feet was measured at the bottom of monitoring well W5. Some of the DNAPL is slowly dissolving into groundwater and providing chemical mass to a groundwater contaminant plume. DNAPL recovery efforts are currently in progress.

## 5.3   Permeable Reactive Barrier Evaluation

A properly operating PRB creates a near zero concentration boundary within the aquifer. Thus, groundwater flowing out of the PRB is expected to be at or below target concentrations, which are typically USEPA MCLs. The PRBs at NAS and FEW are thought to be constructed downgradient of any current or past occurrences of DNAPL. Thus, over time, chemical concentrations in groundwater downgradient of a PRB should decrease as this area is flushed with non-impacted groundwater. If groundwater concentrations do not decrease systematically, or if concentrations reach plateau values, a chemical source may be operating that is not related to the occurrence of DNAPL.

5.3.1  NASFtW Permeable Reactive Barrier

The alluvial aquifer in the NAS area is heterogeneous with sand layers and interbedded silt/clay layers. Sampling within the wall indicates that the PRB effectively creates a near-zero concentration boundary within the alluvial aquifer that extends across most of the groundwater contaminant plume.

There are four sampling transects, each with an upgradient well, a well installed in the PRB, and a downgradient well. Other downgradient sampling wells are located at various distances from the PRB, and the groundwater travel times between the PRB and these wells are variable. Depending on the local groundwater conditions and aquifer properties, these wells should exhibit the effects of the PRB at various times

after PRB installation.

Chemical concentrations of TCE, cis-1,2-DCE, and VC in water samples obtained from selected monitoring wells are provided in Table 21.  The data include sampling events conducted during June, September, and December 2002 and March 2003.

# Table 21    Groundwater VOC concentrations in wells near the NASFtW PRB

| General Location | TCE | | | | DCE | | | | VC | | | |
|---|---|---|---|---|---|---|---|---|---|---|---|---|
| | 1 | 2 | 3 | 4 | 1 | 2 | 3 | 4 | 1 | 2 | 3 | 4 |
| **TRANSECT 1** | | | | | | | | | | | | |
| WHGLTA070 — Just upgradient of PRB | 1600 J | 1,300 | 1,400 | 1200 | 390 J | 330 | 350 | 300 | 22 | 29 | 25 | 18 |
| WHGLFE001 — Within the PRB | 700 J | 910 | 1,000 | 1600 | 400 J | 440 | 350 | 340 | 19 | 21 | 16 | 15 |
| WP07-10C — Just downgradient of PRB | 3.9 | 7.6 | 0.81 F | 5 | 160 | 28 | 8.2 | 4 | 7.3 | 1.4 | ND | ND |
| **TRANSECT 2** | | | | | | | | | | | | |
| WP07-10B — Just upgradient of PRB | 1800 J | 1,800 | 1,500 | 1400 J | 470 J | 430 | 360 | 360 J | 2.8 | 3.3 | 2.8 | 4.1 J |
| WHGLFE002 — Within the PRB | 1100 J | 1,200 | 1,400 | 1400 | 500 J | 420 | 400 | 420 | 8.1 | 9.2 | 4.7 | ND |
| WHGLTA071 — Just downgradient of PRB | 14 | 11 | 10 | 4.7 | 330 | 460 | 400 | 150 | 5.9 | ND | 9.9 J | 35 |
| CAR-RW10 — 18 ft downgradient | 0.81 F | 20 | 0.8 F | 5.2 | 340 | 86 | 65 | 88 | 3.7 | 24 | 15 | 21 |
| WHGLTA072 — 42 ft downgradient | 1,800 J | 1,800 | 26 | 21 | 290 J | 260 | 79 | 47 | 1.4 | ND | 1.8 | 1 |
| WHGLTA073 — 108 ft downgradient | 2600 J | 4,600 | 2,400 | 2400 | 190 J | 120 | 170 | 210 J | 0.96 F | ND | ND | ND |
| WHGLTA074 — 198 ft downgradient | 2100 J | 2,100 | NA | 140 | 410 J | 500 | NA | 400 | 11 | 12 | NA | 58 |
| **TRANSECT 3** | | | | | | | | | | | | |
| WHGLTA076 — Just upgradient of PRB | 1,700 | 1,500 | 1,300 | 1300 | 490 | 400 | 450 | 490 | 3.2 | 2.4 | 3.2 F | ND |
| WHGLFE003 — Within the PRB | 3.3 | ND | ND | ND | 890 | 700 | 380 | 430 | 6.7 | 6.2 | 4.1 F | 4.6 F |
| WHGLTA075 — Just downgradient of PRB | ND | ND | ND | ND | 1,000 | 750 | 670 | 780 J | 6.4 | 7 | 5.1 | ND |
| LF04-4F — 92 ft downgradient assuming east-southeast flow direction | 410 | 12 | 2 | ND | 400 | 320 | 420 | 340 | 3 | 4.9 | 31 | 21 |
| LF04-02 — 251 ft downgradient | 1,200 | 1,000 | 490 | 280 | 600 | 570 | 350 | 280 | 2.5 | ND | ND | ND |
| LF04-4E — 358 ft downgradient | 1,400 | 880 | NA | 100 | 410 | 670 | NA | 390 | 1.8 | ND | NA | 180 |
| **TRANSECT 4** | | | | | | | | | | | | |
| WHGLTA077 — Just upgradient of PRB | 65 | 28 | 11 | 8.8 | 23 | 9.3 | 3.8 | 3 | ND | ND | ND | ND |
| WHGLFE004 — Within the PRB | ND | 1.3 | ND | ND | 18 | 38 | 10 | 4.8 | 0.57 F | 1 | 0.78 F | 1.7 |
| WHGLTA056 — Just downgradient of PRB | ND | 6.2 | ND | ND | 63 | 37 | 25 | 11 | 1.1 | 1.2 | 1.2 | 1.4 |
| **OTHER WELLS** | | | | | | | | | | | | |
| LF04-4D — 595 ft downgradient | 100 J | 280 | NA | 440 | 39 | 160 | NA | 180 | 1.1 | 5.1 | NA | 9.7 |
| LF05-5G — 475 ft downgradient | 930 | 830 | NA | 1500 | 210 | 210 | NA | 280 | 1.2 | ND | NA | ND |
| WHGLTA069 — 33 ft north of PRB alignment (a) | 960 J | 1200 | 670 | 510 | 600 J | 630 | 640 | 350 | 24 | 32 | 30 | 47 |
| FT09-12E — 67 feet south of PRB alignment (a) | 24 | 20 | NA | 5.5 | 11 | 10 | NA | 1.9 | ND | ND | NA | ND |
| LF05-5H — 288 feet east-northeast of north end of PRB (a) | 68 | 61 | NA | 43 | 500 | 650 | NA | 360 | 22 | 40 | NA | 41 |

Notes:
1  Qtr 1- June 2002
2  Qtr 2 - Sept. 2002
3  Qtr 3 - Dec. 2002
4  Qtr 4 - Mar. 2003
NA - Not analyzed
ND - Not detected

Significant decrease in concentration over time (yellow)

Signficiant increase in concentration over time (blue)

(a)    May not be on downgradient flow path

226

In Table 21, monitoring wells exhibiting significantly increasing or decreasing chemical concentrations are indicated. The criteria for a significant change in concentration are (1) a factor of three or more difference in concentration over the sampling period and/or (2) a clear trend in the concentration values. As shown, there is a clear tendency for decreasing concentrations of TCE and cis-1, 2 -DCE in wells downgradient of the PRB. In some cases, decreasing concentrations of these compounds are observed in wells several hundred feet away from the PRB. There also appears to be a tendency for increasing vinyl chloride concentrations downgradient of the PRB. The processes leading to increases in vinyl chloride are currently under investigation by the Air Force and its contractors. Figure 127 shows time trends in TCE concentrations for selected wells downgradient of the PRB. The relative change in TCE concentrations for these wells is shown on Figure 1208.
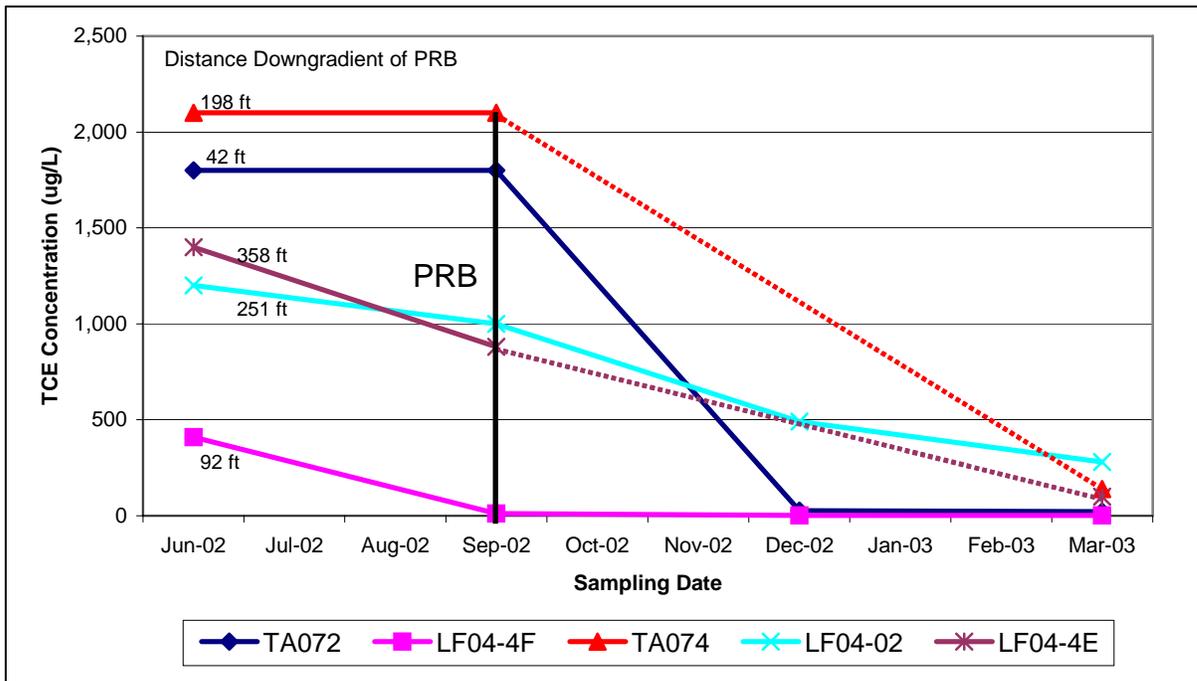


Figure 120 - TCE concentrations in selected wells downgradient of NASFtW PRB
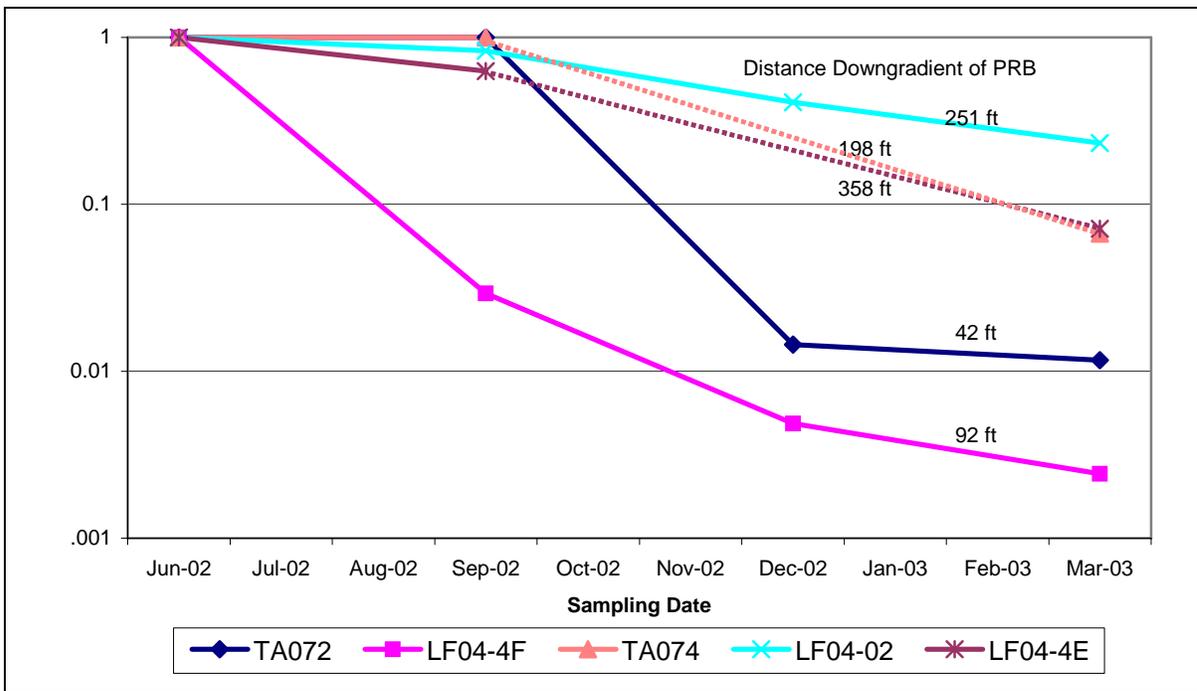
Figure 128 - Relative TCE concentrations in selected wells downgradient of
NASFtW PRB

In some cases, the downgradient concentrations have decreased dramatically.
Since the PRB was recently installed, the decreases are more pronounced at
wells relatively close to the PRB.  As shown on Figure 128, two wells located
within 100 feet of the PRB have experienced a two order-of-magnitude decrease
in TCE concentration and appear to be approaching plateau values.  Three wells
located further from the PRB have decreasing TCE concentrations but have not
yet exhibited plateau behavior.   More complete evaluation of temporal
concentrations in these wells will require future chemical sampling.  The plateau
behavior would not be predicted if chemical migration included only advection,
dispersion, and adsorption.   It is hypothesized that the lower stabilized
concentrations result from diffusive chemical flux from low permeability zones
(silt/clay layers) into groundwater migrating within active flow zones (sand
layers).

5.3.2   FEW Permeable Reactive Barrier

Table 22 presents characteristics of TCE concentrations in wells downgradient of FEW PRB.

Table 22      Characteristics of TCE concentrations in wells downgradient of FEW PRB

| Monitoring Well | Initial TCE Conc. May 2000 (ug/L) | Recent TCE Conc. Nov-Dec 2002 (ug/L) | General Characteristics |
|---|---|---|---|
| MW-173 B | 191 | 21 | **Decreasing** concentration with **plateau** at 20 to 25 ug/L |
| MW-186 | 115 | 17 | **Decreasing** concentration with **plateau** at 10 to 30 ug/L |
| MW-186 (D) | 198 | 22 | **Decreasing** concentration with **plateau** at 10 to 50 ug/L |
| MW-700 B | 2630 | 720 | Generally **decreasing** concentration; no apparent plateau |
| MW-702 B | 90.5 | 63 | Slightly **decreasing** concentration with **plateau** at 60 to 65 ug/L |
| MW-707 A | 3230 | 2200 | Generally **decreasing** concentration with **fluctuations** |
| MW-707 B | 2660 | 4300 | Generally **increasing** concentration with **fluctuations** |
| MW-708 | 970 | 750 | No trend; **fluctuations** only |
| PMW-401 | 120 | 72 | **Decreasing** concentration with **plateau** at 65 to 75 ug/L |
| PMW-501 | 740 | 780 | Initial decrease in concentration to less than 10 ug/L, followed by increase back to initial conditions |

A common characteristic is a TCE concentration that decreased during 2000 and 2001, and then reached a plateau during 2002.  This is observed in five of ten wells.  Seven wells displayed a decreasing concentration with or without such a plateau.  Increasing concentrations or no apparent trends were observed for two wells.

The PRB effectively creates a near-zero concentration boundary within the alluvial aquifer that extends across most of the groundwater contaminant plume. However, because the PRB only penetrates the upper portion (15 feet) of the saturated alluvium, there is some groundwater that flows under the PRB and is not subject to in-situ treatment. Over time, groundwater concentrations downgradient of the PRB should decrease as the area is flushed with non-impacted groundwater (that is, water "created" within the PRB). Actual TCE concentrations and relative TCE concentrations for selected downgradient wells are shown on Figure 29 and Figure 0, respectively.
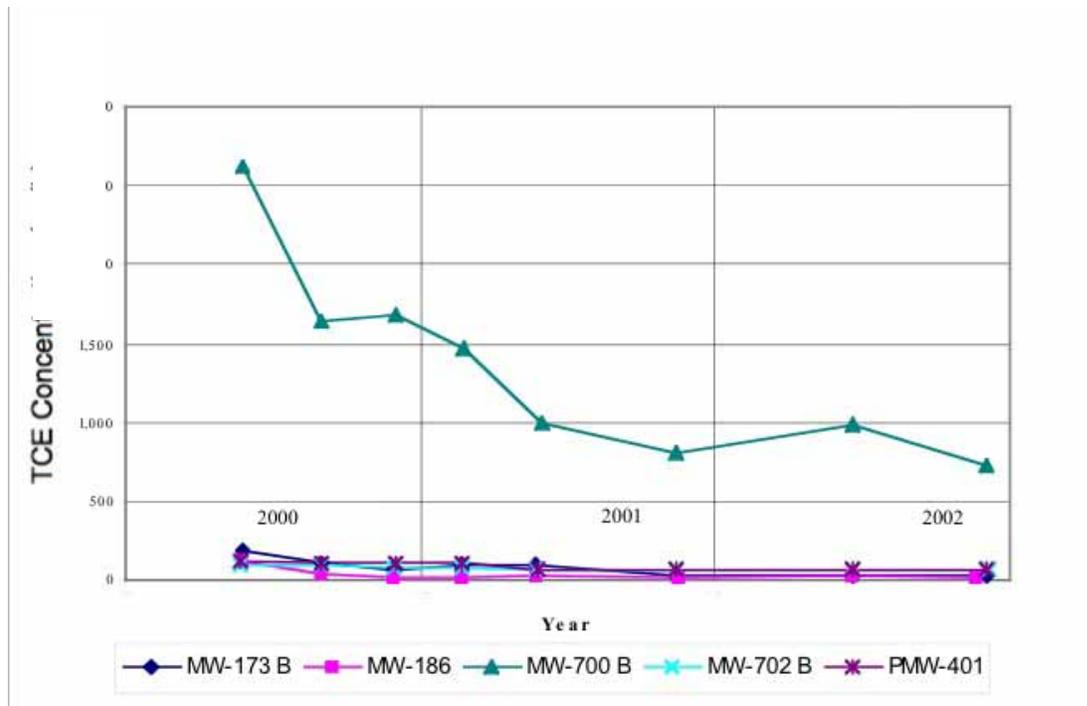


Figure 129 - TCE concentrations in selected wells downgradient of FEW PRB
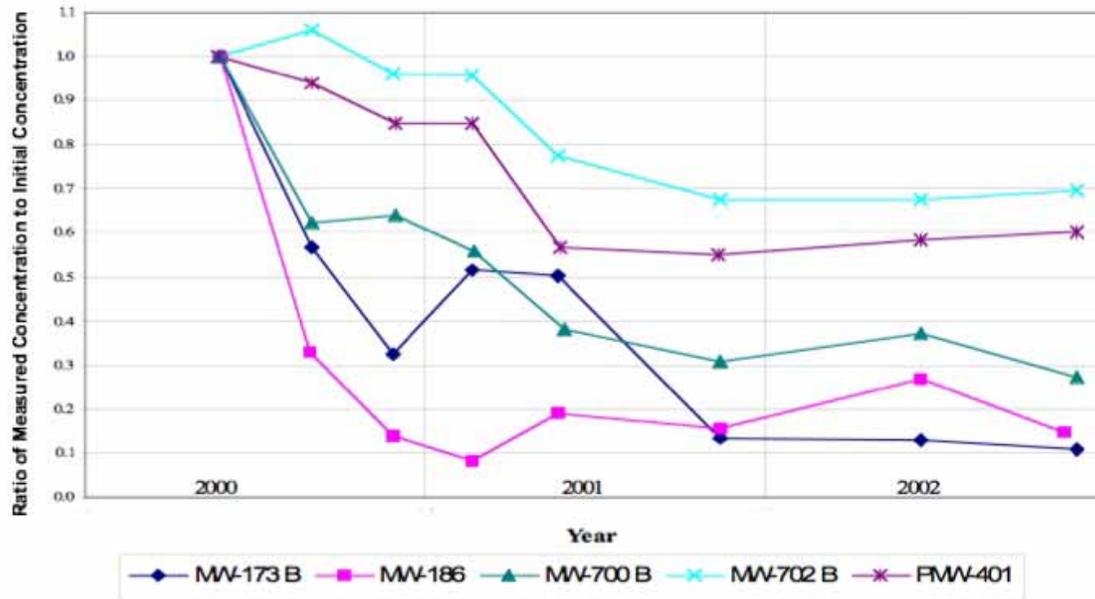
Figure 130 - Relative concentrations in selected wells downgradient of FEW PRB

TCE concentrations have decreased in most monitoring wells located downgradient of the PRB. A common behavior was for TCE concentrations to decrease by 30 to 90 percent after the PRB was installed. However, there was also a tendency for the concentrations to plateau and become somewhat stable at a lower value. This is shown on Figure 130 for selected downgradient wells. It is hypothesized that the lower stabilized concentrations result from diffusive chemical flux from low permeability zones (silt/clay layers) into groundwater migrating within active flow zones (sand layers). This diffusion process supplies chemicals into groundwater that was previously not impacted; that is, after passing through the PRB. It is possible that the plateau behavior may result in part from affected groundwater that flows under the PRB and thus bypasses the treatment system. Site data indicate that deeper groundwater is generally not contaminated or has relatively low chemical concentrations. While by-pass may be a factor contributing to downstream chemical concentrations, it does not appear to be the sole process that is operating.

231

### 5.3.3 Preliminary Conclusions Pertaining to PRB's

At both the NASFtW and FEW sites, a groundwater plume with relatively high TCE concentrations previously existed in an area that is now downgradient of a PRB. Each site has a heterogeneous aquifer with silt/clay layers that likely contain stagnant groundwater. As a consequence, the opportunity would have existed for diffusion of dissolved chemicals from active flow zones (sand layers) into the low permeability zones (silt/clay layers) prior to PRB construction. After PRB installation, non-impacted water was introduced into the active flow zones. This resulted in an eventual reduction in downgradient chemical concentrations. However, the observed plateau behavior in many wells is difficult to explain by traditional transport theory alone, even if adsorption/desorption is considered. The diffusion process discussed in Sections 2, 3, and 4 provides a hypothetical explanation for the observed plateaus in chemical concentrations. According to this hypothesis, diffusion provides chemical mass transfer from low permeability zones in silt/clay materials (at relatively high concentration) into the active flow zones in sand layers (at lower concentrations due to in-situ treatment at the PRB).

The diffusion process supplies chemicals into groundwater that was previously non-impacted; that is, after passing through the PRB. The diffusive process therefore provides a chemical source capable of *re-contaminating* clean groundwater. This source behavior may occur far from the chemical spill sites that originally created the chemical plume.

## 6.0 CONCLUSIONS/ADDITIONAL WORK

Through this project, a set of tools were developed to assist stakeholders in resolving the benefits of source management measures. Key elements include a description of governing processes, illustrative laboratory studies, predictive models, and demonstrative field data. Results from this work indicate that transverse diffusion can drive contaminants into low permeability zones. Initially, this has the effect of attenuating contaminants in transmissive layers. After the DNAPL has been depleted, back diffusion from low permeability zones sustains contaminant concentrations in transmissive layers in source zones and plumes. Primary implications of contaminant storage and release in low permeability zones include:

- Release of stored contaminants can sustain contaminant discharge from source zones. This can explain persistent releases of contaminant from plume heads where little, if any, DNAPL can be found.

- Source zone treatments that solely address transmissive zones may miss substantial contaminant mass in low permeability zones and be subject to post treatment contaminant rebound.

- Given near perfect depletion and/or containment of sources, back diffusion can sustain downgradient plumes for extended periods. As such, removal and/or containment of sources may not provide substantial near-term improvement in groundwater quality.

Per the original objective for this project, the project team hopes that the information presented herein provides an improved basis for selection remedies for releases of chlorinated solvents and other persistent contaminants at DoD facilities.

Pertinent follow-on studies and critical issues recognized during the course of this project include:

1) Better field data is needed to demonstrate and evaluate the effect of source depletion on downgradient water quality under a range of geology-contaminant type and release settings. This will help better manage stakeholder expectations regarding the benefits of source treatment with respect to reducing risk. Furthermore, field data is needed to better test and validate concepts and models developed through this project, and models being developed by others.

2) Models developed in this report provide an important resource for helping decision-makers better anticipate the value of potential investments under a variety of site conditions. It would be useful to develop software packages and decision tools based on the mathematical techniques demonstrated through this project.

3) A protocol is needed for management of sites affected by chlorinated solvent releases. Fortunately, per coordination with AFCEE, the protocol initiative has been picked up by ESTCP.

4) Ideas in this document suggest significant limitations to conventional approaches for modeling contaminant transport in heterogeneous granular geologic media. Specifically, contaminant mass storage-release from hydraulically stagnant zones is often ignored or missed. The study clearly demonstrates the significance of this process that has a major bearing on the plume longevity. The ways in which contaminants are transported in natural granular media needs to be revisited to address the diffusive transport mechanics discussed in this document.